



# Carbon dioxide and vegetable oil for the synthesis of bio-based polymer precursors

Margot Alves

## ► To cite this version:

Margot Alves. Carbon dioxide and vegetable oil for the synthesis of bio-based polymer precursors. Catalysis. Université de Bordeaux; Université de Liège, 2016. English. NNT : 2016BORD0129 . tel-01531823

**HAL Id: tel-01531823**

**<https://theses.hal.science/tel-01531823>**

Submitted on 2 Jun 2017

**HAL** is a multi-disciplinary open access archive for the deposit and dissemination of scientific research documents, whether they are published or not. The documents may come from teaching and research institutions in France or abroad, or from public or private research centers.

L'archive ouverte pluridisciplinaire **HAL**, est destinée au dépôt et à la diffusion de documents scientifiques de niveau recherche, publiés ou non, émanant des établissements d'enseignement et de recherche français ou étrangers, des laboratoires publics ou privés.

THÈSE EN COTUTELLE PRÉSENTÉE  
POUR OBTENIR LE GRADE DE  
**DOCTEUR DE**  
**L'UNIVERSITÉ DE BORDEAUX**  
**ET DE L'UNIVERSITÉ DE LIÈGE**

ÉCOLE DOCTORALE DES SCIENCES CHIMIQUES (Université de Bordeaux)

ÉCOLE DOCTORALE DE CHIMIE (Université de Liège)

SPÉCIALITÉ CHIMIE PHYSIQUE ET POLYMÈRES

Par Margot ALVES

**Carbon dioxide and vegetable oil for the synthesis of bio-based polymer precursors**

Sous la direction de Dr. Thierry TASSAING et de Pr. Christine JÉRÔME

Soutenue à Liège le 17 Novembre 2016

Membres du jury :

Mme. VERTRUYEN, Bénédicte  
Mme. APRILE, Carmela  
M. KLEIJ, Arjan. W  
M. DIDIER, Benoît  
M. TASSAING, Thierry  
Mme. JÉRÔME, Christine  
M. DETREMBLEUR, Christophe  
M. MÉREAU, Raphaël

Professeur, Université de Liège, Belgique  
Professeur, Université de Namur, Belgique  
Professeur, ICIQ, Espagne  
Chef de projet R&D, Saint-Gobain, Belgique  
Directeur de Recherche, CNRS, France  
Professeur, Université de Liège, Belgique  
Directeur de Recherche, FNRS, Belgique  
Ingénieur de Recherche, CNRS, France

Présidente  
Rapporteur  
Rapporteur  
Examineur  
Directeur de thèse  
Directrice de thèse  
Invité, Secrétaire  
Invité



This PhD thesis is the result of a collaboration between the Group of Molecular Spectroscopy (GSM, UMR 5255 CNRS) of the Institute of Molecular Sciences (ISM) from the University of Bordeaux (France) and the Center for Education and Research on Macromolecules (CERM) from the University of Liège (Belgium). It has been co-supervised by Dr. Thierry TASSAING (ISM) and Prof. Christine JÉRÔME (CERM).

This project was equally funded by the “International Doctorate” program of the Initiatives of Excellence (IDEX) of the University of Bordeaux and the University of Liege through the “CO2Green” project granted by the Walloon Region.

This work was performed in the framework of the International Doctoral School in Functional Materials (ISD-FunMat) program funded by the European Community (ERASMUS MUNDUS Doctoral Program).

Computational facilities were provided by the “Pôle Modélisation” of the ISM and the MCIA (Mesocentre de Calcul Intensif Aquitain) of the University of Bordeaux (<http://www.mcia.univ-bordeaux.fr>) financed by the “Conseil Régional d’Aquitaine” and the French Ministry of Research and Technology.







# Remerciements

Après trois ans de thèse partagés entre deux laboratoires, deux équipes, deux ambiances et aussi une école doctorale internationale, j'en sors grandie de cette expérience avec beaucoup de rencontres à la clé.

Je souhaite tout d'abord remercier mes directeurs de thèse et superviseurs car si cette thèse s'est bien déroulée c'est surtout grâce à eux. Je leur suis très reconnaissante de m'avoir fait confiance, encouragée et de m'avoir permis de présenter mes résultats lors de nombreux congrès.

Je remercie Dr. Thierry Tassaing avec qui j'ai passé de nombreuses journées à bricoler des cellules IR et des montages de suivi cinétique et ainsi pris goût à la spectroscopie. Je lui suis très reconnaissante d'avoir été disponible, patient et toujours à l'écoute de mes propositions et de mon ressenti.

Merci à Madame le Professeur Christine Jérôme d'avoir dégagé un peu de temps dans cet emploi du temps bien rempli pour suivre l'avancée de mes résultats. Je tiens à remercier Dr. Christophe Detrembleur pour son implication dans ma thèse, son suivi, son aide et ses conseils.

Je remercie grandement Dr. Raphaël Méreau de m'avoir initiée et formée à la modélisation moléculaire et aux calculs DFT alors que je partais de zéro. J'y ai pris goût rapidement et il y a une certaine satisfaction d'avoir réussi à expliquer l'expérimental avec la théorie mais cela aurait été impossible sans sa patience, sa pédagogie, sa bonne humeur et sa disponibilité.

Enfin, j'adresse un grand merci à Dr. Bruno Grignard qui a supervisé une partie de cette thèse mais aussi partagé mon bureau pendant plus d'un an. Je le remercie pour son aide, sa générosité, sa disponibilité, ses coups de main (et de clés), les heures de corrections des articles et du manuscrit. D'un grand soutien au niveau de la thèse, il a toujours été là pour essayer de me donner un peu plus confiance en moi et me remonter le moral dans les moments de doute ou quand la motivation n'était plus là.

I would like to thanks Professor Kleij and Professor Aprile for accepting to be the rapporteurs of this thesis, Dr. Didier to bring an industrial point of view on this project and Professor Vertruyen for accepting to be the president of the jury.

Du côté de l'ISM, je souhaite remercier Dr. Gwenaëlle Le Bourdon et Dr. Jean-Luc Brunel pour m'avoir initié respectivement à la spectroscopie IR et Raman. Je tiens à remercier Prof. Vincent Rodriguez pour son accueil dans le groupe. Merci à Monsieur le Professeur Joseph Grondin avec qui j'ai partagé le laboratoire, pour ses conseils et à Stéphane RULLIER pour la confection des pièces qui ont permis l'assemblage des cellules haute-pression. Je souhaite remercier Cécile Siméoni pour son implication lors de son stage et Amélie Boyaval pour son aide pour les cinétiques IR réalisées alors que j'étais à Liège.

Au CERM, je voudrais remercier Sandro Gennen qui a mis en route ce projet et obtenu les premiers résultats ainsi que Gregory Cartigny, Charlotte Danemark et Laetitia Defays qui ont tous participé en faisant quelques synthèses, titrages RMN ou analyses.

Je remercie les autres membres du GSM et du CERM pour leur intérêt pour ces travaux et leur aide scientifique, technique et logistique.

Merci également à Monsieur le Professeur Émérite Bernard Gilbert pour les cinétiques par spectroscopie Raman. Je tiens à remercier Dr. Julien de Winter et Monsieur le Professeur Pascal Gerbaux pour les analyses MALDI-ToF et les « prises de tête » qui ont suivi.

Du côté de Bordeaux, j'adresse un grand merci à Elise et Flavie avec qui j'ai partagé mon bureau mais aussi de nombreux weekends, pour leur aide, leur soutien, nos nombreuses discussions mais aussi pour m'avoir accueillie chez elles lors de mes visites à Bordeaux. Je n'oublie pas Mathilde. C, Coralie, Antoine, Thomas, Tatiana, The Thong, Meriem et Claire qui ont partagé mon quotidien, les pauses café et les weekends à la plage ou au ski.

Du côté de Liège, un grand merci à Hélène pour son écoute et surtout les heures à discuter et les mails interminables pour se remonter le moral mutuellement. Je remercie Mathilde D. pour avoir partagé mon quotidien, mon bureau et mes doutes pendant notre période commune de rédaction. Merci aussi pour ces moments simples auxquels j'associe également Tim. I also had great time with Rahmet, Daniela, Zeynep, Mirco, Pauline, Philip, Satya and Nagaraj playing volley-ball, having a coffee/tea/beer or eating a pizza and just chatting away. Merci à tous les membres du CERM pour les parties de tarot, soirées volley-ball et ces moments partagés lors des journées du labo ou au BPG.

J'ai eu la chance de faire partie du programme IDS FunMat où j'ai eu l'opportunité de rencontrer des gens venant de partout dans le monde et cela a été une très bonne expérience. Ce fût toujours un plaisir de croiser Mathilde W.M., Tristan, Floriane, Marie, Gustavo et bien d'autres lors des écoles de printemps ou au détour d'un couloir à Liège ou à Bordeaux. Je remercie le Pr. Laurent Servant et l'équipe d'IDS FunMat.

Enfin, je souhaite remercier sincèrement ma famille, et particulièrement ma maman, pour leur soutien même si mes travaux sont toujours restés abstraits pour eux et qu'il a parfois été difficile de me suivre dans tous mes déplacements, déménagements et voyages. Un énorme merci à Benjamin pour sa confiance, son soutien depuis ces nombreuses années malgré la distance.

Pour terminer, j'ai une pensée pour Dr. Cyrielle Rudaz qui m'avait convaincu au cours de mon stage de fin d'étude qu'une thèse serait épanouissante pour moi ; et aujourd'hui je ne regrette pas de m'être lancée dans cette aventure.

# Résumé en français

Le coût incertain du pétrole et l'épuisement à moyen terme des réserves disponibles poussent la communauté scientifique à identifier de nouvelles sources de carbone abondantes, facilement exploitables et peu coûteuses. La valorisation du dioxyde de carbone qui est actuellement considéré comme un déchet et le principal gaz à effet de serre est donc le sujet de recherche de nombreux groupes de recherche. L'utilisation du CO<sub>2</sub> comme synthon C1 est donc très prometteuse pour la synthèse de molécules et de monomères d'intérêts. Cependant, le dioxyde de carbone est cinétiquement et thermodynamiquement très stable. L'utilisation de catalyseurs est donc nécessaire pour sa conversion chimique. La fixation du CO<sub>2</sub> sur les époxydes et les oxétanes représente un des exemples les plus efficaces de conversion/valorisation du CO<sub>2</sub> et conduit respectivement à la formation de carbonates cycliques à cinq ou six chaînons (Schéma 1).

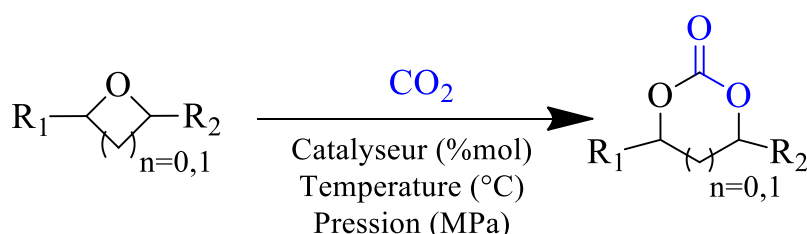


Schéma 1 : Réaction de couplage catalytique du CO<sub>2</sub> avec un époxyde (n=0) ou un oxétane (n=1)

Bien que les catalyseurs métalliques soient efficaces même à température ambiante et pression atmosphérique, la plupart sont peu sélectifs, sensibles à l'hydrolyse ou à l'oxydation et/ou toxiques. Au contraire, les catalyseurs organiques tels que les liquides ioniques ou les sels organiques sont moins toxiques et plus respectueux de l'environnement mais ne sont réellement efficaces qu'à haute température et haute pression. L'amélioration des performances des catalyseurs organiques est donc le sujet de nombreux travaux de recherche.

L'objectif des travaux menés durant cette thèse concerne le développement d'un nouveau système organocatalytique pour la synthèse de carbonates cycliques à partir de CO<sub>2</sub> dans des conditions douces (T < 100°C, P < 5 MPa). Initialement optimisé pour la conversion d'époxydes terminaux en carbonates cycliques *via* des études cinétiques et mécanistiques approfondies, l'utilisation de ce catalyseur a ensuite été extrapolée à la conversion d'huiles végétales époxydées et d'oxétanes en synthons (bio- et) CO<sub>2</sub>-sourcés d'intérêts.

Comme cela a été précédemment démontré dans la littérature, l'activité catalytique des sels organiques et des liquides ioniques peut être améliorée grâce à l'ajout d'un co-catalyseur donneur de liaisons hydrogènes. Nous avons démontré qu'une synergie existe entre les sels de tétrabutylammonium et les alcools fluorés. Alors qu'aucune activité n'a été mise en évidence lorsqu'il est utilisé comme solvant, l'ajout en

quantité catalytique d'alcool fluoré permet la synthèse rapide et sélective de carbonates cycliques par réaction entre l'époxyde et le CO<sub>2</sub> sans ajout de solvant. La cinétique de la réaction a été suivie grâce à un montage utilisant la spectroscopie FTIR ou Raman *in-situ*. Le CO<sub>2</sub> étant utilisé en large excès, la réaction répond à une cinétique de pseudo-ordre 1 et les constantes cinétiques peuvent être facilement extraites. Pour un époxyde modèle (1,2-epoxydodecane), l'addition de 1,1,1-trifluoro-2-méthyl-2-propanol (TFMP, Schéma 2 a), permet d'augmenter la constante cinétique de 300% comparée à celle déterminée en présence de sels de tetrabutylammonium comme unique catalyseur. De plus, l'activité catalytique augmente avec le nombre de groupements trifluorométhyle de l'alcool fluoré dans l'ordre suivant : 1,1,1-trifluoro-2-méthyl-2-propanol (TFMP) < hexafluoro-*tert*-butanol (HFB, Schéma 2 b) < perfluoro-*tert*-butanol (PFB, Schéma 2 c). En outre, les études cinétiques ont mis en évidence qu'un diol fluoré, le 1,3-bis-(2-hydroxyhexafluoroisopropyl)benzene (1,3-bis-HFAB, Schéma 2 d), était le donneur de liaisons hydrogène le plus efficace permettant une réaction rapide et sélective entre le CO<sub>2</sub> et l'époxyde dans des conditions douces (60 - 80°C) et même à pression atmosphérique. La conversion d'oligomères de poly(éthylène glycol) diglycidylether (Mn= 500 g/mol) dans lesquels tous les composés sont solubles a démontré que l'activité n'était pas liée à un effet de co-solvant de l'alcool fluoré. On peut noter que le diol équivalent non-fluoré n'a aucune activité co-catalytique. Par conséquent, ce résultat démontre l'impact positif des groupements trifluorométhyles pour promouvoir et accélérer la réaction.

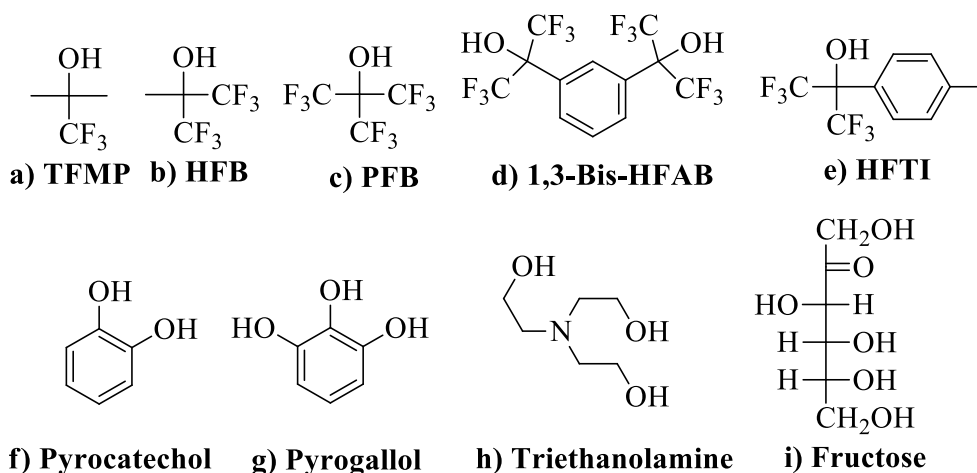


Schéma 2 : Structure chimique des activateurs donneurs de liaisons hydrogène utilisés comme co-catalyseurs.

Dans le but de mettre en évidence l'activité supérieure des alcools fluorés, un criblage catalytique de différents co-catalyseurs organiques commerciaux a ensuite été réalisé pour la conversion d'époxydes modèles dans les mêmes conditions (60°C, 2 MPa) en présence de TBABr comme catalyseur (3 mol%). *Via* des suivis cinétiques *in-situ* par spectroscopie proche infrarouge, il a été démontré que les performances co-catalytiques des alcools fluorés surpassent celles de la triethanolamine, du fructose et des dérivés phénoliques (Figure 1). En effet, la cinétique de la réaction est significativement plus rapide avec le perfluoro-*tert*-butanol (PFB), l'hexafluoro-*p*-

tolyl-isopropanol (HFTI, Scheme 2 e) et le 1,3-bis-HFAB. La cinétique avec le 1,3-bis-HFAB est accélérée de 230% par rapport à celle réalisée en présence de pyrogallol qui était connu dans la littérature comme le co-catalyseur le plus performant. A 60°C et 2 MPa, la conversion de l'oxyde propylène est quantitative après seulement 100 minutes. Sans surprise, une augmentation de la température et de la pression accélère significativement la réaction de couplage entre le CO<sub>2</sub> et l'époxyde. Ensuite, la réaction a été étudiée avec d'autres époxydes modèles (oxyde de styrène, glycidol, oxyde de cyclohexène). Quel que soit la nature de l'époxyde, les systèmes catalytiques composés de TBABr et d'un alcool fluoré accélèrent la cinétique de la réaction sans formation de sous-produits. Cependant, la conversion d'époxydes disubstitués, tels que l'oxyde de cyclohexène, en carbonates cycliques correspondants est beaucoup plus lente que celle des époxydes terminaux comme cela a déjà été reporté dans la littérature.

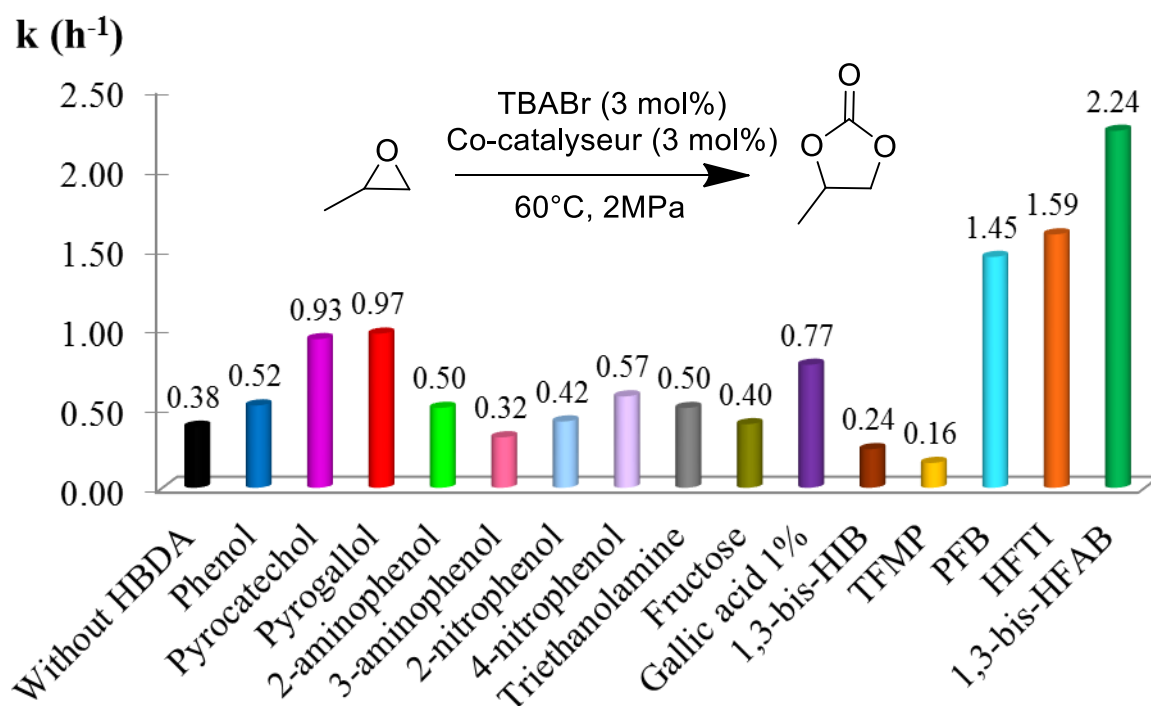


Figure 1: Constantes de vitesse déterminées pour la réaction de couplage entre le CO<sub>2</sub> et l'oxyde de propylène catalysée par les systèmes catalytiques composés de TBABr et d'un donneur de liaisons hydrogène. Conditions expérimentales : T = 60°C, P = 2 MPa, TBABr = 3 mol%, [TBABr]/[HBD] = 1.

Ensuite, la synthèse d'huile de lin carbonatée par réaction entre le CO<sub>2</sub> et l'huile de lin époxydée a été étudiée. Premièrement, un criblage de liquides ioniques et de sels organiques utilisés comme catalyseurs a été réalisé. L'activité catalytique du cation diminue dans l'ordre suivant : guanidinium > ammonium ~ imidazolium > phosphonium ~ amidinium > pyrrolidinium > pyridinium. D'autre part, l'influence de l'anion halogène a également été étudiée. Le brome est l'anion le plus efficace car il offre le meilleur compromis entre le caractère nucléophile et la taille (encombrement stérique). En effet, bien qu'il soit moins nucléophile, le brome est plus petit que l'iode ce qui facilite sa diffusion rapide vers les époxydes internes dans l'huile visqueuse.

Dans une deuxième étape, une étude de systèmes catalytiques composés de TBABr et de dérivés multiphénoliques ou d'alcools fluorés a été réalisée. Les activateurs mutiphénoliques dérivés du catéchol et du pyrogallol ainsi que les alcools fluorés présentent les performances catalytiques les plus élevées. Une étude par spectroscopie FTIR *in-situ* a mis en évidence que le 1,3-bis-HFAB reste le donneur de liaisons hydrogène le plus efficace. L'influence de nombreux paramètres (pression, température, pourcentage de catalyseur, quantité de CO<sub>2</sub> dissoute dans l'huile végétale époxydée) a également été évaluée. La réaction entre l'huile végétale époxydée et le CO<sub>2</sub> est favorisée à hautes température (120°C) et pression (5 MPa) bien que la quantité de CO<sub>2</sub> dissoute dans l'huile soit plus faible lorsque la température augmente. La synthèse d'huile végétale carbonatée est totale après 600 minutes dans ces conditions (Figure 2). La conversion d'époxydes bio-sourcés est donc beaucoup plus lente que celle des époxydes modèles même à plus haute pression et plus haute température. En effet, comme cela a été montré avec l'oxyde de cyclohexene, les époxydes internes (disubstitués) sont beaucoup moins réactifs que les époxydes terminaux à cause de l'encombrement stérique. Cependant, l'utilisation d'alcools fluorés comme co-catalyseurs permet d'accélérer sensiblement la cinétique de réaction en comparaison avec les autres systèmes décrits dans la littérature.

## Yield (%)

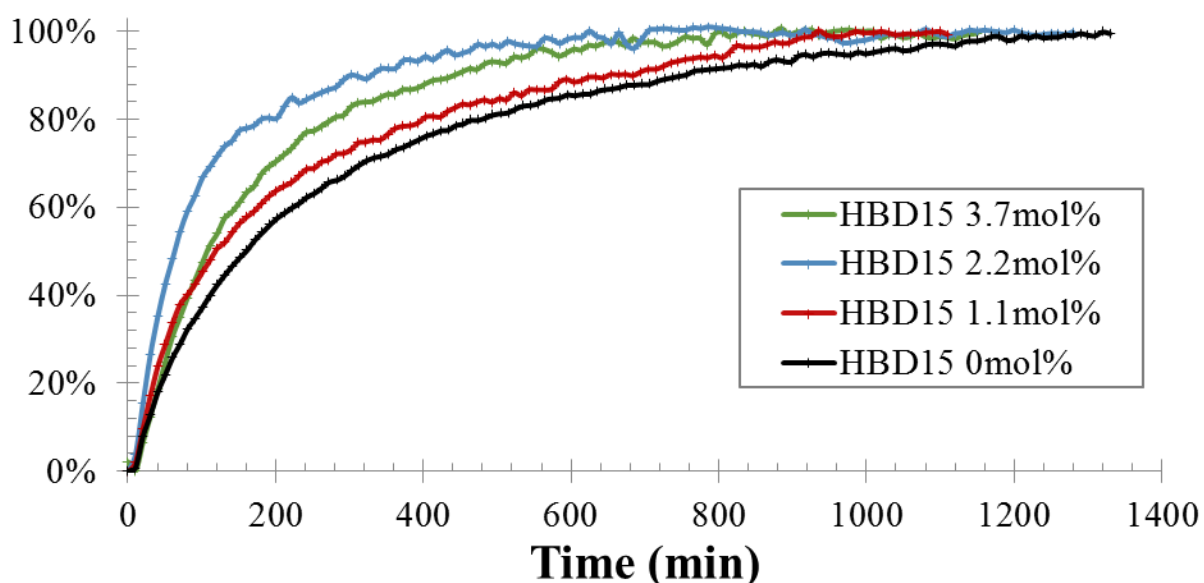


Figure 2: Etude cinétique de la réaction entre le CO<sub>2</sub> et l'huile de lin époxydée catalysée par le système catalytique TBABr/1,3-HFAB: effet de la quantité de co-catalyseur donneur de liaisons hydrogène. Conditions expérimentales : T = 120°C, P = 5 MPa, TBABr = 2.2 mol%.

Une étude par modélisation moléculaire utilisant la méthode de la Théorie de la Fonctionnelle de la Densité (DFT) a été conduite afin de déterminer de manière approfondie le mécanisme d'activation et les paramètres clés expliquant l'activité élevée du co-catalyseur. Le mécanisme réactionnel le plus probable est composé de trois étapes : l'ouverture de l'époxyde par attaque nucléophile du contre-ion halogéné, l'insertion du CO<sub>2</sub> et enfin la fermeture du carbonate cyclique. Les calculs DFT ainsi que les titrages RMN ont montré une forte interaction par liaisons

hydrogène entre l'oxygène de l'époxyde et le 1,3-bis-HFAB. En plus des deux liaisons hydrogène avec les groupements hexafluoroisopropanol, une troisième interaction plus faible entre le proton aromatique en position *ortho* des groupements hexafluoroisopropanol et l'oxygène de l'époxyde a été mise en évidence. Cette triple interaction permet de stabiliser l'ensemble des intermédiaires réactionnels et des états de transition (Figure 3 a). Par conséquent, l'énergie libre de la réaction est diminuée de 33.7 kcal/mol avec TBABr comme seul catalyseur à 3.8 kcal/mol en utilisant le 1,3-bis-HFAB comme co-catalyseur. Le mécanisme d'activation est similaire avec le pyrogallol mais uniquement deux liaisons intermoléculaires avec deux groupements OH vicinaux permettent de stabiliser les intermédiaires et les états de transition (Figure 3 b). En effet, l'oxygène du groupement phénolique central est stabilisé *via* une liaison hydrogène intramoléculaire par le troisième groupement OH. L'activité catalytique supérieure du 1,3-bis-HFAB comparé au pyrogallol est donc attribuée à une stabilisation par liaisons hydrogènes plus forte. De plus, l'activité co-catalytique de monoalcools fluorés a été attribuée à l'action simultanée de deux molécules (Figure 3 c). Cette étude détaillée démontre que la présence de groupements trifluorométhyles influence la distribution de charge du donneur de liaison hydrogène et augmentent l'acidité du proton du groupement alcool ce qui permet de former des liaisons hydrogènes plus fortes qu'un analogue non fluoré.

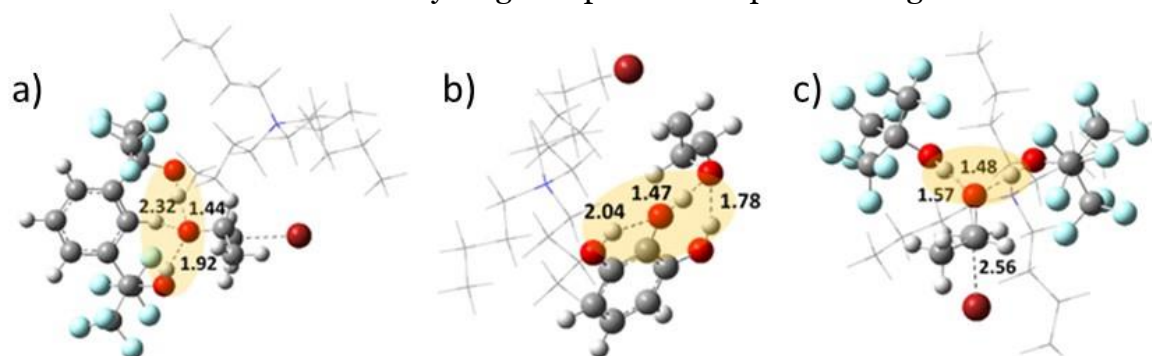
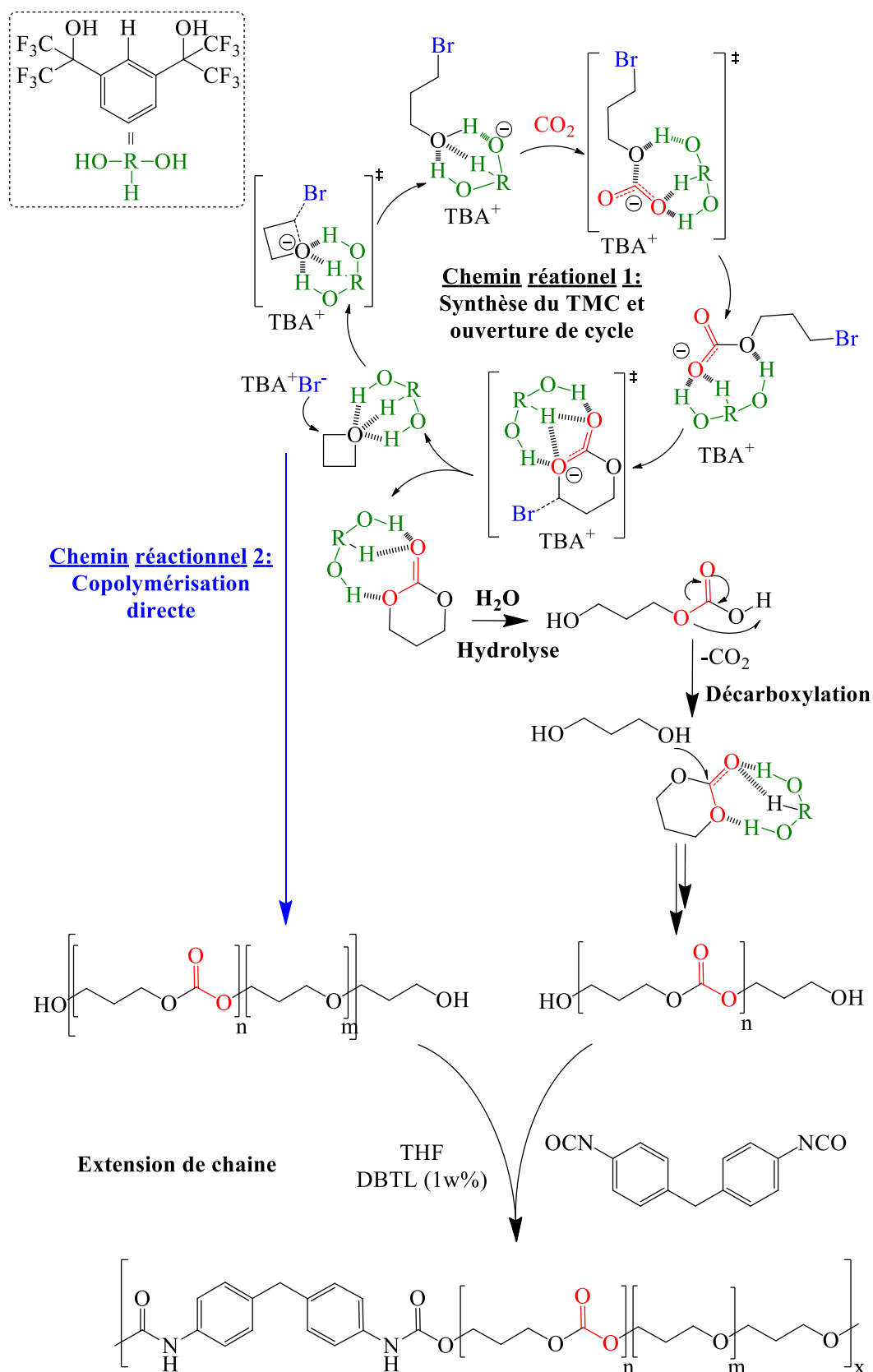


Figure 3 : Structure de la géométrie optimisée (M06-2X/6-311G(d,p)) de l'état de transition d'ouverture de cycle de l'époxyde par l'ion bromure (TS1) pour la réaction entre le CO<sub>2</sub> et l'oxyde de propylène catalysée par a) TBABr/1,3-bis-HFAB, b) TBABr/Pyrogallol et c) TBABr/2 molécules de PFB (TBABr est représenté sous forme de squelette pour une meilleure visualisation).

Finalement, grâce à la versatilité et l'activité catalytique remarquable du système catalytique composé d'un sel de tétrabutylammonium (iodure de tétrabutylammonium) et d'un alcool fluoré (1,3-bis-HFAB), des oligocarbonates hydroxyles téléchéliques ont été synthétisés par réaction entre le CO<sub>2</sub> et un oxétane. Ce système catalytique bicomposant est le premier permettant la conversion sélective d'oxétanes sans utilisation de catalyseur métallique en produits à valeur ajoutée. Toutefois, les oxétanes sont moins réactifs que les époxydes et leur conversion requiert des conditions expérimentales plus drastiques (130°C, 10 MPa). Le 1,3-bis-HFAB est thermiquement stable alors que d'autres co-catalyseurs organiques tels que le pyrogallol se dégradent dans ces conditions. Des titrages RMN et des calculs DFT ont mis en évidence que le diol fluoré (1,3-bis-HFAB) interagit très fortement avec



l'oxétane par liaisons hydrogène et ainsi réduit significativement l'énergie libre de Gibbs de l'étape limitante (ouverture de l'époxyde) à  $\Delta G = 6.4$  kcal/mol par rapport à la réaction avec TBABr comme unique catalyseur ( $\Delta G = 39.9$  kcal/mol). L'étude du mécanisme de réaction par spectroscopie FTIR *in-situ* a mis en évidence la formation du carbonate de triméthylène (TMC) (Scheme 3) qui se dégrade rapidement en 1,3-propanediol par hydrolyse en présence de traces d'eau. Le 1,3-propanediol amorce alors l'ouverture du carbonate de triméthylène pour former des oligocarbonates ( $M_n = 2000$  g.mol<sup>-1</sup>,  $\bar{D} = 1.3$ ). De plus, études DFT et titrages RMN à l'appui, il est probable que le 1,3-bis-HFAB puisse catalyser l'ouverture de cycle du carbonate de triméthylène car il interagit également avec le carbonate cyclique à 6 chaînons. La structure des oligocarbonates et la nature des bouts de chaîne ont été déterminées en combinant des analyses par MALDI-ToF et RMN qui ont mises en évidence que la majorité des chaînes (90%) étaient terminées à chacune de leurs extrémités par des groupements hydroxyles ou par des doubles liaisons oléfiniques (10%). Dans une deuxième étape, des poly(uréthane-co-carbonate)s CO<sub>2</sub>-sourcés avec une  $M_n$  atteignant jusqu'à 9200 g/mol ( $\bar{D} = 2.24$ ) ont été synthétisés par extension de chaîne des oligomères en présence de diisocyanate (Scheme 3). Alors que les oligomères se dégradent à 135°C, ces polymères sont stables jusqu'à 250°C et leur température de transition vitreuse augmente de -41°C pour les oligocarbonates ( $M_n = 2000$  g/mol) à -3°C pour un PU de  $M_n = 9200$  g/mol. L'insertion d'un segment rigide permet d'améliorer les propriétés des poly(uréthane-co-carbonate)s offrant ainsi des perspectives d'application en tant que revêtements, mousses PU ou matériaux à des fins médicales.



Scheme 3: Mécanisme proposé pour la synthèse d'oligocarbonates par couplage entre le CO<sub>2</sub> et l'oxyde de propylène catalysée par le système organocatalytique TBAI/1,3-bis-HFAB. RH(OH)<sub>2</sub> représente le 1,3-bis(2-hydroxyhexafluoroisopropyl)benzene.



# Table of contents

List of abbreviations.....	15
General introduction.....	17
<u>Chapter I:</u> Background and literature review: Organocatalytic CO <sub>2</sub> /epoxide coupling: catalysts development and mechanistic studies.....	23
<u>Chapter II:</u> Fluorinated alcohols as activators for the solvent-free chemical fixation of carbon dioxide into epoxides.....	87
<u>Chapter III:</u> Organocatalytic promoted coupling of carbon dioxide with epoxides: a rational investigation of the co-catalytic activity of various hydrogen bond donors.....	109
<u>Chapter IV:</u> Organocatalytic synthesis of bio-based cyclic carbonates from CO <sub>2</sub> and vegetable oils.....	127
<u>Chapter V:</u> A comprehensive Density Functional Theory study of the key role of fluorination and dual hydrogen bonding in the activation of the epoxide/CO <sub>2</sub> coupling by fluorinated alcohols.....	147
<u>Chapter VI:</u> Organocatalytic coupling of CO <sub>2</sub> with oxetanes.....	169
General conclusion and outlooks.....	203
<u>Appendix:</u> DFT investigation of the reaction mechanism for the guanidine catalysed ring-opening of cyclic carbonates by aromatic and alkylamines.....	209



# List of abbreviations

1,3-bis-HIB:	$\alpha,\alpha$ -(dihydroxy-1,3-diisopropyl)benzene
1,3-bis-HFAB:	1,3-bis(2-hydroxyhexafluoroisopropyl)-benzene
$\beta$ -CD:	$\beta$ -cyclodextrin
AA:	Amino acid
AAIL:	Amino acid-derived ionic liquid
AN:	Acceptor number
ATR:	Attenuated Total Reflectance
Bet:	Betaine
CLSO:	Carbonated Linseed oil
CU6:	Cucurbit[6]uril
C <sub>x</sub> -MIm:	C <sub>x</sub> methylimidazolium
C <sub>x</sub> -PyX:	C <sub>x</sub> -Pyridinium X <sup>-</sup>
CO:	Cyclohexene oxide
DABCO:	1,4-diazabicyclo[2,2,2]octane
DBTL:	Dibutyltin dilaurate
DBU:	1,8-diazabicyclo[5.4.0]undec-7-ene
DCTB:	trans-2-[3-(4-tert-butyl-phenyl)-2-methyl-2-propenylidene] malononitrile
DFT:	Density Functional Theory
DMA:	Dimethylacetamide
DMAP:	4-(N,N-dimethylamino)pyridine
DMF:	N,N-Dimethylformamide
DMSO:	Dimethyl sulfoxide
DSC:	Differential scanning calorimetry
DTGS:	Deuterated TriGlycine Sulphate
ED:	1,2-epoxydodecane
EDTA:	Ethylenediaminetetraacetic acid
ELSO:	Epoxidized linseed oil
EO:	Ethylene oxide
FHBD:	Fluorinated Hydrogen Bond Donor
FTIR:	Fourier transform infrared spectroscopy
g-C <sub>3</sub> N <sub>4</sub> :	Graphitic carbon nitride
GDO:	Glycidol
GO:	Graphite oxide
HA:	Amidinium halide
HBD:	Hydrogen Bond donor
HFB:	Hexafluoro- <i>ter</i> -butanol
HFIP:	1,1,1,3,3,3-hexafluoroisopropanol
HFTI:	Hexafluoro-( <i>p</i> -tolyl)-isopropanol
HMTA:	Hexamethylene tetramine
IL:	Ionic liquid
Im:	Imidazole

IR:	Intermediate (of the reaction)
IRC:	Intrinsic reaction coordinate
k:	Rate constant ( $\text{h}^{-1}$ or $\text{min}^{-1}$ )
MALDI-ToF:	Matrix-assisted Laser Desorption/Ionization Time-of-Flight
MDI:	4,4'-methyldiphenyldiisocyanate
MOF:	Metal organic framework
MTBD:	7-methyl-TBD (7-Methyl-1,5,7-triazabicyclo[4.4.0]dec-5-ene)
MTHP:	Methyltetrahydropyrimidine
NBO:	Natural Population Analysis
NBS:	N-bromosuccinimide
NHC:	N-heterocyclic carbene
NHO:	N-heterocyclic olefin
NIPU:	Non Isocyanate Polyurethane
NIR:	Near Infrared Spectroscopy
NMP:	N-Methyl-2-pyrrolidone
NMR:	Nuclear magnetic resonance
NO <sub>x</sub> :	Nitrogen oxide
PC:	Propylene Carbonate
PETT:	Pentaerythritol
PFB:	Perfluoro- <i>tert</i> -butanol
PHU:	Poly(hydroxyurethane)
PO:	Propylene oxide
PTMC:	Poly(trimethylene carbonate)
PU:	Polyurethane
REACH:	Registration, Evaluation, Authorization and Restriction of Chemicals
ROP:	Ring-opening polymerization
SEC:	Size-exclusion chromatography
SO:	Styrene oxide
SO <sub>x</sub> :	Sulphur oxide
TA:	Tannic acid
TBD:	1,5,7-triazabicyclo[4.4.0]dec-5-ene
TBAX:	Tetrabutylammonium X <sup>-</sup>
TEAX:	Tetraethylammonium X <sup>-</sup>
TFMP:	1,1,1-Trifluoro-2-methyl-2-propanol
TGA:	Thermogravimetric analysis
THAX:	Tetrahexylammonium X <sup>-</sup>
THF:	Tetrahydrofuran
TMC:	Trimethylene carbonate
TMO:	Trimethylene oxide
TOAX:	Tetraoctylammonium X <sup>-</sup>
TON:	Turn Over Number
TS:	Transition state

---

# General introduction

---





Concerns related to fossil resources utilization (price, depletion, climate change) prompted the scientific community to search for inexpensive, abundant and easily exploitable new sources of carbon while responding to the challenges of green and sustainable chemistry. To answer this challenge, valorizing CO<sub>2</sub> as a renewable C1 feedstock for producing added value building blocks has become the scope of many academic and industrial researches. Carbon dioxide is a thermodynamically and kinetically stable molecule that can be converted into five- and six-membered cyclic carbonates by coupling with epoxides or oxetanes, respectively, using appropriate catalysts. By merging bio-based epoxides derived from vegetable oils and carbon dioxide, cyclic carbonates can be synthesised with a total atom economy. Although transition metal catalysts are efficient under atmospheric pressure and ambient temperature for CO<sub>2</sub>/oxiranes coupling, most of them are poorly selective, sensitive to hydrolysis and/or oxidation and/or toxic whereas less/non-toxic and eco-friendly organocatalysts such as ionic liquids and halide salts are generally only efficient at very high temperature and pressure favoring their thermal degradation. Thus, although these areas of research have been the subject of many works, the catalytic performance still need to be further enhanced in particular for the coupling of CO<sub>2</sub> with more demanding oxetanes and disubstituted epoxides such as epoxidized vegetable oils while respecting environmental standards. This thesis aims at synthesizing CO<sub>2</sub>-based building blocks by developing a new versatile organocatalytic platform enabling both the fast and selective cycloaddition of CO<sub>2</sub> onto terminal epoxides and epoxidized oils and the conversion of oxetanes into useful CO<sub>2</sub>-based products (Figure 1).

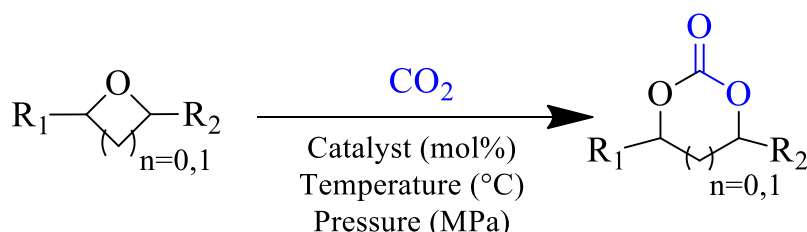


Figure 1: Catalytic coupling of CO<sub>2</sub> with epoxide (n=0) or oxetane (n=1)

To achieve this purpose, the Institute of Molecular Sciences (ISM) from the University of Bordeaux (France) and the Centre for Education and Research on Macromolecules (CERM) from the University of Liège (Belgium) have combined their respective expertise in i) developing analytical spectroscopic tools to investigate *in situ* complex phenomena such as phase diagrams, molecular interactions, reaction kinetics... and DFT calculations using molecular modeling enabling to identify the key parameters involved in the reaction mechanisms and ii) in polymer synthesis, processing and characterization including a strong activity in CO<sub>2</sub> transformation, CO<sub>2</sub> processing and CO<sub>2</sub> utilization. The development of the catalytic platform and the characterizations of the CO<sub>2</sub>-based precursors and polymers were performed at CERM. Online FTIR kinetics studies, determination of thermodynamics parameters such as phase diagram and DFT calculations were done at the ISM.

This thesis is composed of six chapters written as communications that have been submitted or published in scientific journals except for the literature review.

The first chapter is dedicated to a detailed background and a state of the art overview related to homogeneous organocatalytic systems for the epoxide/ $\text{CO}_2$  coupling. In a first part, single component catalysts such as ionic liquids, organic salts, organic bases... are described. The second part focuses on hydroxyl-, carboxylic acid- and amino-functional mono- or bicomponent systems that allow enhancing the catalyst performances. Finally, mixed bicomponent organocatalysts composed of a homogeneous salt or IL and a heterogeneous co-catalyst are reviewed. This introduction also includes mechanistic discussions based on DFT calculations of the most relevant catalytic systems. This review includes results described in the following chapters.

The second chapter deals with the development of a new bicomponent catalytic platform composed of an onium salt and fluorinated alcohols for  $\text{CO}_2$ /epoxides coupling. The combination of online kinetic studies under pressure (Raman/FTIR), NMR titrations and DFT calculations allows understanding the origin of synergistic effect that provides a very active organocatalyst for the conversion of epoxides under mild conditions.

The third chapter focuses on a rational comparative study of the co-catalytic efficiency of a series of commercially available and efficient hydrogen bond donor co-catalysts. The influence of different parameters such as the pressure, the temperature, the catalyst loading, and the nature of the epoxide on the reaction kinetics was evaluated through detailed kinetic studies by *in-situ* FT-IR spectroscopy. This chapter highlights the superior co-catalytic performances of fluorinated alcohols compared with others hydrogen bond donors reported previously in the literature.

In the fourth chapter, bio- and  $\text{CO}_2$ -based cyclic carbonates are synthesized in short reaction times under solvent-free conditions by coupling  $\text{CO}_2$  with epoxidized linseed oil using a bicomponent organocatalytic platform. A screening of the catalytic activity of a series of organic salts and ionic liquids used in combination with hydroxyl-based, (multi)phenolic or fluorinated hydrogen bond donors is realized. The synergistic effect between the ammonium salt and 1,3-bis-HFAB is highlighted by kinetics studies *via* IR spectroscopy under pressure that also enabled to optimize the reaction conditions (pressure, temperature, catalyst loading).

The fifth chapter is dedicated to the fine comprehension by Density Functional Theory (DFT) of the activation mechanism for the coupling of epoxide/ $\text{CO}_2$  using the binary organocatalyst combining TBABr with (multi)phenolic or fluorinated hydrogen bond donors (HBDs). The key role of the hydrogen bonding in the stabilisation of intermediates and transition states is highlighted. In addition, the influence of the number of electron withdrawing trifluoromethyl substituents in HBDs and the mechanism involving two molecules of monofluorinated alcohols is described.

In the sixth chapter, the use of the powerful catalytic system composed of ammonium salts and fluorinated alcohols is then extended to the first example of organocatalytic coupling of CO<sub>2</sub> with less reactive oxetanes. The influence of the main reaction parameters (type of organocatalytic system, pressure and temperature) on the yield, the product formed and the selectivity of the reaction is discussed. The bicomponent organocatalyst promotes the efficient and selective synthesis of CO<sub>2</sub>-sourced  $\alpha,\omega$ -hydroxyl oligocarbonates. NMR characterizations were correlated with MALDI-ToF analyses for elucidating the structure of the oligomers. Online FTIR studies under pressure, NMR titrations and DFT calculations allowed an in-depth understanding of the reaction mechanism. Finally, CO<sub>2</sub>-based poly(carbonate-co-urethane)s were synthesized by step-growth polymerization of hydroxyl telechelic oligocarbonates with 4,4'-methyldiphenyldiisocyanate (MDI).

This manuscript ends with a general conclusion summarizing the key results and future outlooks.

Finally, the appendix is dedicated to the mechanistic investigation using the density functional theory (DFT) of the guanidine catalyzed aminolysis of propylene carbonate. It shows that different reaction pathways are involved depending on the aromatic or aliphatic nature of the amine reactant. The structural ability of 1,5,7-triazabicyclo[4.4.0]dec-5-ene (TBD) to simultaneously transfer and receive protons was demonstrated. The bifunctional activity (base/H-bond donor) of TBD significantly reduces the Gibbs energy of the reaction and allows understanding its higher efficiency compared to its methyl counterpart (MTBD).



---

Chapter I  
Background and literature review:

Organocatalytic CO<sub>2</sub>/epoxide  
coupling: catalysts development and  
mechanistic studies

---



## Table of content

I. CO <sub>2</sub> as chemical feedstock.....	27
II. CO <sub>2</sub> /epoxide coupling using homogeneous metal-free organocatalysts .....	29
II-1. Single-component metal-free homogeneous organocatalysts .....	29
II-1-a) Alkali metal salts.....	29
II-1-b) Organic salts and ionic liquids .....	30
Ammonium salts.....	30
Phosponium ILs .....	31
Imidazolium ILs .....	32
Pyridinium ILs.....	33
Pyrrolidinium ILs .....	33
Others nitrogen containing ILs derived from (super)bases .....	33
II-1-c) Amines and organic bases.....	35
II-1-d) Carbenes, N-heterocyclic olefins and phosphorus-ylides catalysts.....	36
II-1-e) Azaphosphatranes.....	38
II-1-f) Others catalysts .....	39
II -1-g) Mechanistic study .....	40
Activation by a halide .....	40
Halide-free activation mechanism .....	44
II-2. Functionalized one-component metal-free homogeneous organocatalysts....	47
II-2-a) Hydroxyl-functionalized organic salts and ILs catalysts .....	47
Ammoniums and choline derivatives.....	47
Phosponiums .....	48
Imidazoliums .....	49
Others ILs .....	50
II-2-b) Carboxylic acid-functionalized organic salts and ILs catalysts.....	51
Ammonium ILs.....	51
Phosponium ILs .....	52
Imidazolium ILs .....	52
Pyridinium ILs.....	53
Others ILs .....	53
II-2-c) Amino-functionalized organic salts and ILs catalysts .....	53
Phosponium ILs .....	53
Imidazolium ILs .....	53
Others animo-functional ILs .....	54
II-2-d) Urea-functionalized ILs catalysts .....	54

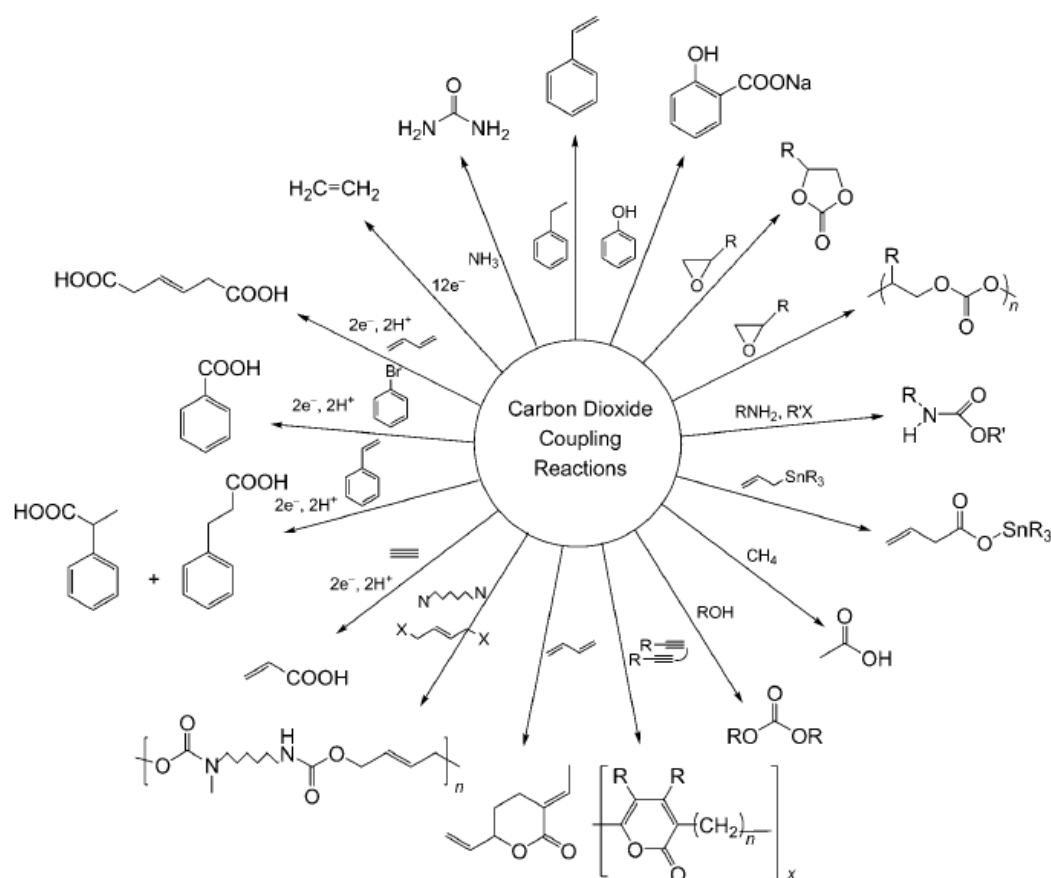


II-2-e) Amino alcohols and amino acids catalysts.....	54
II-3. Bi- and tri-component metal-free homogeneous organocatalysts .....	56
II-3-a) Water .....	56
II-3-b) Alcohols and hydroxyl-functionalized HBDs .....	57
Mono-alcohols .....	57
Di- and polyols.....	57
Saccharides .....	58
Fluorinated alcohols .....	58
Boronic acids .....	59
Silanols.....	59
Phenol and derivatives .....	60
Carboxylic acids .....	62
Aminoalcohols .....	62
Amino acids .....	63
II-3-c) Aliphatic and cyclic amines and their derivatives.....	65
II-3-d) Crown ethers, (poly)ethers and cavitands .....	66
II-4. Mixed homogeneous/heterogeneous organocatalysts.....	69
II-4-a) Oxides of carbon and carbon nitrides .....	69
II-4-b) Biopolymers .....	70
Microcrystalline cellulose.....	70
Chitosan .....	71
Lignin.....	71
Polydopamine .....	72
II-5. Mechanistic study of functionalized single catalysts or bicomponent catalysts .....	73
III. Conclusion.....	78
IV. References .....	79

## I. CO<sub>2</sub> AS CHEMICAL FEEDSTOCK

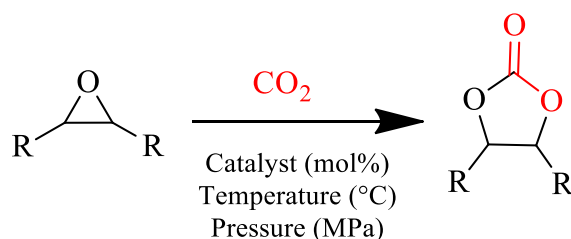
Carbon dioxide (CO<sub>2</sub>) is a well-known greenhouse gas regulated by the global fixation of terrestrial plants, oceans and microorganisms as part of the natural “carbon cycle”. Since the industrial revolution in the mid-18<sup>th</sup> to early 19<sup>th</sup> century, anthropogenic emissions have rapidly increased to reach a CO<sub>2</sub> concentration in the atmosphere of ~ 400 ppm in 2015. Today, CO<sub>2</sub> is considered as an industrial waste directly released in the atmosphere with other harmful compounds (SO<sub>x</sub> and NO<sub>x</sub>) and the excess of CO<sub>2</sub> is no more counterbalanced by nature because of the simultaneous deforestation and ocean acidification, leading to global warming. To limit climate changes, governments are adopting new legislations to decrease CO<sub>2</sub> emissions. Massive efforts focused on (reversible) carbon capture and storage and CO<sub>2</sub> mineralization strategies.<sup>1-7</sup> However, CO<sub>2</sub> sequestration faces problems of costs and public acceptance. Carbon dioxide could also be view as C1 building block and an inexhaustible, cheap, nontoxic, non-flammable green source of carbon.<sup>8-13</sup> Thus, using CO<sub>2</sub> as chemical feedstock may help to mitigate CO<sub>2</sub> emissions and increase independence from fossil fuels.<sup>14</sup>

Since a few decades, CO<sub>2</sub> has been exploited for the synthesis of added-value products, such as organic chemicals<sup>15, 16</sup>, polymers<sup>17</sup>, fuels<sup>18, 19</sup>, pharmaceutical/fine chemicals<sup>2...</sup> Some possible reactions of CO<sub>2</sub> are depicted in Scheme 1.



Scheme 1: Various chemicals produced from CO<sub>2</sub> (reprinted from ref 2)

Industrially, the volume production of CO<sub>2</sub>-sourced products is dominated to a large extent by the synthesis of urea, salicylic acid and (organic) carbonates but these valorisation routes represent only a minute of the worldwide CO<sub>2</sub> emissions (~0.03%).<sup>20</sup> Cyclic carbonates can be produced by coupling CO<sub>2</sub> with epoxides using appropriate catalyst (Scheme 2).



Scheme 2: Synthesis of cyclic carbonate by CO<sub>2</sub>/epoxide coupling

This 100% atom economy reaction is very attractive as it represents a greener and safer alternative to the conventional synthesis of cyclic carbonates from diols and toxic phosgene. Today, these precursors find applications as electrolytes in Li-ion batteries, intermediates for fine chemicals synthesis and polar aprotic solvents replacing DMF, DMSO, NMP and acetonitrile. They also serve as raw materials for the synthesis of polycarbonates (Asahi Kasei Chemicals process)<sup>21</sup> and isocyanates-free polyurethanes<sup>22-24</sup> (NIPUs) for which recent interest is supported by REACH regulation changes banning/limiting the use of harmful isocyanates entering in the synthesis of classical PUs. In view of the broad scope of applications of cyclic carbonates and their strong economic potential, there is still a need to improve their synthesis and decrease their production costs. However, CO<sub>2</sub> is a thermodynamically very stable molecule with a standard heat of formation of  $\Delta_f H^\circ = -394$  kJ/mol and the CO<sub>2</sub>/epoxide coupling doesn't occur spontaneously even though it is highly exothermic. Depending on the calculation methods<sup>25-28</sup>, the activation barrier was estimated between 50 and 70 kcal.mol<sup>-1</sup>. The use of a catalyst is then mandatory for activating the epoxide or/and carbon dioxide and facilitating the reaction. The development of new catalysts was extensively studied and included metal complexes and metal oxides<sup>29,30</sup>, metal oxide frameworks (MOF)<sup>31</sup>, onium salts, ionic liquids<sup>32,33</sup>, Schiff bases, functionalized (bio-)polymers and mono- or binary metal-free catalysts<sup>34</sup>. The activity is influenced by several parameters such as the temperature, the CO<sub>2</sub> pressure, the nature and composition of the catalyst... Homogeneous catalysts are far more efficient than heterogeneous analogues allowing the conversion of CO<sub>2</sub> into cyclic carbonates with lower catalyst loadings, at lower temperatures and reduced reaction times whereas the lower activity of heterogeneous catalysts originates from diffusion limitations of the reactant to the catalytic sites. Due to evolution of environmental and economic considerations, the global trend is now to develop catalysts very active under conditions as mild as possible. Homogeneous metal complexes (Al, Co, Mn, Zn, Cr, Mg, etc.) were the first catalysts enabling the conversion of CO<sub>2</sub> into cyclic carbonates under atmospheric pressure and ambient temperature.<sup>35</sup> However, many metal catalysts are poorly selective, sensitive to

hydrolysis and/or oxidation and/or toxic. Moreover, in order to fully respect the regulations about the absence of metal residues in the final product, organocatalysts should be preferred. Metal-free catalysts are assumed to be efficient only under high pressure and temperature favoring their thermal degradation. To overcome these limitations, functionalized organocatalysts and binary or ternary catalysts were successfully developed in the past few years and some of them were reported to be as competitive as metal-based catalysts. Additionally, organocatalysts are generally composed of low cost, readily available and non-toxic compounds exhibiting good chemical stability towards moisture, water and air. This literature review will then focus on the advances of metal-free organocatalysts for the CO<sub>2</sub>/epoxide coupling.

## **II. CO<sub>2</sub>/EPOXIDE COUPLING USING HOMOGENEOUS METAL-FREE ORGANOCATALYSTS**

### **II-1. Single-component metal-free homogeneous organocatalysts**

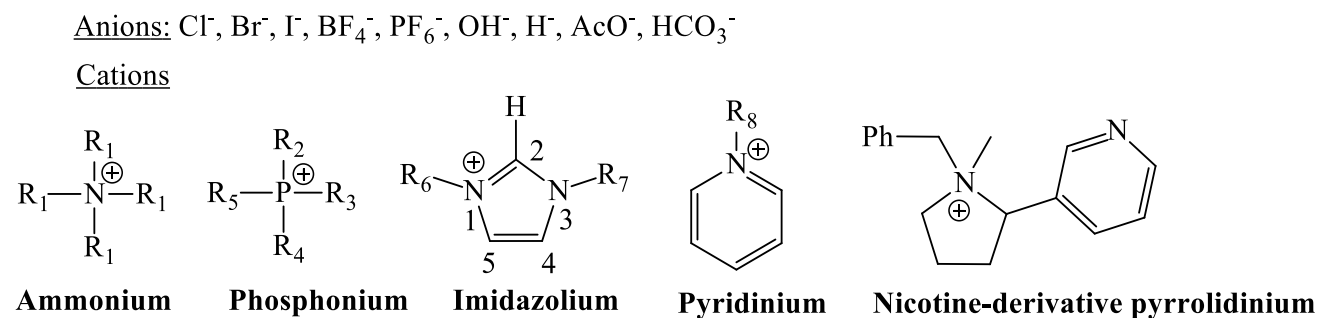
Historically, the first metal-free catalysts promoting the coupling of CO<sub>2</sub> with epoxides were one-component alkali metals salts, organic salts and ionic liquids composed of a nucleophile halide anion and a cation.<sup>29, 32, 34, 35</sup>

#### **II-1-a) Alkali metal salts**

Abundant, inexpensive and nontoxic alkali metal salts of sodium, lithium or potassium<sup>36-38</sup> were found to catalyse the CO<sub>2</sub>/epoxide coupling. For example, Union Carbide (now Dow), Shell and a Japanese research group patented the use of KI as catalyst for the synthesis at the industrial scale of ethylene carbonate from CO<sub>2</sub> and ethylene oxide (EO) under harsh experimental conditions, i.e. T = 190°C and P = 1.3 MPa.<sup>38</sup> Through a detailed study, Endo *et al.* established a structure-activity relationship of various sodium and lithium salts for the coupling of CO<sub>2</sub> with 2,3-epoxypropyl phenyl ether chosen as model oxirane at 100°C under atmospheric pressure using N-methylpyrrolidone as aprotic polar solvent.<sup>36</sup> In 2009, Sun *et al.* highlighted that without water, NaBr, KBr and KI salts exhibited poor catalytic activity for the coupling of CO<sub>2</sub> with propylene oxide (PO) even under harsh experimental conditions because of solubility issues of the catalyst in neat epoxide.<sup>37</sup> Now, it is generally admitted that activity of the alkali metal catalyst is in agreement with the order of the cation Lewis acidity and, for a same cation, the catalyst activity depends on both the nucleophilicity and the leaving ability of the halide counter anion that evolves in the order I<sup>-</sup> > Br<sup>-</sup> > Cl<sup>-</sup> > F<sup>-</sup> (for neat epoxides). It should be noted that the nucleophilicity of the anion depends on the solvent.

## II-1-b) Organic salts and ionic liquids

Organic salts and ionic liquids (ILs), i.e salts with melting point lower than 100°C in which ions are poorly coordinated <sup>39</sup>, are the most widely studied catalysts for the CO<sub>2</sub>/epoxide coupling.<sup>32, 33</sup> Organic salts and ILs can be differentiated according to their cation structure, i.e. ammonium, phosphonium, imidazolium and pyridinium (Scheme 3).



Scheme 3: Structures of the organic salts and ionic liquids catalysts

### Ammonium salts

The industrial synthesis of ethylene or propylene carbonate from CO<sub>2</sub> and EO or PO promoted by tetraethylammonium bromide (TEABr) is known since the 1950s.<sup>40, 41</sup> However, these reactions are efficient at very high temperature (150 - 175°C) favouring the catalyst degradation into tributylamine by Hofmann elimination.<sup>42</sup> Later, Calo *et al.* reported on the catalytic coupling under atmospheric pressure of CO<sub>2</sub> with a broad variety of epoxides using mixture of molten tetraalkylammonium salts, i.e tetrabutylammonium bromide (TBABr) and tetrabutylammonium iodide (TBAI) in a 1:1 w/w ratio, acting as both solvent and catalyst.<sup>43</sup> Most of the epoxides were converted in high yields into the corresponding cyclic carbonates after 1 to 24 h at 120°C. When TBAI was used in catalytic amount (10 mol%) instead of solvent at 60°C, the conversion of neat epoxides drastically plummeted even after extended reaction times. These results have to be relativized as the author makes comparison between two different catalytic systems operating at two different temperatures. However, through comparative study, Sun showed that TBAX salts (with X = halide anion) are more efficient under the same experimental conditions than potassium and sodium halides for converting epoxides into cyclic carbonates.<sup>37</sup>

Through detailed kinetic studies, Park *et al.* investigated the effect of the alkyl chain of various quaternary ammonium chloride salts on the coupling of glycidyl methacrylate with CO<sub>2</sub> in toluene at 80°C under ambient pressure. They demonstrated that the rate constant decreased in the order: tetraoctylammonium chloride (TOACl) > tetrahexylammonium chloride (THACl) > tetrabutyl ammonium chloride (TBACl) <sup>44</sup> and concluded that ammonium salts with bulky cations exhibit higher activity because of the longer distance between the NR<sub>4</sub><sup>+</sup>/Cl<sup>-</sup> ions pair. This makes the electrostatic interactions between the two ions weaker which increases the nucleophilicity of the halide anion.<sup>45, 46</sup> Additionally, they highlighted that the halide

catalytic activity evolves in the order  $I^- > Br^- > Cl^-$  but reverses when neat butyl glycidyl ether was converted into the corresponding cyclic carbonate.<sup>46</sup> The effect of the steric hindrance is dominant regarding the nucleophilicity of the anion.

Ema *et al.* investigated the use of various quaternary ammonium hydroxides as catalysts for neat 1,2-epoxyhexane/ $CO_2$  coupling at 120°C and 1 MPa for 24h.<sup>47</sup> Tetrabutylammonium hydroxide (TBAH) was identified as the most active halide-free catalyst whereas  $Me_4NOH$  displays no catalytic activity because of its low solubility in 1,2-epoxyhexane. However, it should be noted that TBAH was less efficient than TBABr.

Lecithin is a quaternary ammonium zwitterion containing a diglyceride and a phosphate that doesn't display catalytic activity for the fixation of  $CO_2$  onto epoxides. However, in the presence of KI, the resulting salt promoted the reaction of epoxides with  $CO_2$  under harsh conditions ( $T = 100^\circ C$ ,  $P = 2$  MPa).<sup>48</sup> Cyclic carbonates with yields higher than 94% and selectivities between 96 and 99% were produced in 4 to 12 h. The synergetic effect between lecithin and KI results from the formation of quaternary ammonium halide catalyst by complexation of the alkali halide salt by lecithin.

### *Phosphonium ILs*

Few articles reported the use of phosphonium halides ILs as catalysts for the  $CO_2$ /epoxide coupling.<sup>37, 47, 49-51</sup> Sun *et al.* reported that triphenylbutylphosphonium bromide was the most active phosphonium-based IL, with a catalytic activity similar to the one of TBABr, for the synthesis of propylene carbonate by coupling of neat PO and  $CO_2$  at 20 MPa and 125°C (conv. = 54%,  $t = 1$ h).<sup>37</sup> At the opposite, whatever the halide counter-ion, Takahashi *et al.* found that tetrabutylphosphonium salts were very poor catalysts for converting neat PO under supercritical conditions (conv. < 10%,  $t = 1$ h,  $T = 100^\circ C$ ,  $P = 10$  MPa).<sup>49</sup>

Halide-free phosphonium ILs with hydroxyl, acetate or carbonate anions were also used as organocatalysts for converting epoxides into cyclic carbonates. Contrary to tetrabutylammonium hydroxide, the phosphonium analogue ( $Bu_4P^+OH^-$ ) was a poor catalyst even under harsh conditions ( $T = 120^\circ C$ ,  $P = 1$  MPa, conv. = 22%,  $t = 24$ h).<sup>47</sup> Similar conclusions were reported by Galvan *et al.* who studied the coupling of neat styrene oxide (SO) with  $CO_2$  by using methyl-n-trioctylphosphonium carbonate or acetate ILs under atmospheric pressure and high temperature ( $100^\circ C < T < 140^\circ C$ ).<sup>50</sup> At a 1 to 5 mol% catalyst loading, the  $CO_2$ /epoxide coupling was slow and never reached SO conversions higher than 40% even by increasing the pressure up to 9 MPa. The poor catalytic activity was attributed to the catalyst deactivation resulting from the progressive transformation of phosphonium ILs into phosphine oxides in the presence of acetate or carbonate anions and/or the epoxides.<sup>50</sup>

### *Imidazolium ILs*

The first use of imidazolium ILs as catalysts for the epoxide/ $\text{CO}_2$  coupling was pioneered by Peng *et al.*<sup>52</sup> 1-Butyl-3-methylimidazolium ( $\text{C}_4\text{-MIm}$ ) salts with hexafluorophosphate ( $\text{PF}_6^-$ ), chlorine ( $\text{Cl}^-$ ) or tetrafluoroborate ( $\text{BF}_4^-$ ) were shown to catalyse the addition of  $\text{CO}_2$  onto PO at  $110^\circ\text{C}$  and 2 MPa. Results highlighted that the best catalytic performance was achieved with the ionic liquid consisting of the  $\text{C}_4\text{-MIm}^+$  cation and  $\text{BF}_4^-$  anion. The performance of methylimidazolium ILs with  $\text{BF}_4^-$  anion, could be significantly improved i) by increasing their alkyl chain length from C2 to C8 ( $\text{C}_8\text{-MIm} > \text{C}_4\text{-MIm} > \text{C}_2\text{-MIm}$ )<sup>53, 54</sup> or ii) by using supercritical conditions increasing the mass transfer between the two phases of the  $\text{scCO}_2/\text{IL}$  biphasic system while reducing the viscosity of the IL. Indeed, Kawanami *et al.* reported that PO was completely converted in 5 min at  $100^\circ\text{C}$  and 14 MPa which represents a 33-fold increase of the reaction rate determined under the same conditions below 5 MPa.

The origin of the higher catalytic activity  $\text{BF}_4^-$  anion was elucidated by FTIR studies<sup>55</sup> evidencing that  $\text{BF}_4^-$  interacts with  $\text{CO}_2$  dissolved in the IL and the less hindered carbon atom of the epoxide. The new anion species created by Lewis acid-base interactions between  $\text{BF}_4^-$  and  $\text{scCO}_2$  is more basic than  $\text{BF}_4^-$  of pure  $\text{C}_4\text{-MImBF}_4$  and than the one formed by the interaction between  $\text{CO}_2$  and  $\text{PF}_6^-$ .<sup>55, 56</sup> In addition, a shift of the C-H bands of the imidazolium-ring highlighted that the cation also interacts with  $\text{CO}_2$ . Consequently, the Lewis acid-base interaction between  $\text{CO}_2$  and  $\text{BF}_4^-$  can be also tuned by the choice of the cation.

Neat epoxides were also converted into cyclic carbonates at  $\text{CO}_2$  pressures lower than 2 MPa using catalytic amounts of imidazolium ILs with various structures and counter-ions.<sup>57-61</sup> Under those conditions, the catalytic activity of  $\text{C}_4\text{-MIm}$ -based ILs decreases with the nature of the counter ion in the order  $\text{Br}^- \sim \text{I}^- > \text{HCO}_3^- > \text{Cl}^- > \text{AcO}^-$ .<sup>57</sup> The lower catalytic activity of chloride compared to iodide and bromide probably results from the best compromise between nucleophilicity and leaving ability.<sup>37, 57, 58</sup> Contrary to the results reported under supercritical conditions, the catalytic activity of ILs decreased with the increase of alkyl length chain of the  $\text{C}_n\text{-MIm}^+$  cation.<sup>58</sup> This observation was related to the change of imidazolium IL acidity that decreased in the order:  $\text{C}_1\text{-MImBr} > \text{C}_2\text{-MImBr} > \text{C}_4\text{-MImBr}$ , which is beneficial for forming hydrogen bond between the proton in position 2 of the  $\text{C}_x\text{-MIm}$  ring with the O-donor group of epoxide. The acidity of the proton on the 2-position of the imidazolium ring and the solubility of  $\text{CO}_2$  in ILs could be enhanced by replacing the methyl substituent of  $\text{C}_x\text{-MIm}^+$  by a fluorinated pentafluorobenzyl group.<sup>59</sup> This observation was supported by Anthofer's work who demonstrated that 1-(2,3,4,5,6-pentafluoro)-benzyl-3-n-octylimidazolium bromide is more efficient than the non-fluorinated analogue for the PO/ $\text{CO}_2$  coupling at  $70^\circ\text{C}$ , 0.4 MPa for 22h (conv. = 91% and 73%, respectively).

Finally, the substituent effect on the catalytic activity of imidazolium bromide ILs has been briefly evaluated by replacing the methyl group in position 1 and/or the alkyl group in position 3 by different linear or tertiary alkyl groups or by replacing the

proton in position 2 on the imidazolium ring by a methyl group.<sup>57, 59</sup> However, data were insufficient to draw rational conclusions even if no drastic change of the catalytic performances was noticed.

### *Pyridinium ILs*

In his pioneer study, Peng compared the catalytic activity of imidazolium salts (C4-MImBF<sub>4</sub>, C4-MImCl and C4-MImPF<sub>6</sub>) with the one of pyridinium ILs. Whatever the counter ion (BF<sub>4</sub><sup>-</sup>, Cl<sup>-</sup> or PF<sub>6</sub><sup>-</sup>), ILs derived from n-ButylPyridinium cation (C4-Py<sup>+</sup>) were less efficient than the imidazolium counterpart (C4-MIm<sup>+</sup>).<sup>52</sup> Contrary to imidazolium ILs, no shift of the pyridinium-ring bands was observed by FTIR under scCO<sub>2</sub> conditions<sup>55</sup> highlighting the absence of specific interaction between the pyridinium cation and CO<sub>2</sub>. However, the catalytic activity of those ILs can be enhanced using the microwave-assisted cycloaddition of allyl glycidyl ether and CO<sub>2</sub> under ambient pressure.<sup>62</sup> Molecules with a high dipole moment can easily be activated by microwave radiations reducing significantly the reaction time. At a microwave power of 200W, the reactor reached a temperature of 180°C during the reaction so that allyl glycidyl ether was nearly completely converted into the corresponding cyclic carbonate in less than 30 seconds (conv. = 95%) when 1-ButylPyridinium bromide (C4-PyBr) was used as catalyst. The authors also evaluated the effects of both the alkyl chain length and the nature of the counter ions of pyridinium ILs on the reaction rate. The conversion was found dependent on the alkyl chain length and increased in the order EthylPyridinium (C2-PyCl) < PropylPyridinium (C3-PyCl) < ButylPyridinium (C4-PyCl). Nevertheless, the conversion dropped with HexylPyridinium (C6-PyCl) because of the steric hindrance of the cation whereas the catalytic activity of the anion decreased in the order: I<sup>-</sup> ≈ Br<sup>-</sup> > Cl<sup>-</sup> > PF<sub>6</sub><sup>-</sup>.

### *Pyrrolidinium ILs*

Pyrrolidinium-based ILs were scarcely studied. Only nicotine-derived pyrrolidinium ILs were developed by Hajipour *et al.* as catalysts for the CO<sub>2</sub>/epoxide coupling.<sup>63</sup> The conversion of styrene oxide was total after 5h at 100°C and 4 MPa using 1-benzyl-1-methyl-2-pyridin-3-yl-pyrrolidinium bromide as catalyst. Notably, the dibromide pyridinium counterpart was inactive highlighting the positive role of the basic pyridine active site.

### *Others nitrogen containing ILs derived from (super)bases*

Lewis bases ionic liquids derived from 1,8-diazabicyclo[5.4.0]undec-7-ene (DBU), 1,4-diazabicyclo[2.2.2]octane (DABCO), hexamethylene tetramine (HMTA) and TBD (Scheme 4 a-c and e) were found to catalyse the neat PO/CO<sub>2</sub> coupling at 140°C and 1 MPa.<sup>64</sup> Both the structure of the cation and the anion were crucial to enhance the catalyst activity and the selectivity toward the formation of cyclic carbonates. Cations with the highest ability to delocalize the positive charge and stabilize the epoxy ring-opened intermediates displayed the better catalytic activity that decreased in the

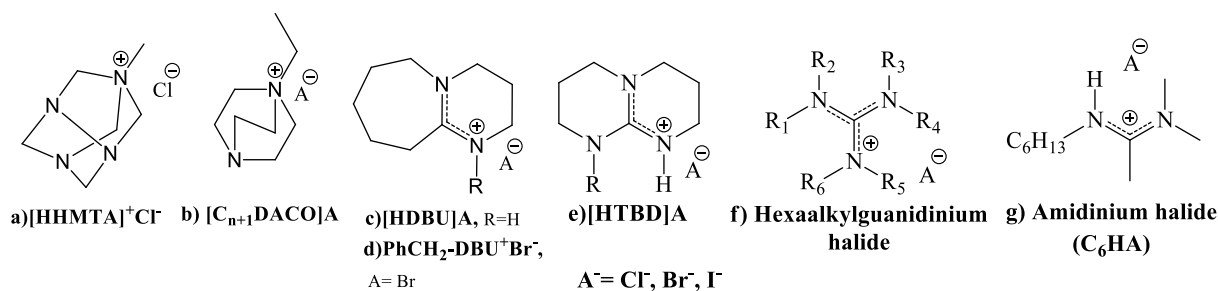


order  $\text{HDBU}^+ > \text{HTBD}^+ > \text{C}_4\text{DABCO}^+ > \text{HHMTA}^+$ . Indeed, if reaction yields of 97% were obtained with HDBUCl, PO conversion progressively decreased to only 33% with HHMTAcl. At the exception of HHMTAcl, the selectivity toward PC formation remained good (93 to 99%) for each catalyst. Besides, as reported for alkali metals salts and others ILs, halides anions showed the highest performances due to their good nucleophilicity and leaving ability. In addition, acetate anion and the  $\text{OH}^-$  anion that can easily react with  $\text{CO}_2$  also fastened the  $\text{CO}_2$ /epoxide coupling. However, the acetate anion was thermally unstable and induced a slight decrease of the catalyst selectivity ( $\sim 90\%$ ). Finally,  $\text{Tf}_2\text{N}^-$ ,  $\text{PF}_6^-$ ,  $\text{BF}_4^-$  anions were poorly effective (conv.  $< 10\%$ ) and selective towards the cyclic carbonate formation (lower than 50%).

The DBU/benzyl bromide ( $\text{PhCH}_2\text{Br}$ ) system was reported as an efficient catalytic system for the selective synthesis of chloromethylethylene carbonate from epichlorhydrin and  $\text{CO}_2$  under atmospheric pressure and mild temperature ( $T = 65^\circ\text{C}$ ).<sup>65</sup> The catalytic activity of the present DBU/ $\text{PhCH}_2\text{Br}$  system arises from the initial *in-situ* formation of an  $\text{PhCH}_2\text{-DBU}^+\text{Br}^-$  amidinium salt (Scheme 4 d) that catalyzes the ring-opening reaction through nucleophilic attack of its bromide ion onto the less sterically hindered  $\beta$ -carbon atom of epichlorhydrin. The  $\text{pK}_a$  and the steric hindrance of the organic base are key factors influencing the catalyst efficiency. Quaternary benzyl bromide salts of DBN, DABCO, Pyridine, (methyl)imidazole or DMAP were less efficient than salts derived from DBU. Wang also demonstrates that the structure of the halide compound affects the performances of the catalyst that decrease in the order  $\text{PhCH}_2\text{Br} > p\text{-tBuPhCH}_2\text{Br} > \alpha\text{-bromodiphenylmethane} > 4\text{-nitrobenzyl bromide} > \text{BuBr}$ . Interestingly,  $\text{PhCH}_2\text{-DBU}^+\text{Br}^-$  was a more efficient catalyst than TBABr and allowed for the conversion of terminal, disubstituted or enantiomerically pure epoxides with good yields, selectivity above 99% and enantiomeric excess higher between 84 and 99%.

Tassaing *et al.* studied the catalytic efficiency of several ILs for the SO or PO coupling with  $\text{CO}_2$  under neat conditions at  $80^\circ\text{C}$  and 8 MPa for 20h. Through this comparative study, they demonstrated that the guanidinium halide [HTBDBr] (Scheme 4 e) gave very good catalytic performances comparable to the ones of the best imidazolium salts (C1-MimI and C2-MimBr).<sup>66</sup> Besides, hexaalkylguanidinium salts (Scheme 4 f) were efficient catalysts for the epoxide/ $\text{CO}_2$  coupling even under atmospheric pressure.<sup>67-70</sup> Duan *et al.* showed that larger size guanidinium cations exhibit a better catalytic activity.<sup>67</sup> The conversion of SO catalysed by hexabutylguanidinium chloride reached 82% at  $60^\circ\text{C}$  for 20h under atmospheric pressure that is higher than using quaternary ammonium salt (conv. = 42% and 40% with TBABr and TBAI respectively).

Finally, the amidinium halides (C6-HA, Scheme 4 g) were efficient catalysts for the conversion of SO at low temperature ( $T = 50^\circ\text{C}$ ) and pressures ranging from 0.1 to 6 MPa in acetonitrile or room temperature IL solvent even if the presence of water traces affects the catalytic performances probably because of the formation of an amidinium bicarbonate salts.<sup>71</sup>



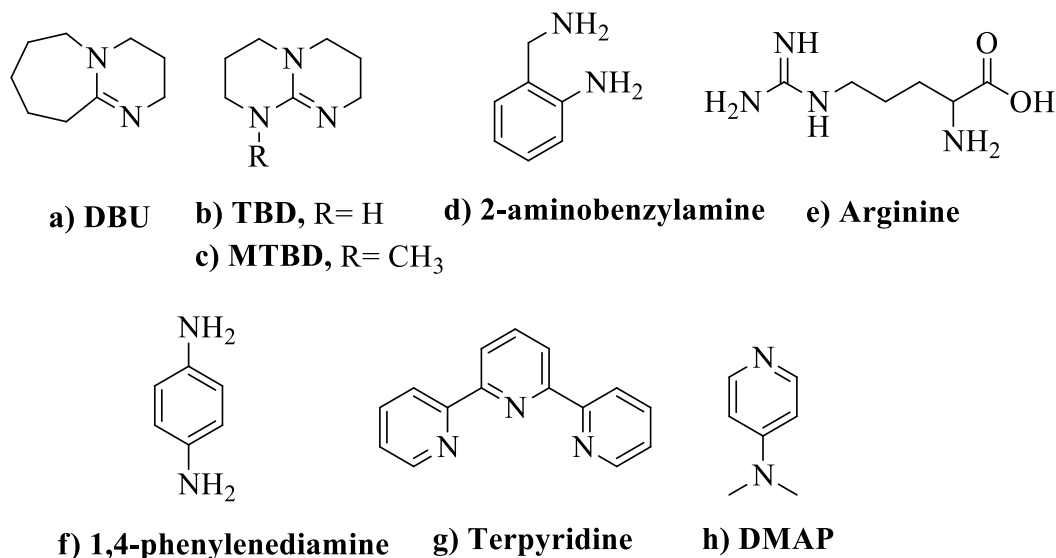
Scheme 4: Structure of the nitrogen containing ILs catalysts derived from (super)bases

### II-1-c) Amines and organic bases

Primary and secondary amines are known to reversibly react with CO<sub>2</sub> to form fairly stable carbamates <sup>2, 3</sup> or generate bicarbonate adducts in the presence of additional water. In a similar way, facile chemisorption of CO<sub>2</sub> onto organic (super)bases such as 1,8-diazabicyclo[5.4.0]undec-7-ene (DBU), 1,5,7-diazabicyclo[4.4.0]dec-5-ene (TBD) (Scheme 5 a and b)... leads to formation of a (super)base-CO<sub>2</sub> zwitterionic adducts. For example, the N-methyl derivative of TBD (MTBD, Scheme 5 c) was reported to form a white precipitate corresponding to the carbamate zwitterionic compound even under atmospheric conditions.<sup>72</sup> Amines derivatives and heterocyclic amines (super)bases such as guanidine, amidine... represent potential metal-free and halide-free organocatalysts able to activate CO<sub>2</sub> and facilitate its coupling with epoxides. Series of primary amines with pK<sub>a</sub> values between 4.5 and 13.6 were tested as sole catalyst for the coupling of PO with CO<sub>2</sub>.<sup>73</sup> Under harsh conditions (T = 150 °C, P = 5 MPa, t = 24h) in dichloromethane, the PO conversion progressively increases from 49% for non-conjugated methanolamine to 70% for 2-aminobenzylamine (Scheme 5 d). If no correlation between the basicity and the catalyst activity could be established, unsaturated amines with a C=N-C structure were found more efficient than primary non-conjugated amines as evidenced by higher PO conversion of 80 and 90% respectively with arginine and 1,4-phenylenediamine (respectively Scheme 5 e and f). Under those conditions, PO was fully converted in propylene carbonate by replacing unsaturated primary amines by TBD. The higher activity of superbases was further confirmed by using DBU <sup>74,75</sup>, TBD <sup>72-74</sup> and MTBD <sup>72</sup> as catalysts for the coupling of various internal or terminal epoxides with CO<sub>2</sub>. Good to excellent yields (60 – 98%) were reported although reaction conditions were quite harsh (120 °C < T < 150 °C, 2 MPa < P < 5 MPa) and chemo-selectivities varied from 90 to 98% (formation of 1,2-propanediol as by-product). In a comparative study of the catalytic activity of various nitrogen containing compounds, Liu reported that 2,2',2''-terpyridine (Scheme 5 g) was more efficient than DBU and TBD for the conversion of epichlorohydrin and other terminal epoxides into the corresponding cyclic carbonates at 130 °C and 3 MPa (conv. ~ 90% after 10h even at catalyst loading of 1 mol%).<sup>76</sup>

Contradictory examples of cyclic carbonates synthesized by 4-(N,N-dimethylamino)pyridine (DMAP) promoted coupling of CO<sub>2</sub> with epoxides were briefly described in the literature (Scheme 5 h). Whereas Shen *et al.*<sup>74</sup> found that this organic base was an inactive catalyst for the cycloaddition of CO<sub>2</sub> onto PO at 120 °C

and 3.6 MPa in  $\text{CH}_2\text{Cl}_2$ , Shiels <sup>77</sup> demonstrated the selective formation of PC with a yield of 92% under drastically anhydrous and identical conditions. The catalytic activity of DMAP was further confirmed by Sankar's <sup>78</sup> and Park's <sup>79</sup> observations who showed that epichloridrin or neat PO were selectively converted into their respecting cyclic carbonates.



Scheme 5: Structure of the amines and organic bases catalysts

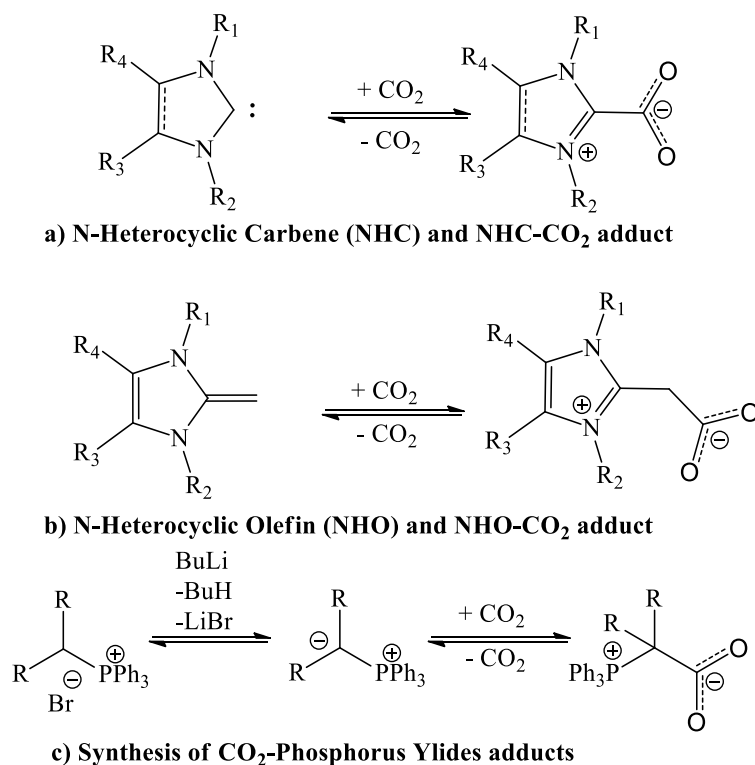
### II-1-d) Carbenes, N-heterocyclic olefins and phosphorus-ylides catalysts

N-heterocyclic carbenes (NHCs) are generally obtained by deprotonation of the corresponding imidazole(in)um salt with strong bases (Scheme 6 a). Since they are highly reactive basic nucleophiles, NHCs are air- and moisture-sensitives and, as amines, amidines or guanidines, react with  $\text{CO}_2$  to form stable NHC- $\text{CO}_2$  adducts making them potential efficient halogen-free organocatalysts for the conversion of epoxides.<sup>80-83</sup> Zhou *et al.* highlighted by FTIR that NHC- $\text{CO}_2$  adducts decomposed easily within 1h at 100°C. Decomposition was inhibited by an excess of  $\text{CO}_2$  but fastened in the presence of PO while simultaneously and selectively affording propylene carbonate with retention of stereochemistry at 120°C, 2 MPa after 24h in  $\text{CH}_2\text{Cl}_2$ .<sup>84</sup> They also established a NHCs structure-catalytic activity correlation by highlighting that N,N-disubstituted saturated imidazolium-2-carboxylate catalysts with bulky 2,6-diisopropylphenyl groups were more efficient than catalysts with 2,6-dimethylphenyl- or methyl- substituents. Simultaneously, Ikariya *et al.* briefly showed that a NHC- $\text{CO}_2$  adduct with less bulky tBu- substituents, i.e. N,N'-*t*-butyl-imidazolium-2-carboxylate, was also an efficient catalyst for the synthesis of cyclic carbonate with yields up to 89% at 4.5 MPa and 100°C from neat epoxides and  $\text{CO}_2$ .<sup>82</sup>

Thanks to their specific structure enabling the stabilization of a positive charge by aromatization of the ring making the terminal carbon of the olefin more electronegative, N-heterocyclic olefins (NHOs) are potent strong nucleophiles

forming with CO<sub>2</sub> NHO-CO<sub>2</sub> adducts acting as efficient organocatalysts for the synthesis of cyclic carbonate by CO<sub>2</sub>/epoxide coupling (Scheme 6 b).<sup>85, 86</sup> Even if NHO-CO<sub>2</sub> adducts exhibit poorer thermal stability than NHC-CO<sub>2</sub> adducts, the coupling of neat PO with CO<sub>2</sub> is only efficient at temperatures and pressure of 100 - 120°C and 2 MPa respectively but reaction times were reduced from 24h to 12h. As observed with NHCs, NHOs with 2,6-diisopropylphenyl bulky N-substituents showed superior catalytic activity than NHOs with methyl, isopropyl or tert-butyl groups. Finally, Wang *et al.* also prepared NHO-COS and NHO-CS<sub>2</sub> adducts being less efficient catalysts for converting neat PO into propylene carbonate as a result of their higher thermal stability than NHO-CO<sub>2</sub> adducts.<sup>86</sup>

By analogy with NHC-CO<sub>2</sub> and NHO-CO<sub>2</sub>, moisture and thermally stable CO<sub>2</sub>-phosphorus ylides adducts were synthesized from CO<sub>2</sub> and triphenylphosphonium ylide derivatives (Scheme 6 c). These catalysts were shown to be very efficient organocatalysts for the fast CO<sub>2</sub>/neat PO coupling even under ambient conditions (P = 0.1 MPa and T = 25°C) as evidenced by a PO conversion up to 90% within 6h and a selective formation of propylene carbonate.<sup>87</sup> The activity of the catalyst was dependent on the nature of the R substituent on the ylidic carbon; CO<sub>2</sub>-phosphorus ylides adducts with alkyl electron donating substituents being more performant than analogues with electron withdrawing fluorine atoms. The versatility of these catalysts was highlighted by the synthesis of a broad scope of cyclic carbonates from terminal (enantiopure) epoxides with alkyl, phenyl, alkenyl, halide, amino, ether and ester functionalities with moderate to excellent yields ranging from 46 to 99% with no observable by-product formation (and retention of the configuration). However, it was regrettable that the alkyltriphenylphosphonium bromide were not tested as catalysts under similar conditions to evaluate the relevance of the catalytic efficiency of the CO<sub>2</sub>-phosphorus ylide adducts. Indeed, the CO<sub>2</sub> fixation is reversible and phosphonium bromide derivatives are known for promoting the CO<sub>2</sub>/epoxide coupling.

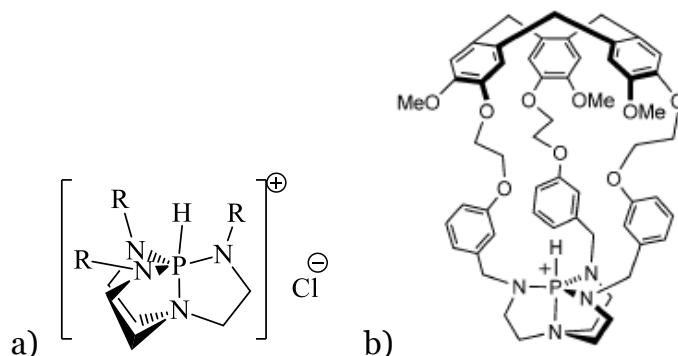


Scheme 6: Formation of the N-Heterocyclic Carbenes-CO<sub>2</sub> adducts, the N-Heterocyclic Olefins-CO<sub>2</sub> adducts and the CO<sub>2</sub>-phosphorus ylides adducts

### II-1-e) Azaphosphatranes

The azaphosphatranes (Scheme 7 a) are the acidic counterparts of the proazaphosphatrane superbases (Verkade's superbases). In these protonated aminophosphines, the phosphorous atom is stabilized by tertiary nitrogens and the catalytic site behaves like a lipophilic pocket. As the charge is delocalized around the H-P-N core, the cation does not strongly associate with halide anions which facilitates the ring-opening of the epoxide by nucleophilic attack. Azaphosphatranes with different steric properties and Cl<sup>-</sup> anion were tested as organocatalysts for the conversion of SO into styrene carbonate at 100°C and 0.1 MPa. The catalyst activity and stability were found dependent on the structure of the N-substituent of the azaphosphatrane. Methylsubstituted azaphosphatrane was rapidly deactivated in less than 4h due to the insertion of CO<sub>2</sub> into the P-N bond affording SO conversion of 10%. Dufaud *et al.* showed that steric protection of the P-H site by bulky *neo*-pentyl or aromatic substituents improves the stability and activity of the catalyst for the CO<sub>2</sub>/SO coupling even after four days under higher substrate-to-catalyst ratio (1000:1).<sup>88</sup> However, the activity of azaphosphatrane depends on the ability of substituents to create H-bonds with the acidic P-H<sup>+</sup> site.<sup>89</sup> Therefore, the highest TONs were obtained with benzyl substituents bearing Lewis base groups such as fluorine and methoxy groups. Indeed, they are able to i) strongly interact with the P-H<sup>+</sup> site, ii) stabilize the catalyst structure and iii) enhance the catalytic activity by preventing its degradation. Finally, cage azaphosphatrane-hemicryptophane complex structures (Scheme 7 b) were found twice active than the model non-cage

counterpart.<sup>90</sup> This cage structure induced a constraint around the P-H<sup>+</sup> site that prevents the catalyst degradation. However, the recognition and accessibility to the reactive site and the easy release of the carbonate product are crucial highlighting how the volume of the inner cavity of cage azaphosphatrane is important in optimizing the performances of such catalysts.



Scheme 7: General structure of azaphosphatrane a) and azaphosphatrane-hemicryptohane b) (reprinted from ref 90)

## II-1-f) Others catalysts

Kozak *et al.* developed a continuous flow system for the rapid (45 min) synthesis of cyclic carbonates from CO<sub>2</sub>/epoxides coupling using N-bromosuccinimide (NBS) or NBS/benzoyl peroxide (BPO) as catalysts at 120°C and 0.7 MPa.<sup>91</sup> This catalytic system composed of electrophiles goes against the previous observations claiming that a good nucleophile is required for the CO<sub>2</sub>/epoxide coupling. However, solvents such as DMF and DMA were critical to achieve good yields. DMF and DMA can i) convert NBS into Br<sub>2</sub><sup>92</sup>, ii) transfer electrophilic bromine from NBS<sup>93</sup> or iii) activate CO<sub>2</sub><sup>94</sup>. A plausible mechanism was proposed to explain the catalytic activity of this system and suggests the simultaneous activation of epoxide with electrophilic Br<sub>2</sub> instead of bromine anion and the activation of CO<sub>2</sub> by DMF as nucleophile. If no DFT calculations were reported to confirm such hypothesis, a test experiment for which propylene carbonate was synthesized from PO with only pure bromine as catalyst confirmed that Br<sub>2</sub> was the active species formed *in-situ* from NBS. When used as solvent, DMF activated CO<sub>2</sub> as it promoted the catalyst-free conversion of styrene oxide but with no styrene carbonate formation.<sup>95</sup> Hirose *et al.* confirmed that DMF could act as solvent and activator for the CO<sub>2</sub>/epoxide coupling catalysed by benzyl bromide.<sup>96</sup> Styrene carbonate was obtained in good yield (73%) under atmospheric pressure at 120°C after 24h. The yield of cyclic carbonates decreased by replacing DMF with other common solvents (toluene and DMSO) or commercially available amides (DMAc, N-formylmorpholine, N-methylpyrrolidone, and N-formylpiperidine). NMR characterization of a 1:1 benzyl bromide/DMF mixture highlighted that benzylbromide was activated by DMF to generate an iminium salt. It was then supposed that this species induces electrophilic activation of epoxides while DMF induces nucleophilic activation of CO<sub>2</sub> which accelerates the CO<sub>2</sub>/epoxide coupling.

## II -1-g) Mechanistic study

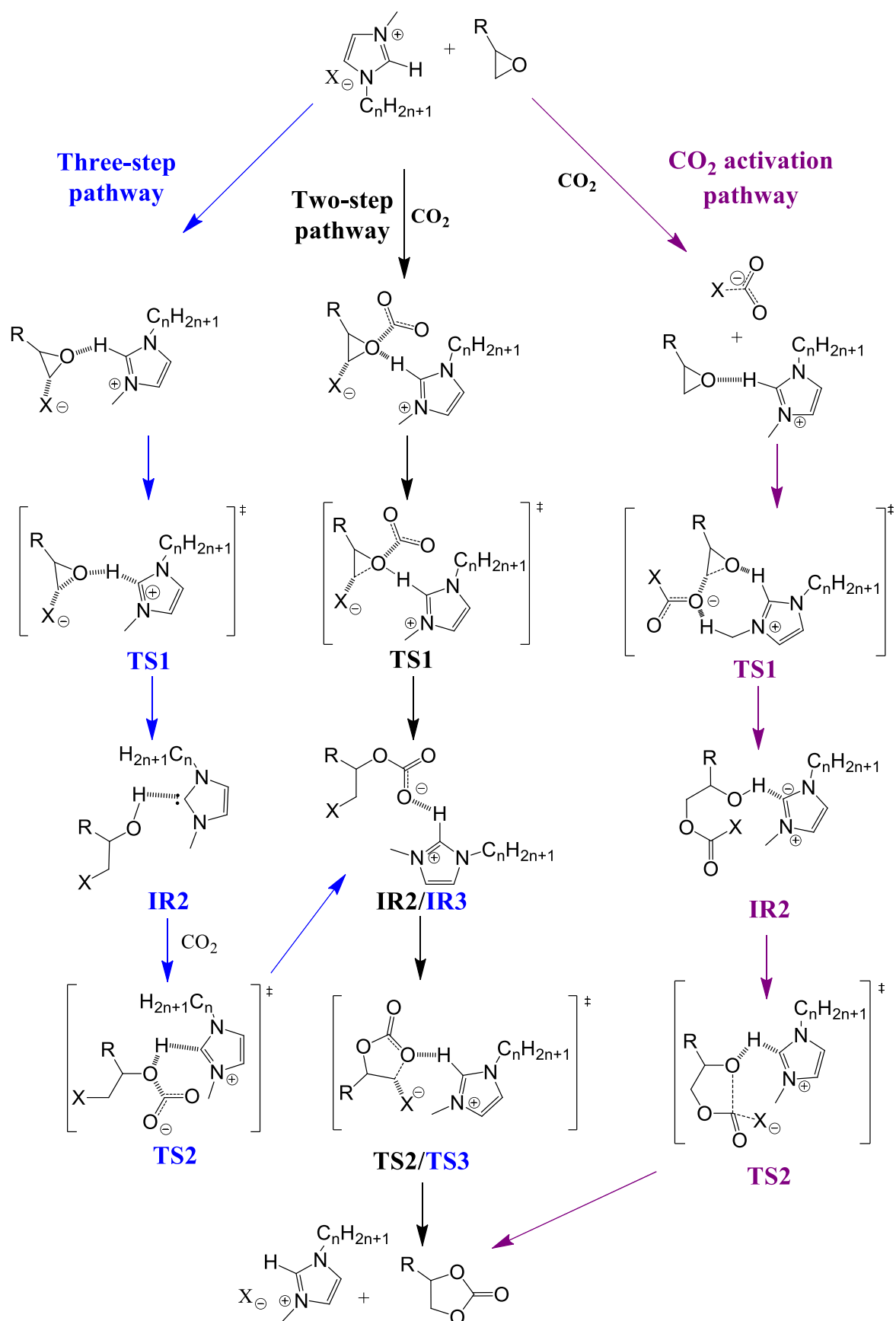
Computational organic chemistry has been increasingly recognized as a bridge between theory and experiment in establishing the mechanisms of chemical reactions. Few years after the first experimental studies, the catalytic activation mechanism was investigated by DFT calculations in the gas phase approximation. Although the non-catalyzed epoxide/ $\text{CO}_2$  coupling is a single-step concerted mechanism<sup>97</sup>, the presence of a catalyst increases the number of elementary steps making more complex the reaction mechanisms. In this section, DFT investigations will only be detailed for the most relevant catalytic systems.

### *Activation by a halide*

Computational study elucidating the mechanism of the  $\text{CO}_2$ /PO coupling was first reported for ethylmethylimidazolium chloride ILs, i.e. C2-MImCl, (Scheme 8).<sup>98</sup> Three different pathways were investigated.

The first path involves three elementary steps consisting of the epoxide ring-opening followed by the  $\text{CO}_2$  insertion and the carbonate ring-closure. Initially, PO and C2-MImCl interact *via* hydrogen bonds before ring-opening of the epoxide by nucleophilic attack of the chlorine anion onto the  $\beta$  carbon (TS1). Simultaneously, the proton of the  $\text{CH}_2$  in position 2 of the N atoms of the imidazolium ring migrates toward the O atom of the epoxide and leads to the formation of a chlorohydrin and a carbene (IR1). Then, the O atom of the chlorohydrin links to  $\text{CO}_2$  through a nucleophilic attack and the proton migrates back to the imidazolium ring (TS2). The resulting chloroalkylcarbonate ion intermediate (IR2) induces the breaking of the C-Cl bond *via* a  $\text{S}_{\text{N}}2$ -type reaction after a torsional rotation (TS3) enabling the ring closure of the carbonate. The epoxide ring-opening of PO was identified as the rate determining step. The activation energy is lower for the nucleophilic attack of  $\text{Cl}^-$  onto the  $\beta$  carbon ( $\Delta G = 28.5 \text{ kcal.mol}^{-1}$ ) than onto the substituted carbon ( $\Delta G = 29.9 \text{ kcal.mol}^{-1}$ ) because of reduced steric hindrance.

The second pathway proposes a two-step mechanism including the formation of an initial PO/ $\text{CO}_2$ /C2-MImCl trimolecular complex. The first step, that is rate determining, corresponds to the simultaneous epoxide ring-opening by nucleophilic attack of the chlorine anion on the  $\beta$  carbon and the  $\text{CO}_2$  insertion (TS1) to form the chloroalkylcarbonate ion (IR1) before ring closure (TS2). The activation energy of the two-step pathway was found similar to the one of the three-step pathway ( $\Delta G = 27.9 \text{ kcal.mol}^{-1}$ ). Similarly, Marmitt and Gonçalves found that a competition between the three-step and the two-step activation takes place for the SO/ $\text{CO}_2$  coupling catalyzed by C4-MImBr.<sup>99</sup>



Scheme 8: Possible mechanistic routes for the  $\text{CO}_2$ /epoxide coupling catalyzed by imidazolium liquid ionic  $[\text{C}_n\text{-MImX}]$ .<sup>98</sup>



Finally, the third two-step pathway involving the activation of CO<sub>2</sub> by the halide <sup>25, 98, 100</sup> was proposed but can be excluded as it is energetically less favourable than the other pathway by about 10 kcal.mol<sup>-1</sup>.

In order to discriminate between the two remaining pathways which one is the most probable, Tassaing *et al.* investigated the CO<sub>2</sub>/PO coupling using TBABr or HTBDBr IL as catalyst by combining kinetic studies and DFT calculations.<sup>25</sup> The Gibbs energy decreases in the order  $\Delta G(\text{HTBDBr}) > \Delta G(\text{TBABr})$  for the two-step pathway which was not consistent with kinetic studies highlighting that HTBDBr was a more efficient catalyst than TBABr. By considering a three-step pathway, the Gibbs energy evolved in the order  $\Delta G(\text{TBABr}) > \Delta G(\text{HTBDBr})$  in good agreement with experimental observations. Then, the three-step activation mechanism including epoxide ring-opening, CO<sub>2</sub> insertion and carbonate ring-closure <sup>66</sup> is now recognized and was generalized for the CO<sub>2</sub>/epoxide coupling catalysed by quaternary ammonium salts<sup>27, 101</sup>, pyridinium and imidazolium ILs <sup>57, 102-104</sup>, LiBr <sup>100</sup>, KI <sup>105</sup> and azaphosphatranes <sup>106</sup> using different calculation levels.

In such catalytic systems, the role of the cation is to stabilize the intermediates and transition states. Depending on their structures, stabilization occurs either by Van der Waals or H-bonds interactions which changes the structure of some intermediates. In one hand, only Van der Waals interactions exist between quaternary ammonium, phosphonium or alkali cations and the O atom of the former epoxide. However, as the Van der Waals interactions are weak, the bromoalkoxide-cation ion pair resulting from the epoxide ring-opening (IR1) is not stable. The weak energy gap between TS1 and IR1 makes the system vulnerable to undergo the reverse reaction. This intermediate instantaneously reacts with CO<sub>2</sub> without formation of a transition state to form a more stable bromoalkylcarbonate. As alternative, Kleij *et al.* reported that the ring opening of epoxide and the CO<sub>2</sub> insertion take place simultaneously.<sup>26</sup> However, in their calculations, the contribution of the quaternary ammonium cation was neglected. On the other hand, cations with acidic protons such as the N-H proton of HTBDBr, the N=CH-N proton of the imidazolium ring, or the P-H proton of azaphosphatranes (Figure 1) allow a strong interaction by H-bond with the O atom of the former PO. The charge delocalisation stabilizes the transition states and intermediates especially for the epoxide ring-opening step. At the difference of ammonium, phosphonium or alkali cations, a bromohydrin is formed by the proton migration toward the O atom of the opened epoxide, intermediate that was found more stable than the [bromoalkoxide-quaternary ammonium] ion-pair as the Gibbs energy is decreased by 17.3 kcal.mol<sup>-1</sup>.<sup>25</sup>

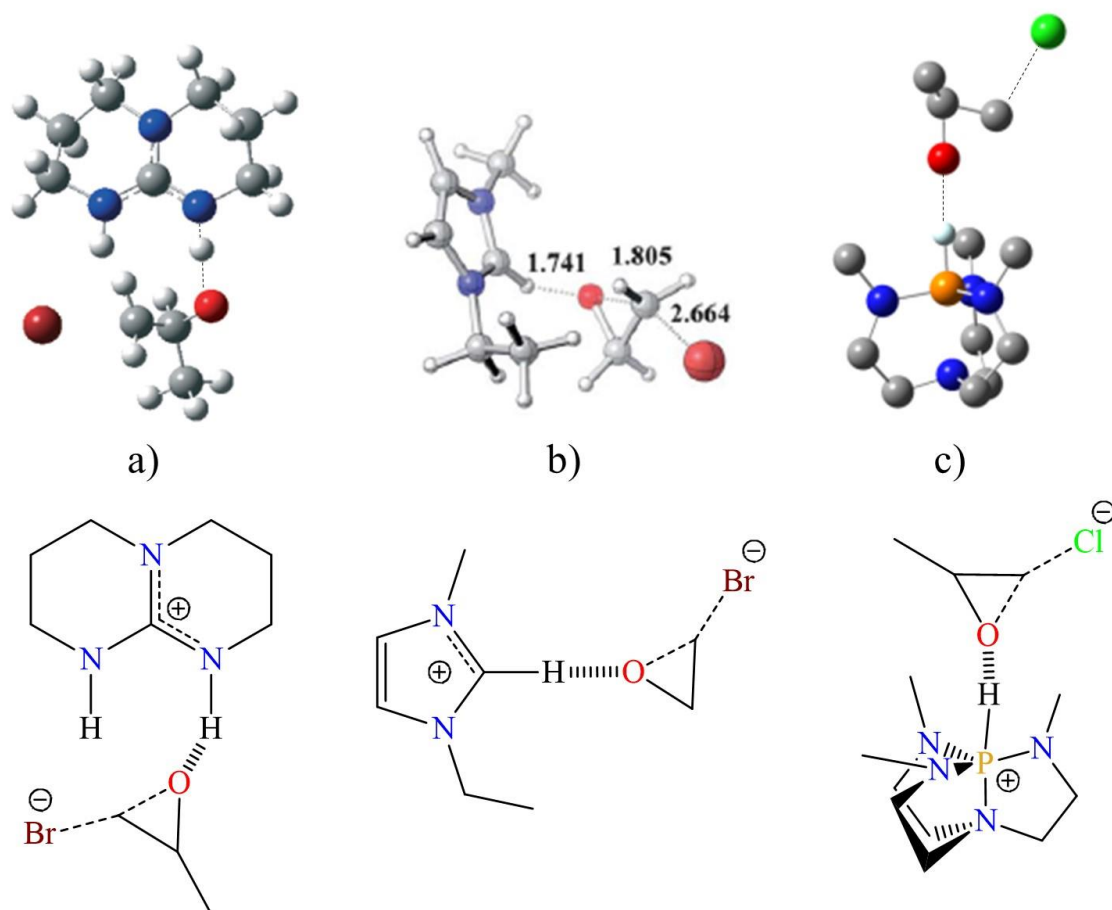


Figure 1: Optimized geometries and Lewis structures of the first transition state for the coupling of  $\text{CO}_2$  with respectively a) PO catalyzed by HTBDBr (reprinted from ref <sup>25</sup>), b) EO catalyzed by C2-MImBr (reprinted from ref <sup>103</sup>) and EO catalyzed by azaphosphatrane (reprinted from ref <sup>106</sup>).

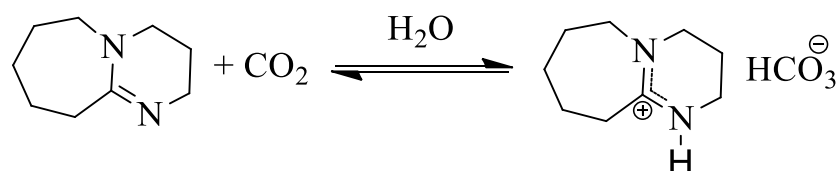
Besides, as briefly mentioned in the catalyst description part, enlarging the cation by increasing the length of the alkyl chain is beneficial for the catalyst activity. This positive effect is related to the decrease of the Gibbs energy value of 1.5 kcal.mol<sup>-1</sup> for TBABr compared to Et<sub>4</sub>NBr <sup>27</sup> and of 2.4 kcal.mol<sup>-1</sup> for 1-butylpyridinium chloride (BPyCl) compared to 1-ethylpyridinium chloride (EtPyCl) <sup>102</sup>. Indeed, the halide charge determined by NBO analysis increases with the alkyl chain length from -0.527 e for EtPyCl to -0.815 e for BPyCl rendering the anion more nucleophilic.<sup>102</sup> However, above a critical chain length, the catalytic activity drops because of the steric hindrance that negatively affects the stabilization of the transitions states and intermediates by Van der Waals or hydrogen bond interactions. At the exception of Wu's contradictory DFT study who claims that the carbonate ring closure is the rate determining step for the LiBr promoted coupling of  $\text{CO}_2$  with 2,3-epoxypropylphenylether <sup>100</sup>, in most simulations, the epoxide ring-opening is rate determining in gas phase. The energy barrier for the formation of the first reactive intermediate is reduced by using a strong nucleophile.<sup>25, 27, 57, 98, 99, 101, 102, 106</sup>. By using halide anions, the activation energy decreased in the order  $\text{Cl}^- > \text{Br}^-$ .<sup>25, 27, 102</sup> However, being a good nucleophile anion is not a sufficient condition for tailoring effective

catalyst. Indeed, if the activation barrier determined with azide anion ( $\text{N}_3^-$ ) was one of the lowest <sup>25</sup>, tetrabutylammonium azide ( $\text{TBAN}_3$ ) was a poor catalyst for the  $\text{CO}_2$ /epoxide coupling <sup>66</sup> as the azide carbonate intermediate was highly stable ( $\Delta G = -20.3 \text{ kcal.mol}^{-1}$ ) because of the very low leaving ability of the  $\text{N}_3^-$  anion. Finally, the regioselectivity of the ring-opening of terminal epoxides was also modelled by DFT calculations. For the coupling of PO with  $\text{CO}_2$  catalyzed by  $\text{TBABr}$  <sup>25</sup>,  $\text{C4-MImBr}$  <sup>99</sup> or  $\text{MImCl}$  <sup>98</sup>, the Gibbs energy value is lower for the nucleophilic attack of the halide anion onto the less substituted  $\beta$  carbon of the epoxide of respectively  $1.5 \text{ kcal.mol}^{-1}$ ,  $2.1 \text{ kcal.mol}^{-1}$  and  $1.4 \text{ kcal.mol}^{-1}$ .

### Halide-free activation mechanism

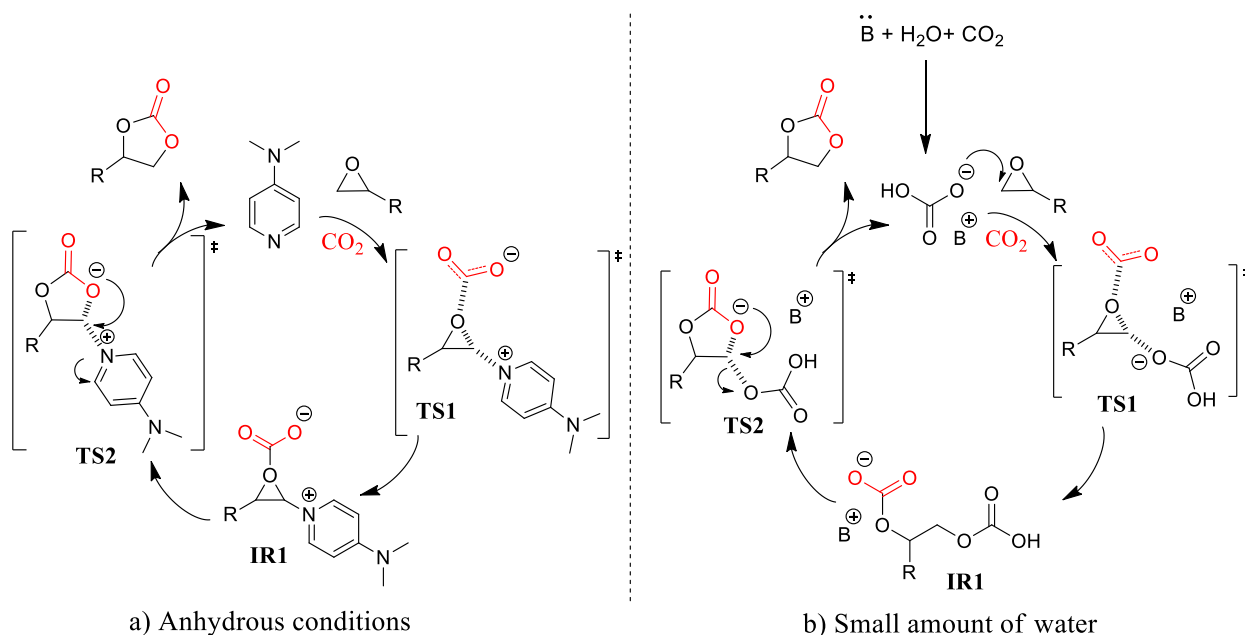
In depth mechanistic investigation of organic bases promoted  $\text{CO}_2$ /epoxide coupling was described using DMAP, pyridine or imidazole. <sup>79</sup> Two distinct reaction pathways were proposed with DMAP as catalyst depending on the presence or not of water. Under anhydrous conditions, Sankar *et al.* <sup>78</sup> postulated that the reaction occurred through a bimolecular mechanism involving the activation of the epoxide by polarization of the C-O bond through nucleophilic interaction between the  $\beta$ -carbon of the oxirane and DMAP and parallel activation of  $\text{CO}_2$  by DMAP forming a carbamate active species able to ring open the epoxide while simultaneously adding  $\text{CO}_2$  before carbonate ring closure. However, this proposal couldn't be confirmed by calculation. The most probable mechanism reported by Roshan *et al.* <sup>79</sup> relies on a two-step pathway in which the electron lone pair from aromatic nitrogen of DMAP attacks the less hindered C atom of the epoxide forming a N-C bond and a ring-opened complex (Scheme 10 a). The activation energy value of this rate determining step was estimated to  $27.62 \text{ kcal mol}^{-1}$  which is twice lower than the non-catalyzed reaction. Subsequently, this reactive intermediate adds  $\text{CO}_2$  forming a carbonate ion while the C-N bond partially breaks before ring closure *via* nucleophilic attack of the  $\beta$  carbon atom of the epoxide by the carbonate ion. Pyridine and imidazole bases answered the same reaction pathway but DMAP ( $E_a = 27.62 \text{ kcal.mol}^{-1}$ ) was a more efficient catalyst than pyridine ( $E_a = 30.66 \text{ kcal.mol}^{-1}$ ) and imidazole ( $E_a = 32.25 \text{ kcal.mol}^{-1}$ ).

The activity of Lewis bases was enhanced in presence of small amount of water. Yet Heldebrant *et al.* reported that a bicarbonate salt could be formed by reaction between  $\text{CO}_2$  and water in presence of a DBU (Scheme 9).<sup>107</sup>



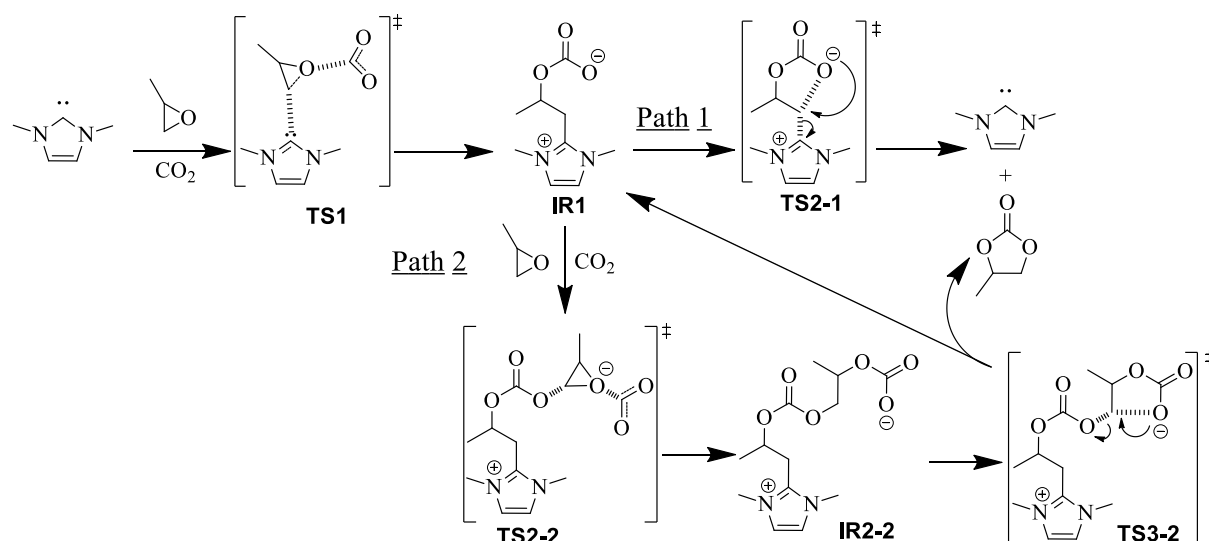
Scheme 9: Formation of bicarbonate salt of DBU (reprinted from ref <sup>79</sup>)

Hence, Roshan *et al.* assumed that the bicarbonate anion could be the active species for the CO<sub>2</sub>/epoxide coupling catalysed by imidazole, pyridine or DMAP.<sup>79</sup> The favoured activation mechanism still followed a two-step pathway similar to the one reported under anhydrous conditions (Scheme 10 b). However, the DFT calculations showed that the energy barrier was decreased from 27.62 kcal.mol<sup>-1</sup> to 12.34 kcal.mol<sup>-1</sup> with the bicarbonate anion compared to the activation mechanism of pyridine and DMAP in the absence of water. However, a contradictory investigation of Carvalho *et al.* showed that the bicarbonate anion allowed both the epoxide ring opening and the stabilization of the O atom by transfer of proton in the first step.<sup>95</sup> This mechanism was ruled out by Roshan *et al.* who investigated the mechanism with the acetate anion for preventing the proton transfer and found that the bicarbonate anion only act as a nucleophile for the epoxide ring-opening. The DFT calculations clearly elucidated that the energy values obtained with the HCO<sub>3</sub><sup>-</sup> ( $E_a = 12.34$  kcal.mol<sup>-1</sup>) and CH<sub>3</sub>COO<sup>-</sup> ( $E_a = 10.9$  kcal.mol<sup>-1</sup>) were significantly lower than those obtained with the Lewis bases in water-free systems (Scheme 10). Similarly, as the nucleophilic hydroxide anion has a poor leaving ability, Ema *et al.*<sup>47</sup> assumed that the activity of the hydroxide quaternary ammonium arises from the *in-situ* formation of tetrabutylammonium bicarbonate salts (TBABC) by reaction between TBAH and CO<sub>2</sub>. Indeed, DFT calculations highlighted that the formation of TBABC is very exothermic ( $\Delta G = -49$  kcal.mol<sup>-1</sup>) and proceeds without activation barrier. The catalytic activity originates from the bicarbonate ion (HCO<sub>3</sub><sup>-</sup>) that combines good nucleophilicity and leaving character.



Scheme 10: Catalytic pathway for the CO<sub>2</sub>/epoxide coupling catalyzed by a) DMAP in anhydrous conditions and b) the H<sub>2</sub>O/Lewis base (B) catalytic system <sup>79</sup>

Then, the reaction mechanism of NHC catalysed coupling of CO<sub>2</sub> with epoxide was investigated in detail by Ajitha *et al.*<sup>80</sup> Six different pathways including NHC or NHC-CO<sub>2</sub> adducts as active nucleophilic species were studied. Although the Gibbs energy of the NHC-CO<sub>2</sub> adduct formation is low ( $\Delta G = 4.1$  kcal.mol<sup>-1</sup>), the Gibbs energy of the epoxide ring-opening rate determining step is dramatically reduced with NHC ( $\Delta G = 25.6$  kcal.mol<sup>-1</sup>) compared to the NHC-CO<sub>2</sub> adduct ( $\Delta G = 44.4$  kcal.mol<sup>-1</sup>). From these DFT calculations, the authors postulated that NHC was the catalytic species involved in the activation mechanism. More precisely, a highly stable zwitterionic acyclic carbonate (IR1) was first generated by a termolecular reaction involving the nucleophilic attack of NHC on the less substituted carbon atom of the epoxide while the forming alkoxide oxygen attacked simultaneously CO<sub>2</sub> (TS1). This reactive intermediate can then undergo direct cyclization (IR2-1) for forming the cyclic carbonate and regenerating the NHC catalyst (Scheme 11, path 1) or reacts through a second termolecular pathway with an additional molecule of epoxide and CO<sub>2</sub> (IR2-2) to generate a new reactive intermediate that undergoes ring closure while reforming the first zwitterionic acyclic carbonate intermediate (Scheme 11, path 2). However, the pathway involving direct cyclization ( $\Delta G = 44.9$  kcal.mol<sup>-1</sup>, path 1) is energetically disfavored compared to the second route ( $\Delta G = 30.6$  kcal.mol<sup>-1</sup>, path 2).



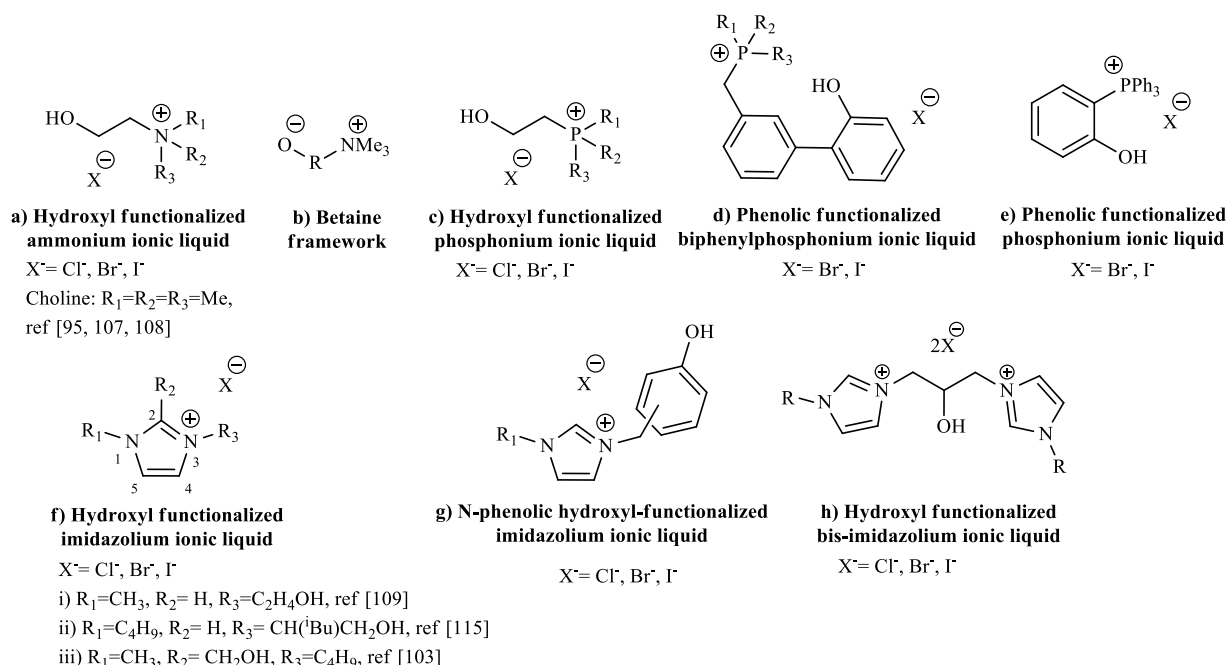
Scheme 11: The catalytic pathway for the CO<sub>2</sub>/epoxide coupling catalysed by NHC<sup>80</sup>

## II-2. Functionalized one-component metal-free homogeneous organocatalysts

In an effort to enhance the activity of organocatalysts, one-component organic salts and ILs with -OH, -COOH or -NH<sub>2</sub> functionalities were developed. The presence of these hydrogen-bond donors groups induces synergistic effects with the catalysts facilitating the CO<sub>2</sub>/epoxide coupling.

### II-2-a) Hydroxyl-functionalized organic salts and ILs catalysts

Hydroxyl-functionalized ammonium, phosphonium and imidazolium ILs catalysts were developed to enhance their activity by hydrogen bonding (Scheme 12)



Scheme 12: Structures of hydroxyl-functionalized ionic liquids catalysts

#### Ammoniums and choline derivatives

Biological choline derivatives, i.e. 2-(hydroxyethyl)trimethylammonium halide salts, or tetraalkylammonium halides derivatives with 2-hydroxyethyl substituents (Scheme 12a) synthesized by easy quaternization of tertiary amines by a halohydrin were used as active functional organocatalysts for the coupling of various terminal epoxides. For examples, Amaral *et al.*<sup>108</sup> and Büttner *et al.*<sup>109</sup> reported that choline were inefficient for the coupling of neat 1,2-epoxybutane with CO<sub>2</sub> at 1 MPa for 2h at 85°C or 90°C respectively probably because of catalyst solubility issues. The catalytic activity drastically increased in the presence of alcohol solvents (ethanol and isopropanol) or in benzonitrile with an almost complete conversion of 1,2-

epoxybutane after 6h while selectively forming the corresponding cyclic carbonate. Similar conclusions were reported by Carvalho *et al.*<sup>95</sup> for the synthesis of styrene carbonate from SO and CO<sub>2</sub> at 120°C and 1.5 MPa. Using choline chloride as catalyst, both the SO conversion and selectivity towards the formation of the cyclic carbonate increase with the increase of the solvent permittivity. Among all the tested solvents, benzonitrile that has a permittivity ( $\epsilon = 25.9$ ) similar to the one of ethanol ( $\epsilon = 25.3$ ) led to the best selectivity (93%) and carbonate yield (35%).

As reported for non-functional analogues, Büttner *et al.*<sup>109</sup> and Sun *et al.*<sup>110</sup> figure out for the coupling of neat 1,2-epoxybutane with CO<sub>2</sub> that the activity of hydroxyl-functional tetraalkylammonium halide salts is significantly influenced by the steric environment of the ammonium cation and increases with the steric effect induced by the N-alkyl substituents in the order Methyl < Ethyl < n-Butyl. The distance between the N atom and hydroxyl group of the ammonium salt was also crucial for optimizing the activity of the catalyst. If the ethyl spacer of the chain bearing the alcohol function is replaced by a propyl group, the carbonate yield formation dropped from 96% to 81%.<sup>109, 110</sup> In addition, the conversion of the epoxide was influenced by the nucleophilic character and the leaving ability of the halide and decreased in the order: I<sup>-</sup> > Br<sup>-</sup> > Cl<sup>-</sup>. Thus, 2-(hydroxyethyl)tributylammonium iodide as catalyst showed the highest epoxide conversion. Performance of both cholines and hydroxyl-functional tetraalkylammonium halide salts were found superior to their non-functionalized catalyst analogues.<sup>95, 109, 110</sup>

Zwitterionic ammonium betaines with aryloxy anion (Scheme 12b) were found to be efficient halide-free organocatalysts for the coupling of various terminal epoxides with CO<sub>2</sub>. Betaines of various structures were screened for the selective conversion of neat 1,2-epoxyhexane into cyclic carbonate at 1 MPa and 120 °C.<sup>111</sup> *Ortho*-substituted betaines with trimethylammonium cations were more efficient than the analogues with allyl and benzyl groups. This was related to the steric hindrance of these bulky substituents hindering the access of CO<sub>2</sub>/epoxide to the phenolate anion. The nucleophilicity of the phenolate was one of the most important parameter for the catalytic activity of trimethylammonium betaines. Results highlighted that the phenolic *meta*-isomer is the more active because of the highest nucleophilicity of the phenolate ion resulting from the lack of conjugation stabilization. As CO<sub>2</sub> reacts with the alkoxide moieties of the betaine to form a CO<sub>2</sub>-betaine adduct that thermally decomposed, this adduct was supposed to be the active catalytic species allowing the epoxide ring-opening.

### *Phosphoniums*

In 2015, Büttner *et al.* studied the catalytic activity of air-stable hydroxyl-functionalized phosphonium ILs (Scheme 12c) for the coupling of neat 1,2-epoxybutane with CO<sub>2</sub>.<sup>112</sup> This work was performed under the same conditions (catalyst structure, temperature, reaction time, pressure) than that reported previously by the same author for the hydroxyl-functionalized ammonium catalyst and identical conclusions were drawn.<sup>109</sup> The activity of hydroxyl functional

quaternary phosphonium halide was strongly influenced by the length and steric hindrance of the alkyl chains as well as the nature of the halide anion. The activity increased by increasing alkyl chain length in the order Methyl < Ethyl < n-Butyl and, for the halide anion in the order  $I^- > Br^- > Cl^-$ . As for ammonium counterparts, increasing the alkyl chain length bearing the OH group from ethyl to propyl decreased the activity. Therefore, 2-(hydroxyethyl)tributylphosphonium iodide was the most efficient catalyst and a high yield of cyclic carbonate (95%) can be achieved at 90°C, 1 MPa in 2 hours whereas non-functionalized tetrabutylphosphonium iodide was a poor catalyst (19%), which is consistent with Wei-Li's observations.<sup>113</sup> Moreover, no difference in the catalytic activity of both hydroxyl-functionalized phosphonium salts and ammonium analogues could be highlighted by this comparative study.

Liu *et al.*<sup>114</sup> developed various efficient biphenyl quaternary phosphonium halide possessing a phenolic hydroxyl group (Scheme 12 d) for the conversion of terminal epoxides under mild conditions. The distance between the phosphonium and the phenolic hydroxyl groups and the nature of the halide anion had a strong influence on the activity that decreased by changing the position of the hydroxyl-phenolic group in the order *ortho* > *meta* > *para* and for the anion in the order  $I^- > Br^-$ . Therefore, the o-phenol-2-arylmethyl triphenylphosphonium iodide was the most active catalyst allowing achieving a high and selective conversion of styrene oxide (91%) at 60°C for 24h under atmospheric pressure without using a solvent.<sup>114</sup> Then, Toda *et al.* studied various tetraarylphosphonium halide (Scheme 12 e) at higher temperature (120°C) using high catalyst loading (15 %mol).<sup>115</sup> The best performances were found using (2-hydroxyl-5-methylphenyl)triphenylphosphonium bromide that allowed the conversion of styrene oxide in high yield (90%) at 120°C and atmospheric pressure using chlorobenzene as solvent and.<sup>115</sup>

### Imidazoliums

The higher catalytic activity of hydroxyl functionalized imidazolium ILs (Scheme 12 f) for the CO<sub>2</sub>/epoxide coupling was first reported by Sun *et al.*<sup>110</sup> Compared to C2-MImBr, 1-(2-hydroxyl-ethyl)-3-methylimidazolium bromide (HO-C2-MImBr) allowed for the selective and complete conversion of PO and other terminal epoxides into carbonates in less than 1h at 125°C and 2 MPa. The chemical structure of HO-C2-MImBr was then modified by several groups to improve the performance of the catalyst i) by introducing branching on the OH-C2 and long alkyl chains on the C1<sup>116</sup>, ii) by introducing hydroxymethyl group on the carbon in 2 position (N=C-N) of the imidazole ring<sup>103</sup>, iii) by replacing the 2-hydroxyethyl group of the imidazole ring by N-phenolic groups (Scheme 12 g)<sup>117</sup>, or iv) by using ILs of more complex structure composed of two N-alkylimidazolium rings linked by a propan-2-ol bond (Scheme 12 h).<sup>118</sup>

Denizalt showed that β-hydroxyl-functionalized imidazolium were efficient catalysts under mild conditions.<sup>116</sup> The length of the C1 alkyl chain had a strong influence as the activity increased from ethyl to butyl but decreased from butyl to hexyl. In



addition, the performances increased when the isopropyl chain on the  $\alpha$ -carbon atom of C3 was replaced by an isobutyl. The synthesis of propylene carbonate was quantitative and selective with OH-(*i*Bu)-C2-BuImI (Scheme 12 f (ii)) after 8h at 60°C and 1 MPa.

As demonstrated by Wang *et al.*<sup>103</sup>, changing the position of the hydroxyl group from the N-alkyl substituent to the carbon 2 of the imidazole ring has no impact on the catalyst activity (Scheme 12 f (iii)). Both the PO conversion and the selectivity against the formation of propylene carbonate determined after 1h at 110°C and 2 MPa were identical whatever the OH position and the alkyl chain length of the N-substituent of the MIm ring.

Wu *et al.* compared the catalytic activity of series of N-phenolic hydroxyl-functionalized butylimidazolium ILs (Scheme 12 g) for the coupling of epichlorohydrin with CO<sub>2</sub> at 70°C and 1 MPa for 3h before extending the use of the most efficient catalyst to the successful and selective conversion of others various terminal and disubstituted oxiranes.<sup>117</sup> The spatial position of the phenolic OH group was crucial for tailoring a functional catalyst with optimum performances. The highest activity was attributed to imidazolium IL with phenolic meta-isomer and a proton in position 2 (N=CH-N) of the ring. The cooperative catalytic effect of the phenolic OH group and the C-H bond was highlighted by the lowest conversion of epichlorohydrin when the N=CH-N proton was replaced by a methyl group. In addition, multi-phenolic derivative did not improve the catalytic activity because of the steric hindrance on the second N-atom of the imidazolium ring. The authors concluded that phenolic hydroxyl-functionalized imidazolium ILs displayed a higher activity than HO-C2-MImBr indicating that a phenolic group may activate epichlorohydrin more effectively than the hydroxyl one.

Finally, ILs with bis-N-alkylimidazolium ring linked by a propan-2-ol bond (Scheme 12 h) were investigated for the selective synthesis of propylene carbonate from PO and CO<sub>2</sub> under mild conditions (T = 70°C, P = 0.4 MPa).<sup>118</sup> The PO conversion increased with the alkyl chain length in the order methyl < benzyl < n-octyl. This trend was attributed to the higher solubility of the catalyst bearing long alkyl chain in neat epoxide whereas the catalysts with shorter alkyl chains were not soluble in PO. For sake of comparison, whatever the alkyl chain length, propan-2-ol linked bis-alkylimidazolium bromide displayed a higher catalytic activity than the hydroxyl-functionalized mono-alkylimidazolium counterpart. It's worth mentioning that for all studied catalytic systems, the activity of the halide anion respects the order Cl<sup>-</sup> < Br<sup>-</sup>.

57, 103, 110, 117, 118

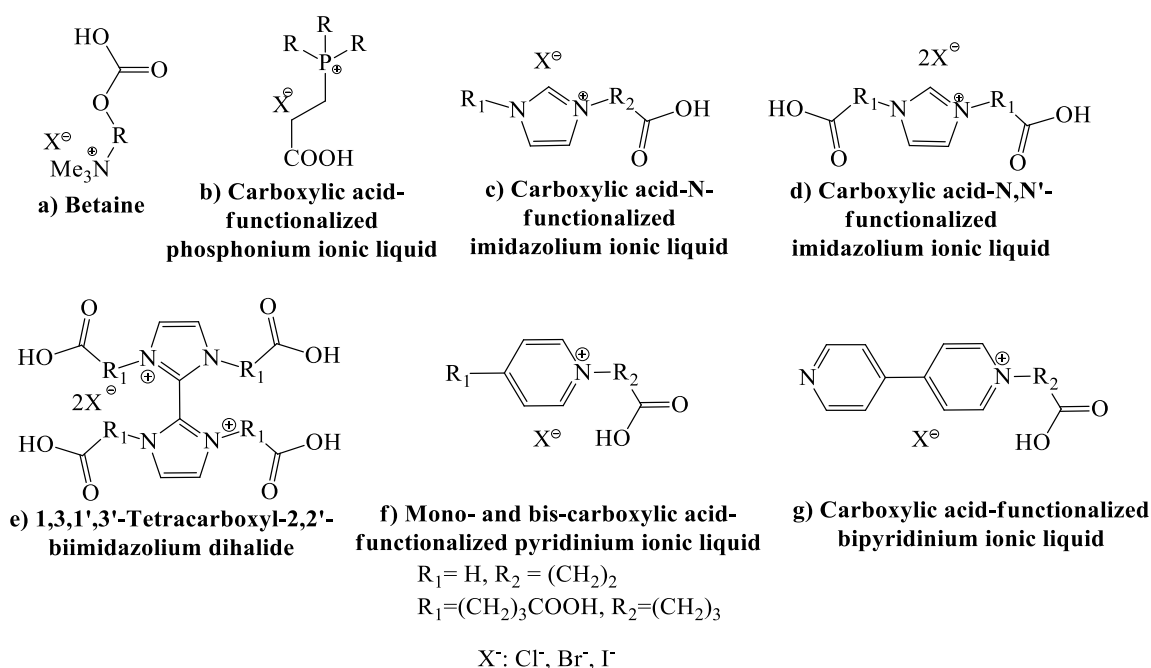
### *Others ILs*

Wei-Li *et al.* reported a unique experiment comparing the catalytic activity of hydroxyl-based tetramethylguanidinium bromide ILs with the one of the non-functional analogue. For the coupling of PO with CO<sub>2</sub> at 130°C and 2 MPa<sup>119</sup>, they suggested that the epoxide conversion increased from 63% for

tetramethylethylguanidinium bromide to 89% with the OH functionalized one. However, these data should be confirmed by additional experiments.

## II-2-b) Carboxylic acid-functionalized organic salts and ILs catalysts

Carboxylic acids are stronger Brønsted acids than alcohols. As a consequence, the hydrogen bond donor ability of these groups is different from the one of alcohols and affects the catalytic activity of ammoniums, phosphoniums, imidazoliums or pyridinium organocatalysts (Scheme 13).



Scheme 13: Structures of the carboxylic acid-functionalized ionic liquids catalysts

### Ammonium ILs

Trimethylglycine or betaine (Bet) is a natural zwitterionic quaternary ammonium that widely exists in plants and animals (Scheme 13 a). Its structure differs from cholines by the presence of a carboxylate group instead of an OH functionality.<sup>108</sup> Various betaines were prepared by protonation of anhydrous betaine with acids<sup>108</sup> or by quaternization of glycine with MeI<sup>120</sup> and tested as catalysts for the PO/CO<sub>2</sub> coupling under harsh conditions ( $T = 140^\circ\text{C}$ ,  $P = 8 \text{ MPa}$ ).<sup>121</sup> The catalytic activity of carboxylic acid functionalized betaines was dependent on the anion and evolved in the order  $\text{PF}_6^- < \text{BF}_4^- < \text{Br}^- < \text{Cl}^- < \text{I}^-$ . The lower activity of the protonated betaine bromide (HBetBr) compared to the chloride one (HBetCl) was explained by the lower solubility of the bromide salt in the reaction mixture. The most active HBetI catalyst was then successfully exploited to produce terminal and internal cyclic carbonates with almost 100% selectivity from terminal epoxide or cyclohexene oxide. Interestingly, HBetCl was more efficient than the choline chloride attesting for the better epoxide activation capability of the carboxylic acid groups.

### Phosphonium ILs

Catalytic performances of carboxylic acid functionalized phosphonium ILs with  $[(\text{Ph})_3\text{P}-\text{C}_n\text{H}_{2n}-\text{COOH}]\text{X}$  structures (Scheme 13 b) were evaluated by Dai *et al.*<sup>113</sup> for the coupling of PO and various epoxides with  $\text{CO}_2$  at  $130^\circ\text{C}$  and 2.5 MPa for 3 h. If, under such experimental conditions, it was impossible to discriminate about the best catalytic performance between hydroxyl and carboxylic acid-functionalized ILs,  $[(\text{Ph})_3\text{P}-\text{C}_n\text{H}_{2n}-\text{COOH}]^+\text{X}^-$  ILs were more efficient than the non-functional catalysts. Additionally, a slight spacer effect between the P center and the carboxylic acid group was highlighted by a maximum PO conversion of  $\sim 97\%$  with  $\text{C}_2\text{H}_4$  or  $\text{C}_3\text{H}_6$  spacers that decreased in the order  $\text{C}_2\text{H}_4 \sim \text{C}_3\text{H}_6 > \text{C}_4\text{H}_8 > \text{CH}_2$ . Without surprise, catalysts with  $\text{Cl}^-$  anion were less efficient than  $\text{Br}^-$  and  $\text{I}^-$  as counter anion that showed similar performances.

### Imidazolium ILs

Series of carboxylic acid-functionalized imidazolium ILs (Scheme 13 c) were developed and the influence of the cation structure, the halide anion and the distance between the N center and the carboxylic acid group on the catalytic performances were studied.<sup>60, 122-124</sup> Compared to the non-functionalized counterpart, the activity of such ILs as catalysts is enhanced by the presence of the carboxylic acid function and selectively leads to the formation of cyclic carbonates. However, they systematically show lower performances than hydroxyl-functionalized analogues.<sup>60, 124, 125</sup> As reported for functional ammonium or phosphonium ILs, the length of the  $-\text{C}_n\text{H}_{2n}-$  alkyl chain bearing the carboxylic group influences the epoxide conversion. For instance, by using  $[\text{HOOC}-\text{C}_n\text{H}_{2n}-\text{MIm}]\text{X}$  catalysts, the PO conversion decreases with the reduction of the  $-\text{C}_n\text{H}_{2n}-$  chain length in the order  $\text{C}_2\text{H}_4\text{CO}_2\text{H} > \text{CH}_2\text{CO}_2\text{H}$ <sup>124</sup> or  $\text{C}_3\text{H}_6\text{CO}_2\text{H} > \text{CH}_2\text{CO}_2\text{H}$ <sup>60</sup> for model reactions respectively performed at  $110^\circ\text{C}$  and 1.5 MPa or at  $125^\circ\text{C}$  and 2 MPa. This trend was ascribed to the stronger acidity of shorter alkyl chains bearing  $\text{COOH}$  that is detrimental for the catalytic activity. On one hand, strong interaction between the halide and the carboxylic acid weakens the nucleophilicity of the anion which hardens the epoxy ring-opening.<sup>60</sup> On the other hand, a too strong H-bond between the  $\text{COOH}$ -functionalized catalyst and the oxygen donor group of the opened epoxide could baffle the  $\text{CO}_2$  insertion.<sup>124</sup> Effect of the imidazolium structure was briefly explored by comparing the activity of  $\text{COOH}$ -functional methyl- and butylimidazolium bromide<sup>125</sup> ILs or mono- and biscalboxylic acid functionalized methylimidazolium bromide ILs<sup>60, 122</sup> (Scheme 13 d). If the length of the N-alkyl substituent has negligible effect, the activity of the bifunctional catalyst was somewhat superior to the one of monofunctional methylimidazolium IL as evidenced by a PO conversion of respectively 78% and 66% at  $125^\circ\text{C}$  and 2 MPa.<sup>60</sup> Finally, 1,3,1',3'-tetracarboxyl-2,2'-biimidazolium dibromide was developed but the catalytic activity was poor even under harsh conditions (Scheme 13 e).<sup>123</sup>

### Pyridinium ILs

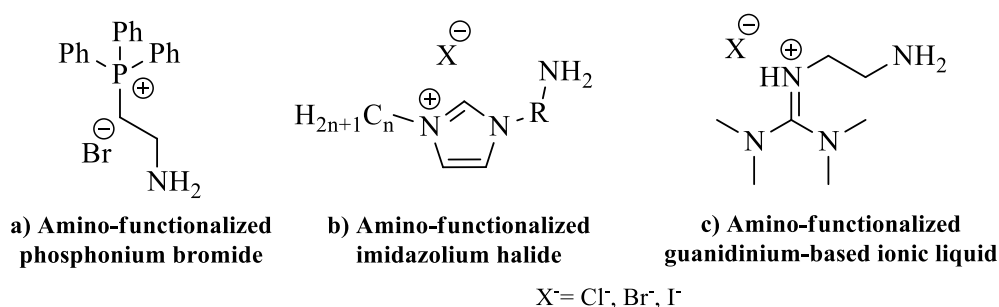
Mono- and bis-carboxylic acid-functionalized-N-pyridinium and bipyridinium ILs were scarcely developed for coupling PO with CO<sub>2</sub> (Scheme 13 f and g).<sup>60, 124</sup> Unfortunately, reported data are insufficient to draw general trends. However, under similar experimental conditions (T = 125 °C and P = 2 MPa), both types of catalyst were less efficient than COOH-based alkylimidazolium ILs.

### Others ILs

As reported for OH functional guanidinium ILs, Wei-Li *et al.* suggested that the PO conversion increased from 63% for tetramethylethylguanidinium bromide to 91% with COOH functional tetramethylguanidinium bromide at 130°C and 2 MPa.<sup>119</sup> Additional data are however needed to support this observation.

## II-2-c) Amino-functionalized organic salts and ILs catalysts

Beside their ability to reversibly capture CO<sub>2</sub> by the way of ammonium carbamate formation<sup>126, 127</sup>, primary amines are potential hydrogen bond donor groups that can act as catalyst for fastening the CO<sub>2</sub> fixation onto epoxides. Only few amino-functionalized catalysts were reported in the literature (Scheme 14).



Scheme 14: Structures of amino-functionalized organic salts and ILs catalysts

### Phosphonium ILs

NH<sub>2</sub>-functionalized phosphonium bromide ILs with a [(Ph)<sub>3</sub>P-C<sub>2</sub>H<sub>4</sub>-NH<sub>2</sub>][Br] structure were tested for the synthesis of PC from PO and CO<sub>2</sub> at 130°C and 2.5 MPa for 3h (Scheme 14 a). According to the very few data reported by Dai *et al.*, [(Ph)<sub>3</sub>P-C<sub>2</sub>H<sub>4</sub>-NH<sub>2</sub>][Br] were as effective as [(Ph)<sub>3</sub>P-C<sub>2</sub>H<sub>4</sub>-OH][Br] and [(Ph)<sub>3</sub>P-C<sub>2</sub>H<sub>4</sub>-COOH][Br] ILs as evidenced by a PO conversion between 95 and 97% for the three catalysts.<sup>113</sup>

### Imidazolium ILs

Amino-functionalized ILs with structure [NH<sub>2</sub>-C<sub>3</sub>H<sub>6</sub>-MIm]X were also exploited as catalysts for the synthesis of cyclic carbonate by the CO<sub>2</sub>/PO coupling (Scheme 14 b). Both the cation structure and the anion influence the catalytic performances.<sup>128</sup> At 120°C and 1.5 MPa, catalytic performances of [NH<sub>2</sub>-C<sub>3</sub>H<sub>6</sub>-MIm]X increase with the nucleophilicity of the halide (Cl<sup>-</sup> < Br<sup>-</sup> < I<sup>-</sup>). For a Cl<sup>-</sup> anion, the PO conversion evolved from 59 to 69% with the lengthening of the N-alkyl substituent of the

imidazolium ring in the order methyl- (MIm)  $\sim$  ethyl- (EIm)  $<$  butyl- (BIm). Interestingly, amino functional ILs displayed superior efficiency than a non-functionalized analogues confirming the capability of  $\text{NH}_2$  to facilitate the coupling of epoxide with  $\text{CO}_2$  by hydrogen bonds formation but discrimination between the best activity of  $\text{NH}_2$  and  $\text{COOH}$  catalysts was impossible as, under identical experimental conditions, the PO conversion slightly differ between 84% ( $\text{COOH}$ -based IL) and 88% ( $\text{NH}_2$ -based IL).

#### *Others animo-functional ILs*

Benefits of functionalizing guanidinium bromide ILs with a  $\text{NH}_2$  group (Scheme 14 c) were once again briefly highlighted by Wei-Li *et al.* for the model coupling reaction of PO with  $\text{CO}_2$  ( $T = 130^\circ\text{C}$ ,  $P = 2 \text{ MPa}$ ).<sup>119</sup> The author showed that the PO conversion evolved from 63% for non-functional tetramethylethyl guanidinium bromide to 95 % with the  $\text{NH}_2$  functional analogue while, for both catalysts, the selectivity against formation of propylene carbonate was closed to 100%. By a comparative study, they also demonstrated that the activity slightly increased with the nature of the functional group in the order  $\text{CH}_3 < \text{OH} < \text{COOH} < \text{NH}_2$ . The most efficient amino-based guanidinium IL was exploited with success to selectively produce various cyclic carbonates from terminal or internal epoxides with conversions closed to 100% in 1 to 20 h.

### **II-2-d) Urea-functionalized ILs catalysts**

Thermally stable urea-functionalized imidazolium ILs were developed by Liu *et al.* for both capturing  $\text{CO}_2$  and catalysing the  $\text{CO}_2/\text{PO}$  coupling.<sup>129</sup> Catalysts of various structure were screened under relatively harsh conditions ( $T = 130^\circ\text{C}$ ,  $P = 1.5 \text{ MPa}$ ) and the activity was dependent on the anion nucleophilicity and responds to the order  $\text{NO}_3^- \sim \text{CH}_3\text{COO}^- \sim \text{HSO}_4^- \ll \text{Cl}^- < \text{Br}^- < \text{I}^-$ . The co-catalytic effect of urea was attested by the superior PO conversion measured with the functional IL (84% instead of 74%). This enhanced activity was ascribed to the synergetic effects between  $\text{CO}_2$  activation/capture by the  $\text{N}=\text{CH}-\text{N}$  group of the imidazolium ring and hydrogen bond formation between the  $-\text{NH}$  group of urea with the epoxide. For a same halide anion, they also observed that the steric hindrance reduced the catalyst activity by replacing the  $\text{NH}$  proton of the N in position 1 of the imidazolium cation by a n-butyl chain.

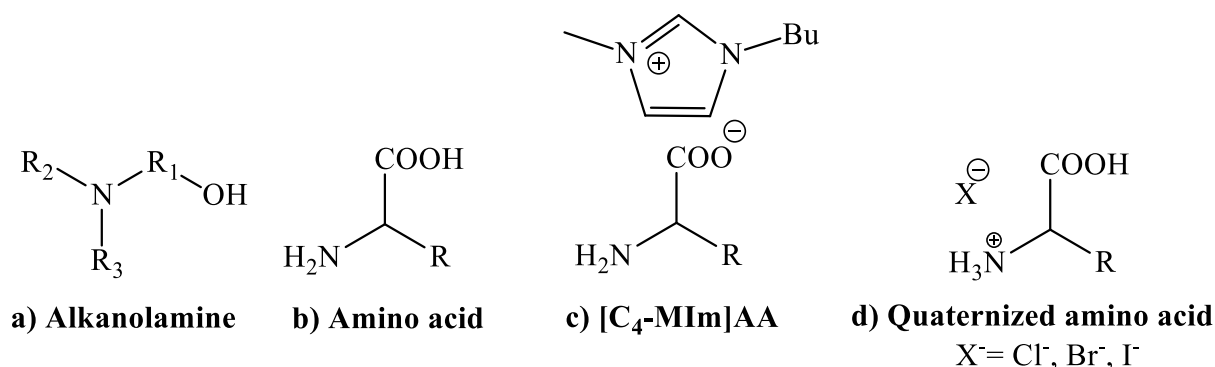
### **II-2-e) Amino alcohols and amino acids catalysts**

Alkanolamines (Scheme 15 a) are metal-free and halide-free organocatalysts for the synthesis of cyclic carbonates.<sup>130</sup> Series of (multifunctional) alkanolamines bearing primary, secondary or tertiary amines and one or several hydroxyl groups were screened for the  $\text{CO}_2/\text{PO}$  coupling at  $120^\circ\text{C}$  and  $1 \text{ MPa}$ . Under those conditions, depending on the alkanolamine structure, PO conversion varied from 6% with *N-tert*-butyldiethanolamine to 91% with *N,N*-dimethylpropanolamine after 3h and, whatever the alkanolamine, propylene carbonate was selectively produced. As a global trend, the catalytic activity increased in the order primary  $<$  secondary  $<$

tertiary amines. In addition, aminoalcohols with short N-alkyl chains had a favourable impact on the reaction yields because of the reduction of the steric hindrance. These results clearly highlight synergistic effects between the -OH and the amino-groups.

Natural and non-toxic amino acids (AAs, Scheme 15 b) are amphoteric compounds that can exist as zwitterion depending on the pH and their pKa. Indeed, the primary amino groups are basic and can be protonated while the carboxylic acid can be deprotonated to form a carboxylate anion. This make the 20 AAs potential metal and halide-free catalysts able to promote the CO<sub>2</sub>/PO coupling under harsh conditions (130°C, 6 MPa) and prolonged reaction times (48h) using CH<sub>2</sub>Cl<sub>2</sub> as solvent.<sup>131</sup> By virtue of their side-chain functionalities, structure of the AAs had a strong impact on the catalytic activity. L-leucine, L-proline, L-phenylalanine, L-methionine, L-histidine and L-lysine were the most performant AAs allowing a complete conversion of PO into propylene carbonate in CH<sub>2</sub>Cl<sub>2</sub>. As a general trend, basic amino acids performed better than the acid ones. However, it was not possible from those results to determine the key structural factors influencing the activity or to establish a generalized plausible reaction mechanism. The study of Qi and Jiang confirmed the higher efficiency of L-histidine under supercritical conditions compared to the others AAs.<sup>132</sup> However, as the reaction was realized under solvent-free conditions, the results differ from the ones reported in CH<sub>2</sub>Cl<sub>2</sub> because of polarity and solubility changes.

Amino acid-derived ionic liquids (AAILs) consisting of amino acid anions and 1-butyl-3-methylimidazolium cation, i.e. [C4-MIm]AA (Scheme 15 c), show strong hydrogen bond ability<sup>133, 134</sup> making them halogen-free catalysts for coupling various terminal epoxides with CO<sub>2</sub>. Good to excellent epoxide conversions (69 – 96%) with selectivities higher than 96% were reported for experiments realized at 130°C, 4 MPa for 18h using [C4-MIm]AA with an alanine AA anion ([Ala]) as catalyst.<sup>135</sup> The activity of [C4-MIm][Ala] was compared to the one of [C4-MIm] catalyst with lysine [Lys], serine [Ser] and glutamic acid [Glu] anions respectively bearing -NH<sub>2</sub>, -OH and -COOH functional groups (CH<sub>3</sub> for alanine) for the coupling of PO with CO<sub>2</sub> at 130°C and 4 MPa for 8 h. If low PO conversions between 20 and 40% were obtained, [C4-MIm][Lys] with NH<sub>2</sub> function was identified as the most efficient AAIL. Similar trend was reported by Park *et al.*<sup>136</sup> for the coupling of SO with CO<sub>2</sub> at 120°C and atmospheric pressure using AAILs synthesized by simple quaternization of AAs (Scheme 15 d). They demonstrated that the AAIL derived from histidine was the most efficient catalyst with a selective conversion of SO of 92% in 6h. In a general way, basic (or NH<sub>2</sub> containing) quaternized AAs afford much better SO conversion than the acidic ones containing OH or COOH groups.<sup>136</sup>



Scheme 15: General structure of alkanolamine, amino acid, amino acid-derived imidazolium ionic liquid and quaternized amino acid used as catalysts

### II-3. Bi- and tri-component metal-free homogeneous organocatalysts

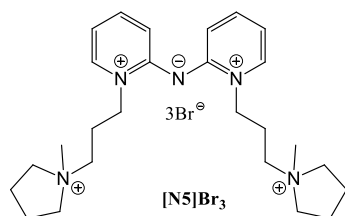
Instead of monocomponent functionalized catalysts, bi- and tri-component catalysts were used to promote the CO<sub>2</sub>/epoxide coupling. The catalytic platform consists of the combination of an alkali or organic salt, an ionic liquid or a base with a hydrogen bond donor (HBD). The HBD allow the activation of the epoxide by interaction with the epoxide and the OH or COOH group by H-bonds. Potassium and tetrabutylammonium salts are the most widespread catalysts. In most case, the development of efficient catalytic platform is easy as the components are commercially available.

#### II-3-a) Water

Water is a green and cheap protic compound that was used to activate the CO<sub>2</sub>/epoxide coupling by acting as HBD co-catalyst, by enhancing the catalyst solubility of the most common imidazolium, ammonium, phosphonium ILs organocatalysts and alkali metal halides in the reaction medium or by reacting with CO<sub>2</sub>.<sup>37, 78, 107, 125, 137-141</sup> However, in some cases, the presence of water may affect the selectivity of the reaction by formation of diols as by-product *via* hydrolysis of the epoxy ring. Compared to anhydrous analogues, hydrated alkali metal halide salts with MX.nH<sub>2</sub>O structure fasten the synthesis of PC. At 120°C and 2 MPa, PO conversion rises after 1h from 8 and 13 % in the absence of water to 94 and 96% by using respectively NaI.2H<sub>2</sub>O or LiI.3H<sub>2</sub>O without affecting the selectivity of the reaction.<sup>139</sup> This spectacular booster effect was attributed not only to the improved solubility of hydrated salts in PO but also the release of free water in the reaction medium. The coordination of a H atom from a water molecule with an O atom from PO by hydrogen bonding resulted in the polarization of the C–O bonds, which facilitates PO ring opening.

ILs/H<sub>2</sub>O dual systems were sparsely reported in the literature. For C2-MImBr, 1-(2-carboxyl-ethyl)-3-butyylimidazolium bromide (HO-EBimBr)<sup>125</sup> and ILs with more

complex structure composed of two pyridinium and two pyrrolidinium moieties (Scheme 16)<sup>140</sup>, the activity of the catalyst against the coupling of CO<sub>2</sub> with PO and various terminal epoxides was systematically enhanced by the addition of catalytic amount of water. In some cases, water is not only a co-catalyst but it allows liquefying polar hygroscopic ILs improving their compatibility with non-polar epoxides. For all these systems, the selectivity remained generally higher than 98%.



Scheme 16: Structure of [N5]Br<sub>3</sub> co-catalyst

As previously mentioned, the coupling of CO<sub>2</sub> with epoxides promoted by amino acids is slow even under harsh experimental conditions. The low catalytic activity of amino acids was significantly improved by using 30 equivalents of water (compared to AAs) as co-catalyst at 120°C and 1.2 MPa. Histidine, the most efficient basic AA, allowed to convert PO into PC with good yield (93%) with a selectivity of 91% whereas no PC was produced under similar conditions in the absence of water.<sup>138</sup> However, with other AAs, both the PO conversion and selectivity respectively fall down to 3 - 9% and 71 - 76% with the most acidic AAs. Park *et al.*<sup>138</sup> also established a PO conversion/water content dependence and demonstrated that if the increase of the water content is beneficial on the PO conversion, the selectivity dramatically falls down.

### II-3-b) Alcohols and hydroxyl-functionalized HBDs

#### *Mono-alcohols*

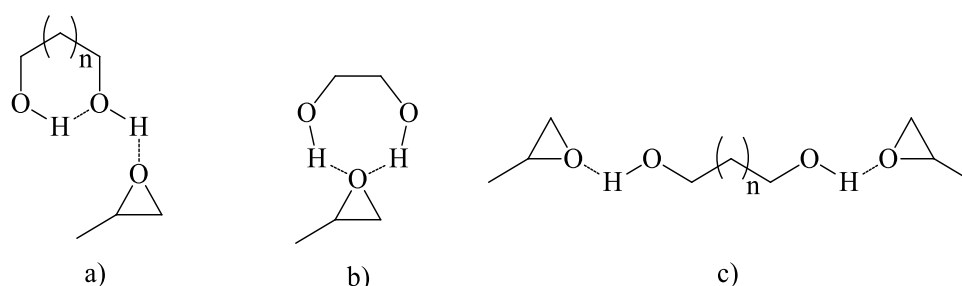
The potential of various alcohols such as ethanol, propanol... to accelerate the TBABr catalysed PO/CO<sub>2</sub> coupling at 100°C and 3 MPa was screened by Zhang *et al.*<sup>137</sup> However, all the tested mono-ols displayed a poor co-catalytic activity even at high loading (100 eq. compared to TBABr) as evidenced by a ~ two-fold increase of the PO conversion compared to the same model reaction without HBD. This comparative study also points out that such activators are not more efficient than water as PC yields after reaction are similar and close to 50%.

#### *Di- and polyols*

Surprisingly, the catalytic activity of KI was significantly improved by using diols<sup>125, 142</sup> which co-catalytic activity evolved in the order vicinal diols > 1,3-propanediol > 1,4-butanediol > 1,6-hexanediol >> mono-alcohols >> water for the synthesis of PC at 90°C and 2 MPa. Such positive effect was assigned to the ability of diols to simultaneously interact by intra-molecular hydrogen bonds formation and inter-molecular bonding with the oxygen atom of the epoxide (Scheme 17 a). However, as 1,2-diols cannot form intramolecular bonds, their higher activity can be only



explained by the stabilisation of the oxygen atom of the epoxide by two intermolecular H-bonds forming a seven-membered ring (Scheme 17 b).<sup>143</sup> The lowest efficiency of 1,6-hexanediol was related to the long distance between both OH groups making impossible the creation of intramolecular H-bonds (Scheme 17 c). Synergistic effects between 1,2-ethylene glycol and HO-EBImBr were further reported for the selective synthesis of PC from coupling of PO with CO<sub>2</sub>.<sup>125</sup> However, these results are in contradiction with those reported by Zhang *et al.*<sup>137</sup> for the TBABr catalysed PO/CO<sub>2</sub> coupling who showed that ethylene glycol exhibited similar activity than mono-alcohols. This rise the question on how the catalyst solubility in the epoxide rich mixture is affected by the addition of alcohols co-catalysts.



Scheme 17: Possible ways of interaction of diols co-catalysts with propylene oxide a) diols with  $1 \leq n \leq 5$ , b) 1,2-diols, c) diols with  $n \geq 6$ .

Cheap pentaerythritol (PETT)/KI dual system was described as an efficient catalyst to fasten the coupling of various terminal epoxides (Scheme 18 a).<sup>144</sup> Under solvent-free conditions, at 130°C and 2.5 MPa, epoxides conversion between 90 and 99% were obtained after 2-10 h. The supposed activation mechanism involved the complexation of the potassium cation by PETT but it was not confirmed by DFT calculations. However, under lower temperature and pressure ( $T = 70^\circ\text{C}$ ,  $P = 0.4 \text{ MPa}$ ), this bicomponent system was less efficient than combinations of PETT with nucleophilic halide ammonium salts or imidazolium ILs systems for the cycloaddition of CO<sub>2</sub> with PO or others epoxides.<sup>145</sup> The activation mechanism remained unclear but the chelation of TBAI by PETT is not possible because of the cation size suggesting that PETT acts as a HBD interacting with the epoxide.

### Saccharides

Halide- and metal-free CO<sub>2</sub>/PO coupling was reported with binary DBU/saccharides catalysts.<sup>146</sup> At 120°C and 2 MPa, only sucrose, fructose, galactose and 2-deoxy-D-ribose displayed very low co-catalytic activity. The PO conversion only slightly increased from 80% for a model reaction using DBU as sole catalyst to 87 % in the presence of the most efficient bicomponent DBU/2-deoxy-D-ribose (Scheme 18 b) catalyst.

### Fluorinated alcohols

Finally, as the Brønsted acidity influenced the catalytic activity, monohydroxyl fluorinated alcohols/TBAX ( $X = \text{I}^-, \text{Br}^-$ ) bicomponent catalyst (Scheme 18 c) has been reported to efficiently enhance the CO<sub>2</sub>/epoxide coupling under mild conditions ( $T =$

60-80°C, P = 0.1-2 MPa) allowing the complete and selective formation of terminal cyclic carbonates within 20 to 60 minutes.<sup>147</sup> The co-catalytic activity of fluorinated alcohols increased with the number of trifluoro groups:  $(\text{CH}_3)_3\text{COH} < \text{CF}_3(\text{CH}_3)_2\text{COH} < (\text{CF}_3)_2\text{CH}_3\text{COH} < (\text{CF}_3)_3\text{CH}_3\text{COH}$ . Indeed, fluorine is a strong electronegative atom that attracts electrons and increases the acidity and the positive charge of protons of neighbouring hydroxyl groups, creating stronger hydrogen bond interactions with the O atom of the epoxide. Interestingly, the fluorinated double hydrogen bond donor 1,3-bis-(2-hydroxyhexafluoroisopropyl)-benzene (Scheme 18 d), has been reported to be a most efficient activator than perfluoro-*tert*-butanol allowing the conversion of terminal epoxides within few minutes whereas its non-fluorinated counterpart was a poor co-catalyst.

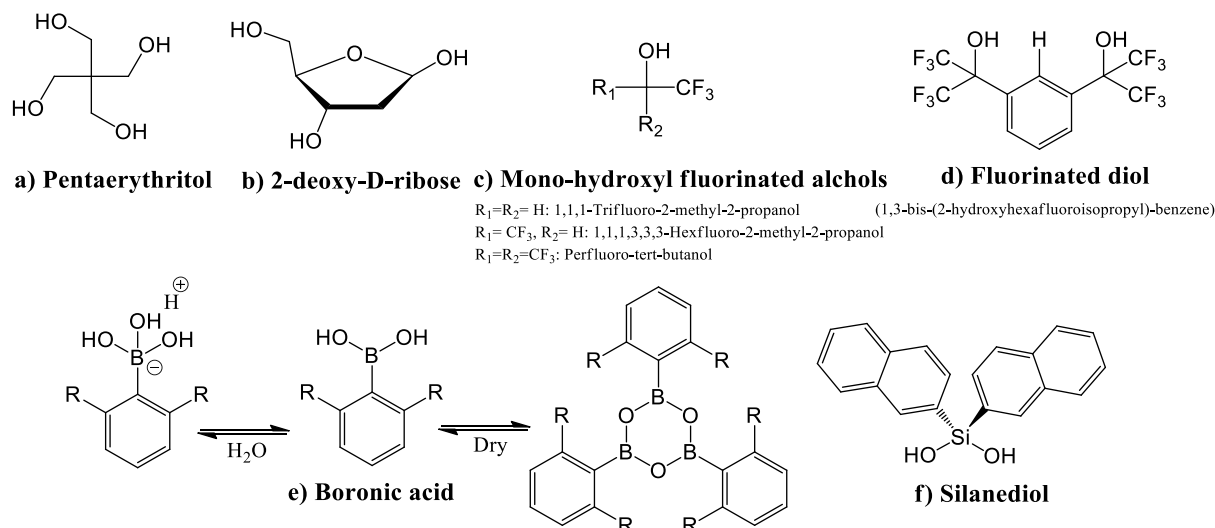
### Boronic acids

Boronic acids (BA) with  $\text{RB}(\text{OH})_2$  structures (Scheme 18 e) are weak Lewis acids that can potentially act as hydrogen bond donor because of the presence of OH groups. BAs exist as mixture of oligomeric anhydrides in particular six-membered boroxines under dry conditions that decompose in the presence of water. In a very recent publication, Zhang *et al.* screened more than 25 boronic acids/TBAI onium salts combinations to promote the coupling of  $\text{CO}_2$  with model (glycidyl phenyl ether) and various epoxides under mild conditions ( $T = 50^\circ\text{C}$ ,  $P = 1 \text{ MPa}$ ) using water as solvent.<sup>148</sup> Under those conditions, moderate to good yields (13 - 90%) were obtained after 4h and cyclic carbonates were produced with a 100% selectivity. From this study, phenylboronic acid with isopropyl substituent in *ortho* position of the aromatic ring was found to be the most efficient co-catalyst. In addition, the catalytic efficiency and reaction yields were correlated to the boron positive charge thanks to the calculated natural bond orbital (NBO) charges on boron derivatives highlighting that both higher positive charge on the boron atom and the substitution on the 2,6 positions of the aromatic ring increase the Lewis acidity. The authors concluded that those BAs behave like strong Brønsted acids providing strong H-bonds. At the same time, our group was testing more than 20 BAs derivatives, most of them being similar to the ones reported by Zhang, for the coupling of 1,2-epoxydodecane or poly(ethyleneglycol diglycidylether) under solvent-free conditions at  $80^\circ\text{C}$  and 5 MPa (unpublished results). Under those conditions, cyclohexylboronic acid was the most efficient co-catalyst allowing for the epoxide conversion of ~ 80% after 30 min while selectively producing the corresponding cyclic carbonate. Interestingly, in our comparative study, we highlighted that BAs remained less efficient than fluorinated alcohols.

### Silanols

Silanols compounds and more particularly silanediols exhibit excellent hydrogen-bonding capabilities. In 2014, Mattson *et al.* reported one of the only examples of room temperature ( $T = 23^\circ\text{C}$ ) and atmospheric pressure ( $P = 0.1 \text{ MPa}$ ) fixation of  $\text{CO}_2$  onto epoxides (mainly SO and SO derivatives).<sup>149</sup> Using the bicomponent TBAI/silanediol catalyst (Scheme 18 f), the conversion of neat SO reached 93% after

18h whereas the methoxylated silane analogue displayed no co-catalytic activity. Interestingly, optically pure (R)-SO was converted into styrene carbonate in 95% enantiomeric excess attesting for minimal racemization of the initial epoxide. However, whatever the epoxide, very high catalyst loadings (10 mol% silanediol, [TBAI]/[silanediol]= 1) were necessary to achieved high conversion under reasonable time.



Scheme 18: Structure of (multi-hydroxyl) alcohols used as co-catalysts

### Phenol and derivatives

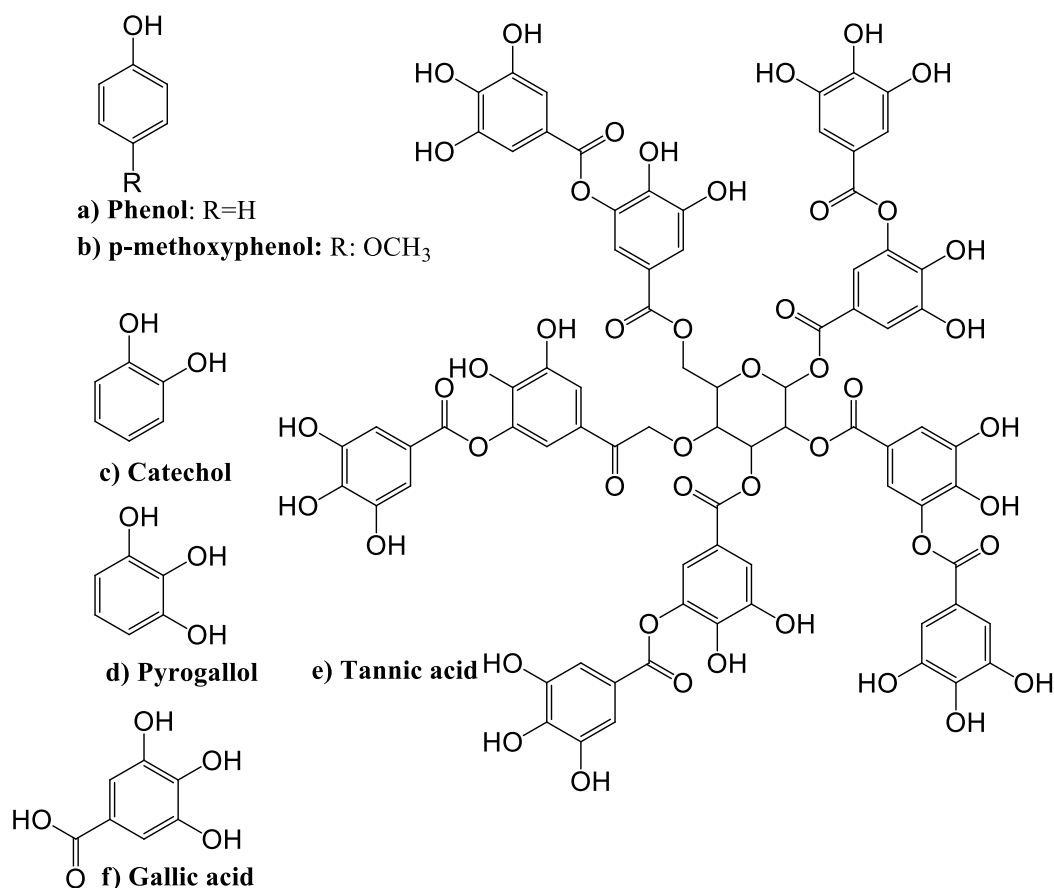
Phenol and derivatives are one of the most widely investigated classes of hydrogen bond donors to accelerate the fixation of CO<sub>2</sub> onto epoxides. Phenol is a moderate activator used in combination with organic bases (DMAP, DBU, NEt<sub>3</sub>...) <sup>150</sup>, ammonium or phosphonium halide salts and triphenylphosphine (Scheme 19 a). <sup>26, 137, 151, 152</sup>

Shen *et al.* highlighted that both the pK<sub>a</sub> of the phenol and the structure of the organic base play important roles in the coupling of PO and others terminal epoxides with CO<sub>2</sub> at 120°C and 3.6 MPa for 24 - 48 h and showed that p-methoxyphenol <sup>150</sup> (Scheme 19 b) and Schiff base <sup>74</sup> used in combination with DMAP or DBU provided effective bicomponent catalytic systems. However, the development of new phenolic derivatives/organic base dual catalysts was limited as more acidic phenol would react with the base by proton transfer and the co-catalytic activity of phenol was poor under mild conditions. <sup>26, 152</sup> This system being far from optimum, Kleij *et al.* developed bicomponent catalysts composed of substituted phenols or multiphenolic derivatives (catechol or pyrogallol, Scheme 19 c and d) with TBAI. Through detailed studies, they correlated the catalytic activity of the bicomponent organocatalyst with the variation of electron withdrawing or attractive substituents in *ortho*-, *meta*- or *para*-position of phenol. Binary catechol or pyrogallol/TBAI systems were powerful catalysts allowing ample substrate scope to be converted into the corresponding cyclic carbonate with yields up to 96% and 100% selectivity under very mild reaction conditions (T = 25 - 45°C, P = 1 MPa) at low catalyst loading (2 - 5

mol%).<sup>26</sup> Interestingly, catechol displays a higher activity and selectivity for the cyclic carbonate formation than two independent phenol units<sup>26, 137</sup> demonstrating that vicinal hydroxyl groups of multiphenolic HBDs allowed stronger interaction by H-bonds with the O atom of the epoxide. These conclusions are supported by Zhang's less detailed similar work that also highlighted that phenolic HBDs were more efficient than alcohols.<sup>137</sup> Tannic acid (TA), a polyphenol composed of 5 catechols and 5 pyrogallols units was tested as HDB in presence of TBAI for the coupling of various terminal and disubstituted epoxides with CO<sub>2</sub> in methylethylketone at 1 MPa (Scheme 19 e).<sup>153</sup> Cyclic carbonates were obtained in good to nearly quantitative yields (9 – 94%) with selectivities higher than 99% using very low TA co-catalyst loading (0.01 – 0.5 mol%). However, temperature of 80°C was required to ensure reasonable solubility of TA in the reaction medium as it was assumed that under lower temperature, the solvent is not able to break up intra- and inter-molecular hydrogen bonds of TA. Interestingly, at same low co-catalyst loading of 0.03 or 0.15 mol%, the activity of the TBAI/TA system was higher than the one reported for TBAI/pyrogallol and TBAI/catechol. Unfortunately, at temperature higher than 80°C, pyrogallol and TA deactivate by reaction with TBAI and the epoxide to form unreactive ammonium phenolate salt and a halohydrin species.<sup>153-155</sup>

In addition, gallic acid (Scheme 19 f), a pyrogallol analogue displaying an additional carboxylic acid group, was one of the most efficient HDB under mild conditions at very low loading.<sup>152</sup> In their rational investigation, Tassaing *et al.* showed that under similar conditions (T = 60°C, P = 2 MPa, t = 4h), the PC yield was significantly higher with the gallic acid/TBAI catalytic system (95%) than the pyrogallol/TBAI one (82%). However, as reported for tannic acid, the carboxylic acid-functionalized pyrogallol was no more soluble in PO for loadings higher than 1 mol%.

If PPh<sub>3</sub> displays no catalytic activity (except for the conversion of epichlorhydrin<sup>151</sup>), addition of NaI allowed for the direct incorporation of CO<sub>2</sub> into poly(glycidyl methacrylate).<sup>156</sup> It turns out that the activity of this binary system arises from the *in-situ* formation of a  $\beta$ -hydroxyl triphenylphosphonium salt and could be enhanced by addition of phenol.<sup>151</sup> Huang *et al.* reported that the tri-component system NaI/PPh<sub>3</sub>/PhOH effectively catalysed and fastened the fixation of CO<sub>2</sub> onto PO in 4h at 120 °C and 4 MPa with selective formation of PC.



Scheme 19: Structure of (multi-) phenolic derivatives co-catalysts

### Carboxylic acids

Carboxylic acids were rarely and sparsely reported as potential HBDs as  $\beta$ -hydroxy ethers and esters are produced by ring-opening with epoxides.<sup>157</sup> Only traces of PC were formed with the TBABr/acetic acid system because of the conversion of PO into ring-opened products.<sup>137</sup> In contrast, PC was synthesized with good yields and selectivity using bifunctional systems composed of acetic acid and HO-C2-MImBr, imidazole or pyridine.<sup>79, 125</sup> Fast and selective synthesis of cyclic carbonates from allyl glycidyl ether and other various epoxides were developed at 1 MPa by combining KI/formic acid catalyst and microwave irradiations.<sup>158</sup> The co-catalytic activity of carboxylic acids was found dependent on the alkyl chain length and decreases in the order  $\text{HCOOH} > \text{CH}_3\text{COOH} > \text{C}_2\text{H}_5\text{COOH} > \text{C}_3\text{H}_7\text{COOH}$  and much more superior than the one of the analogue alcohol. The high catalytic efficiency of carboxylic acid probably arises from the effective polarization of the carboxylic acid co-catalysts under microwaves allowing them to interact strongly with the epoxide through H-bonding resulting in higher epoxides conversion.

### Aminoalcohols

Series of aminoalcohols were explored as potential HBDs to fasten the coupling of epoxides with CO<sub>2</sub>. Synergistic effects between TBAI and pyridinemethanol (Scheme 20 a) allowed to convert epichlorhydrin in good yield (up to 92%) under ambient

conditions ( $T = 25^{\circ}\text{C}$ ,  $P = 0.1\text{ MPa}$ ) at high catalyst loading of 8 mol% whereas low conversion of 26% was reached in the absence of co-catalyst.<sup>159</sup> The importance of the N atom of pyridinemethanol on the activation was highlighted by a decrease of the epichlorohydrin conversion using the benzylalcohol/TBAI catalyst. The use of the pyridinemethanol/TBAI catalyst was successfully extended to the selective conversion of terminal, internal and enantiomerically pure epoxides with moderate to excellent yields (15 - 97%) and enantiomeric excess higher than 94%.

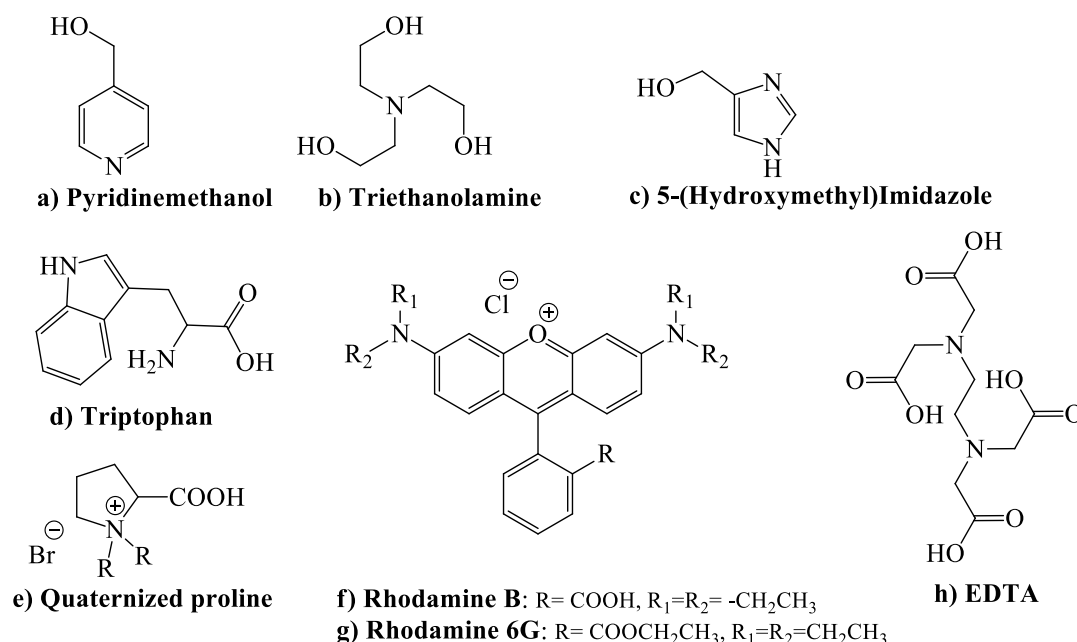
The catalytic activity of KI was dramatically enhanced by addition of aminoalcohols for the fixation of  $\text{CO}_2$  onto various epoxides at  $90^{\circ}\text{C}$  and 1 MPa.<sup>160, 161</sup> Notably, the co-catalytic activity slightly evolved with the length of the alkyl chain between the amino and the OH group in the order 1,2-aminoethanol < 1,3-aminopropanol < 1,5-aminopentanol to reach a maximum yield of 88% after 3h. Consistently with Roshan's study<sup>130</sup>, Werner *et al.* found that triethanolamine (Scheme 20 b) was the most efficient co-catalyst with a 1,2-epoxybutane conversion of 98%<sup>161</sup> which highlights the beneficial effect of increasing the number of hydroxyl groups and substituent of the amine (ethanolamine < diethanolamine < triethanolamine) on the co-catalytic activity.<sup>160</sup> Both amino and hydroxyl groups played an important role in optimizing the reaction. Under strictly identical experimental conditions, the triethanolamine/KI system exhibited lower performance than 4- or 5-(hydroxymethyl)imidazoles (Scheme 20 c).<sup>162</sup> Werner suggested that the better catalytic performances of hydroxyl-functionalized imidazoles/KI system arose from the *in-situ* formation of imidazolium IL in presence of water and  $\text{CO}_2$  (with potassium carbonate by-product formation) that acts as catalyst.

### Amino acids

By virtue of their acidic and basic hydrogen bonding groups, AAs induce synergism with alkali halide salts, especially KI, facilitating the selective formation of PC from PO/ $\text{CO}_2$  cycloaddition at  $120^{\circ}\text{C}$  and 1 MPa.<sup>105</sup> The co-catalytic activity of AAs depends on their inherent charge, polar/non polar nature and decreases in the order: basic AAs > neutral AAs with polar side chains > acidic AAs ~ neutral AAs > neutral AAs with hydrophobic amino acid chain. As reported for AAs single component catalysts, histidine was the most efficient co-catalyst enabling PO conversion up to 99% after 3h. According to Yang *et al.*<sup>163</sup>, tryptophan (Scheme 20 d) was even more efficient than histidine but this result is in contradiction with Roshan's study.<sup>105</sup> The necessary role played by the functional groups of AAs co-catalysts in promoting the epoxide/ $\text{CO}_2$  coupling was highlighted by comparing the activity of L-tryptophan with the one of analogues which chemical structure differs by the (partial) absence of  $\text{COOH}$ ,  $\text{NH}_2$  or  $\text{NH}$  functional groups. Yang showed that the co-catalytic performance evolved in the order: L-tryptophan > 3-indolepropionic acid > indole > 1-methylindole. It may be noted that compared to amino alcohols, the use of a bifunctional AAs/KI catalyst didn't allow to promote the reaction in milder conditions ( $T > 120^{\circ}\text{C}$ ) even if it enabled to shorten the reaction time.

Even though the neutral L-proline was not evaluated in Yang or Roshan's studies, quaternized proline (by 1-bromobutane, Scheme 20 e) associated with  $\text{NEt}_3$ , DMAP or DBU catalyses the selective styrene carbonate synthesis at 90 °C under atmospheric pressure with reasonable yields (75 to 83%) after 24h.<sup>164</sup> Under comparable experimental conditions, rhodamine B, a chlorine ammonium salt possessing both carboxylic acid and tertiary amino group (Scheme 20 f) displayed identical activity than quaternized proline when used in combination with  $\text{Net}_3$ .<sup>165</sup> Whatever the organic base, SO conversion was somewhat enhanced to ~ 94% by replacing quaternized proline or rhodamine B by rhodamine 6G, a chlorohydrate analogue salt with 2 secondary amines and no carboxylic acid (Scheme 20 g). If the  $\text{Cl}^-$  anion of Rhodamines 6G was less nucleophile than the bromide anion of the quaternized proline, the higher co-catalytic activity of this co-catalyst was explained by the presence of secondary amino groups interacting with the epoxide by H-bonds.<sup>165</sup>

Recently, Liu *et al.* postulated that molecules with multiple carboxylic groups more effectively activate epoxides through multi-sites hydrogen bonding than monofunctional activators. By employing a TBABr/Ethylenediaminetetraacetic acid (EDTA, Scheme 20 h) as dual catalytic platform, the coupling of epoxides with  $\text{CO}_2$  proceeded under mild conditions ( $T = 70^\circ\text{C}$  and  $P = 0.5 \text{ MPa}$ ) and reached a quantitative yield after 24h.<sup>166</sup> Above  $70^\circ\text{C}$ , EDTA decomposed preventing the authors to evaluate the catalytic performances of the binary system at higher temperatures. These results highlight synergisms between the four carboxylic acids of the amino acid and the bromine anion of TBABr.



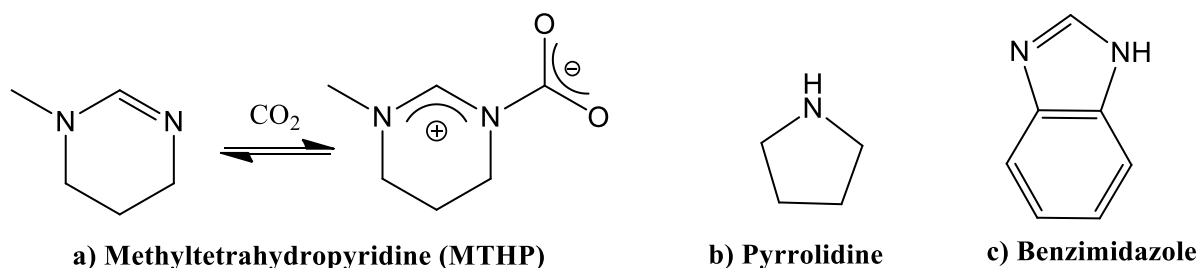
Scheme 20: Structure of aminoalcohols and amino acids co-catalysts

### II-3-c) Aliphatic and cyclic amines and their derivatives

The catalytic efficiency of amines and amidines superbases could be enhanced by the addition of KI, I<sub>2</sub> or other nucleophilic co-catalysts.<sup>83, 162, 167-169</sup>

Ramidi *et al.* explored the synergistic influence of various organic bases/alkali metal salts bifunctional catalysts on various substrates at 130°C and 2 MPa.<sup>167</sup> The most efficient catalytic platform was identified as LiBr/DMAP. The results indicate that the catalyst activity ( $\text{Li}^+ > \text{Na}^+ > \text{K}^+$ ) is inversely related to the size of the alkali metal ions ( $\text{Li}^+ < \text{Na}^+ < \text{K}^+$ ) which is correlated with the higher Lewis acidity of Li<sup>+</sup>, compared to Na<sup>+</sup> and K<sup>+</sup> and related i) to the higher basicity of DMAP compared to triethylamine or pyridine or ii) the less bulkiness and the nucleophilicity of the nitrogen atom. A similar strategy was reported by Endo *et al.* to promote the quantitative conversion of epoxides under ambient temperature and atmospheric pressure using LiBr in combination with N-methyltetrahydropyrimidine (MTHP, Scheme 21 a) as organic base that activates CO<sub>2</sub>.<sup>168</sup> However, very high catalyst loadings (25 mol% LiBr and 10 mol% MTHP) and a solvent (N-methylpyrrolidone) were required for the reaction to proceed in homogeneous conditions and reasonable time.

Then, Werner *et al.* compared the co-catalytic activity of linear and cyclic amines with KI for the conversion of 1,2-butylene oxide into cyclic carbonate at 90°C and P = 1 MPa.<sup>162</sup> The screening highlighted that cyclic amines such as pyrrolidine (Scheme 21 b) and DBU were more efficient than aliphatic ones but the catalyst performances were significantly enhanced using aromatic amines such as imidazole and benzimidazole (Scheme 21 c) that afforded cyclic carbonate yields higher than 96% after 3h. The same group also applied the concept of convergent activation to facilitate the CO<sub>2</sub>/epoxides coupling by using suitable carbene catalysts activating CO<sub>2</sub> and KI co-catalyst complexed by 18-crown-6 interacting with the epoxide.<sup>83</sup> The carbene/KI/18-crown-6 tricomponent catalyst allowed converting various epoxides with moderate to excellent yields (34 – 91%) at 100°C and 1 MPa within 3h but its activity drastically dropped at higher pressures. This detrimental CO<sub>2</sub> pressure effect might be explained by a dynamic equilibrium between CO<sub>2</sub>, the free carbene and the corresponding carboxylated adduct that is shifted towards the formation of the unreactive imidazolium-2-carboxylate upon high CO<sub>2</sub> pressure.



Scheme 21: Structure of methyltetrahydropyrimidine a), pyrrolidine b) and benzimidazole c) co-catalysts.



Coulembier *et al.* reported on a DBU/I<sub>2</sub> cooperative catalyst that afforded high and selective conversion (96%) of 1,2-epoxybutane after 4.75h under mild conditions (T = 65°C, P = 0.1 MPa).<sup>169</sup> Indeed, as already mentioned, DBU is able to activate CO<sub>2</sub> to form an adduct while iodine activates the cyclic ether by formation of a charge transfer complex.

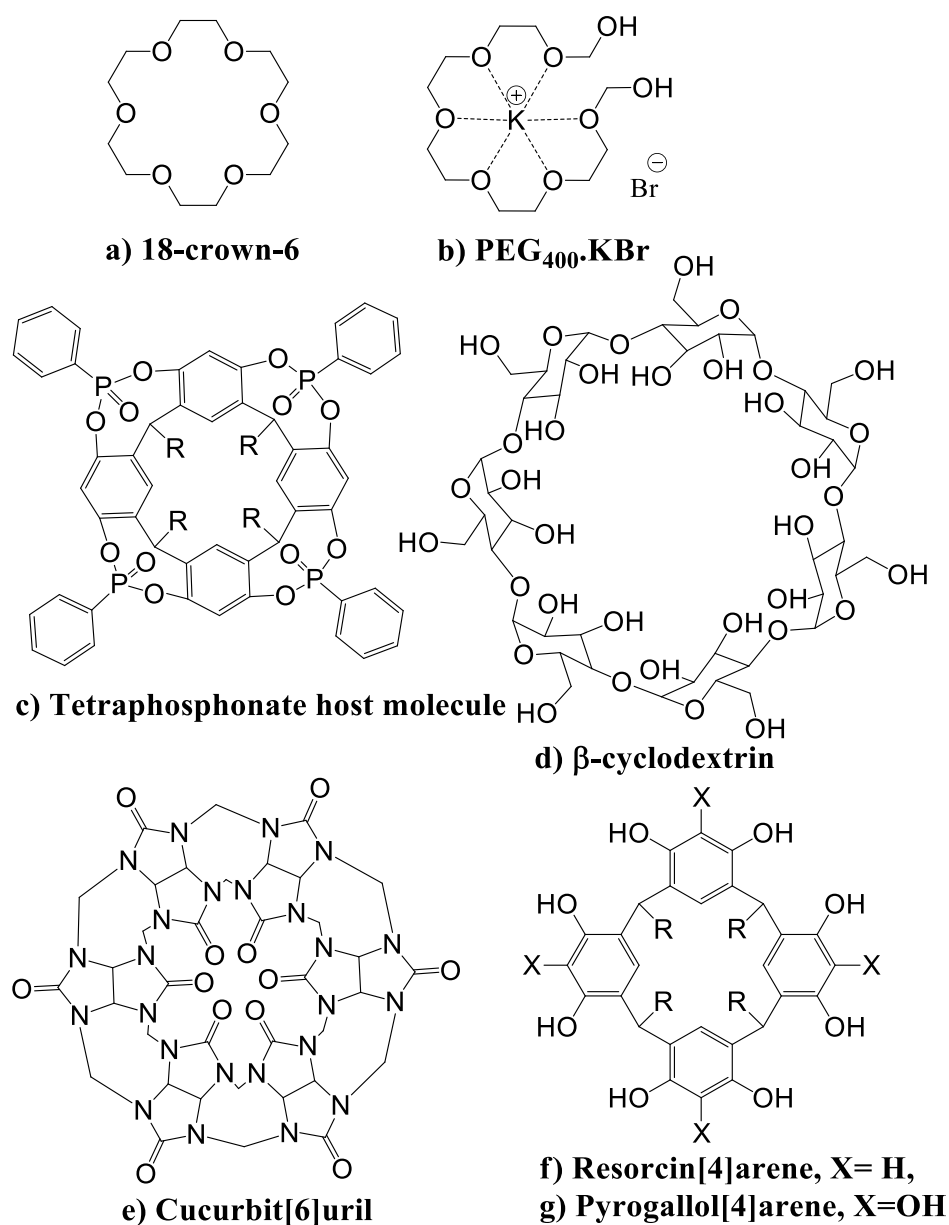
### II-3-d) Crown ethers, (poly)ethers and cavitands

Crown ethers such as 15-crown-5 or 18-crown-6 and polyethers enhanced the catalytic activity of alkali metal halides and carbonate salts. For the CO<sub>2</sub>/epichlorhydrin coupling (T = 120°C, P = 4 MPa), the catalytic performances of the bicomponent catalyst composed of alkali metal and crown ethers increased with the cation size in the order Li<sup>+</sup> < Na<sup>+</sup> < K<sup>+</sup> and yields reached almost 100% even with a poor nucleophilic anion such as CO<sub>3</sub><sup>2-</sup>.<sup>170</sup> By using KI in combination with 18-crown-6 (Scheme 22 a), various epoxides were converted into cyclic carbonates with moderate to good yields (25 – 97%) after 4h at 120°C and 4 MPa. Besides, similarly to crown ethers, Kumar *et al.* exploited  $\alpha,\omega$ -hydroxyl telechelic polyethylene glycol (PEG<sub>400</sub>) to chelate the potassium cation of KBr and activate the oxygen atom of the epoxide by hydrogen bond interactions with the OH chain ends (Scheme 22 b).<sup>171</sup> This catalytic system was efficient under mild temperature (T = 60°C) and atmospheric pressure for converting various substrates within 1.5 to 6h with yields above 93%. It may be noted that the pre-synthesized PEG<sub>400</sub>/KBr complex was more efficient than the use of the KBr/PEG<sub>400</sub> bifunctional catalyst. Let's also briefly mention that, even if it doesn't consist of bicomponent catalyst, fluorethers were used as solvent in combination with ammonium salts to enhance the solubility of CO<sub>2</sub> in the epoxide and fasten the coupling under low pressure (0.1 – 0.5 MPa) at 80°C.<sup>172</sup>

As crown ethers, cavitands are (macro)cyclic molecules with a cavity able to accommodate a guest molecule or a cation. Bowl-shape tetraphosphonates cavitands (Scheme 22 c) have been reported as suitable receptors for the tetraalkylammonium halide recognition by host-guest association.<sup>173</sup> The affinity towards cations arises from the strong donating capability of the four inward (i) oriented P=O phosphoryl groups towards the nested cationic species, ii) the potential strong hydrogen bonds, and the cooperative effect of the aromatic cavity in forming cation-CH  $\pi$ - $\pi$  interactions. Me<sub>4</sub>N<sup>+</sup>/cavitand inclusion complex provided efficient charge separation increasing the nucleophilicity, thus the activity of iodide anion. By using this binary catalyst, the SO conversion reached 92% in 24h at 1 MPa and 100°C whereas only traces of styrene carbonate were obtained without host molecules. However, the catalytic activity was affected by the tetraphosphonates cavitands structure as the halide anion can be located in-between the substituents at the narrow rim of the host with dramatic effect on the ion-pair breaking especially when cavitands with long alkyl chain are used. Therefore, the host-guest chemistry was extended to the wrapping of epoxides instead of the cation into the cavities.  $\beta$ -cyclodextrin ( $\beta$ -CD), a cyclic oligosaccharide with 7 glucose units (Scheme 22 d), encapsulates and activates epoxides *via* hydrogen bonds which facilitates their coupling with CO<sub>2</sub>.<sup>174</sup>  $\beta$ -CD used

in combination with KI enables a 4-fold increase of the PO conversion (conv. = 97% in 4h) at 120°C and 6 MPa compared to similar reactions promoted by KI as sole catalyst (conv. = 27%). Under relatively similar experimental conditions ( $T = 120\text{ }^{\circ}\text{C}$ ,  $P = 4\text{ MPa}$ ), cucurbit[6]uril (CU6, Scheme 22 e), a six glycoluril units cyclic oligomer, displayed slightly higher co-catalytic activity than  $\beta$ -CD as evidenced by a complete conversion of PO in 2h at lower catalyst loading (1.5 instead of 2.5 mol%).<sup>175</sup> These higher co-catalytic performances were assigned to the simultaneous inclusion of epoxides into the rigid hydrophobic cavity of CU6 and additional interactions of the potassium cation with the carbonyl groups of the macrocycle increasing the nucleophilicity of the halide salt. Interestingly, the activity of both KI/cavitand systems didn't decrease when considering the conversion of terminal sterically hindered epoxides such as SO.

In an effort to improve both the thermal/chemical stability and the co-catalytic activity of phenolic HBDs, Kleij *et al.* developed polyphenolic cavitands derived from resorcinol and pyrogallol.<sup>155</sup> They illustrated that the preorganization of the phenolic units within the cavitand structures by modulating the length of the R-alkyl chains was beneficial for optimizing the catalytic efficiency of both resorcin[4]- and pyrogallol[4]arenes (Scheme 22 f and g). Cooperative catalytic effects between onium salt and resorcin[4]arenes and pyrogallol[4]arenes cavitands with nonyl alkyl chains were reported under mild experimental conditions ( $50^{\circ}\text{C} < T < 80^{\circ}\text{C}$ ,  $P = 1\text{ MPa}$ ) for the coupling of various terminal, internal or enantiomerically pure substrates with  $\text{CO}_2$  in methylethylketone (conversion from 44 up to 99% with full retention of the configuration). Even though pyrogallol was a more efficient HBD than resorcinol, TBAI/resorcin[4]arenes bicomponent system performed better than the binary TBAI/pyrogallol[4]arene catalyst. As pyrogallol is more acidic, pyrogallol-based cavitand undergoes easier deprotonation than resorcinol units, especially under harsher temperature conditions ( $T = 80^{\circ}\text{C}$ ), decreasing its ability to activate epoxide through H-bonds and thus, the lifetime of the catalyst. A second reason for such a lower activity could be found in the more facile self-assembly of pyrogallol-based cavitands into hexamers. Interestingly, under harsher temperature conditions ( $80^{\circ}\text{C}$ ), both cavitands retained their activity after prolonged used compared to pyrogallol/TBAI (or resorcinol/TBAI) simple systems for which the epoxide conversion reached a plateau at  $\sim 70\%$  after few hours.



Scheme 22: Structure of crown ethers, (poly)ethers and cavitands used as co-catalysts

## II-4. Mixed homogeneous/heterogeneous organocatalysts

The CO<sub>2</sub>/epoxide coupling was also illustrated using binary “mixed” catalysts composed of one component soluble in the CO<sub>2</sub>/epoxide phase, generally a halide salt and a heterogeneous hydrogen bond donor. Thus, the reaction occurs at the liquid-solid interface generally *via* a solid/liquid interfacial hydrogen-bond assisted mechanism. In this last paragraph, solid supports with surface active sites such as silica or catalysts/HBDs immobilized onto polymers are not described.

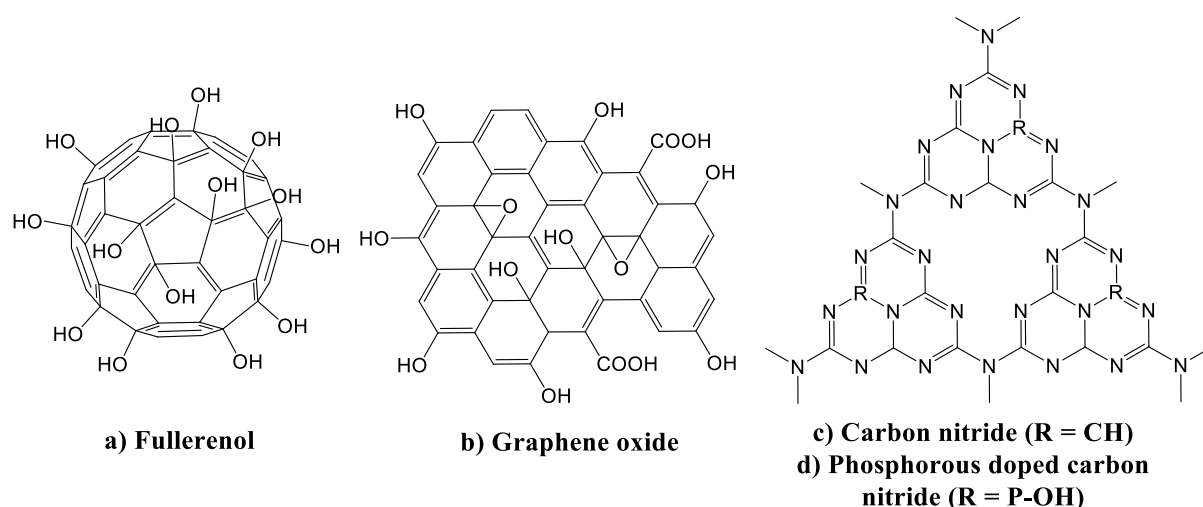
### II-4-a) Oxides of carbon and carbon nitrides

Series of carbon-based materials have been reported to enhance the catalytic properties a series of organocatalysts. Stable fullerenol, an oxidized fullerene C<sub>60</sub> molecule bearing up to forty hydroxyl groups per molecule (Scheme 23 a), promoted the CO<sub>2</sub>/epoxide coupling in the presence of KI.<sup>176</sup> This binary system was very effective for the coupling of various terminal epoxides or cyclohexene oxide at 120°C and 2 MPa, affording the corresponding cyclic carbonate with high yields comprised between 89 - 99% in reaction time of 3 – 24h. However, the catalyst activity was influenced by the temperature and significantly decreased below 120°C. Additionally, while fullerenol has a cage structure, encapsulation of small molecules was not observed.

Graphite oxide (GO) is a carbon material functionalized with hydroxyl and carboxylic acid (and even epoxide) groups that interacts and activates the epoxide (Scheme 23 b). Luo *et al.* and Lan *et al.* respectively illustrated that the inherent Brønsted acidic groups of the graphite oxide and the halide anion of imidazolium and pyridinium based ILs with C<sub>n</sub>-MImX structure (n = 2 or 4 and X = I<sup>-</sup>, Br<sup>-</sup>, Cl<sup>-</sup>, PF<sub>6</sub><sup>-</sup> or BF<sub>4</sub><sup>-</sup>)<sup>177</sup> or onium salts<sup>178</sup> exhibited synergistic effect in promoting the epoxide/CO<sub>2</sub> coupling. At pressures of 0.1 – 1 MPa and temperatures of 50 - 135°C, cyclic carbonates yields evolved with the cation nature in the order C<sub>4</sub>-Py<sup>+</sup> < TBA<sup>+</sup> < C<sub>2</sub>-MIm<sup>+</sup> to reach 95% with C<sub>4</sub>-MImBr. The styrene carbonate yield was found twice superior by using the mixed GO/C<sub>4</sub>-MImBr system compared to carbon nanotube or graphite-based catalysts as a result of the higher OH and COOH functionalities content. The efficiency of the mixed GO/C<sub>4</sub>-MImBr catalyst was slightly improved without compromising the selectivity i) by using graphene oxide, the exfoliated form of graphite oxide, as it exhibits higher surface area and active sites<sup>177, 178</sup> or ii) by addition of water. Indeed, the dispersion of GO is better in H<sub>2</sub>O than in neat PO and reaction between water and GO increases the amount of acidic functional groups on the surface.<sup>179</sup>

Mesoporous graphitic carbon nitrides (g-C<sub>3</sub>N<sub>4</sub>) are carbon material possessing in their structures nitrogen atoms able to activate CO<sub>2</sub> (Scheme 23 c). Ansari *et al.* were the first to exploit g-C<sub>3</sub>N<sub>4</sub> in combination with DMF to synthesize PC from PO and CO<sub>2</sub>. However, the activity of this catalytic system was far from being optimal as

attested by PC yields lower than 34% and selectivities between 92 and 98% obtained after 10h for reactions performed at 100°C and 0.55 MPa.<sup>180</sup> Many strategies were developed to improve the activity of g-C<sub>3</sub>N<sub>4</sub> i) by increasing their surface area <sup>181</sup>, ii) by improvement of defect sites <sup>182</sup>, and iii) by immobilizing functional groups <sup>183</sup>. Unfortunately, none of these approaches gave satisfactory results. Recently, Lan *et al.* developed a catalytic system composed of TBABr and phosphorous doped graphitic carbon nitride prepared by thermolysis of melanine and hexachlorotriphosphazene, urea or dicyandiamide (Scheme 23 d).<sup>184</sup> The modified solid HBDs combine basic amino groups able to activate CO<sub>2</sub> and P-OH acidic sites interacting with the epoxide and offer synergism with the nucleophilic anion for facilitating the CO<sub>2</sub>/PO coupling under mild conditions. This doped catalytic system was significantly more efficient than TBABr/mesoporous carbon nitride <sup>183</sup> as complete PO conversion was achieved within 4h at 100°C and 2 MPa without formation of by-products.



Scheme 23: Structure of oxides of carbon and carbon nitrides co-catalysts

## II-4-b) Biopolymers

Biopolymers such as cellulose, lignin, chitosan, polydopamine... possess (complex) chemical structures characterized by the presence of multiple hydroxyl, amino and carboxylic acid groups, making them valuable solid HBDs for the coupling of CO<sub>2</sub> with epoxides.

### *Microcrystalline cellulose*

Cellulose, a poly(D-glucose), promoted the epoxide/CO<sub>2</sub> coupling in the presence of alkali halide salts <sup>142, 185</sup>, C2-MImBr <sup>186</sup> or organic bases such as DBU, DMAP, TBD... <sup>75</sup> This abundant carbohydrate polymer, rich in vicinal OH groups, activates the epoxide through formation of a seven-membered ring (Scheme 24 a) and facilitates the selective fixation of CO<sub>2</sub> onto PO (or other various epoxides) above 110°C and 2 MPa as evidenced by PC yields of 75-100% in less than 2h and without formation of by-products. However, the cellulose/KI binary catalyst was slightly less efficient than the most performant cellulose/DBU system under relatively similar conditions.

Through a detailed screening, the catalytic efficiency of the dual cellulose/strong base system decreased in the order DBU > DMPA > DABCO > MIm > Im > MTBD > TBD which doesn't strictly respect the pKa value order indicating that both the basicity and the steric hindrance of the catalyst are key factors to promote the reaction. It may be noted that the PC yields dropped using acetylated methyl iodide-quaternized cellulose demonstrating how secondary vicinal hydroxyl groups are crucial to fasten the reaction.<sup>185</sup>

### *Chitosan*

Chitosan is a polysaccharide composed of acetylated and non-acetylated D-glucosamine units (Scheme 24 b). The substitution of the primary OH groups of cellulose by amino groups in chitosan was beneficial for improving the catalyst activity.<sup>185, 186</sup> In a comparative study, Sun *et al.* showed that the PC yield was higher with the chitosan/C2-MImBr catalytic system (80%) than with the cellulose/C2-MImBr (75%).<sup>186</sup> The better performances of chitosan co-catalyst were assigned to the additional nucleophilic activation of CO<sub>2</sub> by the amino groups of the biopolymer. However, in opposition to Sun's observations, the performances of a dual mixed chitosan/DBU catalyst decreased compared to the cellulose/DBU system. Finally, Boutevin *et al.* recently reported on the use of chitosan functionalized by both carboxylic acid and quaternary ammonium chloride moieties in combination with KI.<sup>187</sup> If this binary mixed catalyst seems efficient for synthesizing various cyclic carbonate with yields of 81 – 100 % and 100% selectivity at 80°C and 0.7-1.2 MPa, it is impossible to evaluate how the supported ammonium or the free K<sup>+</sup> cations and the possible exchange of Cl<sup>-</sup> and I<sup>-</sup> anions affects the performances of the catalysts.

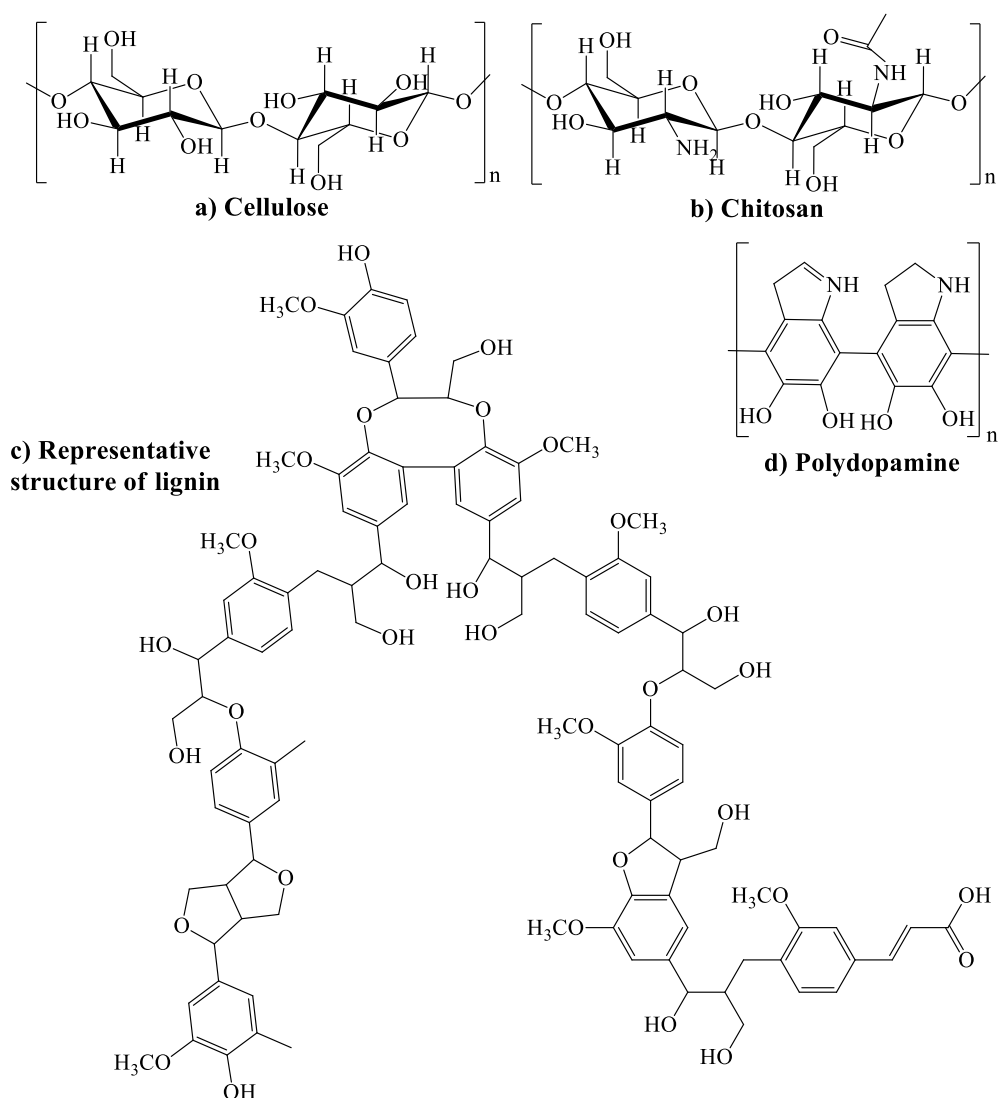
### *Lignin*

Enzymatic hydrolytic lignin from corn stover is a multiphenolic cross-linked polymer (Scheme 24 c) that could fasten the CO<sub>2</sub>/epoxide coupling with KI.<sup>188</sup> However, the chemical composition of lignin varies depending on the vegetal species. Surprisingly, lignin was found less active than cellulose whereas simple multiphenolic compounds such as pyrogallol or catechol were more efficient than aliphatic alcohols. The lower co-catalytic activity of lignin compared to cellulose or chitosan might probably arise from the lower amount of vicinal hydroxyl groups. Harsher temperature of 140°C and pressure between 1 and 4 MPa were required to obtain satisfactory propylene carbonate yields (above 63%) in 12h. Despite the low activity of the lignin/KI system, other cyclic carbonates were produced with good to excellent yields from various terminal epoxides. Besides, sugarcane bagass, one of the largest agricultural waste derived from the sugarcane industry, is composed of cellulose (40 - 50%), hemicellulose (25 - 30%) and lignin (20 - 25%) and is consequently rich in hydroxyl and phenolic groups. Thus, in line with cellulose and lignin catalytic performances, bagass/KI was able to promote the epoxide/CO<sub>2</sub> coupling at 120°C and 2 MPa within 6 h affording PC or various cyclic carbonates in yields higher than 82%. As expected

regarding to the bagass structure and composition, the activity of the bagass/KI system was found intermediate between the cellulose/KI and lignin/KI catalysts.

### *Polydopamine*

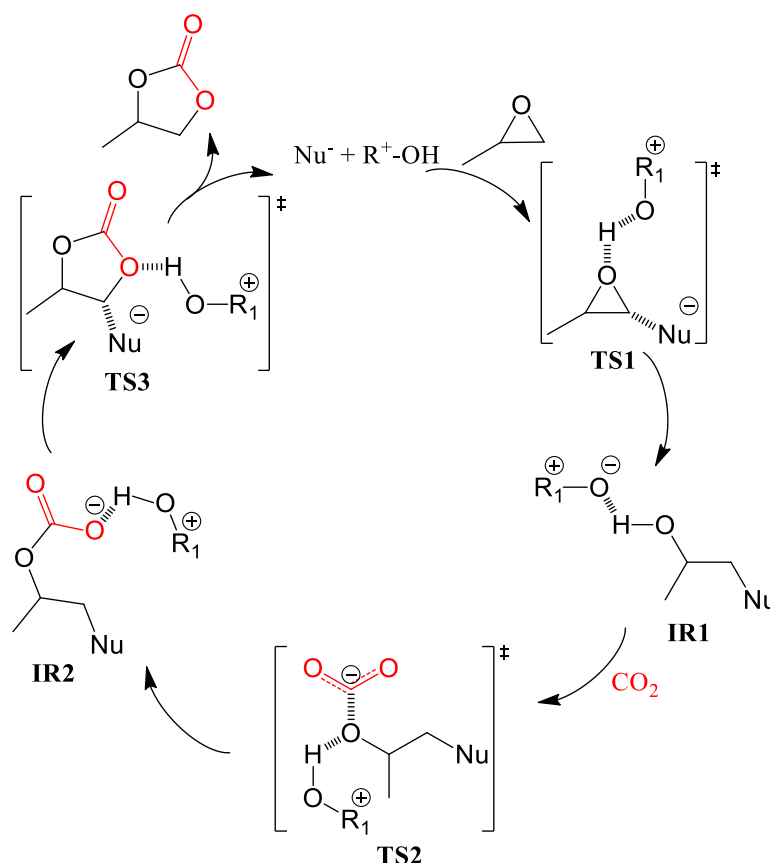
Inspired by the composition of adhesive proteins secreted by mussels, nanosized polydopamine beads were prepared by polymerization of catecholamine and tested as catalysts in the presence of KI for the selective synthesis of cyclic carbonates (Scheme 24 d).<sup>189</sup> A synergism was found between the Lewis base character of the halide anion of KI and the Lewis acidity of polydopamine as evidenced by a ~15-fold increase of the PO conversion at 120°C and 2 MPa after 1h compared to the reference reaction using KI as sole catalyst. However, this mixed system is much less efficient than the TBAI/catechol homogeneous catalyst that promotes the coupling of CO<sub>2</sub> with epoxide under much milder conditions (T = 25-45°C, P = 1 MPa).<sup>26</sup>



Scheme 24: Structure of the bio-based Hydrogen-Bond Donors co-catalysts

## II-5. Mechanistic study of functionalized single catalysts or bicomponent catalysts

In-depth mechanistic studies illustrate how the cooperative effect of the halide anion and the functional group(s) of single component or binary catalysts facilitates the CO<sub>2</sub>/epoxide coupling. The favoured reaction pathway respects a three-step activation mechanism involving the epoxide ring-opening, the CO<sub>2</sub> insertion and the carbonate ring-closure (Scheme 25).<sup>97, 101-103, 105, 117, 118, 125, 130, 137, 147</sup>



Scheme 25: General activation mechanism with functional single or binary catalysts (represented as R-OH)

For all catalytic systems, DFT calculations evidenced the important role played by single or multiple hydrogen bonding in the strong activation of epoxides and stabilization of all reactive intermediates (IR) and transition states (TS). This interaction decreases the Gibbs energy of most IR and TS and consequently decreases the activation barriers. Water, alcohols, vicinal diols, (multi)phenolic compounds and carboxylic acids respond to a similar mechanism. In a representative example, Wang *et al.* highlighted that the OH group on the N atom or the C2 atom of hydroxyl-functional imidazolium interacts by H-bonds with the O atom of the epoxide.<sup>97, 103, 118</sup> Then, simultaneously, the ring opening of the epoxide by nucleophilic attack of the halide anion (TS1) and the migration of the proton of the OH group towards the O atom of the epoxide form a first stable halohydrin intermediate (IR1). Then, the second step involves the concerted carbon dioxide insertion and the migration of the



proton back from the halohydrin towards the catalyst (TS2). An acyclic carbonate in interaction with the hydroxyl-functionalized IL by H-bonds is formed as IR2. Finally, the carbonate ring-closure assisted by the OH group of the catalyst and the halide-C bond rupture form the cyclic carbonate and regenerate the catalyst. The Gibbs energy of the reaction is decreased by 7 kcal.mol<sup>-1</sup> compared to the non-functionalized IL.<sup>103</sup>

Interestingly, by replacing the OH group of monocomponent functional imidazolium catalyst by a more acidic COOH substituent, Wang *et al.*<sup>122</sup> highlighted by DFT calculations that the activation barrier is slightly lower for the carboxylic acid-functionalized ILs (16.27 kcal.mol<sup>-1</sup>) than for the hydroxyl-functionalized one (16.80 kcal.mol<sup>-1</sup>).<sup>97</sup> In addition, the NBO analysis showed that shortening the N-alkyl chain bearing the COOH group of the imidazolium ring has a detrimental effect on the catalytic activity. This observation, correlated with experimental data, is explained by the simultaneous increase of the charge of the proton on the C2 atom and the decrease of the negative charge of the halide that consequently decreases its nucleophilic character.

For water/TBABr binary catalyst, the stabilisation of the O atom of the epoxide by interaction by H-bonds with water (Figure 2 a) makes the cycloaddition easier by decreasing the activation barriers of 8 kcal.mol<sup>-1</sup> compared to the reaction catalysed by TBABr.<sup>137</sup> It may be noted that in this mechanism, the CO<sub>2</sub> insertion occurred without energy barrier.

By using (multi)phenolic co-catalysts, Kleij *et al.* showed that the activation barrier decreased with the number of OH group in the following order: phenol (1 OH) > catechol (2 OH) > pyrogallol (3 OH).<sup>26</sup> Phenol and catechol typically respect the same reaction mechanism than alcohols functionalized ILs. The acidic proton of phenolic derivatives is transferred to the oxygen atom of the epoxide simultaneously with the epoxide ring-opening by the halide attack to form the halohydrin. Notably, pyrogallol activates epoxides and stabilizes the IRs and TSs by multiple hydrogen bonds. The proton of the central hydroxyl group was transferred to the epoxide (Figure 2 b) creating a halohydrin (IR1) which OH group was stabilized by a second OH group from pyrogallol. The third OH group of pyrogallol stabilized the oxygen atom of the phenoxide anion through an intramolecular H-bond. Tassaing *et al.*<sup>101</sup> found that pyrogallol also stabilized the halocarbonate (IR2) formed after the CO<sub>2</sub> insertion and TS3 after the rotation of the halocarbonate. The Gibbs energy of the reaction was lowered by 26 kcal.mol<sup>-1</sup> with pyrogallol compared to the one with TBABr as sole catalyst. Consequently, this detailed mechanism highlights the origin of the higher efficiency of co-catalysts with vicinal hydroxyl groups. The same activation mechanism was proposed with the HO-C2-BImBr/ethylene glycol (EG) bifunctional system.<sup>125</sup> Indeed, EG interacts with the O atom of the epoxide by two hydrogen bonds while the hydroxyl-functionalized imidazolium stabilized one O atom of EG (Figure 2 c).

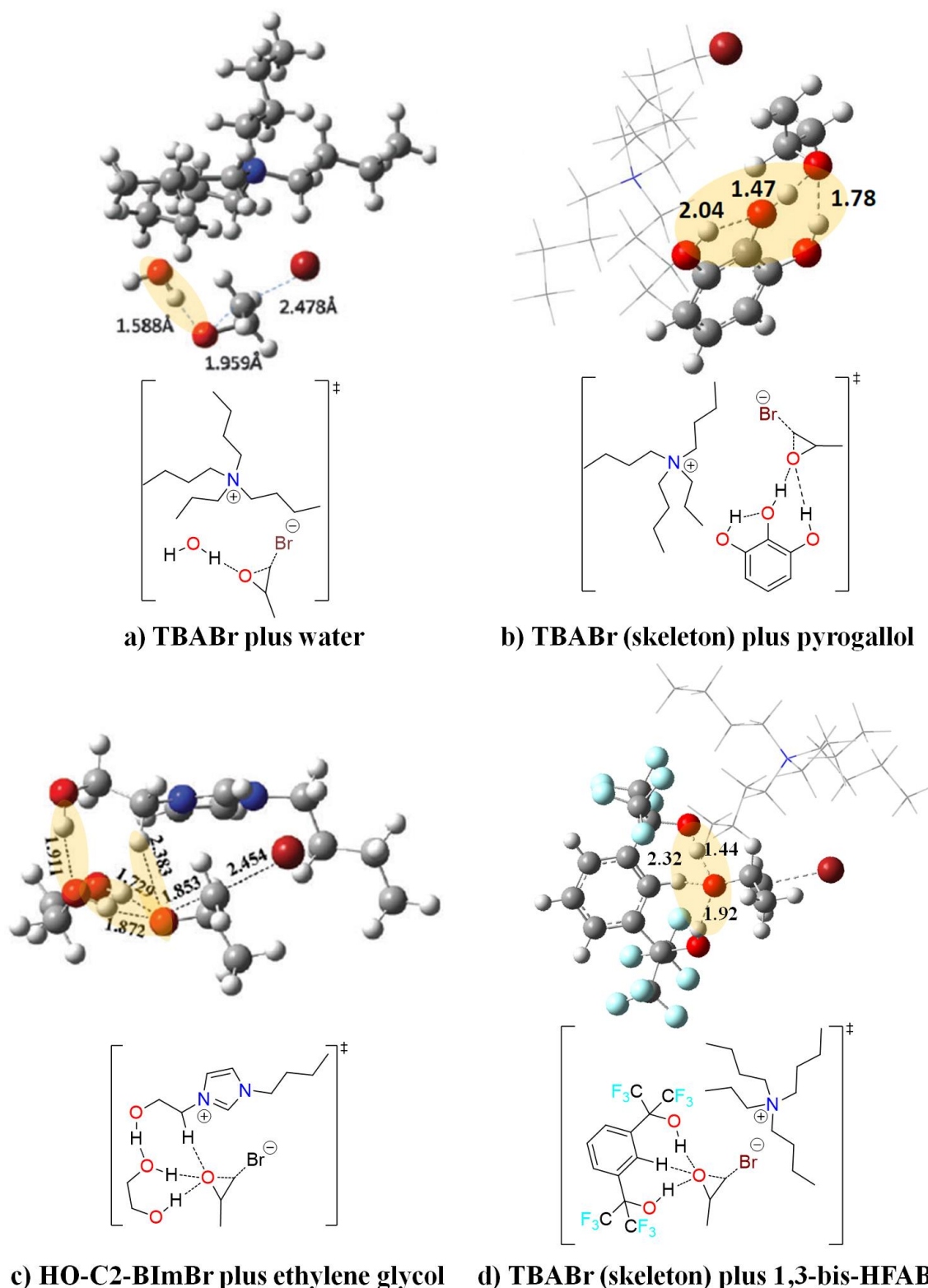


Figure 2: Optimized geometries of the structures and Lewis representations of the epoxide ring-opening (TS1) for the CO<sub>2</sub>/PO coupling in the presence of a) TBABr plus H<sub>2</sub>O (reprinted from ref <sup>137</sup>), b) TBABr plus pyrogallol (reprinted from ref <sup>101</sup>), c) HO-C2-BImBr plus ethylene glycol (reprinted from ref <sup>125</sup>) and d) TBABr plus 1,3-bis-HFAB (reprinted from ref <sup>142</sup>). The dashed lines depict the intermolecular distances in angstrom.

Then, Tassaing *et al.* investigated the activation mechanism with the TBABr/1,3-bis-HFAB bifunctional catalyst.<sup>101, 147</sup> As it was previously reported, the epoxide ring-opening was the determining step. Both the OH groups of the hexafluoroisopropyl groups interact by H-bonds with the O atom of the epoxide. However, both NMR titrations and DFT calculations highlight a third intermolecular H-bond of the proton on the aromatic ring in the *ortho* position of the hexafluoroisopropyl groups and the O atom (Figure 2 d). This strong stabilization mechanism through triple hydrogen bonding allowed an easier epoxide ring-opening. Then, one of the hydroxyl group transferred its proton to the O atom leading a bromohydrin (IR1). The mechanism for the two next steps is similar to the one of pyrogallol. However, the Gibbs energy for the epoxide/CO<sub>2</sub> coupling catalysed by TBABr/1,3-bis-HFAB is lower (3.8 kcal.mol<sup>-1</sup>) than with pyrogallol (7.7 kcal.mol<sup>-1</sup>). Indeed, due to the three intermolecular interactions, the stabilization by H-bond is stronger with 1,3-bis-HFAB than with pyrogallol. Besides, DFT calculations showed that the activity of fluorinated monoalcohols arose from the dual hydrogen bonding induced by two molecules.<sup>101</sup>

The activation mechanism of the amino-functionalized ILs globally respects the well accepted three-steps reaction pathway. However, activation of the epoxide and stabilization of the IR and TS do not directly arise from the NH<sub>2</sub> group but from a carbamic acid species formed *in-situ* by reaction between two molecules of amine and CO<sub>2</sub>.<sup>102, 190</sup> This carbamic acid stabilized the O atom of the epoxide for the epoxide-ring opening (Figure 3).

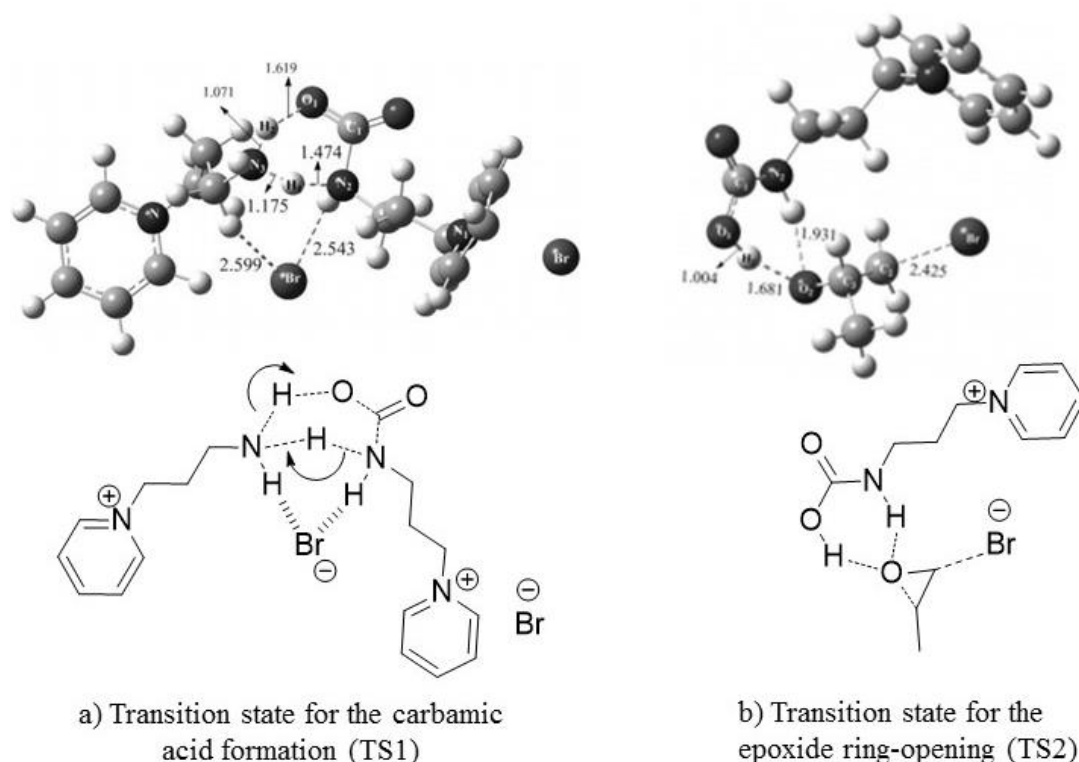
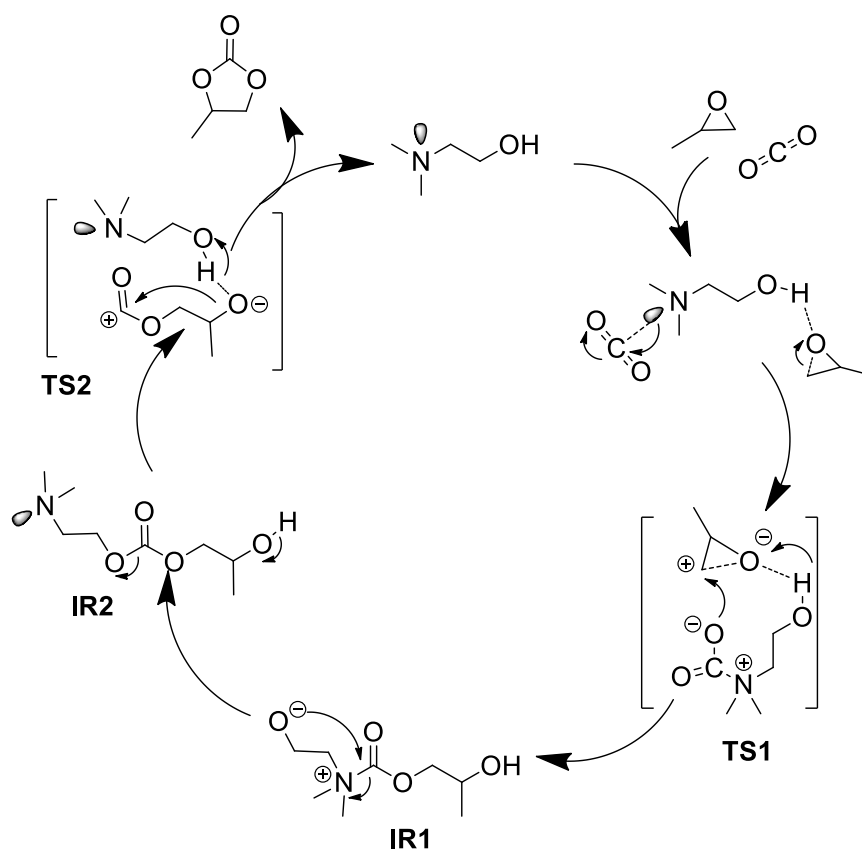


Figure 3: Optimized geometries and schematic representation of the transition states for a) the formation of the carbamic acid and b) the epoxide ring-opening for the CO<sub>2</sub>/propylene oxide coupling catalysed by the N-aminopropylpyridinium bromide at the Mo6/6-311+G(2d,2p)//B3PW91/6-31G(d,p) levels (reprinted from ref <sup>102</sup>)

This preliminary reaction proceeds easily even at room temperature with a lower energy barrier ( $\Delta G = 17.1 \text{ kcal.mol}^{-1}$  and  $\Delta G = 11.03 \text{ kcal.mol}^{-1}$  respectively for pyridinium-based and guanidinium-based ILs) than the carbonate ring-closure that is the rate-determining-step ( $\Delta G = 26.0 \text{ kcal.mol}^{-1}$  and  $\Delta G = 18.24 \text{ kcal.mol}^{-1}$  respectively for pyridinium-based and guanidinium-based ILs).<sup>102, 190</sup>

Finally, the activation mechanism of alkanolamines promoted coupling of  $\text{CO}_2$  with PO was studied by Roshan *et al.* using DFT with the B3LYP correlation functional considering N,N-dimethylethanamine as representative alkanolamine. The mechanism follows a two-step pathway (Scheme 26).<sup>130</sup> A synergistic i) nucleophilic activation of  $\text{CO}_2$  *via* the attack of the nitrogen's lone pair of the tertiary amino group and ii) an interaction between the epoxide and the hydroxyl group facilitating the breaking of the  $\beta$  C-O bond of the oxirane was highlighted as TS1 ( $\Delta G = 37.5 \text{ kcal.mol}^{-1}$ ). The nucleophilic attack of the  $\text{CO}_2$ -activated form onto the  $\beta$  carbon of the epoxide and the proton transfer from the OH group toward the O atom of the epoxide form a stable intermediate (IR1) in which the  $\text{CO}_2$  molecule is tethered between the epoxide and the alkanolamine. Then, a possible nucleophilic attack of the terminal oxy anion onto the N-C bond of the carbamate could lead to the formation of a carbonate bond (IR2). Finally, the proton migrates back to the parent alkanolamine with simultaneous ring closure of the carbonate (TS2,  $\Delta G = 20.3 \text{ kcal.mol}^{-1}$ ).



Scheme 26: Plausible mechanism of the alkanolamine halide-free catalysed cycloaddition of PO and  $\text{CO}_2$ , illustrated using DMEA catalyst.<sup>130</sup>

### III. CONCLUSION

This chapter summarized the recent advances in the organocatalytic coupling of epoxide with CO<sub>2</sub> and correlated the catalytic activity of the most relevant systems to in-depth mechanistic studies by DFT calculations. Today, the privileged approaches in designing efficient catalysts involve cooperative effects between hydrogen bond donors and alkali or organic salts, ILs, organic bases..., CO<sub>2</sub> activation, guest-host chemistry, catalyst spatial pre-organisation, convergent activation... To date, bicomponent organocatalysts are identified as the most active catalysts, few of them competing with metal-based systems as they promote the reaction under atmospheric pressure and relatively low temperature (25-60°C). The quest for highly active organocatalysts still remains challenging and a hot research topic in academic laboratories and industries, especially for converting more demanding di-, tri- or tetrasubstituted epoxides into their corresponding cyclic carbonates or developing halide and metal-free catalysts.

## IV. REFERENCES

1. A. J. Hunt, E. H. K. Sin, R. Marriott and J. H. Clark, *ChemSusChem*, 2010, **3**, 306-322.
2. K. M. K. Yu, I. Curcic, J. Gabriel and S. C. E. Tsang, *ChemSusChem*, 2008, **1**, 893-899.
3. H. Yang, Z. Xu, M. Fan, R. Gupta, R. B. Slimane, A. E. Bland and I. Wright, *Journal of Environmental Sciences*, 2008, **20**, 14-27.
4. P. Markewitz, W. Kuckshinrichs, W. Leitner, J. Linssen, P. Zapp, R. Bongartz, A. Schreiber and T. E. Muller, *Energy & Environmental Science*, 2012, **5**, 7281-7305.
5. S.-W. Lee, S.-B. Park, S.-K. Jeong, K.-S. Lim, S.-H. Lee and M. C. Trachtenberg, *Micron*, 2010, **41**, 273-282.
6. R. Zevenhoven, J. Fagerlund and J. K. Songok, *Greenhouse Gases: Science and Technology*, 2011, **1**, 48-57.
7. R. Zevenhoven and J. Fagerlund, in *Developments and Innovation in Carbon Dioxide (CO<sub>2</sub>) Capture and Storage Technology*, Woodhead Publishing, 2010, vol. 2, pp. 433-462.
8. F. D. Meylan, V. Moreau and S. Erkman, *Journal of CO<sub>2</sub> Utilization*, 2015, **12**, 101-108.
9. I. Omae, *Catalysis Today*, 2006, **115**, 33-52.
10. M. Aresta, Orlando, FL, 2002.
11. M. Aresta and A. Dibenedetto, *Journal*, 2002, **809**, 54-70.
12. M. Aresta, *Carbon Dioxide as Chemical Feedstock*, Wiley-VCH, 2010.
13. M. Mikkelsen, M. Jorgensen and F. C. Krebs, *Energy & Environmental Science*, 2010, **3**, 43-81.
14. A. Otto, T. Grube, S. Schiebahn and D. Stolten, *Energy and Environmental Science*, 2015, **8**, 3283-3297.
15. I. Omae, *Coordination Chemistry Reviews*, 2012, **256**, 1384-1405.
16. J. Rintjema and A. W. Kleij, *Synthesis*, DOI: 10.1055/s-0035-1562520.
17. T. J. Kemp, *Science Progress*, 2014, **97**, 249-260.
18. G. Centi and S. Perathoner, *Catalysis Today*, 2009, **148**, 191-205.
19. X. M. Liu, G. Q. Lu, Z. F. Yan and J. Beltramini, *Industrial and Engineering Chemistry Research*, 2003, **42**, 6518-6530.
20. ADEME, "Valorisation chimique du CO<sub>2</sub> : état des lieux. Quantification des bénéfices énergétiques et environnementaux et évaluation économique de trois voies chimiques", Juillet 2014, <http://www.ademe.fr/sites/default/files/assets/documents/valorisation-chimique-co2-etat-lieux-2014-rapport-final.pdf>
21. S. Fukuoka, M. Kawamura, K. Komiya, M. Tojo, H. Hachiya, K. Hasegawa, M. Aminaka, H. Okamoto, I. Fukawa and S. Konno, *Green Chemistry*, 2003, **5**, 497-507.
22. G. Rokicki, P. G. Parzuchowski and M. Mazurek, *Polymers for Advanced Technologies*, 2015, **26**, 707-761.

23. M. S. Kathalewar, P. B. Joshi, A. S. Sabnis and V. C. Malshe, *RSC Advances*, 2013, **3**, 4110-4129.
24. L. Maisonneuve, O. Lamarzelle, E. Rix, E. Grau and H. Cramail, *Chemical Reviews*, 2015, **115**, 12407-12439.
25. S. Foltran, R. Mereau and T. Tassaing, *Catalysis Science and Technology*, 2014, **4**, 1585-1597.
26. C. J. Whiteoak, A. Nova, F. Maseras and A. W. Kleij, *ChemSusChem*, 2012, **5**, 2032-2038.
27. J.-Q. Wang, K. Dong, W.-G. Cheng, J. Sun and S.-J. Zhang, *Catalysis Science & Technology*, 2012, **2**, 1480-1484.
28. C. H. Guo, H. S. Wu, X. M. Zhang, J. Y. Song and X. Zhang, *Journal of Physical Chemistry A*, 2009, **113**, 6710-6723.
29. J. W. Comerford, I. D. V. Ingram, M. North and X. Wu, *Green Chemistry*, 2015, **17**, 1966-1987.
30. M. North, R. Pasquale and C. Young, *Green Chemistry*, 2010, **12**, 1514-1539.
31. A. C. Kathalikkattil, R. Babu, J. Tharun, R. Roshan and D.-W. Park, *Catalysis Surveys from Asia*, 2015, **19**, 223-235.
32. B.-H. Xu, J.-Q. Wang, J. Sun, Y. Huang, J.-P. Zhang, X.-P. Zhang and S.-J. Zhang, *Green Chemistry*, 2015, **17**, 108-122.
33. J. Sun, S. I. Fujita and M. Arai, *Journal of Organometallic Chemistry*, 2005, **690**, 3490-3497.
34. G. Fiorani, W. Guo and A. W. Kleij, *Green Chemistry*, 2015, **17**, 1375-1389.
35. C. Martín, G. Fiorani and A. W. Kleij, *ACS Catalysis*, 2015, **5**, 1353-1370.
36. N. Kihara, N. Hara and T. Endo, *The Journal of Organic Chemistry*, 1993, **58**, 6198-6202.
37. J. Sun, J. Ren, S. Zhang and W. Cheng, *Tetrahedron Letters*, 2009, **50**, 423-426.
38. M. North, in *New and Future Developments in Catalysis*, Elsevier B.V., 2013, DOI: 10.1016/b978-0-444-53882-6.00014-0, pp. 379-413.
39. T. Welton, *Coordination Chemistry Reviews*, 2004, **248**, 2459-2477.
40. J. F. Cooper and L. Myri, *Journal*, 1956.
41. W. J. Peppel, *Industrial & Engineering Chemistry*, 1958, **50**, 767-770.
42. M. North and R. Pasquale, *Angewandte Chemie - International Edition*, 2009, **48**, 2946-2948.
43. V. Caló, A. Nacci, A. Monopoli and A. Fanizzi, *Organic Letters*, 2002, **4**, 2561-2563.
44. D. W. Park, J. Y. Moon, J. G. Yang and J. K. Lee, *Energy Conversion and Management*, 1997, **38**, S449-S454.
45. C. M. Starks, C. L. Liotta and M. Halpern, *Phase Transfer Catalysis: Fundamentals, Applications and Industrial Perspectives*, 1994.
46. H. Y. Ju, M. D. Manju, K. H. Kim, S. W. Park and D. W. Park, *Journal of Industrial and Engineering Chemistry*, 2008, **14**, 157-160.
47. T. Ema, K. Fukuhara, T. Sakai, M. Ohbo, F.-Q. Bai and J.-y. Hasegawa, *Catalysis Science & Technology*, 2015, **5**, 2314-2321.

48. J. Song, B. Zhang, P. Zhang, J. Ma, J. Liu, H. Fan, T. Jiang and B. Han, *Catalysis Today*, 2012, **183**, 130-135.
49. T. Takahashi, T. Watahiki, S. Kitazume, H. Yasuda and T. Sakakura, *Chemical Communications*, 2006, 1664-1666.
50. M. Galvan, M. Selva, A. Perosa and M. Noè, *Asian Journal of Organic Chemistry*, 2014, **3**, 504-513.
51. N. Aoyagi, Y. Furusho and T. Endo, *Tetrahedron Letters*, 2013, **54**, 7031-7034.
52. J. Peng and Y. Deng, *New Journal of Chemistry*, 2001, **25**, 639-641.
53. P. Jaiswal and M. N. Varma, *Journal of CO<sub>2</sub> Utilization*, 2016, **14**, 93-97.
54. H. Kawanami, A. Sasaki, K. Matsui and Y. Ikushima, *Chemical Communications*, 2003, **9**, 896-897.
55. T. Seki, J. D. Grunwaldt and A. Baiker, *Journal of Physical Chemistry B*, 2009, **113**, 114-122.
56. S. G. Kazarian, B. J. Briscoe and T. Welton, *Chemical Communications*, 2000, 2047-2048.
57. A.-L. Girard, N. Simon, M. Zanatta, S. Marmitt, P. Goncalves and J. Dupont, *Green Chemistry*, 2014, **16**, 2815-2825.
58. L. Xiao, D. Su, C. Yue and W. Wu, *Journal of CO<sub>2</sub> Utilization*, 2014, **6**, 1-6.
59. M. H. Anthofer, M. E. Wilhelm, M. Cokoja, I. I. E. Markovits, A. Pöthig, J. Mink, W. A. Herrmann and F. E. Kühn, *Catalysis Science and Technology*, 2014, **4**, 1749-1758.
60. J. Sun, L. Han, W. Cheng, J. Wang, X. Zhang and S. Zhang, *ChemSusChem*, 2011, **4**, 502-507.
61. J. Sun, W. Cheng, W. Fan, Y. Wang, Z. Meng and S. Zhang, *Catalysis Today*, 2009, **148**, 361-367.
62. J. Tharun, A. C. Kathalikkattil, R. Roshan, D.-H. Kang, H.-C. Woo and D.-W. Park, *Catalysis Communications*, 2014, **54**, 31-34.
63. A. R. Hajipour, Y. Heidari and G. Kozehgary, *RSC Advances*, 2015, **5**, 61179-61183.
64. Z. Z. Yang, L. N. He, C. X. Miao and S. Chanfreau, *Advanced Synthesis and Catalysis*, 2010, **352**, 2233-2240.
65. L. Wang, K. Kodama and T. Hirose, *Catalysis Science and Technology*, 2016, **6**, 3872-3877.
66. S. Foltran, J. Alsarraf, F. Robert, Y. Landais, E. Cloutet, H. Cramail and T. Tassaing, *Catalysis Science and Technology*, 2013, **3**, 1046-1055.
67. H. F. Duan, S. H. Li, Y. J. Lin, H. B. Xie, S. B. Zhang and Z. M. Wang, *Chemical Research in Chinese Universities*, 2004, **20**, 568-571.
68. H. Xie, H. Duan, S. Li and S. Zhang, *New Journal of Chemistry*, 2005, **29**, 1199-1203.
69. H. Xie, S. Li and S. Zhang, *Journal of Molecular Catalysis A: Chemical*, 2006, **250**, 30-34.
70. X. Y. Dou, J. Q. Wang, Y. Du, E. Wang and L. N. He, *Synlett*, 2007, DOI: 10.1055/s-2007-992362, 3058-3062.
71. T. Yu and R. G. Weiss, *Green Chemistry*, 2012, **14**, 209-216.
72. A. Barbarini, R. Maggi, A. Mazzacani, G. Mori, G. Sartori and R. Sartorio, *Tetrahedron Letters*, 2003, **44**, 2931-2934.



73. K. M. K. Yu, I. Curcic, J. Gabriel, H. Morganstewart and S. C. Tsang, *The Journal of Physical Chemistry A*, 2010, **114**, 3863-3872.
74. Y.-M. Shen, W.-L. Duan and M. Shi, *European Journal of Organic Chemistry*, 2004, **2004**, 3080-3089.
75. J. Sun, W. Cheng, Z. Yang, J. Wang, T. Xu, J. Xin and S. Zhang, *Green Chemistry*, 2014, **16**, 3071-3078.
76. H. Liu, R. Zeng and R. Hua, *International Journal of Molecular Sciences*, 2014, **15**, 9945-9951.
77. R. A. Shiels and C. W. Jones, *Journal of Molecular Catalysis A: Chemical*, 2007, **261**, 160-166.
78. M. Sankar, N. H. Tarte and P. Manikandan, *Applied Catalysis A: General*, 2004, **276**, 217-222.
79. K. R. Roshan, R. A. Palissery, A. C. Kathalikkattil, R. Babu, G. Mathai, H.-S. Lee and D.-W. Park, *Catalysis Science & Technology*, 2016, **6**, 3997-4004.
80. M. J. Ajitha and C. H. Suresh, *Tetrahedron Letters*, 2011, **52**, 5403-5406.
81. H. Zhou, Y.-M. Wang, W.-Z. Zhang, J.-P. Qu and X.-B. Lu, *Green Chemistry*, 2011, **13**, 644-650.
82. Y. Kayaki, M. Yamamoto and T. Ikariya, *Angewandte Chemie International Edition*, 2009, **48**, 4194-4197.
83. W. Desens and T. Werner, *Advanced Synthesis & Catalysis*, 2016, **358**, 622-630.
84. H. Zhou, W.-Z. Zhang, C.-H. Liu, J.-P. Qu and X.-B. Lu, *The Journal of Organic Chemistry*, 2008, **73**, 8039-8044.
85. Y.-B. Wang, Y.-M. Wang, W.-Z. Zhang and X.-B. Lu, *Journal of the American Chemical Society*, 2013, **135**, 11996-12003.
86. Y.-B. Wang, D.-S. Sun, H. Zhou, W.-Z. Zhang and X.-B. Lu, *Green Chemistry*, 2015, **17**, 4009-4015.
87. H. Zhou, G.-X. Wang, W.-Z. Zhang and X.-B. Lu, *ACS Catalysis*, 2015, **5**, 6773-6779.
88. B. Chatelet, L. Joucla, J. P. Dutasta, A. Martinez, K. C. Szeto and V. Dufaud, *Journal of the American Chemical Society*, 2013, **135**, 5348-5351.
89. B. Chatelet, E. Jeanneau, J. P. Dutasta, V. Robert, A. Martinez and V. Dufaud, *Catalysis Communications*, 2014, **52**, 26-30.
90. B. Chatelet, L. Joucla, J. P. Dutasta, A. Martinez and V. Dufaud, *Chemistry - A European Journal*, 2014, **20**, 8571-8574.
91. J. A. Kozak, J. Wu, X. Su, F. Simeon, T. A. Hatton and T. F. Jamison, *Journal of the American Chemical Society*, 2013, **135**, 18497-18501.
92. C. Caristi, G. Cimino, A. Ferlazzo, M. Gattuso and M. Parisi, *Tetrahedron Letters*, 1983, **24**, 2685-2688.
93. S. M. Ahmad, D. C. Braddock, G. Cansell and S. A. Hermitage, *Tetrahedron Letters*, 2007, **48**, 915-918.
94. M. Aresta, A. Dibenedetto, L. Gianfrate and C. Pastore, *Journal of Molecular Catalysis A: Chemical*, 2003, **204-205**, 245-252.
95. C. Carvalho Rocha, T. Onfroy, J. Pilmé, A. Denicourt-Nowicki, A. Roucoux and F. Launay, *Journal of Catalysis*, 2016, **333**, 29-39.

96. L. Wang, L. Lin, G. Zhang, K. Kodama, M. Yasutake and T. Hirose, *Chemical Communications*, 2014, **50**, 14813-14816.
97. L. Wang, X. Jin, P. Li, J. Zhang, H. He and S. Zhang, *Industrial & Engineering Chemistry Research*, 2014, **53**, 8426-8435.
98. H. Sun and D. Zhang, *Journal of Physical Chemistry A*, 2007, **111**, 8036-8043.
99. S. Marmitt and P. F. B. Gonçalves, *Journal of Computational Chemistry*, 2015, **36**, 1322-1333.
100. Y. Ren, C. H. Guo, J. F. Jia and H. S. Wu, *Journal of Physical Chemistry A*, 2011, **115**, 2258-2267.
101. M. Alves, R. Mereau, B. Grignard, C. Detrembleur, C. Jerome and T. Tassaing, *RSC Advances*, 2016, **6**, 36327-36335.
102. Y. Li, L. Wang, T. Huang, J. Zhang and H. He, *Industrial & Engineering Chemistry Research*, 2015, **54**, 8093-8099.
103. J.-Q. Wang, W.-G. Cheng, J. Sun, T.-Y. Shi, X.-P. Zhang and S.-J. Zhang, *RSC Advances*, 2014, **4**, 2360-2367.
104. Z. Luo, B. Wang, Y. Liu, G. Gao and F. Xia, *Physical Chemistry Chemical Physics*, 2016, DOI: 10.1039/c6cp05291f.
105. K. R. Roshan, A. C. Kathalikkattil, J. Tharun, D. W. Kim, Y. S. Won and D. W. Park, *Dalton Transactions*, 2014, **43**, 2023-2031.
106. Z. Zhang, L. Xu and W. Feng, *RSC Advances*, 2015, **5**, 12382-12386.
107. D. J. Heldebrant, P. G. Jessop, C. A. Thomas, C. A. Eckert and C. L. Liotta, *Journal of Organic Chemistry*, 2005, **70**, 5335-5338.
108. A. J. R. Amaral, J. F. J. Coelho and A. C. Serra, *Tetrahedron Letters*, 2013, **54**, 5518-5522.
109. H. Büttner, K. Lau, A. Spannenberg and T. Werner, *ChemCatChem*, 2015, **7**, 459-467.
110. J. Sun, S. Zhang, W. Cheng and J. Ren, *Tetrahedron Letters*, 2008, **49**, 3588-3591.
111. Y. Tsutsumi, K. Yamakawa, M. Yoshida, T. Ema and T. Sakai, *Organic Letters*, 2010, **12**, 5728-5731.
112. H. Büttner, J. Steinbauer and T. Werner, *ChemSusChem*, 2015, **8**, 2655-2669.
113. W. L. Dai, B. Jin, S. L. Luo, X. B. Luo, X. M. Tu and C. T. Au, *Applied Catalysis A: General*, 2014, **470**, 183-188.
114. S. Liu, N. Suematsu, K. Maruoka and S. Shirakawa, *Green Chemistry*, 2016, **18**, 4611-4615.
115. Y. Toda, Y. Komiyama, A. Kikuchi and H. Suga, *ACS Catalysis*, 2016, DOI: 10.1021/acscatal.6b02265, 6906-6910.
116. S. Denizalt, *RSC Advances*, 2015, **5**, 45454-45458.
117. S. Wu, B. Wang, Y. Zhang, E. H. M. Elageed, H. Wu and G. Gao, *Journal of Molecular Catalysis A: Chemical*, 2016, **418-419**, 1-8.
118. M. H. Anthofer, M. E. Wilhelm, M. Cokoja, M. Drees, W. A. Herrmann and F. E. Kühn, *ChemCatChem*, 2015, **7**, 94-98.
119. D. Wei-Li, J. Bi, L. Sheng-Lian, L. Xu-Biao, T. Xin-Man and A. Chak-Tong, *Journal of Molecular Catalysis A: Chemical*, 2013, **378**, 326-332.
120. J. Tharun, G. Mathai, R. Roshan, A. C. Kathalikkattil, K. Bomi and D.-W. Park, *Physical Chemistry Chemical Physics*, 2013, **15**, 9029-9033.

121. Y. Zhou, S. Hu, X. Ma, S. Liang, T. Jiang and B. Han, *Journal of Molecular Catalysis A: Chemical*, 2008, **284**, 52-57.
122. L. Wang, X. Jin, Y. Li, P. Li, J. Zhang, H. He and S. Zhang, *Molecular Physics*, 2015, **113**, 3524-3530.
123. M. Feng, G. Zhao, H. Gao and S. Zhang, *Australian Journal of Chemistry*, 2015, **68**, 1513-1517.
124. L. F. Xiao, D. W. Lv, D. Su, W. Wu and H. F. Li, *Journal of Cleaner Production*, 2014, **67**, 285-290.
125. M. Liu, K. Gao, L. Liang, F. Wang, L. Shi, L. Sheng and J. Sun, *Physical Chemistry Chemical Physics*, 2015, **17**, 5959-5965.
126. P. Sharma, S. D. Park, K. T. Park, S. C. Nam, S. K. Jeong, Y. I. Yoon and I. H. Baek, *Chemical Engineering Journal*, 2012, **193-194**, 267-275.
127. H. Peng, Y. Zhou, J. Liu, H. Zhang, C. Xia and X. Zhou, *RSC Advances*, 2013, **3**, 6859-6864.
128. C. Yue, D. Su, X. Zhang, W. Wu and L. Xiao, *Catalysis Letters*, 2014, **144**, 1313-1321.
129. M. Liu, L. Liang, X. Li, X. Gao and J. Sun, *Green Chemistry*, 2016, **18**, 2851-2863.
130. K. R. Roshan, B. M. Kim, A. C. Kathalikkattil, J. Tharun, Y. S. Won and D. W. Park, *Chemical Communications*, 2014, **50**, 13664-13667.
131. C. Qi, H. Jiang, Z. Wang, B. Zou and S. Yang, *Synlett*, 2007, **2007**, 0255-0258.
132. C. Qi and H. Jiang, *Science China Chemistry*, 2010, **53**, 1566-1570.
133. K. Fukumoto, M. Yoshizawa and H. Ohno, *Journal of the American Chemical Society*, 2005, **127**, 2398-2399.
134. K. Fukumoto and H. Ohno, *Chemical Communications*, 2006, 3081-3083.
135. F. Wu, X. Y. Dou, L. N. He and C. X. Miao, *Letters in Organic Chemistry*, 2010, **7**, 73-78.
136. K. R. Roshan, T. Jose, D. Kim, K. A. Cherian and D. W. Park, *Catalysis Science & Technology*, 2014, **4**, 963-970.
137. J.-Q. Wang, J. Sun, W.-G. Cheng, K. Dong, X.-P. Zhang and S.-J. Zhang, *Physical Chemistry Chemical Physics*, 2012, **14**, 11021-11026.
138. J. Tharun, K. R. Roshan, A. C. Kathalikkattil, D.-H. Kang, H.-M. Ryu and D.-W. Park, *RSC Advances*, 2014, **4**, 41266-41270.
139. X. Zhou, Y. Zhang, X. Yang, J. Yao and G. Wang, *Cuihua Xuebao/Chinese Journal of Catalysis*, 2010, **31**, 765-768.
140. W.-L. Wong, P.-H. Chan, Z.-Y. Zhou, K.-H. Lee, K.-C. Cheung and K.-Y. Wong, *ChemSusChem*, 2008, **1**, 67-70.
141. W. L. Wong, L. Y. S. Lee, K. P. Ho, Z. Y. Zhou, T. Fan, Z. Lin and K. Y. Wong, *Applied Catalysis A: General*, 2014, **472**, 160-166.
142. S. Liang, H. Liu, T. Jiang, J. Song, G. Yang and B. Han, *Chemical Communications*, 2011, **47**, 2131-2133.
143. R. A. Watile, K. M. Deshmukh, K. P. Dhake and B. M. Bhanage, *Catalysis Science and Technology*, 2012, **2**, 1051-1055.
144. L. Zhou, Y. Liu, Z. He, Y. Luo, F. Zhou, E. Yu, Z. Hou and W. Eli, *Journal of Chemical Research*, 2013, **37**, 102-104.

145. M. E. Wilhelm, M. H. Anthofer, M. Cokoja, I. I. E. Markovits, W. A. Herrmann and F. E. Kühn, *ChemSusChem*, 2014, **7**, 1357-1360.
146. W. Cheng, F. Xu, J. Sun, K. Dong, C. Ma and S. Zhang, *Synthetic Communications*, 2016, **46**, 497-508.
147. S. Gennen, M. Alves, R. Méreau, T. Tassaing, B. Gilbert, C. Detrembleur, C. Jerome and B. Grignard, *ChemSusChem*, 2015, **8**, 1845-1849.
148. J. Wang and Y. Zhang, *ACS Catalysis*, 2016, **6**, 4871-4876.
149. A. M. Hardman-Baldwin and A. E. Mattson, *ChemSusChem*, 2014, **7**, 3275-3278.
150. Y. M. Shen, W. L. Duan and M. Shi, *Advanced Synthesis and Catalysis*, 2003, **345**, 337-340.
151. J. W. Huang and M. Shi, *Journal of Organic Chemistry*, 2003, **68**, 6705-6709.
152. M. Alves, B. Grignard, S. Gennen, R. Mereau, C. Detrembleur, C. Jerome and T. Tassaing, *Catalysis Science and Technology*, 2015, **5**, 4636-4643.
153. S. Sopena, G. Fiorani, C. Martín and A. W. Kleij, *ChemSusChem*, 2015, **8**, 3248-3254.
154. C. J. Whiteoak, A. H. Henseler, C. Ayats, A. W. Kleij and M. A. Pericàs, *Green Chemistry*, 2014, **16**, 1552-1559.
155. L. Martínez-Rodríguez, J. Otalora Garmilla and A. W. Kleij, *ChemSusChem*, 2016, **9**, 749-755.
156. N. Kihara and T. Endo, *Macromolecules*, 1992, **25**, 4824-4825.
157. J. W. Kim, D. W. Cho, G. Park, S. H. Kim and C. S. Ra, *Bulletin of the Korean Chemical Society*, 2013, **34**, 2286-2290.
158. J. Tharun, G. Mathai, A. C. Kathalikkattil, R. Roshan, J. Y. Kwak and D. W. Park, *Green Chemistry*, 2013, **15**, 1673-1677.
159. L. Wang, G. Zhang, K. Kodama and T. Hirose, *Green Chemistry*, 2016, **18**, 1229-1233.
160. B. Xiao, J. Sun, J. Wang, C. Liu and W. Cheng, *Synthetic Communications*, 2013, **43**, 2985-2997.
161. T. Werner and N. Tenhumberg, *Journal of CO<sub>2</sub> Utilization*, 2014, **7**, 39-45.
162. T. Werner, N. Tenhumberg and H. Büttner, *ChemCatChem*, 2014, **6**, 3493-3500.
163. Z. Yang, J. Sun, W. Cheng, J. Wang, Q. Li and S. Zhang, *Catalysis Communications*, 2014, **44**, 6-9.
164. Q. Gong, H. Luo, J. Cao, Y. Shang, H. Zhang, W. Wang and X. Zhou, *Australian Journal of Chemistry*, 2012, **65**, 381-386.
165. Q. Gong, H. Luo, D. Cao, H. Zhang, W. Wang and X. Zhou, *Bulletin of the Korean Chemical Society*, 2012, **33**, 1945-1948.
166. X.-F. Liu, Q.-W. Song, S. Zhang and L.-N. He, *Catalysis Today*, 2016, **263**, 69-74.
167. P. Ramidi, P. Munshi, Y. Gartia, S. Pulla, A. S. Biris, A. Paul and A. Ghosh, *Chemical Physics Letters*, 2011, **512**, 273-277.
168. B. Barkakaty, K. Morino, A. Sudo and T. Endo, *Green Chemistry*, 2010, **12**, 42-44.
169. O. Coulembier, S. Moins, V. Lemaury, R. Lazzaroni and P. Dubois, *Journal of CO<sub>2</sub> Utilization*, 2015, **10**, 7-11.

170. G. Rokicki, W. Kuran and B. Pogorzelska-Marciniak, *Monatshefte für Chemie Chemical Monthly*, 1984, **115**, 205-214.
171. S. Kumar and S. L. Jain, *Industrial and Engineering Chemistry Research*, 2014, **53**, 541-546.
172. M. Mamone, T. Milcent and B. Crousse, *Chemical Communications*, 2015, **51**, 12736-12739.
173. A. Mirabaud, J. C. Mulatier, A. Martinez, J. P. Dutasta and V. Dufaud, *ACS Catalysis*, 2015, **5**, 6748-6752.
174. J. Song, Z. Zhang, B. Han, S. Hu, W. Li and Y. Xie, *Green Chemistry*, 2008, **10**, 1337-1341.
175. J. Shi, J. Song, J. Ma, Z. Zhang, H. Fan and B. Han, *Pure and Applied Chemistry*, 2013, **85**, 1633-1641.
176. Y. B. Sun, C. Y. Cao, S. L. Yang, P. P. Huang, C. R. Wang and W. G. Song, *Chemical Communications*, 2014, **50**, 10307-10310.
177. R. Luo, X. Zhou, Y. Fang and H. Ji, *Carbon*, 2015, **82**, 1-11.
178. D. H. Lan, F. M. Yang, S. L. Luo, C. T. Au and S. F. Yin, *Carbon*, 2014, **73**, 351-360.
179. A. M. Dimiev, L. B. Alemany and J. M. Tour, *ACS Nano*, 2013, **7**, 576-588.
180. M. B. Ansari, B.-H. Min, Y.-H. Mo and S.-E. Park, *Green Chemistry*, 2011, **13**, 1416-1421.
181. Z. Huang, F. Li, B. Chen, T. Lu, Y. Yuan and G. Yuan, *Applied Catalysis B: Environmental*, 2013, **136-137**, 269-277.
182. Q. Su, J. Sun, J. Wang, Z. Yang, W. Cheng and S. Zhang, *Catalysis Science and Technology*, 2014, **4**, 1556-1562.
183. J. Xu, F. Wu, Q. Jiang and Y.-X. Li, *Catalysis Science & Technology*, 2015, **5**, 447-454.
184. D.-H. Lan, H.-T. Wang, L. Chen, C.-T. Au and S.-F. Yin, *Carbon*, 2016, **100**, 81-89.
185. K. R. Roshan, T. Jose, A. C. Kathalikkattil, D. W. Kim, B. Kim and D. W. Park, *Applied Catalysis A: General*, 2013, **467**, 17-25.
186. J. Sun, J. Wang, W. Cheng, J. Zhang, X. Li, S. Zhang and Y. She, *Green Chemistry*, 2012, **14**, 654-660.
187. V. Besse, N. Illy, G. David, S. Caillol and B. Boutevin, *ChemSusChem*, 2016, **9**, 2167-2173.
188. Z. Wu, H. Xie, X. Yu and E. Liu, *ChemCatChem*, 2013, **5**, 1328-1333.
189. Z. Yang, J. Sun, X. Liu, Q. Su, Y. Liu, Q. Li and S. Zhang, *Tetrahedron Letters*, 2014, **55**, 3239-3243.
190. P. Li, Y. Li, C. Chen, L. Wang and J. Zhang, *RSC Advances*, 2016, **6**, 87036-87043.

---

Chapter II:  
Fluorinated Alcohols as Activators for  
the Solvent-Free Chemical Fixation of  
Carbon Dioxide into Epoxides

---

The results presented in this chapter were published in *ChemSusChem*, 2015, 8, 1845 – 1849

### Abstract

The addition of fluorinated alcohols to onium salts provides highly efficient organocatalysts for the chemical fixation of CO<sub>2</sub> into epoxides under mild experimental conditions. The combination of online kinetic studies, NMR titrations and DFT calculations allows understanding this synergistic effect that provides an active organocatalyst for CO<sub>2</sub>/epoxides coupling.

### Table of contents

Introduction.....	89
Experimental .....	90
1- Materials .....	90
2- Kinetic studies of the chemical fixation of CO <sub>2</sub> onto model epoxides by online high pressure Raman and IR spectroscopy .....	90
a) Kinetic study by Raman spectroscopy.....	91
b) Kinetic study by IR spectroscopy .....	94
3- Characterization .....	96
4- Computational details .....	96
Results and discussion.....	97
References.....	107

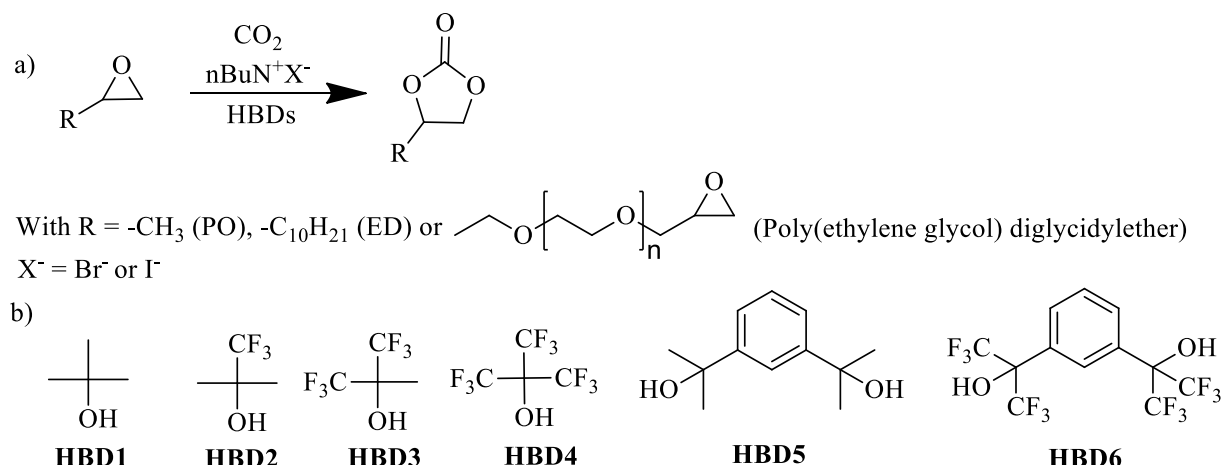
## Introduction

Today, hydrogen-bond donors (HBDs) small molecules are useful tools in (macro)molecular engineering thanks to a catalytic activity arising from (i) the activation of the reactant by polarization through the formation of hydrogen bonds, (ii) the preorganization of the special arrangement of the reactants or (iii) the stabilization of the charges of transition states or intermediates.<sup>1,2-7</sup> Beside the widely used (thio)ureas, alcohols, phenol, phosphoric acid or sulfonamide derivatives, fluorinated alcohols have demonstrated to strongly enhance the rate and the selectivity of various organic reactions as a result of their strong H-bond donors capability, their low nucleophilicity and their high ionizing power.<sup>8</sup> As pertinent examples, polylactides were synthesized by ring opening polymerization of lactide in the presence of a bicomponent organocatalyst based on 1,3-bis(2-hydroxyhexafluoroisopropyl)benzene and an amine.<sup>9</sup> Fluorinated solvents such as 2,2,2-trifluoroethanol and 1,1,1,3,3,3-hexafluoroisopropanol (HFIP) were used in organic chemistry to fasten the epoxidation of olefins and the oxidation of ketones or thioethers in the presence of peroxides.<sup>10-14</sup> Although the use of fluorinated alcohols as solvents has opened perspectives for the improvement of specific organic reactions, HFIP was however found to dramatically affect the phosphonium iodide organocatalyzed synthesis of five-membered cyclic carbonates by chemical fixation of carbon dioxide onto epoxides with no product formation.<sup>15</sup> Aoyagi related this observation to the high acceptor number of HFIP ( $AN_{\text{HFIP}} = 63$ ) and demonstrated that only protic solvents with low acceptor number such as isopropanol ( $AN_{\text{IPA}} = 33.8$ ) could activate the epoxide without decreasing the nucleophilicity of the halide anion by strong solvation. However, even when suitable protic solvents with low acceptor number were used, organocatalysts<sup>16-20</sup> showed poor catalytic activity under mild conditions compared to the traditional strong Lewis acid metal catalysts<sup>21-25</sup>. Ammonium<sup>26-29</sup> or phosphonium halides<sup>30-32</sup> and ionic liquids<sup>33-36</sup> generally showed sufficient catalytic activity at high pressure only, high catalyst loading and generally temperatures higher than 100°C. To overcome these limitations, attempts to identify efficient co-catalysts have been reported in literature. For instance, hydrogen bond donors such as (amino)alcohols<sup>37-41</sup>, carboxylic acids<sup>42, 43</sup>, azaphosphatane<sup>16</sup>, cellulose<sup>20, 44, 45</sup>... have been used as additives to speed up the CO<sub>2</sub>/epoxide coupling with moderate success. In 2012, Kleij *et al.* developed a (multi)phenolic compound/ammonium iodide organocatalytic system that presented high catalytic activity for this reaction at 25°C or 45°C and 1 MPa.<sup>46</sup> Very recently, Mattson *et al.* reported on the use of silanols as a new class of HBDs allowing the synthesis of cyclic carbonates at 0.1 MPa and 25°C. Nevertheless, the conversion of epoxides into cyclic carbonates is very slow (18h) despite the use of a very high catalyst (TBAI) and co-catalyst (silanol) loading (10 mol%).<sup>47</sup>

In this communication, we report a novel combination of an onium salt with catalytic amount of fluorinated hydrogen-bond donor (HBD) for the unprecedented fast synthesis of cyclic carbonates from epoxides and CO<sub>2</sub> under solvent free and mild experimental conditions (Scheme 1). Synergistic effect between the organocatalyst



and the fluorinated activator is demonstrated by kinetics studies, NMR titrations and DFT calculations.



Scheme 1: a) CO<sub>2</sub>/epoxide coupling; b) Representative structures of the H-bonding (HBD) (fluorinated) co-catalysts for the chemical fixation of CO<sub>2</sub> onto epoxides.

## Experimental

### 1- Materials

1,2-epoxydodecane (90%), poly(ethyleneglycol) diglycidylether (Mn = 500 g/mol), *tert*-butanol (99.5%), α,α-(dihydroxy-1,3-diisopropyl)benzene (97%), tetrabutylammonium iodide (98%), tetrabutylammonium bromide (99%), propylene oxide (99%), 1,2-dihydroxybenzene (99%) and pyrogallol (98%) were purchased from aldrich. Perfluoro-*tert*-butanol (99%) and 1,3-bis(2-hydroxyhexafluoroisopropyl)benzene (97%) were purchased from Fluorochem. Hexafluoro-*tert*-butanol (98%) and 1,1,1-trifluoro-2-methyl-2-propanol (98%) were purchased from ABCR. All reactants and catalysts were used as received without any purification.

### 2- Kinetic studies of the chemical fixation of CO<sub>2</sub> onto model epoxides by online high pressure Raman and IR spectroscopy

Kinetic studies of the chemical fixation of CO<sub>2</sub> onto model epoxides were realized using online Raman and online IR spectroscopy under high pressure. Typically, as CO<sub>2</sub> is used in a large excess, the reaction answers a pseudo-first order kinetic so that the kinetic profiles reported in Figure 2 can be plotted by the following equations:

$$v = \frac{d[\text{carbonate}]}{dt} = k_{app}[\text{epoxide}]^{\alpha} \quad \text{with } k_{app} = [\text{CO}_2]^{\beta} [\text{catalyst}]^{\gamma}$$

$$v = \frac{d[x]_t}{dt} = k_{app}[C_0 - x]_t$$

With  $[x]_t$ : concentration of the carbonate at time  $t$  (mol/L)

$C_0$ : initial epoxide concentration (mol/L)

The integration of this equation leads to the following equation:

$$[x]_t = C_0(1 - e^{-k_{app}t})$$

In addition, the epoxide conversion was also determined from the evolution of the relative intensities (proportional to the conversion) of the peak characteristic of the cyclic carbonate and the conversion measured by  $^1\text{H}$  NMR at the end of the reaction and after depressurization of the cell.

### a) Kinetic study by Raman spectroscopy

#### *Set-up*

In a typical experiment, 30 mL of 1,2-epoxydodecane (0.137 mol), 1.26 g of  $\text{nBu}_4\text{NI}$  ( $3.43 \cdot 10^{-3}$  mol) and 0.85 mL of HBD6 (1,3-bis-HFAB) ( $3.43 \cdot 10^{-3}$  mol) are introduced in a 80 mL high pressure view cell. The experimental set-up used to monitor kinetic by Raman spectroscopy under pressure is based on the use of a mobile probe called « power Head » (Horiba-Jobin Yvon) that is connected to a LabRam 300 Jobin Yvon spectrometer (Figure 1). The laser beam, brought to the mobile probe by an optical fibre (100  $\mu\text{m}$  i.d.), is then focused in the reactor with a lens (12 cm focal length, 4 cm o.d). The Raman light is collected at  $360^\circ$  by the same lens, driven through an edge filter to remove the laser line and focused on the entrance of the collecting optical fibre, which is connected to the spectrometer. The excitation wavelength is 785 nm and the laser power at the level of the sample is about 120 mW. It is important to note that several lines belonging to the sapphire window of the cell may appear in the Raman spectra (for example at 418, 577 and  $750 \text{ cm}^{-1}$ ). However, when the position of the mobile probe is well adjusted with the laser beam focused inside the liquid, 2 mm beyond the sapphire window, these bands disappear and do not disturb the measurement of the conversion. The cell is first heated until  $75^\circ\text{C}$  and then, 7 MPa of  $\text{CO}_2$  are added with an isco syringe. Since the reaction is exothermic, rapid equilibration of the temperature to  $80^\circ\text{C}$  occurs and the pressure is then adjusted to 8 MPa. As soon as  $\text{CO}_2$  is added, the conversion is regularly monitored by collecting the Raman spectra at given intervals, depending on the time required for a complete reaction.

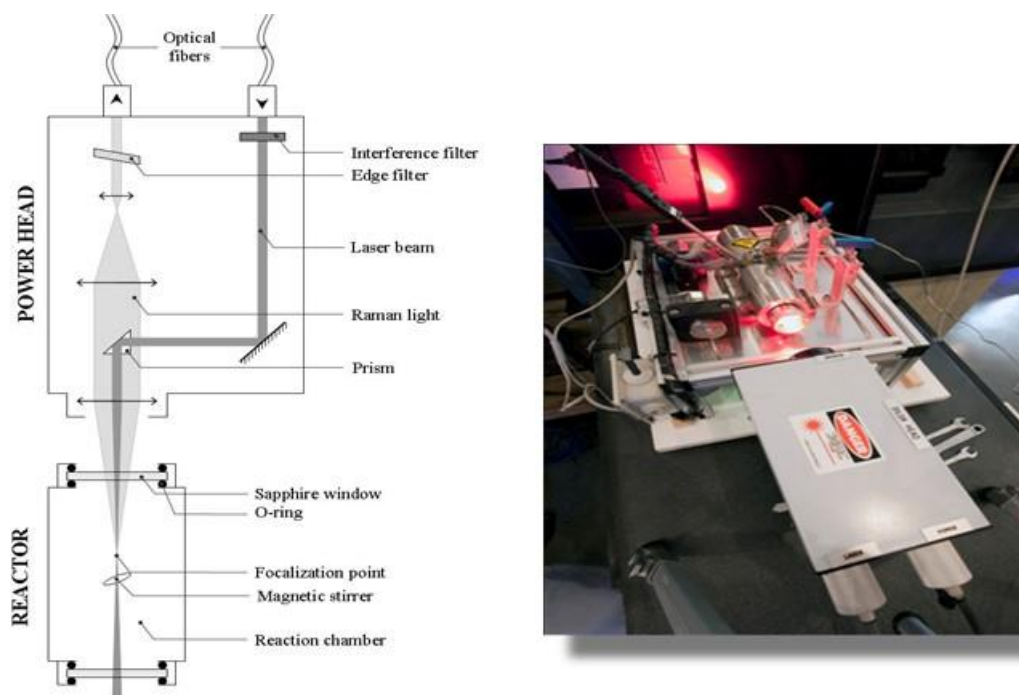


Figure 1: Schematic diagram and picture of the online Raman spectroscopy set-up

*Kinetic study by Raman spectroscopy of the chemical fixation of CO<sub>2</sub> onto 1,2-epoxidodecane in presence of HBD6/nBu<sub>4</sub>NI bicomponent organocatalyst*

The synthesis of cyclic carbonates by chemical fixation of CO<sub>2</sub> onto 1,2-epoxydodecane was monitored at 80°C by online Raman spectroscopy under pressure (ranging from 1 to 10 MPa) using 2.5 mol% of nBu<sub>4</sub>NI as catalyst and HBD6 (1,3-bis-HFAB) as activator in a molar ratio [nBu<sub>4</sub>NI]/[HBD6] = 1. Formation of the cyclic carbonate was monitored either by following the emergence of a peak at 715 cm<sup>-1</sup> characteristic of the carbonate ring or the disappearance of a peak characteristic of the epoxy ring at 1260 cm<sup>-1</sup>. Spectra were recorded every minute and normalized versus the 1441 cm<sup>-1</sup> band corresponding to the central alkyl chain not likely to change during carbonatation (Figure 2). The time dependence of the peak intensity at 715 cm<sup>-1</sup> was fitted by the equation  $[x]_t = [C]_0(1 - e^{-kt})$  (Figure 2). Identical kinetic constants were obtained by following the decrease of the 1260 cm<sup>-1</sup> band intensity (and a fit based on the equation  $[\text{Epoxide}]_t = C_0 \cdot e^{-kt}$ ) although the intensities measurements are slightly complicated by the overlap of a CO<sub>2</sub> Raman band.

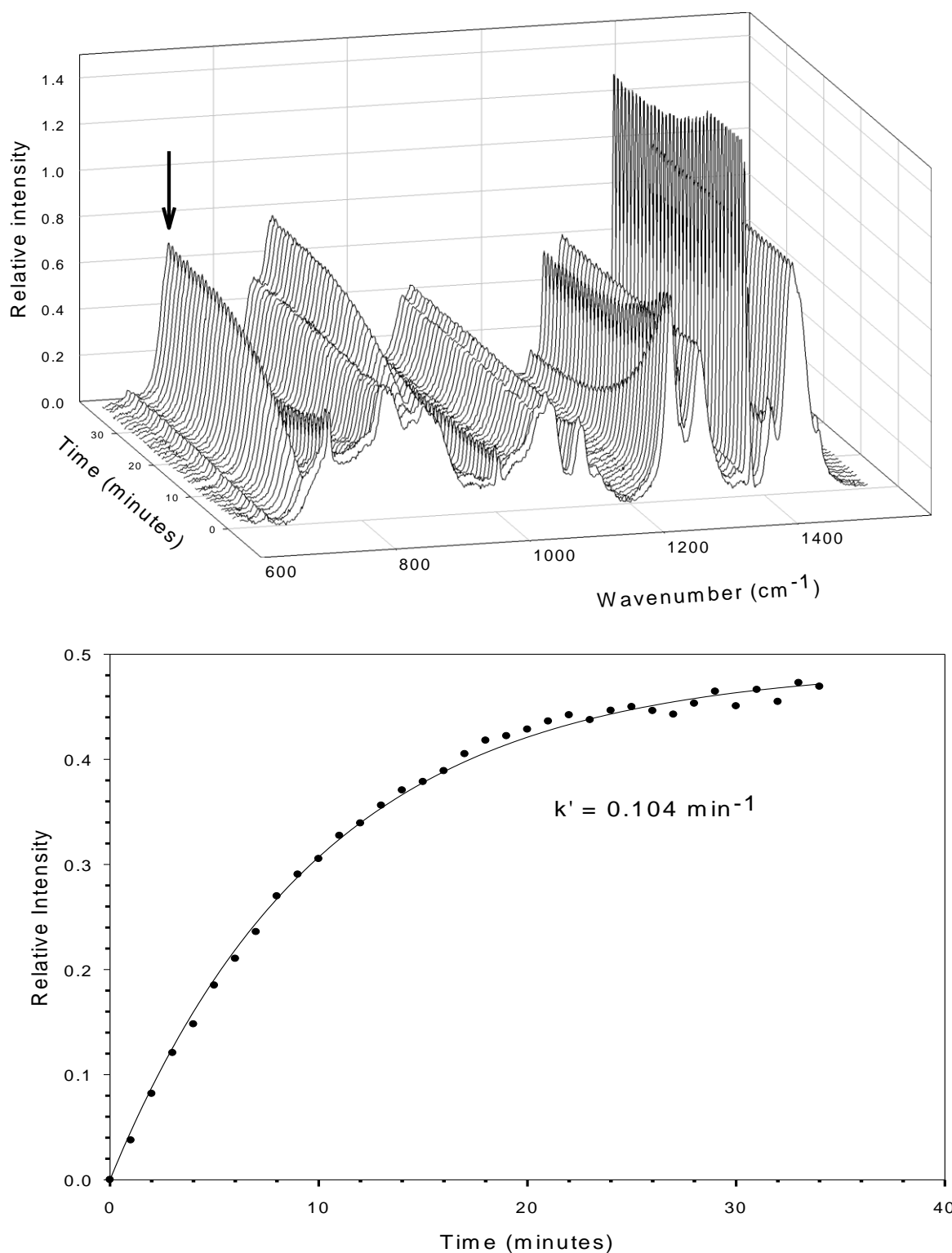


Figure 2: Overlay of the Raman spectra (above) and time dependence of the peak intensity at  $715 \text{ cm}^{-1}$  (below) for the chemical fixation of  $\text{CO}_2$  onto 1,2-epoxydodecane using HBD6/ $\text{nBu}_4\text{NI}$  as bicomponent organocatalyst. Conditions: volume of the cell = 80 ml,  $V_{\text{epoxydodecane}} = 30 \text{ mL}$ ,  $[\text{nBu}_4\text{NI}]/[1,2\text{-epoxydodecane}] = 0.025$ ,  $[\text{nBu}_4\text{NI}]/[\text{HBD6}] = 1$ ,  $T = 80^\circ\text{C}$ ,  $p = 8 \text{ MPa}$ , red incident light ( $\lambda = 785 \text{ nm}$ ,  $P = 120 \text{ mW}$ ). Spectra recorded every minute

**b) Kinetic study by IR spectroscopy***Set-up*

The synthesis of cyclic carbonates from model epoxide and CO<sub>2</sub> was followed *in-situ* using a FTIR microscope (Perkin Elmer Spotlight400) working in transfection coupled with a home-made high pressure cell that allows to record the infrared spectra of the liquid and the gas phase (Figure 3). For our purpose, the cell was fitted with a sapphire window, a polyethylene spacer of 1.1 mm thickness and a liquid volume of approximately 100  $\mu$ L. Single beam spectra of the liquid phase recorded with a 2 cm<sup>-1</sup> resolution were obtained after the Fourier transformation of 300 accumulated interferograms. Spectra were recorded continuously every five minutes for 311 minutes. The cell was heated using cartridge heaters disposed in the periphery of its body. A thermocouple was used located close to a cartridge heater for the temperature regulation with an accuracy of about 2°C. The mixture composed of 1 mL of the epoxide with a given molar percent of catalyst was disposed in the cell at ambient temperature. Then, the cell was heated up to 60°C and carbon dioxide was injected till P = 2 MPa using high pressure high temperature connections.

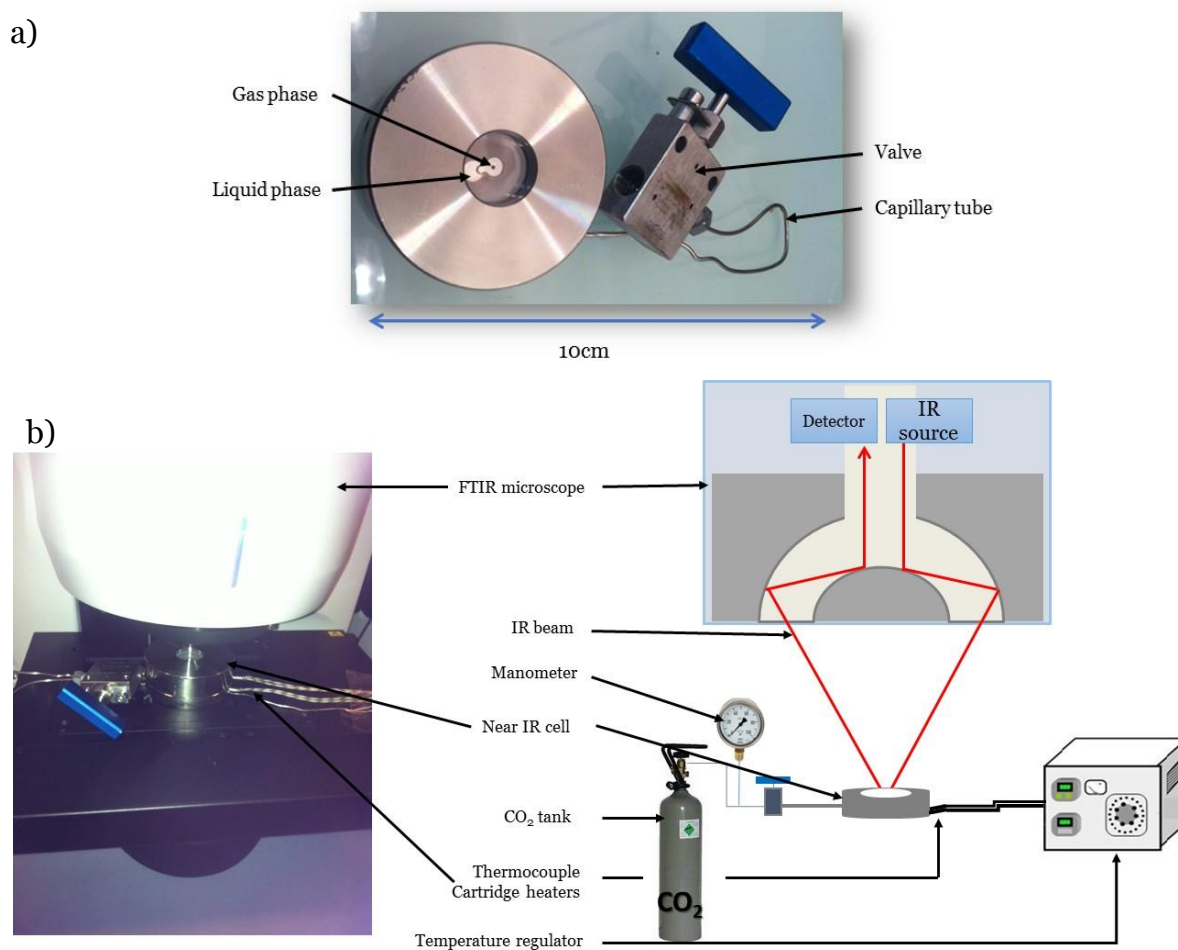


Figure 3: a) Home-made Near-FTIR high pressure cell, b) Picture and schematic representation of the experiment set-up

*Kinetic study by FTIR spectroscopy of the chemical fixation of CO<sub>2</sub> onto propylene oxide in the presence of HBD/nBu<sub>4</sub>NBr bicomponent organocatalysts*

The synthesis of PC was realized at  $T = 60^\circ\text{C}$  and 2 MPa using HBD6 (1,3-bis-HFAB) or pyrogallol in combination with nBu<sub>4</sub>NBr as bicomponent organocatalyst. Under these thermodynamic conditions, the system is under biphasic conditions with an epoxide rich phase which is “swelled” by a significant amount of CO<sub>2</sub> ( $X_{\text{CO}_2} = 0.2$ ). Thus, the epoxide-CO<sub>2</sub> reaction takes place in this epoxide rich phase, knowing moreover that TBABr and the hydrogen bond donors are soluble in this phase and insoluble in the CO<sub>2</sub> rich phase. In this phase, the strong absorption of propylene oxide and propylene carbonate in the mid infrared region between 400 and 4000 cm<sup>-1</sup> requires the use of a very small pathlength (below 20  $\mu\text{m}$ ) that might lead to bad equilibration of the mixture. Therefore, in order to follow the apparition of the carbonate, near infrared absorption spectroscopy (NIR) was used to detect the combination modes of carbonate vibrational modes where a good signal to noise ratio is obtained using a pathlength of about 2 mm. In particular, we choose to monitor the appearance of the peak associated to the  $\nu(\text{C=O}) + \nu(\text{C-H})$  combination mode at 4800 cm<sup>-1</sup> and the disappearance of the peak at 6050 cm<sup>-1</sup> ( $2\nu(\text{C-H})$  mode of the epoxide ring) (Figure 4). In addition, thanks to two peaks centered at 4950 and 5100 cm<sup>-1</sup> that are respectively associated to the combination bands ( $\nu_1 + 2\nu_2 + \nu_3$  and  $2\nu_1 + \nu_3$ ) of CO<sub>2</sub>, the concentration of CO<sub>2</sub> in the mixture as a function of time was easily measured. The cyclic carbonate formation rate was determined by following the evolution of the peak at 4800 cm<sup>-1</sup> with time.

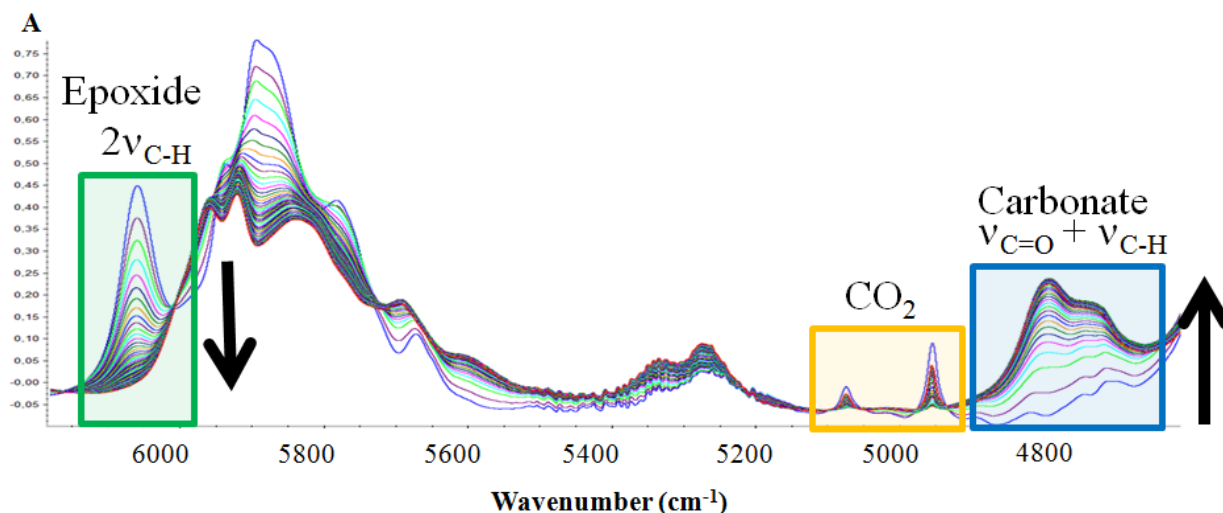


Figure 4: Time evolution of the Near Infrared spectra of the propylene oxide/CO<sub>2</sub>/catalyst mixture at  $T = 60^\circ\text{C}$  and  $P = 2$  MPa using 3 mol% of nBu<sub>4</sub>NBr as organocatalyst.

### 3- Characterization

$^1\text{H}$  NMR spectra were recorded in  $\text{CDCl}_3$  or in  $\text{C}_6\text{D}_6$  at 400 MHz in the FT mode with a Bruker AN 400 apparatus at 25°C.

### 4- Computational details

Preliminary calculations of equilibrium structures were carried out using a semi empirical model (AM1-D3H4<sup>48, 49</sup>) to determine the most stable conformations. These semi-empirical calculations were performed using the AMPAC software<sup>50</sup>. The CHAIN algorithm was used for locating intermediates and transition states along the reaction path. The lowest energy structures obtained at the AM1-D3H4 level were further investigated using the density functional theory (DFT) method implemented in the Gaussian 09 package<sup>51</sup>. DFT calculations of geometries, energies, and vibrational frequencies reported in this paper were carried out with the M06-2X functional<sup>52</sup> using the 6-311G(d,p) basis sets.

All frequencies of each structure have also been calculated to verify the presence of a single imaginary frequency for transition states and the absence of imaginary frequency for ground states. The intrinsic reaction coordinate (IRC) method has been used to verify that most of the obtained transition states were well connected to the desired minima. For all the catalysts tested, a wide range of possible configurations and interactions have been tested and the more stable of them were reported in this work. The energies given in this study correspond to the Gibbs free energy ( $\Delta G$ ) in order to consider entropy effects.

## Results and discussion

Series of single H-bond (*tert*-butanol (HBD1), 1,1,1-trifluoro-2-methyl-2-propanol (HBD2), hexafluoro-*tert*-butanol (HBD3), perfluoro-*tert*-butanol (HBD4)) and double H-bond donors,  $\alpha,\alpha'$ -dihydroxy-1,3-diisopropylbenzene (HBD5), 1,3-bis(2-hydroxyhexafluoroisopropyl)benzene (HBD6, 1,3-bis-HFAB) were used in combination with the classical tetrabutylammonium iodide (nBu<sub>4</sub>NI) organocatalyst for the solvent-free chemical fixation of CO<sub>2</sub> onto 1,2-epoxydodecane (ED). The reaction rates were followed by online backscattered Raman spectroscopy<sup>53</sup> (Figure 2) under pressure using a red incident light ( $\lambda = 785$  nm) and are compared in Figure 5. A reference reaction was first conducted at 80°C and 8 MPa using 2.5 mol% nBu<sub>4</sub>NI (compared to the epoxide) in order to monitor the reaction that answers a pseudo-first order kinetic as CO<sub>2</sub> was used in large excess. In the absence of activator, nBu<sub>4</sub>NI organocatalyst displayed a poor catalytic activity with a  $k'$  value of 0.0005 min<sup>-1</sup>, the reaction being complete in 7300 min (Table 1, Figure 5).

Table 1: Chemical fixation of CO<sub>2</sub> onto ED using fluorinated and non-fluorinated HBDs. Conditions: T = 80°C, P = 8 MPa, [ED]/[nBu<sub>4</sub>NI] = 40, [HBDs] / [nBu<sub>4</sub>NI] = 1. <sup>a</sup> Determined for conversion > 98%

Entry	activator	$k'$ (min <sup>-1</sup> )	Time (min) <sup>a</sup>
1	/	0.0005	7300
2	HBD1	0.0014	2500
3	HBD2	0.0034	1100
4	HBD3	0.0290	130
5	HBD4	0.0826	45
6	HBD5	0.0020	1800
7	HBD6	0.1200	30

The rate constant was increased by 300% by the simple addition of one equivalent (compared to nBu<sub>4</sub>NI) of a common alcohol, *tert*-butanol (HBD1). Table 1 shows that the substitution of one, two or three of the methyl groups of this alcohol by trifluoromethyl groups incredibly speeded up the reaction by 680, 5800 and 16520%, respectively. This impressive improvement of activity seems therefore to be linked to both the acidity and the hydrogen bonding capability of the tertiary alcohol that are both increased with the number of electron-withdrawing -CF<sub>3</sub> substituents. Fluorinated double H-bonding co-catalyst (HBD6, 1,3-bis-HFAB) in combination with nBu<sub>4</sub>NI provided the best activity with a 20800% rate increase compared to the catalytic system without any HBD activator. The reaction was complete in only 30 minutes without the formation of by-products. The importance of the presence of the fluorinated groups was again highlighted by comparing the activity of the non-fluorinated analogue (HBD5) that was about 50 times lower ( $k' = 0.002$  min<sup>-1</sup> for HBD5 vs 0.1040 min<sup>-1</sup> for HBD6 (1,3-bis-HFAB)).



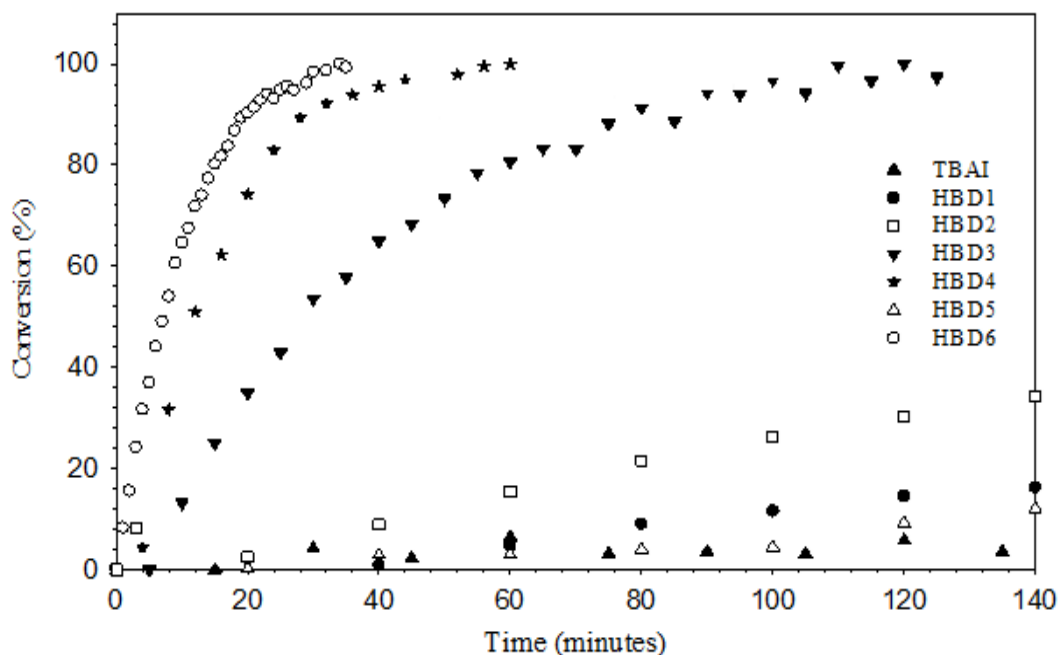


Figure 5: Chemical fixation of CO<sub>2</sub> onto ED using nBu<sub>4</sub>NI as organocatalyst in the presence or not of (non-)fluorinated HBDs: kinetic study by online Raman spectroscopy under pressure. Conditions : T = 80°C, P = 8 MPa, [ED]/[nBu<sub>4</sub>NI] = 40, [HBDs]/[nBu<sub>4</sub>NI] = 1.

To further highlight the efficiency of the nBu<sub>4</sub>NI/HBD6 (1,3-bis-HFAB) co-catalytic system, the CO<sub>2</sub>/epoxide coupling was tested at lower pressure. For each experiment, the CO<sub>2</sub> pressure was maintained constant during the whole reaction so that all kinetics answered a pseudo-first order and could therefore be compared. Results reported in Table 2 demonstrate that a decrease of the CO<sub>2</sub> pressure from 8 to 1.5 MPa had almost no impact on the reaction rate, with a kinetic constant around 0.10 min<sup>-1</sup> corresponding to a complete conversion of the epoxide ring into cyclocarbonate in about 35 minutes. Even at a pressure of 0.1 MPa (Table 2, entry 4), the co-catalytic system still displayed good activity with a reaction that was complete in 600 minutes, thus that remained 12 times faster than the same reaction carried out at 8 MPa without HBD6 (1,3-bis-HFAB) (Table 1, entry 1).

Table 2: Effect of pressure on the chemical fixation of CO<sub>2</sub> onto ED using HBD6/nBu<sub>4</sub>NI bicomponent organocatalyst. Conditions: T = 80°C, [nBu<sub>4</sub>NI]/[HBD6] = 1, [ED]/[nBu<sub>4</sub>NI] = 40

Entry	Pressure (MPa)	k' (min <sup>-1</sup> )	Time (min)
1	8	0.12	30
2	5	0.11	33
3	1.5	0.10	35
4	0.1	0.006	600

As the CO<sub>2</sub>/epoxide couplings were conducted in neat ED, the addition of catalytic amounts of (fluoro)alcohols might slightly change the polarity of the epoxide/CO<sub>2</sub> mixture. They could therefore act as co-solvents that improved the solubility of nBu<sub>4</sub>NI in the epoxide. To demonstrate that their co-catalytic activity is not related to

a simple co-solvent effect, CO<sub>2</sub>/epoxide coupling was performed by homogeneous solvent-free fixation of CO<sub>2</sub> onto viscous oligomers of poly(ethyleneglycol) diglycidylether (M<sub>n</sub> = 500 g/mol) in which all components (ammonium salt, (fluoro)alcohols, CO<sub>2</sub>) present a high solubility. In the presence of 2.5 mol% of nBu<sub>4</sub>NI at 80°C and 10 MPa without alcohol, the kinetic constant was estimated to 0.018 min<sup>-1</sup>, corresponding to a complete reaction in 240 minutes. Remarkably, the addition of 1 equivalent of HBD6 (1,3-bis-HFAB) induced a 12-fold increase of the kinetic constant ( $k' = 0.217 \text{ min}^{-1}$ ) whereas the corresponding non-fluorinated analogue (HBD5) has no co-catalytic activity ( $k' = 0.017 \text{ min}^{-1}$ ). These results confirm that the substitution of the methyl groups of alcohols by trifluoromethyl groups positively impacts the kinetic. They also figure out that the increase of the reaction rate clearly arises from a synergistic effect between the catalyst and the fluorinated H-bond donors, and not from a co-solvent effect.

Finally, the co-catalytic effect of HBD6 (1,3-bis-HFAB) was compared to that of phenolic compounds, recently reported to be the most active organic activators for the coupling of CO<sub>2</sub> with various epoxides.<sup>46</sup> Because phenolic compounds induce fluorescence by Raman spectroscopy, kinetics was monitored by online high pressure infrared spectroscopy (Figure 6). CO<sub>2</sub>/epoxide coupling of neat propylene oxide (PO) was conducted at 60°C and a low CO<sub>2</sub> pressure of 2 MPa in the presence of 3 mol% of nBu<sub>4</sub>NBr as organic salt and HBD6 (1,3-bis-HFAB) or pyrogallol as activator in an equimolar ratio. HBD6 (1,3-bis-HFAB) almost doubled the system activity compared to pyrogallol with a complete conversion of PO into propylene carbonate in 120 minutes (Figure 6). The same conclusions are drawn when catechol is substituted for pyrogallol (Table 3).

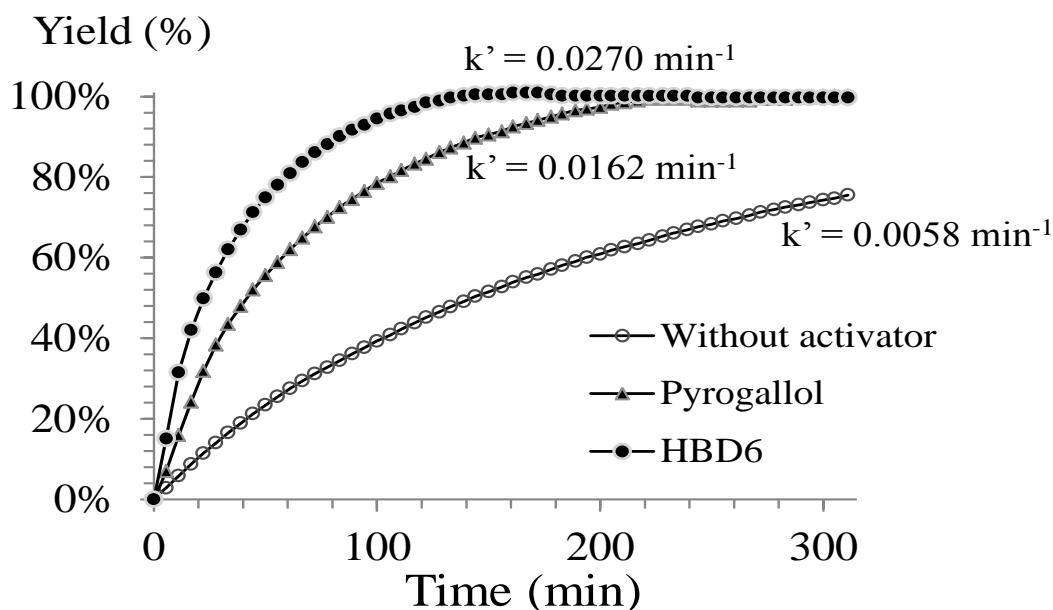
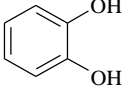
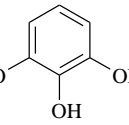
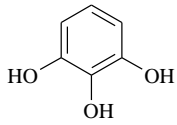


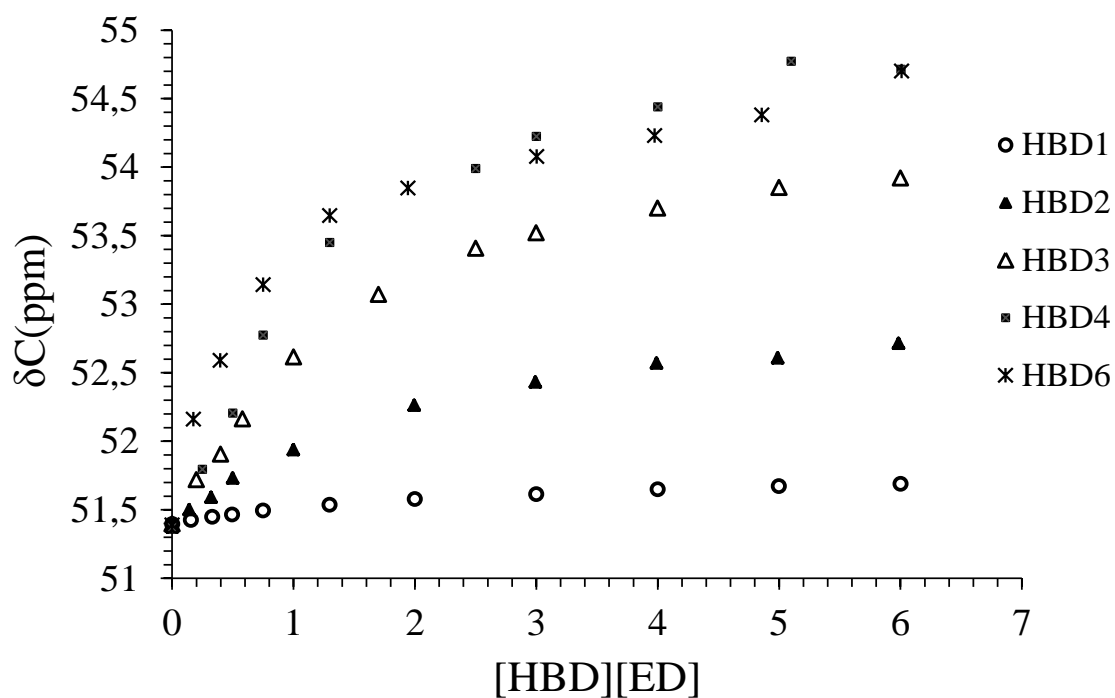
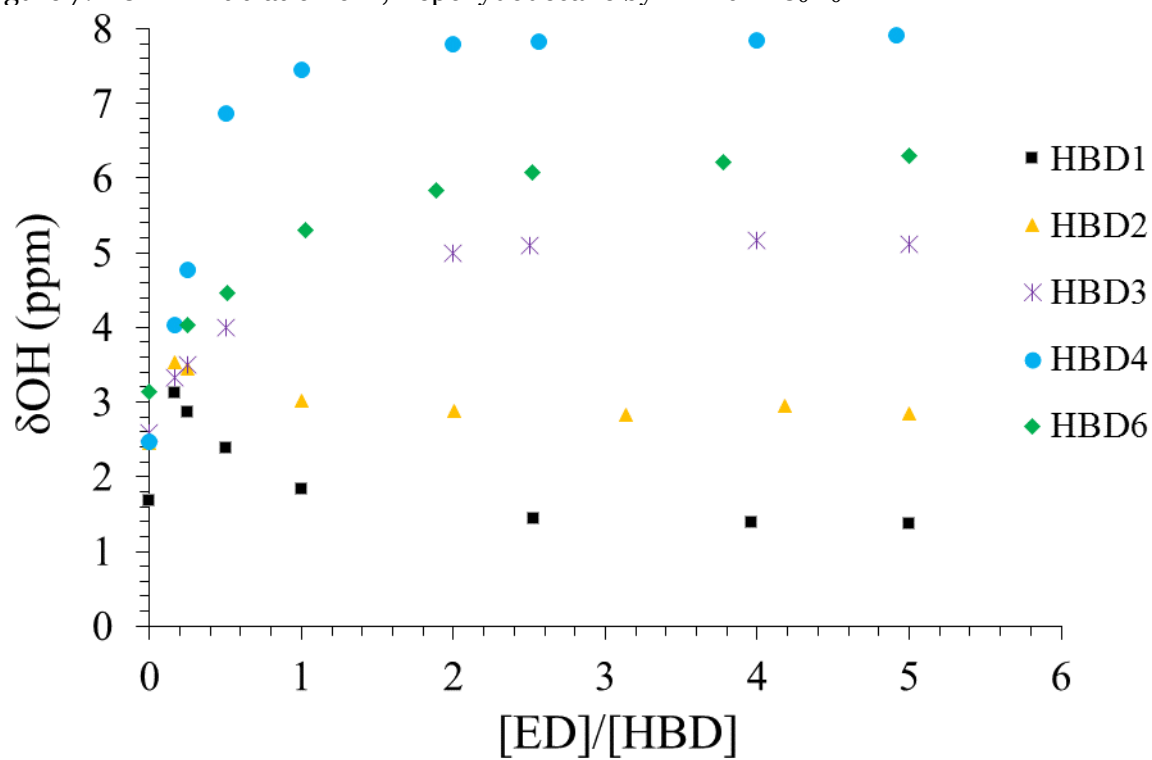
Figure 6: Comparison of rates of fixation of CO<sub>2</sub> onto neat PO in the presence or not of fluorinated or phenolic HBDs by *in-situ* near FTIR spectroscopy. Conditions: T = 60°C, P = 2 MPa, [nBu<sub>4</sub>NBr]/[HBD] = 1, [PO]/[nBu<sub>4</sub>NBr] = 33.3

Table 3: Comparison of the co-catalytic effect of fluorinated and phenolic HBD on the fixation of CO<sub>2</sub> onto neat propylene oxide. Experimental conditions: T = 60°C, P = 2 MPa, [nBu<sub>4</sub>NBr]/[activator] = 1, [propylene oxide]/[nBu<sub>4</sub>NBr] = 33.3

Entry	activator	[HBD] / [nBu <sub>4</sub> NBr]	k' (min <sup>-1</sup> )	Time (min)
1		/	0.0058	600
2		1	0.0156	210
3		1	0.0162	200
4	HBD6	1	0.0270	120

From all these kinetics data, it is assumed that HBDs interact with the epoxide by hydrogen bonding, favouring the epoxide-ring opening which is the limiting step in CO<sub>2</sub>/epoxide coupling. <sup>1</sup>H- and <sup>13</sup>C-NMR titration experiments were therefore carried out in order to probe this interaction.<sup>9</sup> The interaction of HBDs with the epoxide was first investigated by <sup>13</sup>C-NMR titrations of the different epoxide/HBDs couples. A downfield shift of the carbon signal of the oxirane ( $\delta$  = 51.5 ppm) is observed by adding HBDs, suggesting that all alcohols interact with ED, presumably by hydrogen bonding. This shift is increased if 1, 2 or 3 trifluoromethyl electron-withdrawing groups substitute the methyl groups of *tert*-butanol (HBD1) (Figure 7).

The extent of this downfield shift is correlated to the activity observed for the different HBDs/nBu<sub>4</sub>NI organocatalytic systems that were used for the reaction (Table 1), thus HBD6 (1,3-bis-HFAB) > HBD4 > HBD3 > HBD2 > HBD1. <sup>1</sup>H-NMR titrations of ED by HBDs also evidence the hydrogen-bonding interaction between the two components (Figure 8). A large change in the chemical shift of the OH resonance of HBDs is indeed observed. For the single HBDs, change in the  $\delta$ OH value increased with the level of substitution by trifluoromethyl electron-withdrawing groups, in line with the increased acidity of the corresponding HBDs, and therefore their hydrogen-bonding capability. Importantly when the double H-bond donor (HBD6, 1,3-bis-HFAB) is considered, the aromatic proton B in *ortho* position of the two fluorinated substituents is also interacting with the epoxide as indicated by the change in its chemical shift (Figure 9). This hydrogen bonding also slightly affects the chemical shift of all the other aromatic protons as a result of the deformation of the electronic density of the aromatic ring. Protons A of the two hydroxyl groups and aromatic proton B of HBD6 (1,3-bis-HFAB) seem therefore to activate the epoxide for the coupling with CO<sub>2</sub>.

Figure 7:  $^{13}\text{C}$  NMR titration of 1,2-epoxydodecane by HBDs in  $\text{C}_6\text{D}_6$ Figure 8:  $^1\text{H}$  NMR titration of 1,2-epoxydodecane by HBDs in  $\text{C}_6\text{D}_6$ .

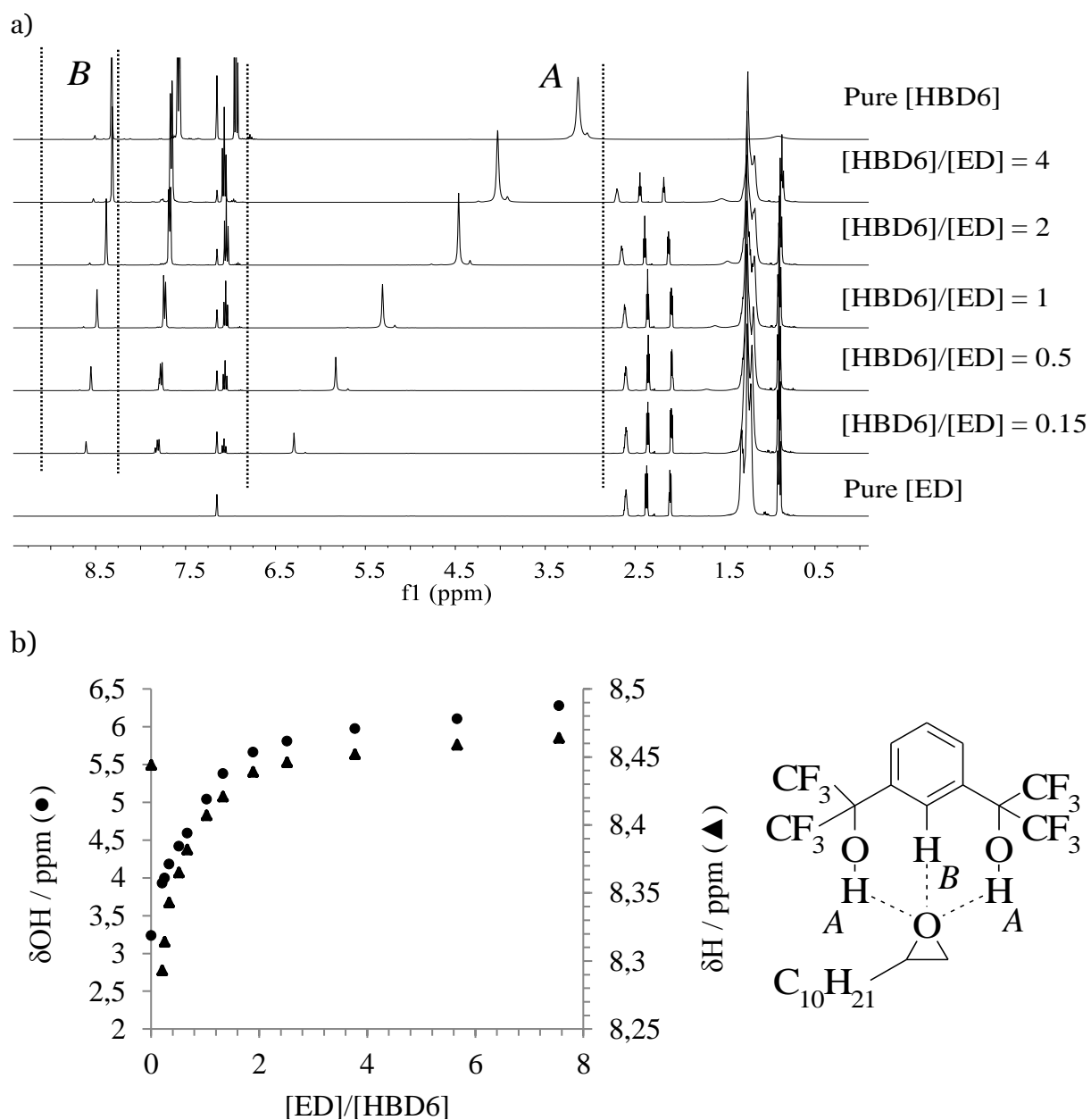


Figure 9:  $^1\text{H}$  NMR titration of ED in  $\text{C}_6\text{D}_6$  by HBD6 (1,3-bis-HFAB): a) overlay of the  $^1\text{H}$  NMR spectra and b) variation of the chemical shift of the hydroxyl protons A ( $\delta\text{OH}$ ) and the proton B ( $\delta\text{H}_\text{B}$ ) with the  $[\text{ED}]/[\text{HBD6}]$  molar ratio.

The hydrogen bonding interaction between HBD6 (1,3-bis-HFAB) and the epoxide was further supported by DFT calculations performed at the Mo6-2X/6-311G(d,p) level. The HBD6 (1,3-bis-HFAB) adduct with PO exhibits two intermolecular H-bonds between each hydroxyl group of HBD6 (1,3-bis-HFAB) and the O atom of the epoxide (Figure 10). The intermolecular distances are not equal (1.91 Å and 2.09 Å) because of the asymmetry of propylene oxide. As observed by  $^1\text{H}$  NMR titrations, a third hydrogen bond exists between the aromatic proton in *ortho* position of the two fluorinated substituents and the O atom of PO (2.40 Å). Gibbs energy of the complex ( $\Delta G = -3.88$  kcal/mol) clearly evidences the strong hydrogen bond interaction between HBD6 (1,3-bis-HFAB) and PO.

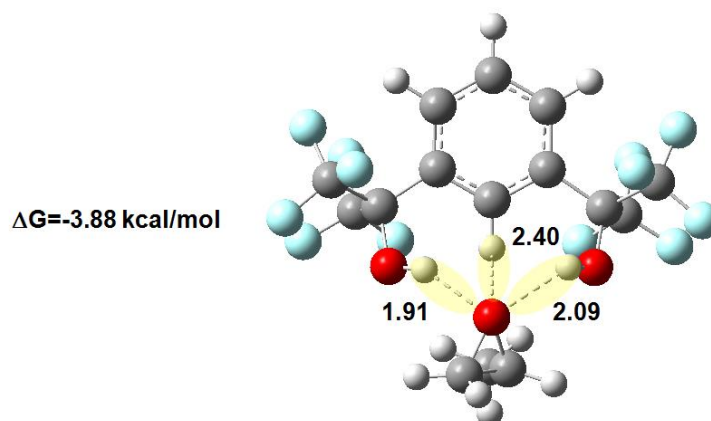


Figure 10: Optimized structure of the HBD6 (1,3-bis-HFAB)-PO adduct at the Mo6-2X level using the 6-311G(d,p) basis set. The dashed lines depict the intermolecular distances in angström.

To go further in the mechanism comprehension and to provide a possible explanation to the different  $\text{CO}_2$ /epoxide coupling rates reported above, quantum chemistry calculations were performed. We have examined and compared the reaction between propylene oxide (PO) and  $\text{CO}_2$  catalysed by (1)  $\text{nBu}_4\text{NBr}$ , (2)  $\text{nBu}_4\text{Br}$  plus pyrogallol, or (3)  $\text{nBu}_4\text{NBr}$  plus HBD6 (1,3-bis-HFAB). The Gibbs energy profiles obtained at the Mo6-2X/6-311G(d,p) level and the schematic intermediate structures are depicted on Figure 11 for the three systems. The  $\text{CO}_2$ /epoxide coupling between PO and  $\text{CO}_2$  has been modelled following a three key elementary process involving the epoxide ring opening, the  $\text{CO}_2$  electrophilic attack, and the intramolecular cyclisation steps. This pathway was reported to be consistent with experimental findings.<sup>54</sup> Initial state (zero energy) corresponds to the sum of the Gibbs energy of each compound ( $\text{nBu}_4\text{NBr}$ /Propylene oxide/ $\text{CO}_2$ /Pyrogallol or HBD6 (1,3-bis-HFAB)) fully optimized.

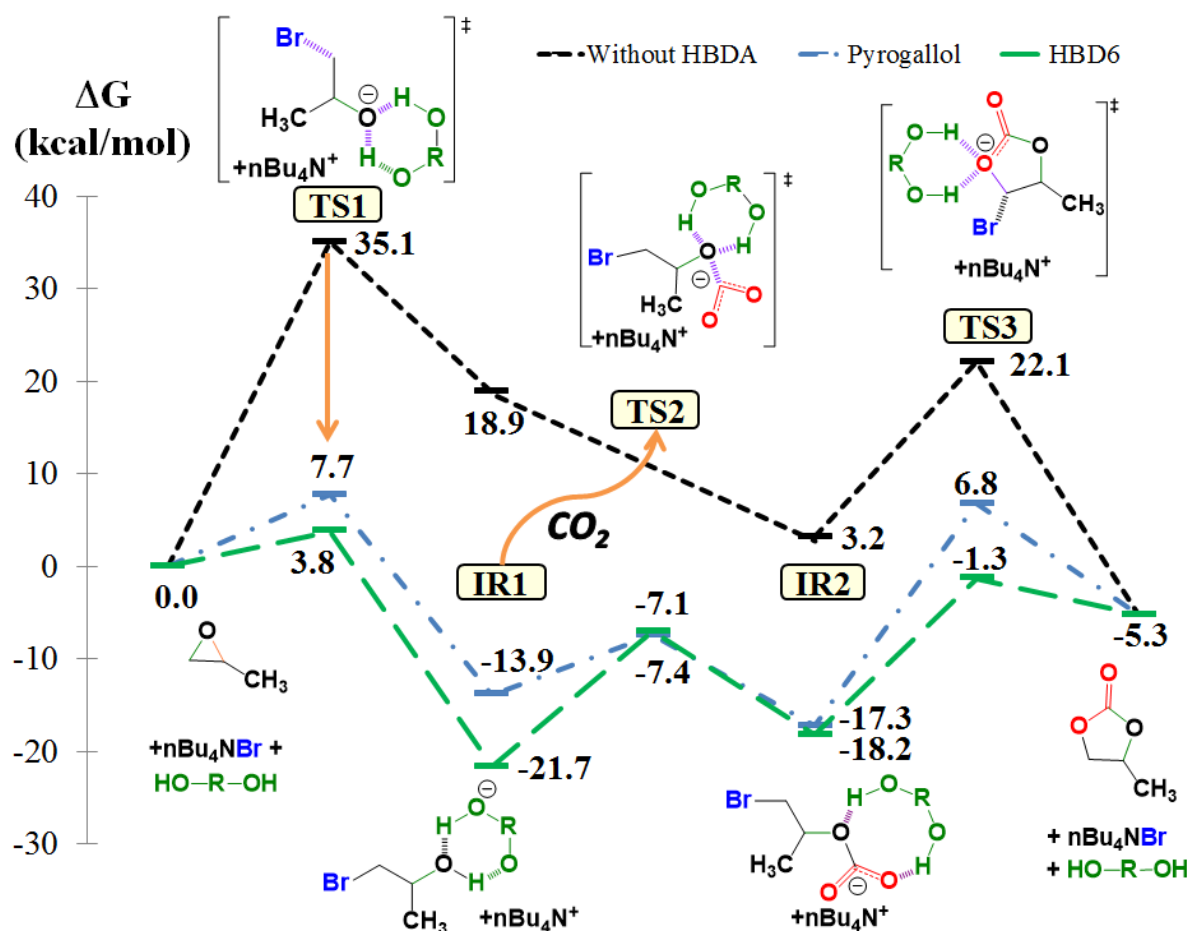


Figure 11: Free energy profile (Mo6-2X/6-311G(d,p)) and Lewis structures for carbonate formation catalyzed by nBu<sub>4</sub>NBr (-), by nBu<sub>4</sub>NBr plus pyrogallol (--) or by nBu<sub>4</sub>NBr plus HBD6 (1,3-bis-HFAB) (---)

Consistently with the literature,<sup>29</sup> by using nBu<sub>4</sub>NBr without hydrogen-bonding donor, the overall reaction is exothermic by 5.3 kcal.mol<sup>-1</sup> and the ring opening is the rate-determining step with a Gibbs energy of 35.1 kcal.mol<sup>-1</sup>. In the presence of HBD6 (1,3-bis-HFAB), the first transition state (TS1) involves H bondings between the O atom of the bromohydrin anion formed by ring-opening with the two OH groups of HBD6 (1,3-bis-HFAB) and the aromatic proton in *ortho* position to hexafluoro alcohol functionalities. The OH distances for these O...H-O fragments are 1.44 Å and 1.91 Å and the O...H<sub>aromatic</sub> distance is 2.32 Å (Figure 12, TS1). This stabilization decreases drastically the energy of the first step to overcome (ΔG<sub>TS1</sub> = 3.8 kcal.mol<sup>-1</sup>) compared to that one previously described without H-bond donor (ΔG<sub>TS1</sub> = 35.1 kcal.mol<sup>-1</sup>). From TS1, the formation of the bromohydrin and the fluorinated oxyanion leads to the stable intermediate IR1. Then, a new transition state (TS2) (ΔG<sub>TS2</sub> = 14.6 kcal/mol) results from the attack of CO<sub>2</sub> onto the O atom of the bromohydrin, with the concomitant O-H breaking and the release of HBD6 (1,3-bis-HFAB) (Figure 12). The bromo-alkylcarbonate (IR2) is then formed and is stabilized by hydrogen bondings: the aromatic hydrogen and one OH group of HBD6 (1,3-bis-HFAB) interact with the terminal O atom of the carbonate ion, and the second OH group stabilizes the O atom situated between the two C atoms of the bromo-alkylcarbonate.

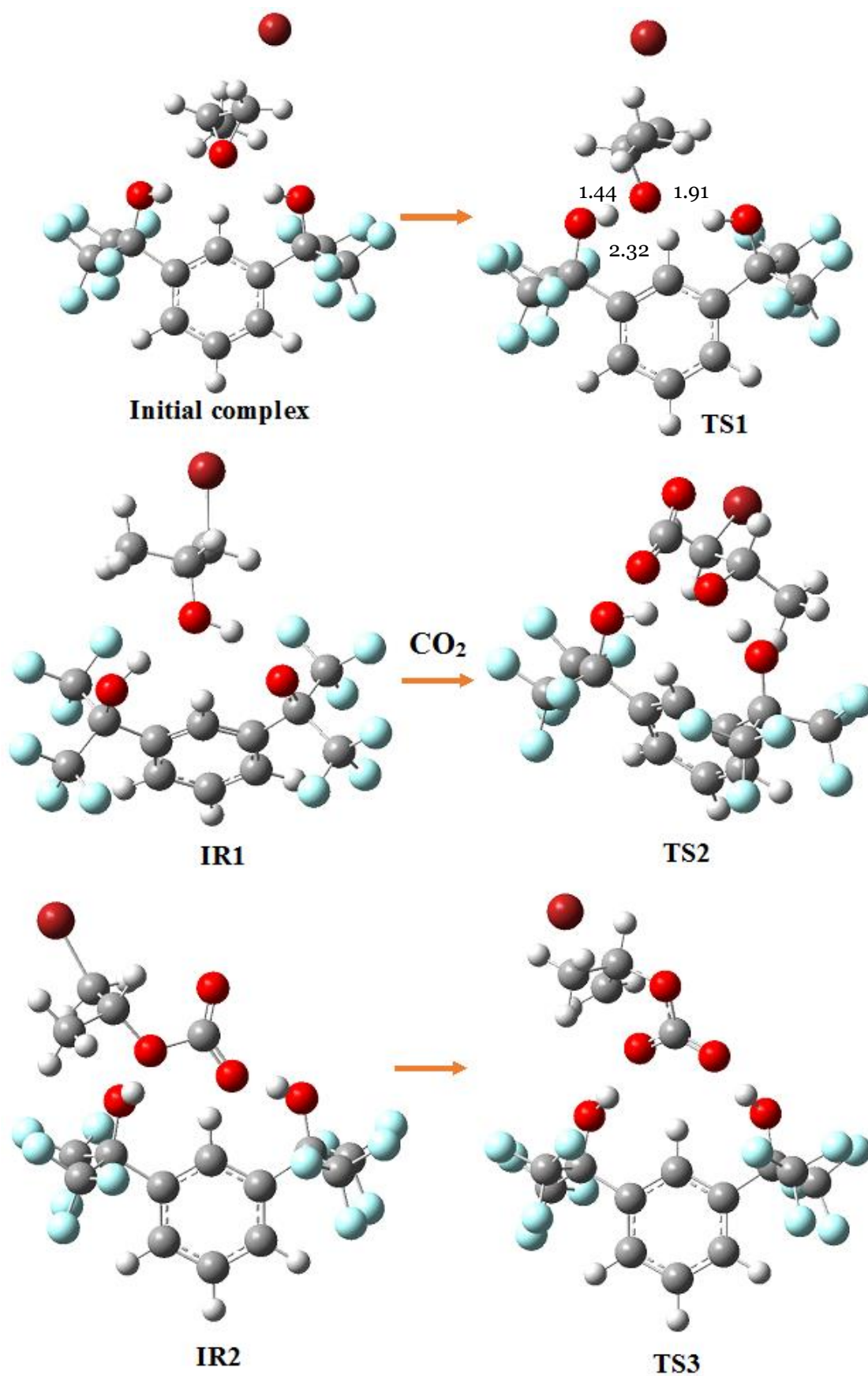


Figure 12: Optimized geometries (M06-2X/6-311G(d,p)) of the structures for the CO<sub>2</sub>/epoxide coupling, in the presence of HBD6/nBu<sub>4</sub>NBr. For a better clarity, nBu<sub>4</sub>NBr is not represented on the structures.



Finally, the last step ( $\Delta G_{TS3} = 16.9$  kcal/mol) involves a torsional deformation of the bromo-alkylcarbonate and the C-Br bond rupture. Propylene carbonate is formed by ring-closure of alkylcarbonate and  $n\text{Bu}_4\text{NBr}$  is regenerated. Consequently, adding a hydrogen-bond donor strongly reduces the relative energy of the reaction in comparison with the system without activator. The hydrogen-bond stabilization mechanism particularly impacts the energy of the epoxide ring-opening step. The same conclusion holds for pyrogallol although the overall energy profile is higher in energy than that reported for HBD6 (1,3-bis-HFAB). This is due to the stabilization mechanism that involves only two intermolecular H-bonds instead of three in the case of HBD6 (1,3-bis-HFAB) (Figure 13).

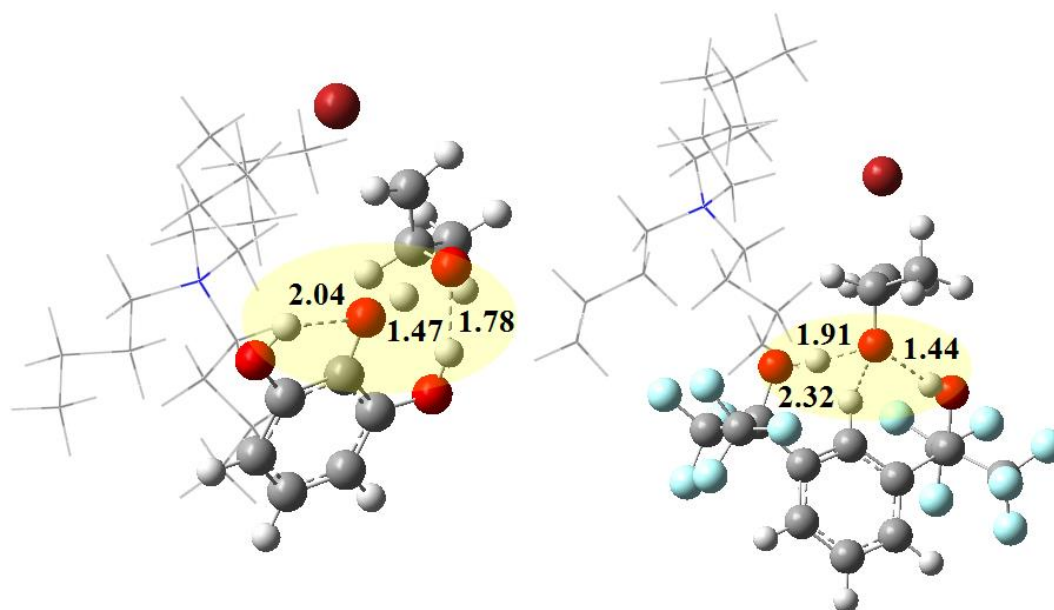


Figure 13: Optimized structures of the transition state TS1 for the ring opening of PO catalyzed by  $n\text{Bu}_4\text{NBr}$  plus pyrogallol (left) and  $n\text{Bu}_4\text{NBr}$  plus HBD6 (right) at the Mo6-2X level using the 6-311G(d,p) basis set. The dashed lines depict the intermolecular distances in angström.

## Conclusion

In this communication, we show that H-bond donors with hexafluoroalcohol functionalities enable to remarkably boost the chemical fixation of  $\text{CO}_2$  onto epoxides when using a conventional onium salt as organocatalyst. This novel bicomponent organocatalytic system is unique for the fast production of cyclic carbonates under mild and solvent free experimental conditions. Kinetic studies combined to NMR titrations and DFT calculations evidence the synergistic effect between onium salt and fluorinated alcohol. We demonstrate here that catalytic amount of fluorinated alcohol activates the epoxide for the ring-opening, the limiting step for the chemical fixation of  $\text{CO}_2$  onto epoxides using this new bicomponent organocatalytic system. This is in sharp contrast to previous works that showed that some fluorinated alcohols had a detrimental effect on the  $\text{CO}_2$ /epoxide coupling when they are used as solvents.<sup>15</sup>

## References

1. Hydrogen Bonding in Organic Synthesis, P.M. Pihko, Weinheim: Wiley VCH, 2009
2. A. G. Doyle and E. N. Jacobsen, *Chemical Reviews*, 2007, **107**, 5713-5743.
3. T. Akiyama, *Chemical Reviews*, 2007, **107**, 5744-5758.
4. M. K. Kiesewetter, E. J. Shin, J. L. Hedrick and R. M. Waymouth, *Macromolecules*, 2010, **43**, 2093-2107.
5. D. Vuluga, J. Legros, B. Crousse, A. M. Z. Slawin, C. Laurence, P. Nicolet and D. Bonnet-Delpon, *Journal of Organic Chemistry*, 2011, **76**, 1126-1133.
6. A. Berkessel, J. A. Adrio, D. Hüttenhain and J. M. Neudörfl, *Journal of the American Chemical Society*, 2006, **128**, 8421-8426.
7. P. I. Dalko and L. Moisan, *Angewandte Chemie International Edition*, 2004, **43**, 5138-5175.
8. J.-P. Bégué, D. Bonnet-Delpon and B. Crousse, *Synlett*, 2004, **2004**, 18-29.
9. O. Coulembier, D. P. Sanders, A. Nelson, A. N. Hollenbeck, H. W. Horn, J. E. Rice, M. Fujiwara, P. Dubois and J. L. Hedrick, *Angewandte Chemie - International Edition*, 2009, **48**, 5170-5173.
10. J. Legros, B. Crousse, D. Bonnet-Delpon and J. P. Bégué, *European Journal of Organic Chemistry*, 2002, 3290-3293.
11. M. C. A. van Vliet, I. W. C. E. Arends and R. A. Sheldon, *Synlett*, 2001, **2001**, 0248-0250.
12. A. Berkessel and J. A. Adrio, *Advanced Synthesis and Catalysis*, 2004, **346**, 275-280.
13. K. Žmitek, S. Stavber, M. Zupan, D. Bonnet-Delpon and J. Iskra, *Tetrahedron*, 2006, **62**, 1479-1484.
14. A. Berkessel, M. R. M. Andreae, H. Schmickler and J. Lex, *Angewandte Chemie - International Edition*, 2002, **41**, 4481-4484.
15. N. Aoyagi, Y. Furusho and T. Endo, *Tetrahedron Letters*, 2013, **54**, 7031-7034.
16. B. Chatelet, L. Joucla, J. P. Dutasta, A. Martinez, K. C. Szeto and V. Dufaud, *Journal of the American Chemical Society*, 2013, **135**, 5348-5351.
17. Y. Tsutsumi, K. Yamakawa, M. Yoshida, T. Ema and T. Sakai, *Organic Letters*, 2010, **12**, 5728-5731.
18. K. R. Roshan, T. Jose, D. Kim, K. A. Cherian and D. W. Park, *Catalysis Science & Technology*, 2014, **4**, 963-970.
19. J. Tharun, G. Mathai, A. C. Kathalikkattil, R. Roshan, J. Y. Kwak and D. W. Park, *Green Chemistry*, 2013, **15**, 1673-1677.
20. K. R. Roshan, G. Mathai, J. Kim, J. Tharun, G.-A. Park and D.-W. Park, *Green Chemistry*, 2012, **14**, 2933-2940.
21. D. Tian, B. Liu, Q. Gan, H. Li and D. J. Darensbourg, *ACS Catalysis*, 2012, **2**, 2029-2035.
22. X.-B. Lu and D. J. Darensbourg, *Chemical Society Reviews*, 2012, **41**, 1462-1484.
23. M. Taherimehr, S. M. Al-Amsyar, C. J. Whiteoak, A. W. Kleij and P. P. Pescarmona, *Green Chemistry*, 2013, **15**, 3083-3090.
24. C. J. Whiteoak, N. Kielland, V. Laserna, E. C. Escudero-Adán, E. Martin and A. W. Kleij, *Journal of the American Chemical Society*, 2013, **135**, 1228-1231.
25. A. Decortes, M. Martinez Belmonte, J. Benet-Buchholz and A. W. Kleij, *Chemical Communications*, 2010, **46**, 4580-4582.

26. N. Aoyagi, Y. Furusho and T. Endo, *Journal of Polymer Science Part A: Polymer Chemistry*, 2013, **51**, 1230-1242.
27. V. Caló, A. Nacci, A. Monopoli and A. Fanizzi, *Organic Letters*, 2002, **4**, 2561-2563.
28. S. Foltran, R. Mereau and T. Tassaing, *Catalysis Science and Technology*, 2014, **4**, 1585-1597.
29. S. Foltran, J. Alsarraf, F. Robert, Y. Landais, E. Cloutet, H. Cramail and T. Tassaing, *Catalysis Science and Technology*, 2013, **3**, 1046-1055.
30. W. L. Dai, J. Bi, S. L. Luo, X. B. Luo, X. M. Tu and C. T. Au, *Catalysis Today*, 2014, **233**, 92-99.
31. T. Sakai, Y. Tsutsumi and T. Ema, *Green Chemistry*, 2008, **10**, 337-341.
32. Q.-W. Song, L.-N. He, J.-Q. Wang, H. Yasuda and T. Sakakura, *Green Chemistry*, 2013, **15**, 110-115.
33. A.-L. Girard, N. Simon, M. Zanatta, S. Marmitt, P. Goncalves and J. Dupont, *Green Chemistry*, 2014, **16**, 2815-2825.
34. E.-H. Lee, J.-Y. Ahn, M. M. Dharman, D.-W. Park, S.-W. Park and I. Kim, *Catalysis Today*, 2008, **131**, 130-134.
35. Y. Zhao, C. Yao, G. Chen and Q. Yuan, *Green Chemistry*, 2013, **15**, 446-452.
36. H. Kawanami, A. Sasaki, K. Matsui and Y. Ikushima, *Chemical Communications*, 2003, **9**, 896-897.
37. T. Werner and H. Büttner, *ChemSusChem*, 2014, **7**, 3268-3271.
38. T. Werner, N. Tenhumberg and H. Büttner, *ChemCatChem*, 2014, **6**, 3493-3500.
39. M. E. Wilhelm, M. H. Anthofer, M. Cokoja, I. I. E. Markovits, W. A. Herrmann and F. E. Kühn, *ChemSusChem*, 2014, **7**, 1357-1360.
40. T. Werner and N. Tenhumberg, *Journal of CO<sub>2</sub> Utilization*, 2014, **7**, 39-45.
41. G. Fiorani, W. Guo and A. W. Kleij, *Green Chemistry*, 2015, **17**, 1375-1389.
42. Y. Zhang, S. Yin, S. Luo and C. T. Au, *Industrial & Engineering Chemistry Research*, 2012, **51**, 3951-3957.
43. L. Han, H. J. Choi, S. J. Choi, B. Liu and D. W. Park, *Green Chemistry*, 2011, **13**, 1023-1028.
44. J. Sun, W. Cheng, Z. Yang, J. Wang, T. Xu, J. Xin and S. Zhang, *Green Chemistry*, 2014, **16**, 3071-3078.
45. S. Liang, H. Liu, T. Jiang, J. Song, G. Yang and B. Han, *Chemical Communications*, 2011, **47**, 2131-2133.
46. C. J. Whiteoak, A. Nova, F. Maseras and A. W. Kleij, *ChemSusChem*, 2012, **5**, 2032-2038.
47. A. M. Hardman-Baldwin and A. E. Mattson, *ChemSusChem*, 2014, **7**, 3275-3278.
48. M. J. S. Dewar, E. G. Zoenisch, E. F. Healy and J. J. P. Stewart, *Journal of the American Chemical Society*, 1985, **107**, 3902-3909.
49. J. Řezáč and P. Hobza, *Journal of Chemical Theory and Computation*, 2012, **8**, 141-151.
50. AMPAC 10, © 1992-2014 Semichem, Inc. PO Box 1649, Shawnee, KS 66222.
51. M. J. Frisch and A. D. Becke, *Gaussian 09, Revision A.02*, 2009, **98**, 5648-5652.
52. Y. Zhao and D. G. Truhlar, *Theoretical Chemistry Accounts*, 2008, **120**, 215-241.
53. B. Grignard, B. Gilbert, C. Malherbe, C. Jérôme and C. Detrembleur, *ChemPhysChem*, 2012, **13**, 2666-2670.
54. J.-Q. Wang, K. Dong, W.-G. Cheng, J. Sun and S.-J. Zhang, *Catalysis Science & Technology*, 2012, **2**, 1480-1484.

---

### Chapter III:

Organocatalytic promoted coupling of carbon dioxide with epoxides:  
a rational investigation of the co-catalytic activity of various hydrogen bond donors

---

The results presented in this chapter were published in *Catalysis Science & Technology*, 2015, 5, 4636-4643.

## Abstract

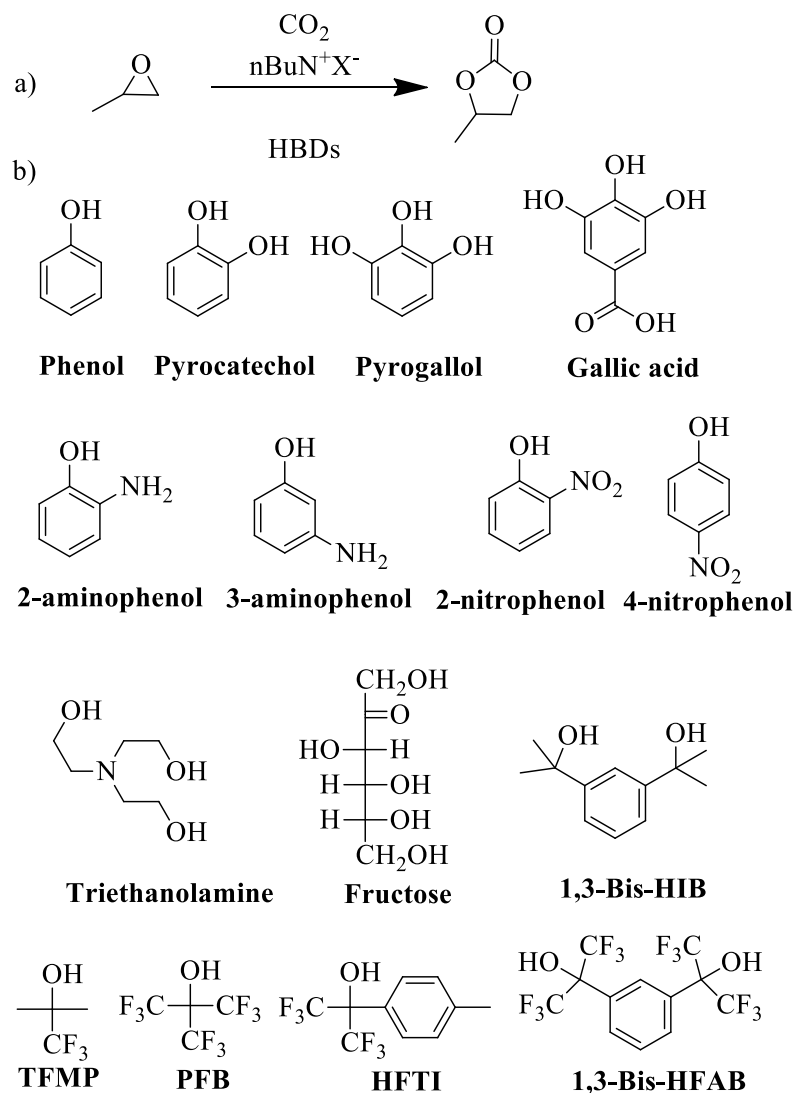
A catalytic platform based on an onium salt used in combination with organic co-catalysts of various structures was developed for the efficient CO<sub>2</sub>/epoxide coupling under mild conditions. Through detailed kinetic studies by *in-situ* FT-IR spectroscopy, a rational investigation of the efficiency of a series of commercially available hydrogen bond donors co-catalysts was realized and the influence of different parameters such as the pressure, the temperature, the catalyst loading, and the nature of the epoxide on the reaction kinetics was evaluated. Fluorinated alcohols were found to be more efficient than other hydrogen bond donor activators proposed previously in the literature under similar conditions.

## Table of contents

Introduction.....	111
Experimental .....	112
Materials .....	112
Infrared set-up.....	113
Experimental procedure .....	113
Results and discussion.....	114
Cyclic carbonates from PO and CO <sub>2</sub> .....	114
A- Without hydrogen bond donors. ....	114
B- Co-catalyst screening.....	116
a) (Multi)phenolic derivatives. ....	116
b) Alcohol and sugar. ....	118
c) Fluorinated alcohols. ....	118
C- Influence of experimental parameters .....	119
a) Influence of the reaction temperature .....	119
b) Influence of the CO <sub>2</sub> pressure .....	119
c) Influence of the HBD loading.....	121
d) Influence of the nature of the epoxide .....	121
Conclusions.....	123
References .....	124

## Introduction

The catalytic synthesis of five-membered cyclic carbonates *via* the coupling of an epoxide with CO<sub>2</sub> is a very promising method to convert CO<sub>2</sub> into valuable organic compounds and is currently the subject of numerous studies.<sup>1-7</sup> Although few catalysts gave satisfactory results under atmospheric pressure and ambient temperature,<sup>3, 8</sup> there is still place for identifying new catalytic platforms to promote an effective cycloaddition under mild conditions while respecting environmental standards. Metallic catalysts have proven to be efficient but their use generally suffers from some drawbacks in particular when metal residues are undesirable in the final product. In this context, organocatalysts have been proposed such as halide salts<sup>9-12</sup> and more recently (functionalized) ionic liquids<sup>13-28</sup> or quaternized glycine<sup>29</sup> and cholinium<sup>30, 31</sup> based ionic liquids were developed. However, halide salts and ionic liquids are generally only efficient at high temperature and pressure that favour their degradation.<sup>4, 32-35</sup> Their activities were enhanced by the addition of suitable hydrogen bond donors (HBDs) such as phenolic derivatives<sup>36-38</sup>, (amino)alcohols<sup>39-41</sup>, carboxylic acids<sup>42-44</sup>, lecithin<sup>45</sup>, cellulose<sup>46, 47</sup>, chitosan<sup>48-51</sup>, graphene oxide.<sup>52</sup> These HBDs interact with the O-donor group of the epoxide, therefore facilitating its ring opening by nucleophilic attack of the halide anion, and they stabilize by hydrogen bonding the oxyanion formed after epoxy-ring opening.<sup>38, 53, 54</sup> For example, Kleij *et al.* proposed a very efficient (multi)phenolic compound/ammonium iodide organocatalytic system that fastened the coupling of CO<sub>2</sub> with epoxides at low temperature (25 - 45°C) and pressure (1 MPa).<sup>38</sup> Very recently, Mattson *et al.* reported on the use of silanols as a new class of HBDs allowing the synthesis of cyclic carbonates at 0.1 MPa and 25°C. Nevertheless, the conversion of epoxides into cyclic carbonates was very slow (18h) despite the use of a very high catalyst (TBAI) and co-catalyst (silanol) loading (10 mol%).<sup>55</sup> By the way, we recently proposed a novel combination of onium salts with catalytic amount of fluorinated HBDs for the fast synthesis of cyclic carbonates within a few minutes by reaction of CO<sub>2</sub> with epoxides under solvent free and mild experimental conditions.<sup>56</sup> To date, if many HBDs were claimed to exhibit high co-catalytic activity, choosing the most efficient additives to fasten the CO<sub>2</sub>/epoxide coupling still remains a challenge as none of the studies reported in the literature were conducted in similar experimental conditions. Herein, we report for the first time a rational investigation of the co-catalytic activity of a series of commercially available HBDs (Scheme 1) for the synthesis of cyclic carbonates from CO<sub>2</sub> and epoxides under mild conditions. Comparative kinetic studies were performed by online FTIR spectroscopy under pressure. Additionally, the influence of the pressure, the temperature, the catalyst loading and the nature of the epoxide on the kinetics and reaction has been evaluated for the most effective HBDs.



Scheme 1: a) CO<sub>2</sub>/epoxide coupling reaction b) Chemical structures of Hydrogen Bond Activators used in this work and their designations

## Experimental

### Materials

Propylene oxide (PO) (purity  $\geq 99\%$ ), styrene oxide (SO, purity  $\geq 97\%$ ), cyclohexene oxide (CO, purity  $\geq 98\%$ ), glycidol (GDO, purity  $\geq 96\%$ ) and tetrabutylammonium bromide (TBABr, purity  $> 99\%$ ) were purchased from Aldrich. Carbon dioxide N45 was supplied by Air Liquide. Phenol, pyrocatechol, pyrogallol, gallic acid, 2- and 3-aminophenol, 2- and 4-nitrophenol and triethanolamine were purchased from Sigma-Aldrich.  $\alpha,\alpha$ -(dihydroxy-1,3-diisopropyl)benzene (1,3-bis-HIB), 1,1,1-trifluoro-2-methyl-2-propanol (TFMP) and hexafluoro-(*p*-tolyl)-isopropanol (HFTI) were supplied by ABCR. Perfluoro-*tert*-butanol (PFB) and 1,3-bis(2-hydroxyhexafluoroisopropyl)-benzene (1,3-bis-HFAB) were purchased from Fluorochem. All reactants were used as received without any further purification.

### *Infrared set-up.*

The synthesis of cyclic carbonates from model epoxides and CO<sub>2</sub> was followed *in-situ* using a FTIR microscope (Perkin Elmer Spotlight400) working in transfection coupled with a home-made high pressure reflection cell. Infrared spectra of the liquid and the gas phases can be successively recorded. For our purpose, the cell was fitted with a sapphire window and a polyethylene spacer of 1.1 mm thickness which could contain a liquid volume of approximately 100 µL. Single beam spectra of the liquid phase recorded with a 2 cm<sup>-1</sup> resolution were obtained after the Fourier transformation of 300 accumulated interferograms. Spectra were recorded continuously every five minutes during 311 minutes. In the liquid phase, the strong absorption of PO and propylene carbonate in the mid infrared region between 400 and 4000 cm<sup>-1</sup> requires the use of a very small pathlength (below 20 µm) that might lead to bad equilibration of the mixture. Therefore, in order to follow the apparition of the carbonate, we have chosen to look at overtones and combinations modes of PO and propylene carbonate in the near infrared region between 4000 and 6000 cm<sup>-1</sup> where a good signal to noise ratio is obtained using a pathlength of about 2 mm. The reflection cell was heated using cartridge heaters disposed in the periphery of its body. A thermocouple located close to a cartridge heater was used to control the temperature with an accuracy of about ±1°C. The cell was connected to the CO<sub>2</sub> tank allowing the pressure to be raised up to 5 MPa.

### **Experimental procedure**

An epoxide/catalyst mixture was introduced in the high pressure cell (100 µL) at ambient temperature and the cell was heated up to the desired temperature before addition of CO<sub>2</sub>. Experiments were conducted under mild conditions of temperature (25 – 100 °C) and pressure (0.3 – 3 MPa) in neat epoxide. To follow kinetics, the infrared beam was focused in the epoxide-rich phase. At the end of the reaction, in order to determine the yield, the near IR (NIR) spectrum of the reaction mixture was compared with the corresponding spectrum of the neat carbonate using the height of the peaks. The absorbance of the peak associated to the ν(C=O) + ν(C-H) combination mode at 4800 cm<sup>-1</sup> of propylene carbonate was normalized using the peak corresponding to 2ν(C-H) stretching mode at 5785 cm<sup>-1</sup> which doesn't evolve during the reaction. The yield for the entire kinetic was deduced by proportionality using the Beer-Lambert law according to Equation 1.

$$Yield (\%) = \frac{\left[ \frac{A_{C=O}}{A_{C-H}} \right]_{Reaction\ mixture}}{\left[ \frac{A_{C=O}}{A_{C-H}} \right]_{Neat\ carbonate}} \quad \text{Eq 1}$$

All these experiments were conducted at least twice in order to check for their reproducibility.



## Results and discussion

### Cyclic carbonates from PO and CO<sub>2</sub>

#### A- Without hydrogen bond donors.

The organocatalysed synthesis of propylene carbonate (PC) by coupling of PO with CO<sub>2</sub> in the presence of 3 mol% of TBABr at 60 °C and 2 MPa was monitored by *in-situ* FTIR spectroscopy. Under these conditions, the system is biphasic with an epoxide rich phase that is “swollen” by a significant amount of CO<sub>2</sub> ( $\chi_{\text{CO}_2} = 0.2$ ).<sup>57</sup> Moreover, knowing that TBABr (and the HBD) is soluble in this phase and insoluble in the gaseous CO<sub>2</sub> rich phase, the epoxide/CO<sub>2</sub> coupling only takes place in the epoxide rich phase. Kinetics studies were realized by monitoring the appearance of the peak associated to the  $\nu(\text{C=O}) + \nu(\text{C-H})$  combination mode at 4800 cm<sup>-1</sup> of propylene carbonate (Figure 1). It is worth noting that the consumption of PO can also be monitored thanks to the decrease of the peak at 6050 cm<sup>-1</sup> (2  $\nu(\text{C-H})$  mode of the epoxide ring). In addition, we also observe two peaks centred at 4950 and 5100 cm<sup>-1</sup> (respectively associated to the combination bands  $\nu_1 + 2\nu_2 + \nu_3$  and  $2\nu_1 + \nu_3$  of CO<sub>2</sub>) that attest for the presence of CO<sub>2</sub> in the mixture. Figure 2a shows the typical time dependence of the reaction yield measured from the height of the peak at 4800 cm<sup>-1</sup> reflecting an increase of the PC concentration in the PO/CO<sub>2</sub> mixture. Figure 2b represents the consumption of PO by the decrease of the absorbance at 6050 cm<sup>-1</sup>. As CO<sub>2</sub> is used in excess, the CO<sub>2</sub>/PO coupling answers a pseudo-first order reaction and kinetic profiles were fitted according to the following equation:  $[x]_t = C_0(1 - e^{-k't})$ . In such experimental conditions, the kinetic constant  $k'$  was estimated to 0.38 h<sup>-1</sup> and the reaction yield reached 42% after 100 minutes (Figure 2). Such fitting was applied for all the TBABr/HBD bicomponent organocatalysts investigated below.

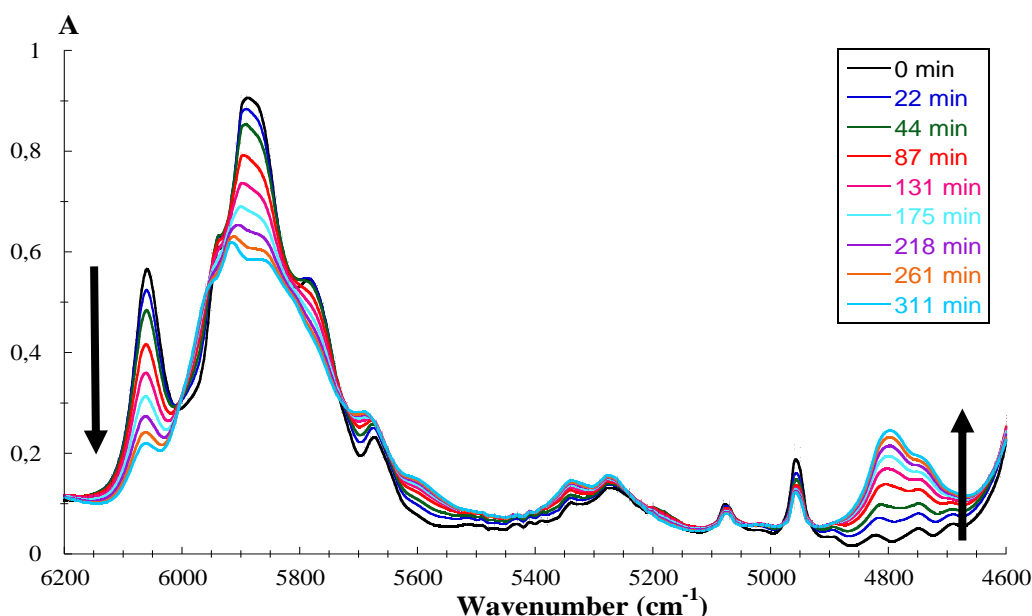


Figure 1: Evolution as a function of time of the Near Infrared spectra of the PO/CO<sub>2</sub>/catalyst mixture at T = 60 °C and P = 2 MPa.

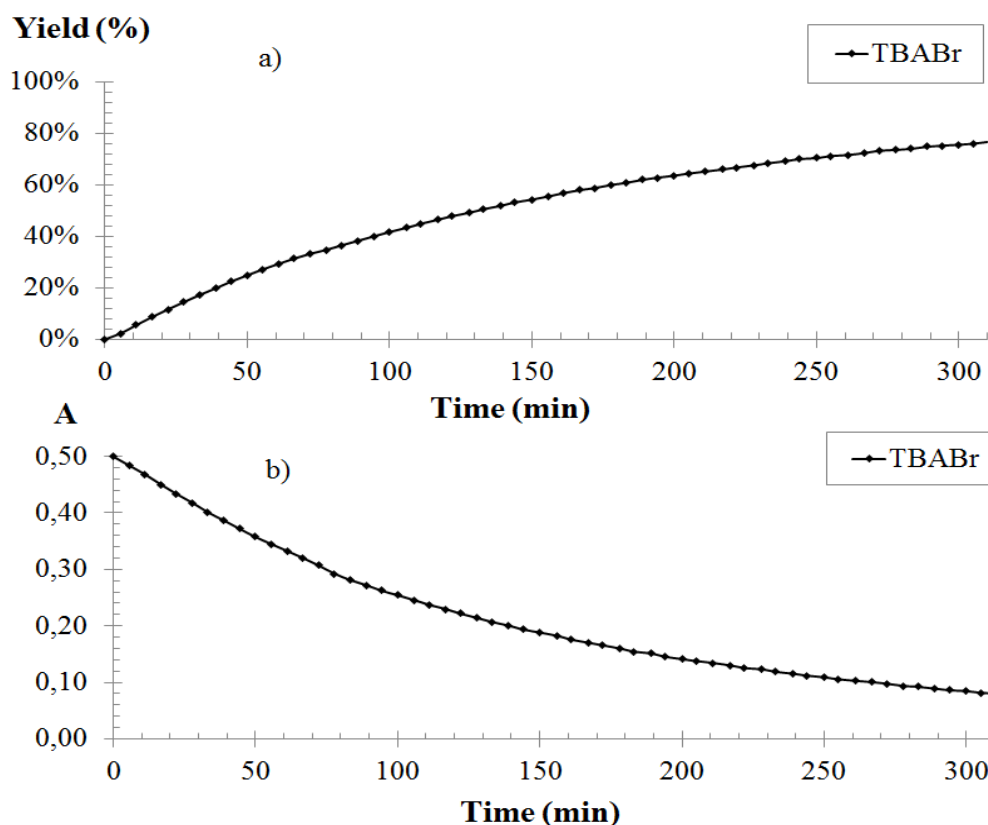


Figure 2: Kinetic study of the TBABr promoted coupling of CO<sub>2</sub> with PO: a) evolution of the reaction yield with time and b) evolution of the absorbance of the PO peak at 6500 cm<sup>-1</sup> with time. Experimental conditions: T = 60°C, P = 2 MPa, TBABr = 3 mol%.

The influence of the ammonium salt concentration on the catalytic efficiency was investigated for the model reaction at 60°C and 2 MPa. The catalytic performances increased when the TBABr loading increased from 0 to 3 mol% (Figure 3). A higher TBABr concentration had a detrimental effect on the kinetics. Indeed, a high TBABr loading might lead to the formation of ion pairs that decrease the nucleophilic activity of the anion.

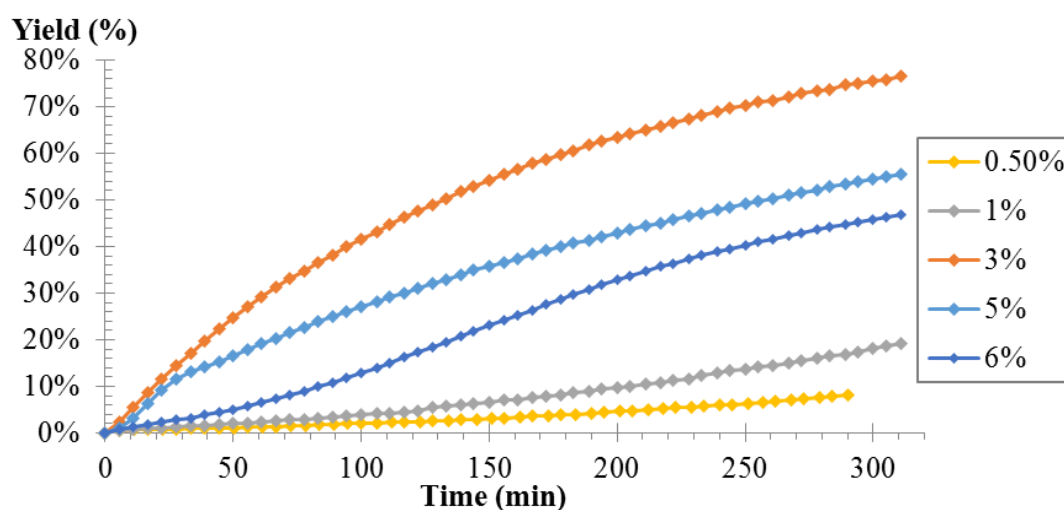


Figure 3: Change as a function of time of the yield of propylene carbonate during the cycloaddition of propylene oxide onto CO<sub>2</sub> (60°C, 2 MPa) with various TBABr loadings (mol%) as catalyst.

### B- Co-catalyst screening

The co-catalytic activity of commercial HBDs was then studied for the same model reaction between PO and CO<sub>2</sub> carried out in the presence of TBABr (3 mol%) at 60°C and 2 MPa. Equimolar amounts of HBDs (relative to TBABr) were used for the reaction.

#### a) (Multi)phenolic derivatives.

In line with the work of Kleij *et al.*,<sup>38</sup> pyrogallol was identified as an efficient HBD that allowed a 2.5-fold increase of the rate constant ( $k' = 0.97 \text{ h}^{-1}$ ) and enabled the full conversion of PO into propylene carbonate in 200 min (Figure 4). Pyrocatechol displayed a similar co-catalytic activity ( $k' = 0.93 \text{ h}^{-1}$ ) while phenol was less efficient with a  $k' = 0.52 \text{ h}^{-1}$  (Figure 4). Those results are in close qualitative agreement with data reported in the literature at lower temperature (between 25 and 40°C) and with a different halide anion (iodide instead of bromide).<sup>38</sup> The difference of activity between these three (multi)phenolic compounds was confirmed by the reaction yields determined after 100 min of reaction (Figure 5). Gallic acid, a pyrogallol analogue displaying an additional carboxylic acid function, was also found to be a very efficient activator at only 1 mol% loading as evidenced by a high conversion (70%) after 100 min. The reaction was not tested for higher gallic acid contents because this compound was insoluble in PO at higher loading. The positive influence of the acidic function was further confirmed by comparing the co-catalytic activity of pyrogallol and gallic acid at 1 mol% loading. The coupling of CO<sub>2</sub> with PO was nearly complete within 250 min (conversion close to 95%) in the presence of gallic acid but only reached 82% with pyrogallol.

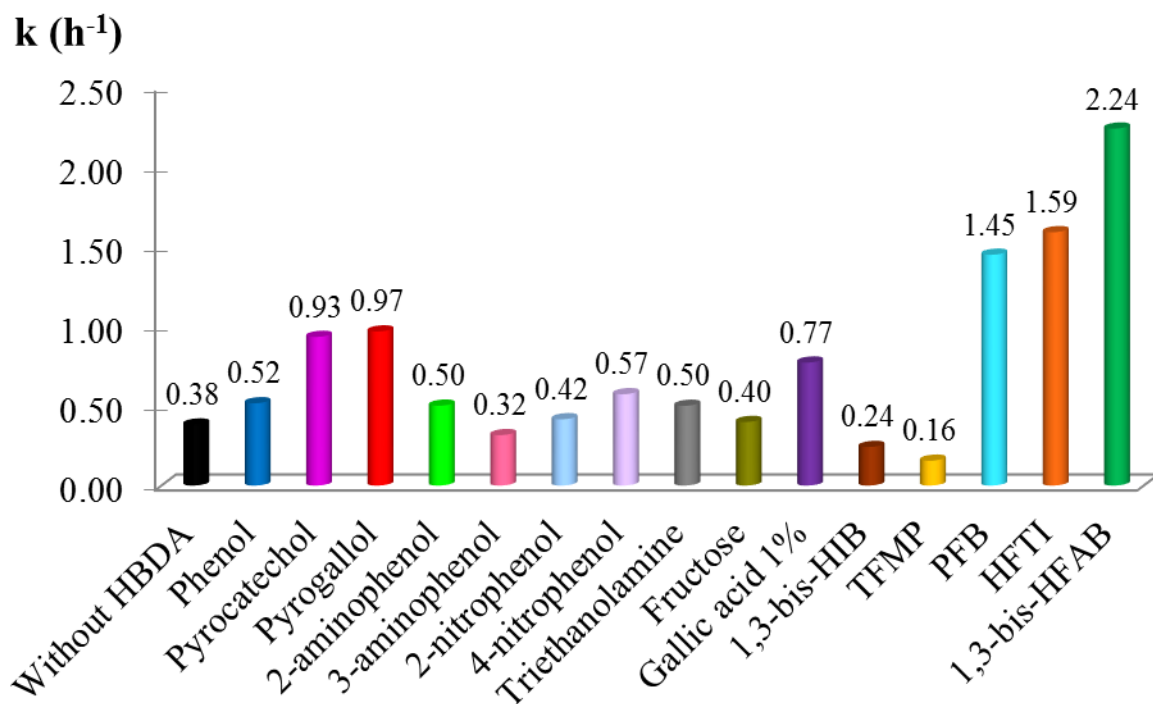


Figure 4: Kinetic rate constant determined for the coupling of CO<sub>2</sub> with PO promoted by TBABr/HBD bicomponent organocatalysts. Experimental conditions: T = 60°C, P = 2 MPa, TBABr = 3 mol%, [TBABr]/[HBD] = 1.

## Yield (%)

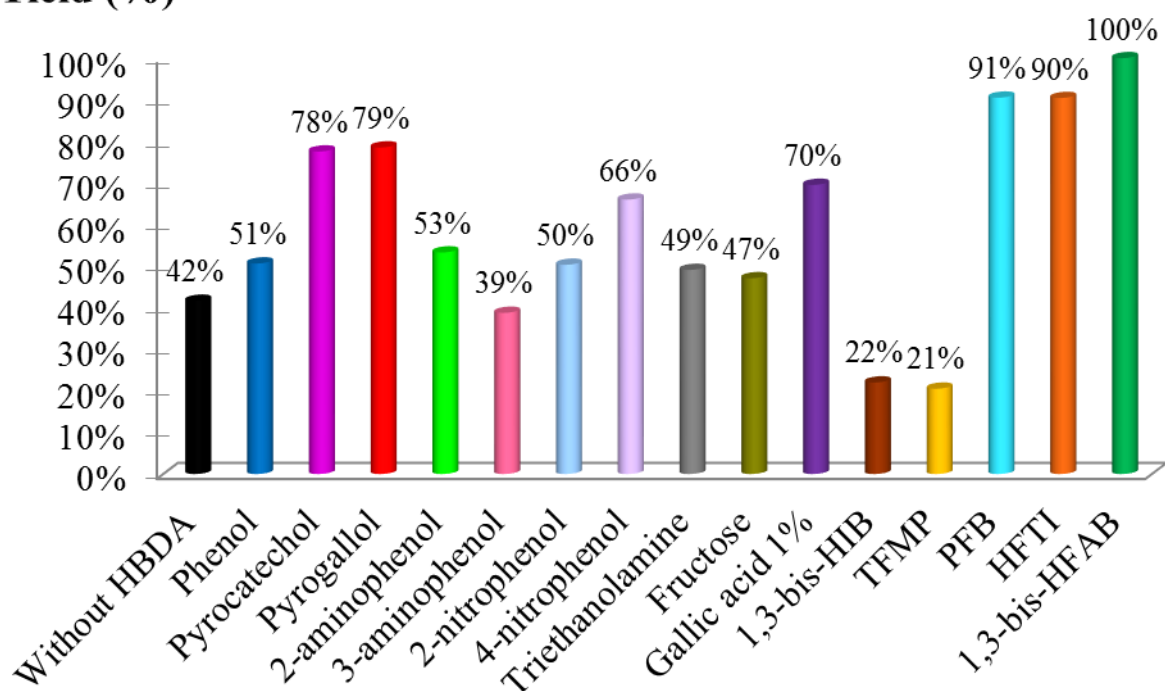


Figure 5: Coupling of CO<sub>2</sub> with PO promoted by TBABr/HBD bicomponent organocatalysts: reaction yields determined after 100 min. Experimental conditions: T = 60°C, P = 2 MPa, TBABr = 3 mol%, [TBABr]/[HBD] = 1.

This result is consistent with those reported in the literature that showed that HBDs with carboxylic acid groups were more efficient than those bearing hydroxyl functions<sup>26, 27, 44</sup> as the proton of the acid moieties also interacted by hydrogen bonding with the oxygen atom of the epoxides. However, the use of carboxylic acid-functionalized phenol derivative as potential HBD was restricted by its low solubility in the epoxide rich-phase. To highlight the crucial role of vicinal hydroxyl groups on the epoxide activation by phenolic HBDs, one OH group of pyrocatechol was replaced by a NH<sub>2</sub> function (Scheme 1b, second line) and its co-catalytic activity was compared with the one of 3-aminophenol. Kinetics studies demonstrated that 2-aminophenol ( $k' = 0.50 \text{ h}^{-1}$ , conv. = 53%) displayed a catalytic activity close to phenol ( $k' = 0.52 \text{ h}^{-1}$ , conv. = 51%) whereas 3-aminophenol had no activity as evidenced by a conversion of 39% and a  $k'$  value of  $0.32 \text{ h}^{-1}$  comparable to the one obtained when using TBABr as sole catalyst (Figure 4 and 5). This result confirms an initial study reported in the literature suggesting that the proximity between the amine functional group and the hydroxyl group is a key parameter that affects the activity of HBDs.<sup>38</sup> However, the amine functional group is a weaker HBD than alcohol as the activity of pyrocatechol was two times higher than the one of 2-aminophenol. Finally, the substitution of an OH group of pyrocatechol by an electron withdrawing NO<sub>2</sub> group that increases the acidity of the phenol derivative and favours the formation of hydrogen bond between the O-donor group of PO and the OH group of the HBD was investigated. If 2-nitrophenol displayed the same activity than phenol, 4-nitrophenol was slightly more efficient (Figure 4 and 5) with a conversion of 66% which

corresponds to a 1.5-fold increase of the reaction yield compared to the reference reaction without HBD. Indeed, the resonance stabilization of 4-nitrophenolate anion is higher than for 2-nitrophenol increasing the proton transfer probability. Moreover, the hydroxyl function of 2-nitrophenol is sterically hindered and could interact with the nitro function. Conclusively, the crucial role of vicinal hydroxyl groups was pointed out and the catalytic activity of phenol could be improved by substitution of the aromatic group by electron attractive substituents (nitro- or carboxylic acid groups).

*b) Alcohol and sugar.*

The co-catalytic efficiency of a variety of alcohols was also evaluated (Scheme 1b, third line). First, triethanolamine, reported recently to fasten the KI promoted coupling of CO<sub>2</sub> with PO, was tested as potential HBD. When it was used in combination with TBABr, the aminoalcohol showed a low co-catalytic activity ( $k' = 0.50 \text{ h}^{-1}$ ; Figure 4) with a conversion of the epoxide into cyclocarbonate of 49% after 100 min of reaction, similar to that of phenol and 2-aminophenol (Figure 5). This result is quite surprising in view of Cheng *et al.*<sup>58</sup> and Werner *et al.*<sup>41</sup> results who claimed that triethanolamine associated with KI had a strong activating role. These results might be explained by the higher temperature at which the coupling of CO<sub>2</sub> with PO was realized in their studies and by the nature of the catalyst used (KI instead of TBABr). Fructose, a sugar exhibiting five hydroxyl groups, was also tested as potential co-catalyst. Unfortunately, fructose had a limited co-catalytic activity as the  $k'$  value ( $0.40 \text{ h}^{-1}$ ) and the reaction yield (47% after 100 min) were close to values observed for the reaction carried out without HBD ( $k' = 0.38 \text{ h}^{-1}$ , conv. = 42%). Finally,  $\alpha,\alpha,\alpha$ -dihydroxy-1,3-disopropylbenzene (1,3-bis-HIB) inhibited the coupling of CO<sub>2</sub> with PO as the propylene carbonate yield and the  $k'$  value are 2 times lower than the one estimated for the reference reaction (Figure 4 and 5).

*c) Fluorinated alcohols.*

Recently, a new class of single and double HBD activators derived from fluorinated alcohols were identified to fasten the epoxide/CO<sub>2</sub> coupling under relatively mild conditions (Scheme 1b, last line).<sup>56</sup> At 60 °C and 2 MPa, hexafluoro-(*p*-tolyl)-isopropanol (HFTI) and perfluoro-*tert*-butanol (PFB), used in equimolar amounts compared to TBABr (3 mol%), were able to convert about 90% of PO into the corresponding cyclic carbonate after 100 min of reaction. The rate constants were 1.45 and 1.59 h<sup>-1</sup> for PFB and HFTI, respectively, thus representing about 50% rate constant increase compared to the best HBD (pyrogallol;  $k' = 0.97 \text{ h}^{-1}$ ). In contrast, 1,1,1-trifluoro-2-methyl-2-propanol (TFMP) had a detrimental effect on the reaction since the rate constant was lower than without HBD ( $0.16 \text{ h}^{-1}$  *vs.*  $0.38 \text{ h}^{-1}$ ). As reported elsewhere, the acidity and the hydrogen bonding capability of the tertiary alcohol that are both increased with the number of electron-withdrawing CF<sub>3</sub>-substituents are important factors affecting the activating efficiency of fluorinated alcohols.<sup>59</sup> Thus, double HBD, 1,3-bis-(hydroxyhexafluoroisopropyl)benzene (1,3-bis-HFAB), combined to TBABr, presented an impressive activity as evidenced by a 6- or 2.3-fold increase of  $k'$  value compared to the system without HBD or with pyrogallol

as HBD, respectively (Figure 4). PO/CO<sub>2</sub> coupling is quantitative in less than 100 min in the presence of 1,3-bis-HFAB, whereas the nonfluorinated analogue displayed no co-catalytic activity (1,3-bis-HIB) (Figure 5). These results highlight the positive impact of substituting methyl groups of alcohols by –CF<sub>3</sub>. Although these fluorinated alcohols are strong activators, they are not organocatalysts by themselves as only traces of propylene carbonate were detected during the cycloaddition of CO<sub>2</sub> onto PO using 3 mol% of fluorinated alcohol without any TBABr.

### C- Influence of experimental parameters

#### a) Influence of the reaction temperature

The impact of the temperature on the PO/CO<sub>2</sub> coupling promoted by the TBABr/HFTI binary catalyst (catalyst loading = 3 mol%, [TBABr]/[HBD] = 1) was investigated at a fixed CO<sub>2</sub> pressure of 2 MPa while varying the temperature from 25 to 100°C (Figure 6a). As expected, the reaction rate was fast at 100°C with a complete conversion of PO into PC within 50 minutes whereas at 60°C, the reaction was 3 times slower. At 25°C, the reaction was very slow and only reached about 35% conversion after 300 min. Using the Arrhenius equation, the activation energy of the reaction was estimated to 68 kJ.mol<sup>-1</sup> (Figure 6b).

#### b) Influence of the CO<sub>2</sub> pressure

One of the main challenges associated to the use CO<sub>2</sub> as a C1 feedstock relies on the development of processes that are efficient at low pressure. The impact of the pressure on the PO/CO<sub>2</sub> coupling was therefore studied at 60°C using the TBABr/1,3-bis-HFAB bicomponent organocatalyst ([TBABr] = 3 mol%, [TBABr]/[1,3-bis-HFAB] = 1) in a pressure range from 0.2 to 3 MPa. Figure 7 depicts the kinetic profiles of the PO/CO<sub>2</sub> coupling which are dependent on the initial CO<sub>2</sub> pressure. The highest reaction rate was measured at the highest pressure of 3 MPa ( $k' = 2.85 \text{ h}^{-1}$ ) that allowed a complete conversion of PO into PC in only 100 min whereas at a lower pressure of 1 and 2 MPa, the  $k'$  values slightly decreased to 2.08 and 2.24 h<sup>-1</sup>, respectively, consistently with the lower amount of CO<sub>2</sub> dissolved in PO at lower pressure. Additionally, even at pressures as low as 0.2 and 0.5 MPa, the reaction rate still remained acceptable with  $k'$  values of respectively 1.08 and 1.47 h<sup>-1</sup>, rendering the reaction quantitative in 200 and 250 min respectively.

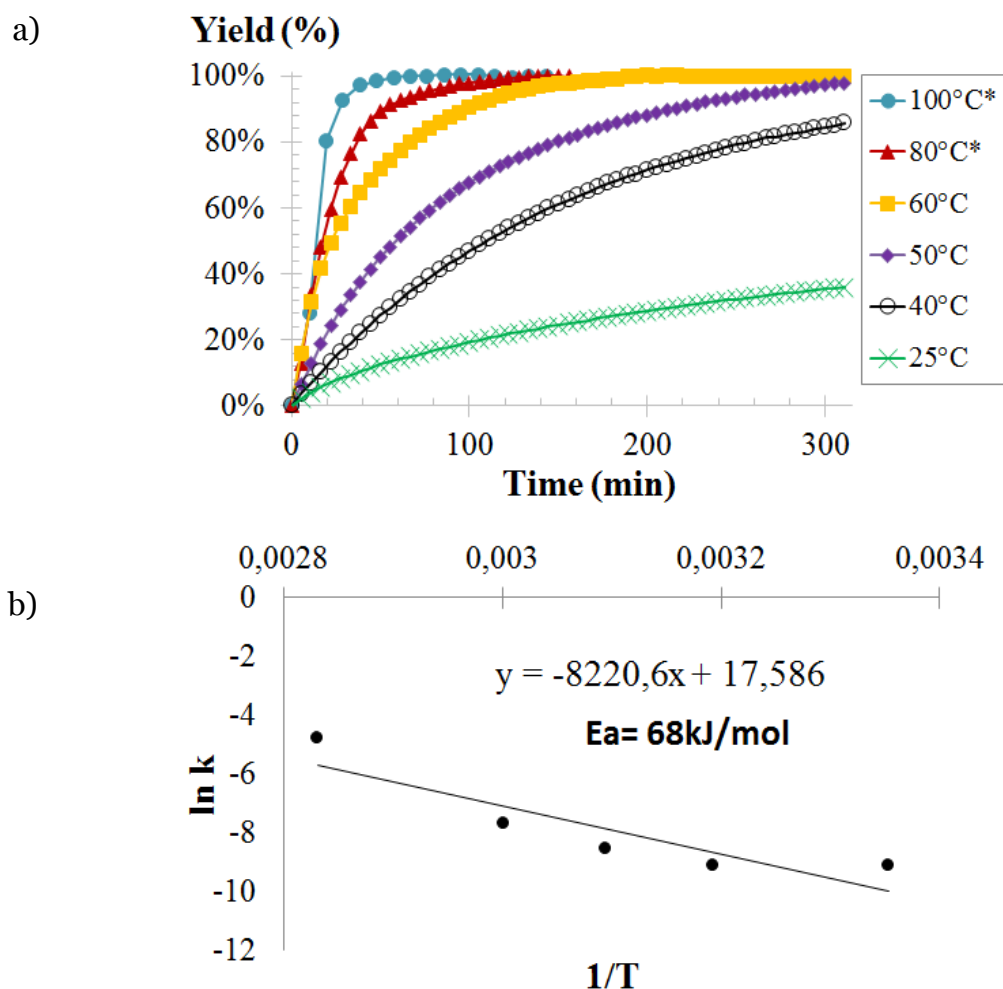


Figure 6: a) Effect of the temperature on the PO/CO<sub>2</sub> coupling promoted by the TBABr/HFTI bicomponent catalyst (\*TBABr/PFTB). b) Determination of the activation energy  $E_a$  using the linear form of the Arrhenius equation ( $\ln(k) = -E_a/RT + \ln(A)$ ). Experimental conditions: [TBABr] = 3 mol%, [TBABr]/[HFTI] = 1, P = 2 MPa.

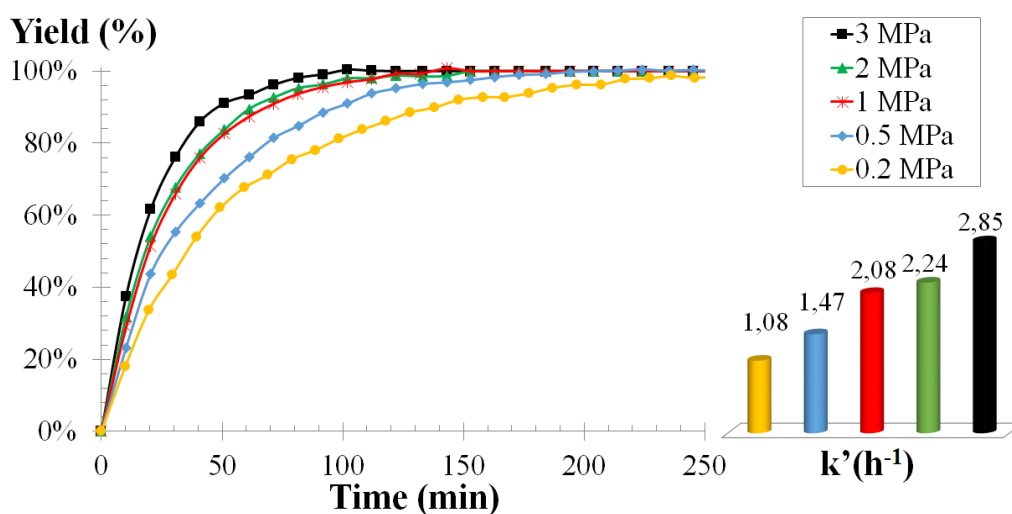


Figure 7: Effect of the pressure on the PO/CO<sub>2</sub> coupling promoted by the TBABr/1,3-bis-HFAB bicomponent catalyst. Experimental conditions: [TBABr] = 3 mol%, [TBABr]/[1,3-bis-HFAB] = 1, T = 60°C.



### c) Influence of the HBD loading

The influence of the HBD concentration on the catalytic platform efficiency was investigated for the model reaction at 60°C and 2 MPa using 3 mol% TBABr and increasing amount of HFTI (from 0 to 5 mol%). The catalytic performances increased when the HFTI loading increased from 0 to 3 mol% (Figure 8). Importantly, the reaction slowed down at higher HFTI concentration (5 mol%), which could be explained by the protonation of the bromine counter-ion by the fluorinated alcohol. This assumption was further supported by previous works that showed that the use of fluorinated alcohols as solvents, thus in large amount, had a detrimental effect on the CO<sub>2</sub>/epoxide coupling.<sup>60</sup> The optimal composition (3 mol% TBABr and 3 mol% HFTI) provided a quantitative conversion of PO into PC in 150 minutes (Figure 9). The reaction slowed down when the total amount of TBABr and HFTI was decreased for an equimolar composition ([TBABr]/[HFTI] = 1).

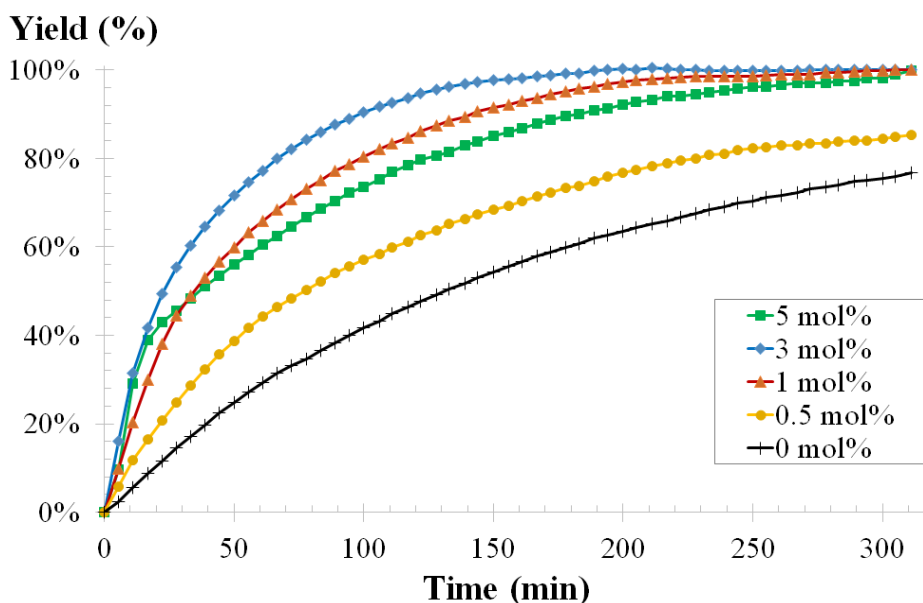


Figure 8: Coupling of PO and CO<sub>2</sub> using the TBABr/HFTI bicomponent catalyst: effect of the co-catalyst loading determined after 100 minutes. Experimental conditions: [TBABr] = 3 mol%, T = 60°C, P = 2 MPa.

### d) Influence of the nature of the epoxide

The coupling of CO<sub>2</sub> with a series of model epoxides such as cyclohexene oxide (CO), glycidol (GDO) or styrene oxide (SO) was finally studied using TBABr as catalyst and HFTI as representative efficient HBD. In the absence of HBD, the synthesis of cyclohexene carbonate from CO and CO<sub>2</sub> was very slow at T = 60°C and P = 2 MPa and the conversion only reached 11% after 300 min (Table 1). Addition of 1 equivalent conversion of HFTI compared to TBABr fastened the reaction with a 2-fold increase of the conversion after the same period of time. Compared to the CO<sub>2</sub>/PO coupling that was quantitative under these experimental conditions, the same reaction performed on CO was much slower as the result of a lower reactivity of di-substituted epoxides due to steric hindrance and charge delocalisation effects. Moreover, for a



given temperature and pressure, the combination with TBABr systematically enhanced the activity of TBABr without the formation of by-products.

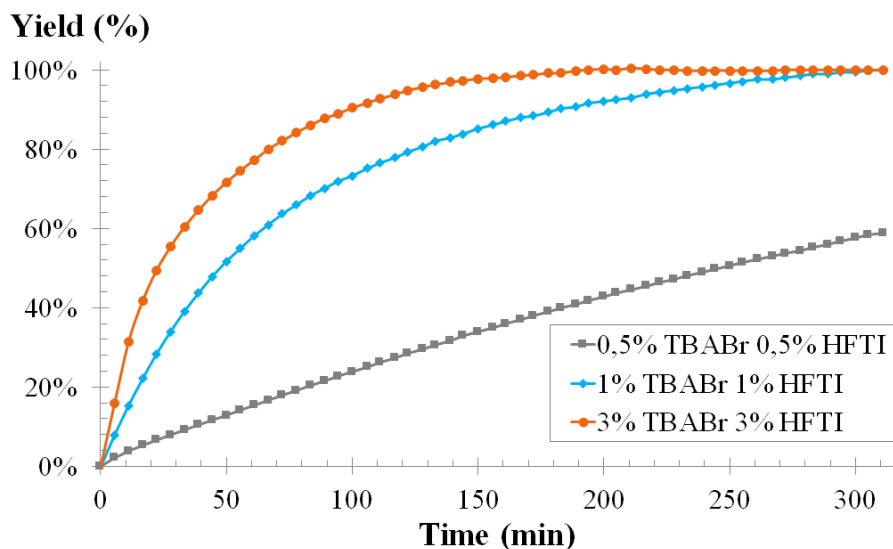


Figure 9: Change as a function of the time of the absorbance of the propylene carbonate during the cycloaddition of CO<sub>2</sub> onto propylene oxide (60°C, 2 MPa) with various loadings of TBABr and HFTI as catalysts and [TBABr]/[HFTI]=1.

Table 1: Coupling of different epoxides and CO<sub>2</sub> using the TBABr/HFTI bicomponent catalyst. Experimental conditions : [TBABr] = 3 mol%, [TBABr]/[HFTI] = 1, T = 60°C, P = 2 MPa, t = 300 min

Entry	Epoxide	Catalyst	HBD	T (°C)	P (MPa)	Conv (%)
<b>1</b>	Propylene oxide	TBABr	-	60	2	76%
<b>2</b>		TBABr	HFTI	60	2	100%*
<b>3</b>	Glycidol	TBABr	-	60	2	2%
<b>4</b>		TBABr	HFTI	60	2	30%
<b>5</b>	Styrene oxide	TBABr	-	60	2	43%
<b>6</b>		TBABr	HFTI	60	2	50%
<b>7</b>	Cyclohexene oxide	TBABr	-	60	2	11%
<b>8</b>		TBABr	HFTI	60	2	22%
<b>9</b>		TBABr	HFTI	100	2	73%

\* Quantitative conversion after 150 minutes

## Conclusions

We report for the first time a rational investigation of the co-catalytic activity of a series of commercially available hydrogen bond donors (HBDs) for the synthesis of cyclic carbonates from CO<sub>2</sub> and epoxides under mild conditions. Through detailed kinetic studies by online IR spectroscopy under pressure, pyrogallol, pyrocatechol, gallic acid, perfluoro-*tert*-butanol, hexafluoro-(*p*-tolyl)-isopropanol and 1,3-bis(2-hydroxyhexafluoroisopropyl)-benzene (1,3-bis-HFAB) were identified as the most efficient commercially available co-catalysts, even if the booster effect of Fluorinated Hydrogen Bond Donors (FHBD) was significantly higher. Then, we have investigated the influence of the temperature, the pressure, the nature of the epoxide and the FHBD loading on the kinetics and yields of the epoxide/CO<sub>2</sub> coupling reaction using the TBABr/FHBD bicomponent catalyst. As expected, increasing the temperature fastens significantly the rate of the reaction. Interestingly, the TBABr/FHBD bicomponent catalyst is active at low CO<sub>2</sub> pressure as quantitative transformation of PO is obtained at 60°C and 0.2 MPa in less than 5h. Additionally, whatever the nature of the epoxide, the use of FHBD in combination with TBABr systematically enhanced the activity of TBABr without formation of by-products. Therefore, the use of suitable hydrogen bond donor activators, more particularly alcohols with hexafluoroisopropanol functionalities, will expand the scope of the metal-free synthesis of cyclic carbonates under mild conditions, especially when considering the cycloaddition of CO<sub>2</sub> onto epoxidized vegetable oils which are expected to be less reactive than model epoxides.<sup>61</sup> This rational investigation is also expected to help researchers to identify suitable organocatalysts that offer the best compromise in terms of activity and cost as a less efficient hydrogen bond activator could remain competitive when its cost is more favourable in regard of the most active and expensive ones.

## References

1. P. Styring, A. Quadrelli and K. Armstrong, *Carbon Dioxide Utilisation, 1st Edition, Closing the Carbon Cycle*, Elsevier, 2015.
2. C. Maeda, Y. Miyazaki and T. Ema, *Catalysis Science & Technology*, 2014, **4**, 1482.
3. M. North, R. Pasquale and C. Young, *Green Chemistry*, 2010, **12**, 1514-1539.
4. P. P. Pescarmona and M. Taherimehr, *Catalysis Science & Technology*, 2012, **2**, 2169-2187.
5. Q. He, J. W. O'Brien, K. A. Kitselman, L. E. Tompkins, G. C. T. Curtis and F. M. Kerton, *Catalysis Science & Technology*, 2014, **4**, 1513-1528.
6. B.-H. Xu, J.-Q. Wang, J. Sun, Y. Huang, J.-P. Zhang, X.-P. Zhang and S.-J. Zhang, *Green Chemistry*, 2015, **17**, 108-122.
7. G. Fiorani, W. Guo and A. W. Kleij, *Green Chemistry*, 2015, **17**, 1375-1389.
8. M. North and C. Young, *Catalysis Science & Technology*, 2011, **1**, 93-99.
9. P. Ramidi, P. Munshi, Y. Gartia, S. Pulla, A. S. Biris, A. Paul and A. Ghosh, *Chemical Physics Letters*, 2011, **512**, 273-277.
10. N. Kihara, N. Hara and T. Endo, *Journal of Organic Chemistry*, 1993, **58**, 6198-6202.
11. T. Werner and H. Büttner, *ChemSusChem*, 2014, **7**, 3268-3271.
12. B. Chatelet, L. Joucla, J. P. Dutasta, A. Martinez, K. C. Szeto and V. Dufaud, *Journal of the American Chemical Society*, 2013, **135**, 5348-5351.
13. J. Sun, S.-I. Fujita and M. Arai, *Journal of Organometallic Chemistry*, 2005, **690**, 3490 - 3497.
14. L. Han, M. S. Park, S. J. Choi, Y. J. Kim, S. M. Lee and D. W. Park, *Catalysis Letters*, 2011, 1-8.
15. S. Zhang, Y. Huang, H. Jing, W. Yao and P. Yan, *Green Chemistry*, 2009, **11**, 935-938.
16. T. Seki, J. D. Grunwaldt and A. Baiker, *Journal of Physical Chemistry B*, 2009, **113**, 114-122.
17. J. Li, L. Wang, F. Shi, S. Liu, Y. He, L. Lu, X. Ma and Y. Deng, *Catalysis Letters*, 2011, **141**, 339-346.
18. S. Udayakumar, S. W. Park, D. W. Park and B. S. Choi, *Catalysis Communications*, 2008, **9**, 1563-1570.
19. Z. Z. Yang, L. N. He, C. X. Miao and S. Chanfreau, *Advanced Synthesis and Catalysis*, 2010, **352**, 2233-2240.
20. H. Y. Ju, M. D. Manju, K. H. Kim, S. W. Park and D. W. Park, *Journal of Industrial and Engineering Chemistry*, 2008, **14**, 157-160.
21. B. Ochiai and T. Endo, *Journal of Polymer Science, Part A: Polymer Chemistry*, 2007, **45**, 5673-5678.
22. S. Foltran, J. Alsarraf, F. Robert, Y. Landais, E. Cloutet, H. Cramail and T. Tassaing, *Catalysis Science & Technology*, 2013, **3**, 1046-1055.

23. W.-L. Wong, L. Y. S. Lee, K.-P. Ho, Z.-Y. Zhou, T. Fan, Z. Lin and K.-Y. Wong, *Applied Catalysis A: General*, 2014, **472**, 160-166.
24. D. Wei-Li, J. Bi, L. Sheng-Lian, L. Xu-Biao, T. Xin-Man and A. Chak-Tong, *Catalysis Today*, 2014, **233**, 92-99.
25. J. Sun, S. Zhang, W. Cheng and J. Ren, *Tetrahedron Letters*, 2008, **49**, 3588-3591.
26. L. Han, H. J. Choi, S. J. Choi, B. Liu and D. W. Park, *Green Chemistry*, 2011, **13**, 1023-1028.
27. W. L. Dai, J. Bi, S. L. Luo, X. B. Luo, X. M. Tu and C. T. Au, *Catalysis Science and Technology*, 2014, **4**, 556-562.
28. O. Coulembier, S. Moins, V. Lemaure, R. Lazzaroni and P. Dubois, *Journal of CO<sub>2</sub> Utilization*, 2015, **10**, 7-11.
29. J. Tharun, G. Mathai, R. Roshan, A. C. Kathalikkattil, K. Bomi and D.-W. Park, *Physical Chemistry Chemical Physics*, 2013, **15**, 9029-9033.
30. A. Zhu, T. Jiang, B. Han, J. Zhang, Y. Xie and X. Ma, *Green Chemistry*, 2007, **9**, 169-172.
31. A. J. R. Amaral, J. F. J. Coelho and A. C. Serra, *Tetrahedron Letters*, 2013, **54**, 5518-5522.
32. J. Łukaszczyk, K. Jaszczyk, W. Kuran and T. Listos, *Macromolecular Rapid Communications*, 2000, **21**, 754-757.
33. D. J. Darensbourg and W.-C. Chung, *Macromolecules*, 2014, **47**, 4943-4948.
34. S. Kumar, S. L. Jain and B. Sain, *Catalysis Letters*, 2012, **142**, 615-618.
35. C. Martín, G. Fiorani and A. W. Kleij, *ACS Catalysis*, 2015, **5**, 1353-1370.
36. J. W. Huang and M. Shi, *Journal of Organic Chemistry*, 2003, **68**, 6705-6709.
37. Y. M. Shen, W. L. Duan and M. Shi, *European Journal of Organic Chemistry*, 2004, 3080-3089.
38. C. J. Whiteoak, A. Nova, F. Maseras and A. W. Kleij, *ChemSusChem*, 2012, **5**, 2032-2038.
39. T. Werner, N. Tenhumberg and H. Büttner, *ChemCatChem*, 2014, **6**, 3493-3500.
40. M. E. Wilhelm, M. H. Anthofer, M. Cokoja, I. I. E. Markovits, W. A. Herrmann and F. E. Kühn, *ChemSusChem*, 2014, **7**, 1357-1360.
41. T. Werner and N. Tenhumberg, *Journal of CO<sub>2</sub> Utilization*, 2014, **7**, 39-45.
42. W. Cheng, Z. Fu, J. Wang, J. Sun and S. Zhang, *Synthetic Communications*, 2012, **42**, 2564-2573.
43. L. Han, H.-J. Choi, S.-J. Choi, B. Liu and D.-W. Park, *Green Chemistry*, 2011, **13**, 1023-1028.
44. J. Tharun, G. Mathai, A. C. Kathalikkattil, R. Roshan, J.-Y. Kwak and D.-W. Park, *Green Chemistry*, 2013, **15**, 1673-1677.
45. J. Song, B. Zhang, P. Zhang, J. Ma, J. Liu, H. Fan, T. Jiang and B. Han, *Catalysis Today*, 2012, **183**, 130-135.
46. S. Liang, H. Liu, T. Jiang, J. Song, G. Yang and B. Han, *Chemical Communications*, 2011, **47**, 2131-2133.

47. J. Sun, W. Cheng, Z. Yang, J. Wang, T. Xu, J. Xin and S. Zhang, *Green Chemistry*, 2014, **16**, 3071-3078.
48. J. Sun, J. Wang, W. Cheng, J. Zhang, X. Li, S. Zhang and Y. She, *Green Chemistry*, 2012, **14**, 654-660.
49. J. Tharun, Y. Hwang, R. Roshan, S. Ahn, A. C. Kathalikkattil and D. W. Park, *Catalysis Science and Technology*, 2012, **2**, 1674-1680.
50. Y. Zhao, J. S. Tian, X. H. Qi, Z. N. Han, Y. Y. Zhuang and L. N. He, *Journal of Molecular Catalysis A: Chemical*, 2007, **271**, 284-289.
51. C. Jing-Xian, J. Bi, D. Wei-Li, D. Sen-Lin, C. Liu-Ren, C. Zong-Jie, L. Sheng-Lian, L. Xu-Biao, T. Xin-Man and A. Chak-Tong, *Applied Catalysis A: General*, 2014, **484**, 26-32.
52. D.-H. Lan, F.-M. Yang, S.-L. Luo, C.-T. Au and S.-F. Yin, *Carbon*, 2014, **73**, 351-360.
53. J.-Q. Wang, K. Dong, W.-G. Cheng, J. Sun and S.-J. Zhang, *Catalysis Science & Technology*, 2012, **2**, 1480-1484.
54. S. Foltran, R. Mereau and T. Tassaing, *Catalysis Science & Technology*, 2014, **4**, 1585-1597.
55. A. M. Hardman-Baldwin and A. E. Mattson, *ChemSusChem*, 2014, **7**, 3275-3278.
56. S. Gennen, M. Alves, R. Méreau, T. Tassaing, B. Gilbert, C. Detrembleur, C. Jerome and B. Grignard, *ChemSusChem*, 2015, **8**, 1845-1849.
57. S. Foltran, E. Cloutet, H. Cramail and T. Tassaing, *The Journal of Supercritical Fluids*, 2012, **63**, 52-58.
58. B. Xiao, J. Sun, J. Wang, C. Liu and W. Cheng, *Synthetic Communications*, 2013, **43**, 2985-2997.
59. D. Vuluga, J. Legros, B. Crousse, A. M. Z. Slawin, C. Laurence, P. Nicolet and D. Bonnet-Delpon, *Journal of Organic Chemistry*, 2011, **76**, 1126-1133.
60. N. Aoyagi, Y. Furusho and T. Endo, *Tetrahedron Letters*, 2013, **54**, 7031-7034.
61. M. Alves, B. Grignard, S. Gennen, C. Detrembleur, C. Jerome and T. Tassaing, *RSC Advances*, 2015, **5**, 53629-53636.

---

Chapter IV:  
Organocatalytic synthesis of bio-  
based cyclic carbonates from CO<sub>2</sub> and  
vegetable oils

---

The results presented in this chapter were published in *RSC Advances*, 2015, 5, 53629-53636

## Abstract

Bio-based cyclic carbonates were synthesized by coupling CO<sub>2</sub> with epoxidized linseed oil using a catalytic platform composed of a bicomponent organocatalyst. Screening of the catalytic activity of a series of organic salts and ionic liquids used in combination with (multi)phenolic or fluorinated hydrogen bond donors was realized before highlighting the synergistic effect between the organocatalyst and the most efficient co-catalysts. These kinetics studies, followed by IR spectroscopy under pressure, enabled optimization of the reaction conditions and to provide quantitative formation of the cyclocarbonated vegetable oil in a short reaction time without using any organic solvent.

## Table of contents

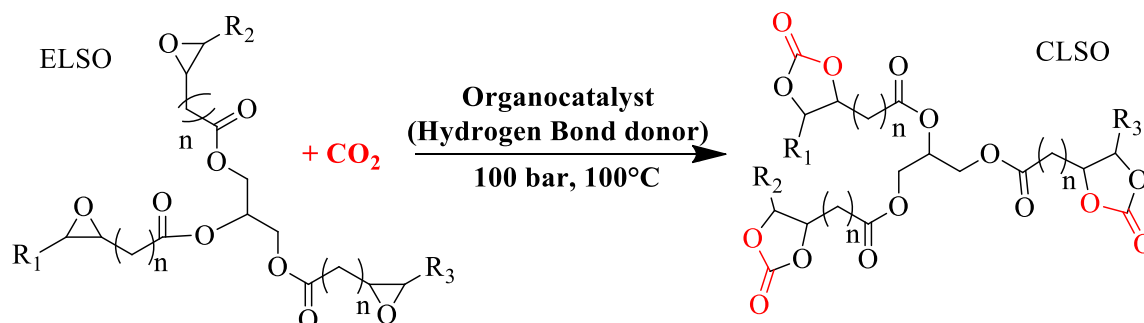
Introduction.....	129
Experimental .....	131
1. Materials .....	131
Infrared set-up .....	132
NMR characterization .....	132
2. Experimental procedure.....	133
Catalyst screening .....	133
Catalyst optimisation .....	133
Kinetic studies .....	133
Solubility of CO <sub>2</sub> into ELSO .....	134
Results and discussion.....	135
1. Catalyst screening for the synthesis of carbonated linseed oil .....	135
2. Detailed kinetic study of the TBABr/HBD promoted ELSO/CO <sub>2</sub> coupling .....	137
Conclusions.....	143
References.....	144

## Introduction

Regarding the economical and environmental issues, finding alternatives to petrochemicals has become one of the most important worldwide challenges. Valorising CO<sub>2</sub> as a C1 feedstock for producing building blocks<sup>1-3</sup> is seducing as it is a free and inexhaustive waste resulting from the human activity. As examples, carbon dioxide can be transformed into added value products such as carboxylic acids<sup>4-8</sup>, esters or lactones<sup>9-12</sup>, urea<sup>13</sup>, carbamates<sup>14-18</sup> or isocyanates<sup>19, 20</sup>. By coupling with epoxides, CO<sub>2</sub> can be converted into cyclic carbonates that find applications as green solvents, electrolytes for lithium batteries or as monomers for the production of polycarbonates and non-isocyanate polyurethanes. However, due to the low reactivity of CO<sub>2</sub> with epoxides, addition of metallic or organic catalysts is necessary, but their use generally suffers from some drawbacks. Indeed, some metal complexes are sensitive to hydrolysis and oxidation or/and are poorly selective. Additionally, some of them are toxic whereas less/non-toxic and eco-friendly organocatalysts such as ionic liquids and halide salts are generally only efficient at high temperature and pressure that favours their degradation.<sup>21-25</sup> In the last years, development of new bicomponent organocatalysts<sup>26</sup> combining the use of organic salts or ionic liquids with hydrogen bond donor activators such as phenolic derivatives<sup>27, 28</sup>, (amino)alcohols<sup>29-31</sup>, carboxylic acids<sup>32-34</sup>, (fluoro)alcohols<sup>35</sup>, silanols<sup>36</sup>, has been proposed to fasten the coupling of CO<sub>2</sub> with epoxides under mild conditions. The efficiency of these catalytic systems has been mainly investigated for the coupling of CO<sub>2</sub> with model petro-sourced small organic molecules such as propylene oxide or styrene oxide. Besides, the synthesis of bio-based cyclic carbonates from CO<sub>2</sub> and epoxidized vegetables oils is a subject of growing interest that allows the synthesis of fully bio-based chemicals. However, the identification and development of efficient (organo)catalysts for synthesizing cyclic carbonates from bio-based epoxides still remains challenging.<sup>37</sup> At the exception of Rokicki's work<sup>38</sup>, coupling of CO<sub>2</sub> with vernonia oil (a naturally epoxy functionalized triglyceride) or epoxidized soybean, linseed or cotton oils was only promoted by tetrabutylammonium bromide (TBABr). At low CO<sub>2</sub> pressure, the reaction was complete within several days at high temperature (110°C < T < 160°C)<sup>39-42</sup> and was fastened by using CO<sub>2</sub> under supercritical conditions.<sup>43, 44</sup> Addition of water or SnCl<sub>4</sub> was also proposed as alternative to improve the catalytic efficiency of the TBABr promoted CO<sub>2</sub>/epoxide coupling at moderate pressure.<sup>45, 46</sup> However, even in the presence of these additives, conversion of the epoxidized vegetables oils into the cyclocarbonated ones was slow (t > 30 h) at high temperature (T = 140°C) and a CO<sub>2</sub> pressure of 1.5 MPa. Therefore, there is a need to develop more efficient (organo)catalysts that are active under milder conditions for the conversion of epoxidized vegetable oils into cyclic carbonates. These cyclocarbonated vegetable oils are indeed attractive synthons for the production of cheap and bio-based non-isocyanate polyurethanes<sup>39, 40, 47-49</sup>, the most promising substitutes for conventional polyurethanes used in paints, coatings or biomaterials.

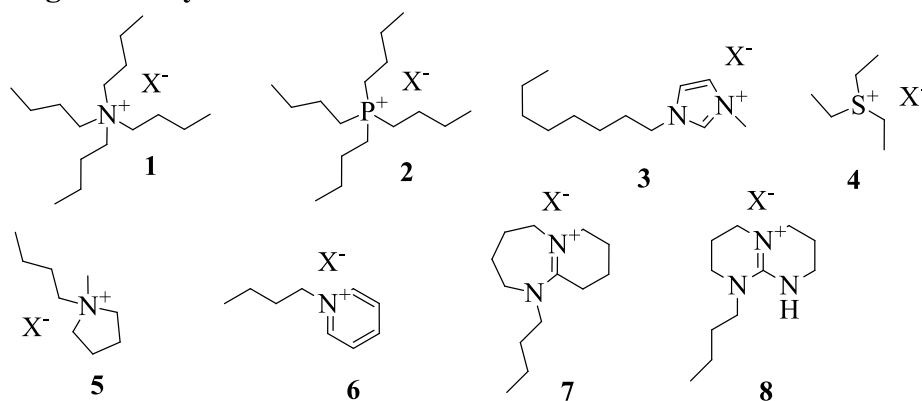


In this contribution, we describe the synthesis of cyclocarbonated linseed oil (CLSO) from epoxidized linseed oil (ELSO) (Scheme 1) by developing a catalytic platform composed of bicomponent organocatalysts (Scheme 2) that fasten the reaction under mild experimental conditions.

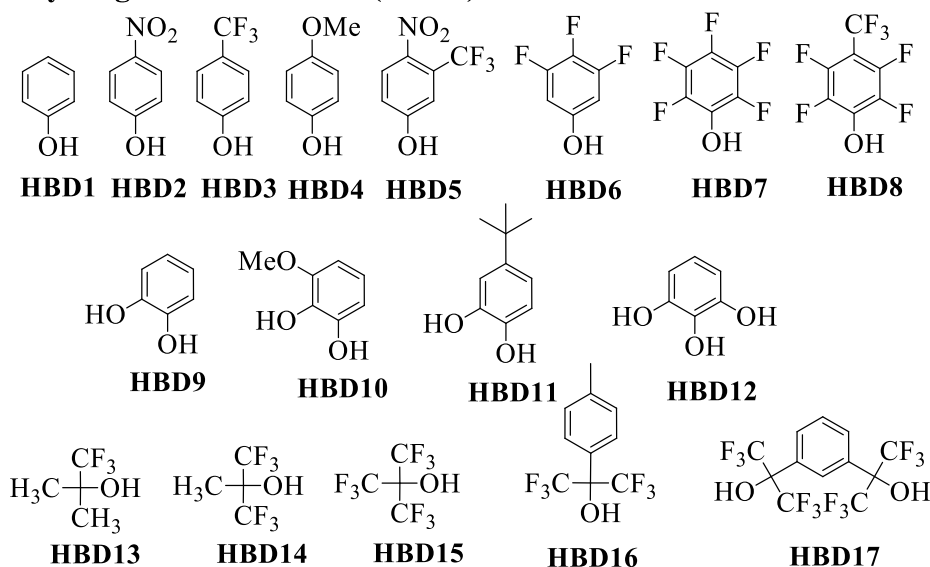


Scheme 1: Synthesis of CLSO by organocatalytic promoted coupling of  $\text{CO}_2$  with ELSO

#### Organocatalysts:



#### Hydrogen Bond Donors (HBDs):



Scheme 2: Catalytic platform developed for the synthesis of CLSO from ELSO and  $\text{CO}_2$

First, a survey of the catalytic activity of a series of organic halide salts or ionic liquids including onium (1), phosphonium (2), imidazolium (3), sulfonium (4), pyrrolidinium (5), pyridinium (6), amidinium (7) and guanidinium (8) (Scheme 1) was studied in order to identify the most active organocatalyst. Then, the catalytic efficiency was improved by the addition of different hydrogen bond donors activators (HBD) derived from (multi)phenolic compounds or fluoroalcohols, and the synergistic effects between the catalyst and the most efficient HBDs are highlighted by online kinetic studies using IR spectroscopy.

## Experimental

### 1. Materials

Epoxidized linseed oil (ELSO) was kindly donated by Vandeputte Oleochemicals (Belgium). Carbon dioxide N45 (purity: 99.95%) was supplied by Air Liquide. Quaternary ammonium salts, phosphonium halides, 1-bromobutane, 1,8-diazabicyclo[5.4.0]undec-7-ene (DBU) and 1,5,7-triazabicyclo[4.4.0]dec-5-ene (TBD), phenol, 4-nitrophenol, 4-trifluoromethylphenol, 4-methoxyphenol, 3,4,5-trifluorophenol, pentafluorophenol, pyrocatechol, 3-methoxypyrocatechol, 4-tert-butoxycatechol, and pyrogallol were purchased from Sigma-Aldrich. 5-hydroxy-2-nitrobenzotrifluoride, 1,3-bis(2-hydroxyhexafluoroisopropyl)benzene, 1,1,1-trifluoro-2-methyl-2-propanol, 1,1,1,3,3,3-hexafluoro-*tert*-butanol, perfluoro-*tert*-butanol were purchased from Fluorochem. 2,3,5,6-tetrafluoro-4-(trifluoromethyl)phenol, hexafluoro-2-(*p*-tolyl)isopropanol, 1,1,1,3,3,3-hexafluoro-2-propanol were supplied by ABCR. Triethylsulfonium iodide, 1-butyl-1-methylpyrrolidinium iodide, 1-butylpyridinium iodide and 1-methyl-3-octylimidazolium halides were purchased from Ioliditec. All reactants or catalysts were used as received.

Amidinium and guanidinium salts, respectively named and 1-butyl-2,3,4,5,7,8,9,10-octahydropyrido[1,2-*a*][1,3]diazepin-1-ium bromide and 1-butyl-3,4,6,7,8,9-hexahydro-2H-pyrimido[1,2-*a*]pyrimidin-1-ium bromide were respectively synthesized by quaternisation of DBU and TBD with 1-bromobutane. In a typical experiment, DBU (1.96 mL, 0.0131 mol) was dissolved in 10 mL CH<sub>2</sub>Cl<sub>2</sub> before slow dropwise addition of 1-bromobutane (1.41 mL, 0.0131 mol). Then, the reaction was allowed to stir for 24 h at room temperature. After reaction, the highly viscous sample was simply collected by removal of the solvent and drying under vacuum. The guanidinium salts was synthesized following the same procedure.

1-butyl-2,3,4,5,7,8,9,10-octahydropyrido[1,2-*a*][1,3]diazepin-1-ium bromide: <sup>1</sup>H NMR, 250MHz (CDCl<sub>3</sub>): δ = 0.85 ppm (t, 3H); δ = 1.27 ppm (m, 2H), δ = 1.52 ppm (m, 2H); δ = 1.71 ppm (broad, 6H); δ = 2.06 ppm (m, 2H); δ = 2.83 ppm (d, 2H); 3.35 ppm < δ < 3.75 ppm (m, 8H).

1-butyl-3,4,6,7,8,9-hexahydro-2H-pyrimido[1,2-*a*]pyrimidin-1-ium bromide: <sup>1</sup>H NMR, 250MHz (CDCl<sub>3</sub>): δ = 0.85 ppm (t, 3H); δ = 1.37 ppm (m, 2H), δ = 1.54 ppm (m, 2H); δ = 1.96 ppm (broad, 6H); 3.15 < δ < 3.35 ppm (m, 9H).

### Infrared set-up

The synthesis of bio-based cyclic carbonates was monitored *in-situ* by IR spectroscopy using a home-made Ge ATR accessory suitable for high-pressure measurements (up to 5 MPa) and high temperature (up to 150°C) coupled with a ThermoOptek interferometer (type 6700) equipped with a globar source, a KBr/Ge beamsplitter and a DTGS (Deuterated TriGlycine Sulphate) detector (Figure 1). Single beam spectra recorded in the spectral range (400 - 4000  $\text{cm}^{-1}$ ) with a 4  $\text{cm}^{-1}$  resolution were obtained after the Fourier transformation of 150 accumulated interferograms. Spectra were recorded every ten minutes for 24 h. The stainless steel cell with a volume of about 3 mL screwed above the Ge crystal provides one port for the inlet of mixture and  $\text{CO}_2$ . A magnetic stirrer was placed into the cell to ensure good homogenization of the mixture. The ATR cell was heated using cartridge heaters disposed in the periphery of its body. A thermocouple was used and located close to a cartridge heater for the temperature regulation with an accuracy of about 2°C. The cell was connected directly to the  $\text{CO}_2$  tank allowing the pressure to be raised up to 5 MPa.

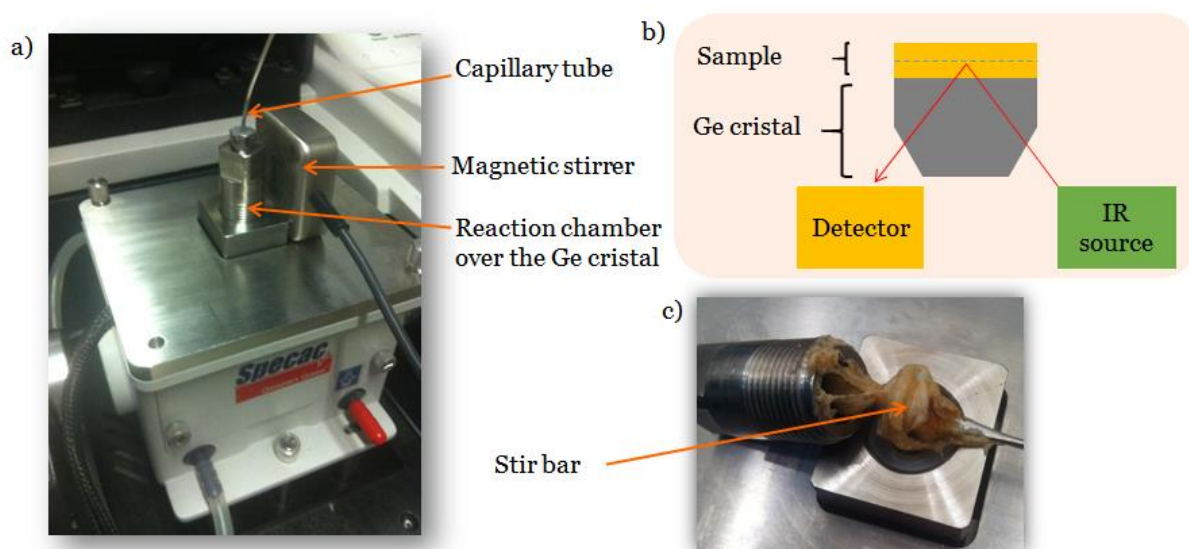


Figure 1: a) Picture and b) schematic representation of the experimental set-up, and c) picture of the set-up after synthesis of CLSO.

### NMR characterization

$^1\text{H}$  NMR spectra were recorded in  $\text{CDCl}_3$  at 400 MHz in the FT mode with a Bruker AN 400 apparatus at 25°C.

## 2. Experimental procedure

### Catalyst screening

30 g of ELSO were introduced in a 80 mL high pressure cell equipped with a mechanical stirrer (Figure 2) using  $2.32 \cdot 10^{-3}$  mol of catalyst (that correspond to 1 mol% of catalyst compared to ELSO). Then the cell was heated to 100°C before addition of CO<sub>2</sub> till the pressure is equilibrated to 10 MPa. After 5 h, the pressure was slowly released and the conversion of ELSO into CLSO was determined by <sup>1</sup>H NMR spectroscopy. The same procedure was applied for all the halide salts or ionic liquids tested in this study while keeping the amount of catalyst constant to  $2.32 \cdot 10^{-3}$  mol.



Figure 2: High pressure cell

### Catalyst optimisation

30 g of ELSO were introduced in a 80 mL high pressure cell equipped with a mechanical stirrer in presence of 1 mol% of TBABr (0.75 g,  $2.32 \cdot 10^{-3}$  mol) and 1,3-bis(2-hydroxyhexafluoroisopropyl)benzene (0.573 mL,  $2.32 \cdot 10^{-3}$  mol). Then the cell was heated to 100°C before addition of CO<sub>2</sub> till the pressure is equilibrated to 10 MPa. After 5h, the pressure was slowly released and the conversion of ELSO into CLSO was determined by <sup>1</sup>H NMR spectroscopy. The same procedure was applied for all HBDs tested in this study.

### Kinetic studies

In a typical experiment, a mixture composed of epoxydized linseed oil (500 µL) and the catalyst ( $5.95 \cdot 10^{-5}$  mol, 2.2 mol%, 32 mg TBABr) and pyrocatechol (11 mg,  $5.95 \cdot 10^{-5}$  mol, 2.2 mol%) were introduced in the ATR reactor at ambient temperature. Then, the cell was heated up to the desired temperature (60 – 120°C) before addition of CO<sub>2</sub> (0.5 – 5 MPa). The infrared spectra were collected online every 10 min. At the end of the reaction, in order to determine the conversion of ELSO into CLSO, the ATR spectrum of the reaction mixture was compared with the corresponding spectrum of the neat carbonate. The absorbance of the carbonate peak at 1808 cm<sup>-1</sup> corresponding to the ν(C=O) stretching mode was normalized using the peak corresponding to a ν(C-H) stretching mode at 2955 cm<sup>-1</sup> which does not evolve during the reaction. The yield for

the entire kinetic was deduced by proportionality using the Beer–Lambert law according to Equation 1.

$$Yield (\%) = \frac{\frac{[AC=O]}{[AC-H]}_{Reaction\ mixture}}{\frac{[AC=O]}{[AC-H]}_{Neat\ carbonate}} \quad \text{Eq 1}$$

The same experimental protocol was applied when pyrogallol, perfluoro-*tert*-butanol, hexafluoro-(*p*-tolyl)-isopropanol and 1,3-bis(2-hydroxyhexafluoroisopropyl)benzene were used as HBDs. All these syntheses were conducted at least twice in order to check the reproducibility of the obtained yields and kinetics.

### Solubility of CO<sub>2</sub> into ELSO

2.3 mL of ELSO were introduced in a high pressure transmission cell (Figure 3) with a pathlength of 0.49 cm and heated up at the desired temperature (from 40 to 100°C). At a fixed temperature, carbon dioxide was added from 0 to 20 MPa. After thermodynamic equilibration (within a few minutes), an infrared spectrum of the liquid phase was collected. The amount of CO<sub>2</sub> solubilized into ELSO was deduced from the height of the combination peak  $\nu_1 + 2\nu_2 + \nu_3$  at 4950 cm<sup>-1</sup> which is characteristic of CO<sub>2</sub>. In addition, the concentration of the ELSO can be followed from the peak at 5712 cm<sup>-1</sup>. The mass fraction of CO<sub>2</sub> dissolved in ELSO can be obtained from Equation 2.<sup>50</sup>

$$X_{CO_2} = \frac{[CO_2]}{[CO_2] + [ELSO]} \quad \text{Eq 2}$$

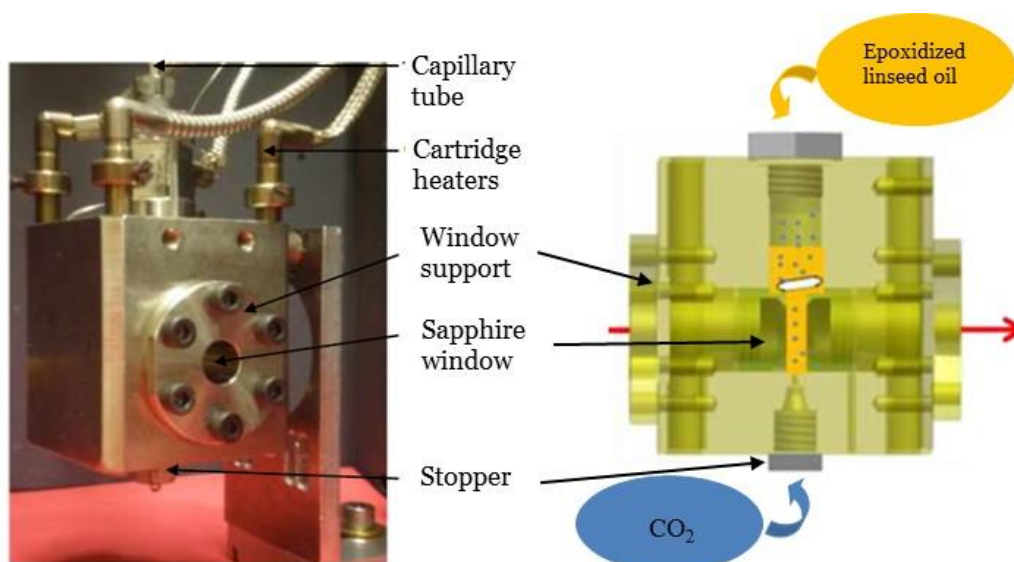


Figure 3: Picture and schematic diagram of the high-pressure optical cell

## Results and discussion

### 1. Catalyst screening for the synthesis of carbonated linseed oil

To identify the most efficient organocatalyst for the conversion of neat ELSO into CLSO, a screening of the catalytic activity of a series of iodide salts was first realized at 100°C and 10 MPa. From the results reported in Table 1, onium, phosphonium and imidazolium salts were found to exhibit the highest catalytic activity with a 25% conversion of ELSO into CLSO after 5h (entries 1, 4, 7), whereas pyrrolidinium, pyridinium or triethylsulfonium salts were less efficient or even ineffective as evidenced by a conversion of 19, 12 and 0% respectively. These very low activities are explained by the poor solubility of these salts in the CO<sub>2</sub>/linseed oil biphasic mixture. Then, the influence of the halide counter anion on the CO<sub>2</sub>/ESLO coupling was investigated for the most efficient onium, phosphonium or imidazolium organocatalysts. Coupling of CO<sub>2</sub> with ESLO was slowed down by using the less nucleophilic chloride counter ion (Table 1, entries 3, 6, 9) as evidenced by a conversion of the epoxide into cyclic carbonate close to 20%.

Table 1: Catalyst screening for the synthesis of CLSO by coupling of CO<sub>2</sub> with ELSO. Conditions: P = 10 MPa, T = 100 °C, catalyst = 2.32 10<sup>-3</sup> mol, t = 5 h, ELSO = 30 g, volume of the cell = 80 mL

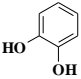
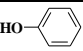
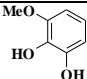
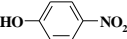
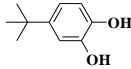

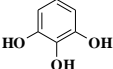
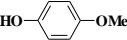
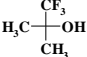
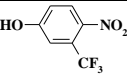
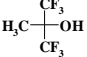
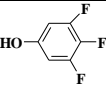
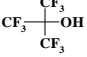
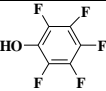
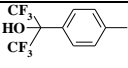
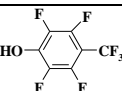
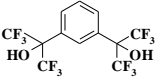
Entry	Catalyst	Halide counter anion	Conv (%)*
1		I <sup>-</sup>	26
2	1	Br <sup>-</sup>	30
3		Cl <sup>-</sup>	17
4		I <sup>-</sup>	21
5	2	Br <sup>-</sup>	28
6		Cl <sup>-</sup>	19
7		I <sup>-</sup>	25
8	3	Br <sup>-</sup>	30
9		Cl <sup>-</sup>	20
10	4	I <sup>-</sup>	/
11	5	I <sup>-</sup>	19
12	6	I <sup>-</sup>	12
13	7	Br <sup>-</sup>	28
14	8	Br <sup>-</sup>	36

\* determined by <sup>1</sup>H NMR spectroscopy by comparison of the relative intensities of the peaks characteristic of the CH groups of the epoxide (2.8 ppm < δ < 3.25 ppm) and the cyclic carbonate (4.6 ppm < δ < 4.9 ppm)

In contrast, substitution of iodine by bromine counter-anion slightly increased the reaction rate (Table 1, entries 2, 5, 8). In view of these results, the bromide counter ion offers the best compromise in terms of reactivity and steric hindrance/size even if it is less nucleophilic than iodide. It is supposed that its higher catalytic activity arises from its smaller size that favours its faster diffusion towards the internal epoxide groups of the fatty chains of the highly viscous vegetable oil. Finally, the coupling of CO<sub>2</sub> with ELSO was carried out in the presence of guanidinium and amidinium salts as organocatalysts (catalysts 7 and 8, Scheme 1). If the amidinium salt showed a similar activity than the previously tested organocatalysts (Table 1, entry 13), the conversion of ELSO into CLSO was increased by 20% in the presence of the guanidinium salt (Table 1, entry 14). These results are consistent with those reported by Foltran *et al.* who demonstrated that the coupling of CO<sub>2</sub> with propylene oxide was improved by replacing tetrabutylammonium bromide by 1,5,7-triaza-bicyclo[4.4.0]dec-5-enium bromide.<sup>51, 52</sup> However, even at high temperature and pressure, the conversion of ELSO into CLSO still remains low compared to results reported for the coupling of CO<sub>2</sub> with model epoxides. These observations are not surprising because the ring-opening of di-substituted epoxides is more difficult than the ring-opening of terminal/monosubstituted epoxides, as the result of increased steric hindrance.

In an effort to boost the reaction and to improve the conversion yield, some activators was added to the reaction medium. The organocatalytic system was therefore composed by the organocatalyst, TBABr, and an activator that was expected to interact with the oxygen of the epoxide ring through hydrogen bonding and to activate it for the ring-opening. The potential activators that were tested are commercially available phenolic compounds and fluoroalcohols (Scheme 2). Some of them have been demonstrated to fasten the coupling of CO<sub>2</sub> with model epoxides but were not tested on hindered epoxidized vegetable oils. The coupling of CO<sub>2</sub> with ELSO was therefore investigated at 100 °C and 10 MPa using 2.2 mol% of TBABr compared to ELSO and a TBABr/HBD molar ratio of 1 (Table 2). As reported by Kleij, phenol (HBD 1) had no co-catalytic activity<sup>28</sup> and a similar trend was observed for the coupling of ELSO with CO<sub>2</sub> using 4-methoxyphenol (HBD 4). Substitution of the hydrogen atom in *para* position by a trifluoromethyl- or a nitro- electron-withdrawing group clearly improved the co-catalytic efficiency of phenol. Indeed, the conversion was increased from 30 to 47% in the presence of 4-nitrophenol (HBD 2), and from 30 to 58% in the presence of 4-trifluoromethylphenol (HBD 3). The latter was therefore doubling the productivity in cyclocarbonated vegetable oils. Finally, a phenolic derivative combining two different electron-withdrawing groups in *meta* (CF<sub>3</sub>) and *para* (NO<sub>2</sub>) positions (HBD 5) or partially/fully fluorinated HBDs (HBDs 6 - 8) were poor activators with a weak increase of the epoxide conversion by 20 to 30%. Coupling of CO<sub>2</sub> with ELSO was also studied using multiphenolic activators derived from catechol (HBDs 9 - 11) and pyrogallol (HBD 12) or fluoroalcohols. (HBDs 13 - 17). At the exception of HBD 13, all these HBDs exhibited the highest co-catalytic activity as evidenced by a 1.85 to 2-fold increase of the conversion of ELSO into CLSO.

Table 2: Hydrogen bond donors screening for the TBABr promoted coupling of CO<sub>2</sub> with ELSO. Conditions: P = 10 MPa, T = 100 °C, catalyst = 2.32 10<sup>-3</sup> mol (1 mol% compared to ELSO), [TBABr]/[HBD] = 1, t = 5 h, ELSO = 30 g, volume of the cell = 80 mL

Entry	HBD	Reference	Conv (%) <sup>*</sup>				
1	/	/	30	10		HBD 9	63
2		HBD 1	32	11		HBD 10	55
3		HBD 2	47	12		HBD 11	57
4		HBD 3	58	13		HBD 12	56
5		HBD 4	31	14		HBD 13	42
6		HBD 5	42	15		HBD 14	58
7		HBD 6	41	16		HBD 15	63
8		HBD 7	45	17		HBD 16	55
9		HBD 8	38	18		HBD 17	58

<sup>\*</sup> determined by <sup>1</sup>H NMR spectroscopy by comparison of the relative intensities of the peaks characteristic of the CH groups of the epoxide (2.8 ppm < δ < 3.25 ppm) and the cyclic carbonate (4.6 ppm < δ < 4.9 ppm)

## 2. Detailed kinetic study of the TBABr/HBD promoted ELSO/CO<sub>2</sub> coupling

After this first organocatalyst and activator screening, a detailed kinetic study of the synthesis of CLSO using the catalytic platform was realized by online IR spectroscopy under pressure and the influence of various experimental parameters, such as CO<sub>2</sub> pressure, catalyst content and the temperature, on the conversion of ELSO into CLSO was investigated. Formation of CLSO was monitored by following the evolution with time of the signal at 1808 cm<sup>-1</sup> reflecting the ν(C=O) stretching mode of CLSO (Figure 4). The presence of CO<sub>2</sub> dissolved in the ELSO rich phase was also highlighted by the presence of a very narrow peak at 2350 cm<sup>-1</sup> corresponding to the antisymmetric stretch ν<sub>3</sub> of CO<sub>2</sub> that is superimposed over a broad doublet profile that is due to atmospheric CO<sub>2</sub>.



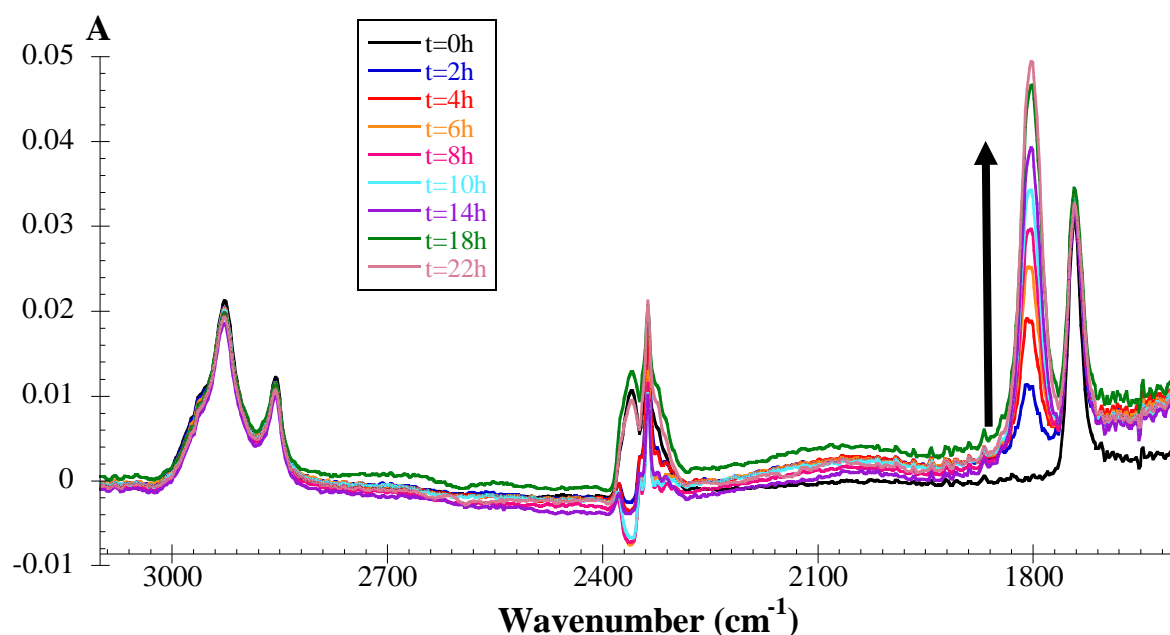


Figure 4: Evolution with time of the ATR-IR spectra for the TBABr/HBD 15 promoted ELSO/CO<sub>2</sub> coupling. Conditions: T = 80°C, P = 2 MPa, TBABr = 2.2 mol%, [TBABr]/[HBD 15] = 1

The yield of reaction was deduced from the comparison of the intensity of the peak at 1808 cm<sup>-1</sup> and the peak at 2955 cm<sup>-1</sup> corresponding to the  $\nu_{\text{(C-H)}}$  stretching modes of the linseed oil that does not evolve during the reaction. Coupling of CO<sub>2</sub> with ELSO was catalysed by TBABr (2.2 mol%) at 80°C and 2 MPa using HBDs 9, 12, 15, 16 and 17 ([TBABr]/[HBD] = 1) that were selected as representative activators as they showed the highest co-catalytic activity for the synthesis of CLSO (Figure 5). In the absence of HBD, the TBABr promoted reaction was slow as evidenced by a conversion of the epoxides into the corresponding cyclic carbonates of 45% after 1200 min. Synergistic effects between TBABr and the co-catalysts are highlighted by an increase of the conversion of ELSO into CLSO after addition of the HBDs. Figure 5 suggests that HBD 17 (1,3-bis-HFAB) is slightly more efficient than the others HBDs as evidenced by an increase after 1200 min of the ELSO conversion from 45% to 66% compared to 64% for HBDs 9 and 16, 60% for HBD 15 and about 50% for HBD 12. The slightly higher co-catalytic activity of HBD 17 (1,3-bis-HFAB) could be explained by the formation of 3 hydrogen bonds between the oxygen atom of ELSO and both protons of the alcohol functions and the aromatic proton in *para* position of both hexafluoroisopropyl alcohol of HBD 17 (1,3-bis-HFAB), which favor the activation of the epoxide groups. This assumption is supported by previous DFT calculations and NMR titration of epoxydodecane with HBD 17 (1,3-bis-HFAB).<sup>28</sup>

The influence of the temperature on the kinetics and the yield of the ELSO/CO<sub>2</sub> coupling was studied from 60 to 120°C at 2 MPa using 2.2 mol% of catalyst (TBABr) in combination with 2.2 mol% of perfluoro-*tert*-butanol (HBD 15) as a model hydrogen bond donor activator.

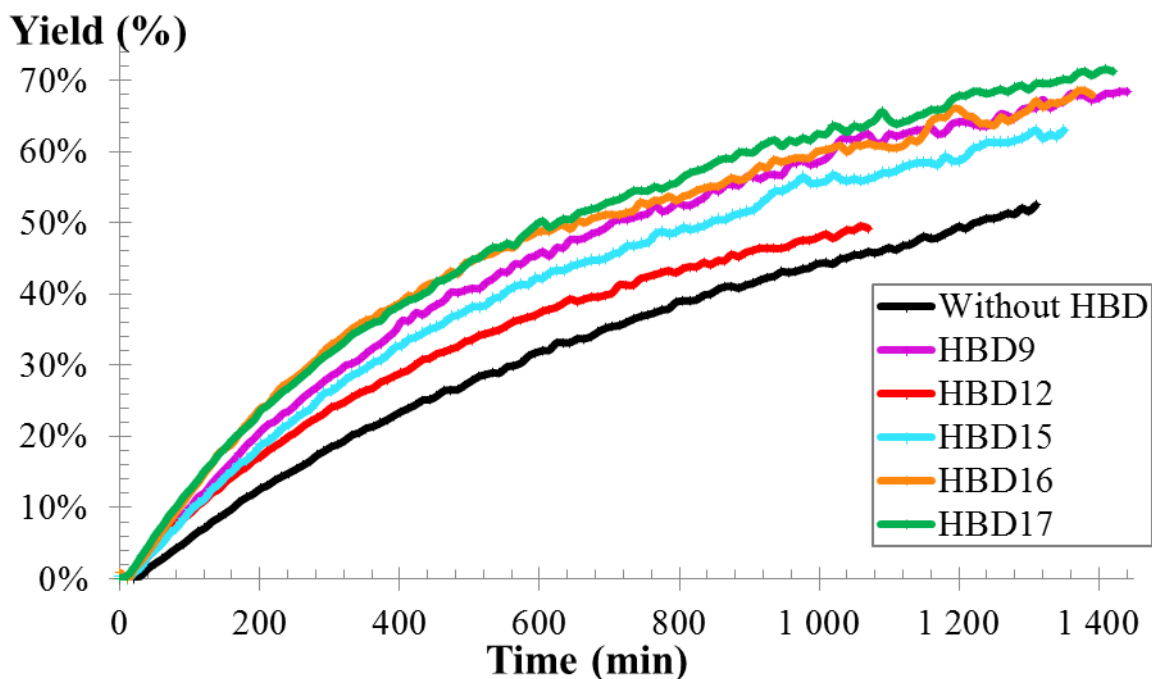


Figure 5: Kinetic study of the TBABr/HBD promoted coupling of CO<sub>2</sub> with ELSO: effect of the HBDs. Conditions: T = 80°C, P = 2 MPa, TBABr = 2.2 mol%, [TBABr]/[HBD] = 1

The resulting kinetic profiles, illustrated in Figure 6, show that the reaction rate was strongly affected by the temperature. At 120°C, ELSO was quantitatively converted into CLSO in 1000 min whereas the conversion only reached 25% at 60°C. Therefore, although the temperature increase (at constant CO<sub>2</sub> pressure) induced a slight decrease of the CO<sub>2</sub> concentration in the ELSO phase (Figure 7 and 8), the CO<sub>2</sub>/epoxide coupling was favored at higher temperature. Moreover, raising the temperature decreased the viscosity of ELSO and was consequently expected to improve the diffusion of the catalytic species in the reaction medium. Thermodynamic considerations show that the concentration of CO<sub>2</sub> dissolved in the oil phase is increased at higher CO<sub>2</sub> pressure as evidenced by an increase of the intensity of the peak at 4950 cm<sup>-1</sup> (Figure 7). At 2 MPa and 80°C, the CO<sub>2</sub> molar fraction is low ( $X_{\text{CO}_2} < 0.05$ ) but doubled by increasing the pressure to 5 MPa ( $X_{\text{CO}_2} \approx 0.1$ ) (Figure 8).

Therefore, the impact of the pressure on the synthesis of CLSO from ELSO and CO<sub>2</sub> was also investigated. Reaction was performed in the presence of 2.2 mol% TBABr and 2.2 mol% of HBD 15 at 80°C in a pressure range of 0.5 to 5 MPa (Figure 9). For low CO<sub>2</sub> pressures of 0.5 and 1 MPa, the reaction was slow and the yield reached a plateau between 40 and 50% after 1400 min. At such low pressure, the amount of CO<sub>2</sub> dissolved in the epoxide rich phase is insufficient ( $X_{\text{CO}_2} < 0.02$ ) to completely convert ELSO into CLSO. Increasing the pressure had a positive impact on both the solubility of CO<sub>2</sub> into ELSO and the kinetics. At 2 MPa, the molar fraction of CO<sub>2</sub> dissolved in the epoxidized vegetable soybean oil was increased to 0.035, and the ELSO conversion into CLSO reached 60% after 1400 minutes whereas at 5 MPa, it

was almost quantitative (90%) after the same period of time. This last result is the consequence of the highest concentration of  $\text{CO}_2$  dissolved in the oil ( $X_{\text{CO}_2} \sim 0.1$ ).

### Yield (%)

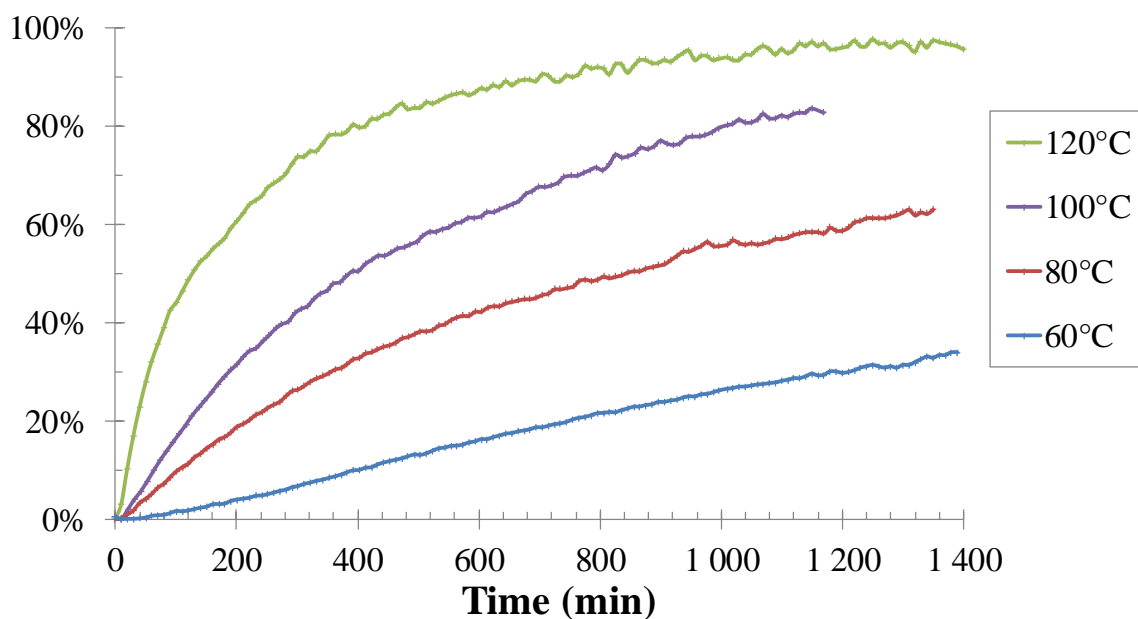


Figure 6: Kinetic study of the TBABr/HBD 15 promoted coupling of  $\text{CO}_2$  with ELSO: effect of the temperature. Conditions:  $P = 2 \text{ MPa}$ ,  $\text{TBABr} = 2.2 \text{ mol\%}$ ,  $[\text{TBABr}]/[\text{HBD 15}] = 1$

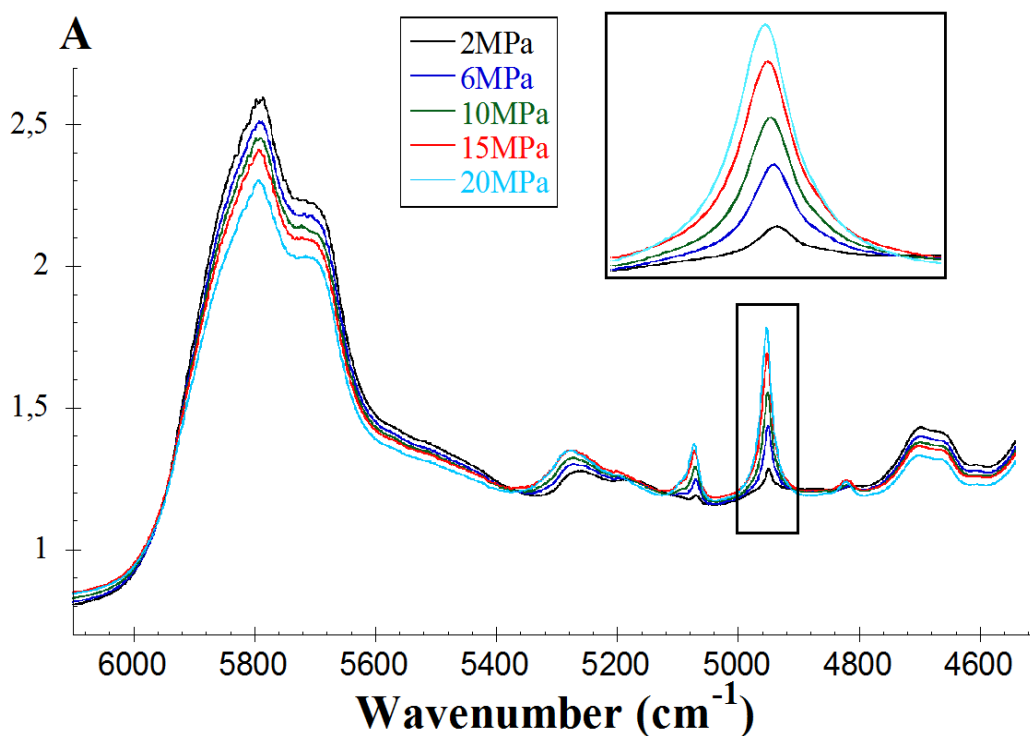


Figure 7: IR absorption spectra of the ELSO rich phase of the ELSO/ $\text{CO}_2$  mixture at  $T = 100^\circ\text{C}$  for different  $\text{CO}_2$  pressures.

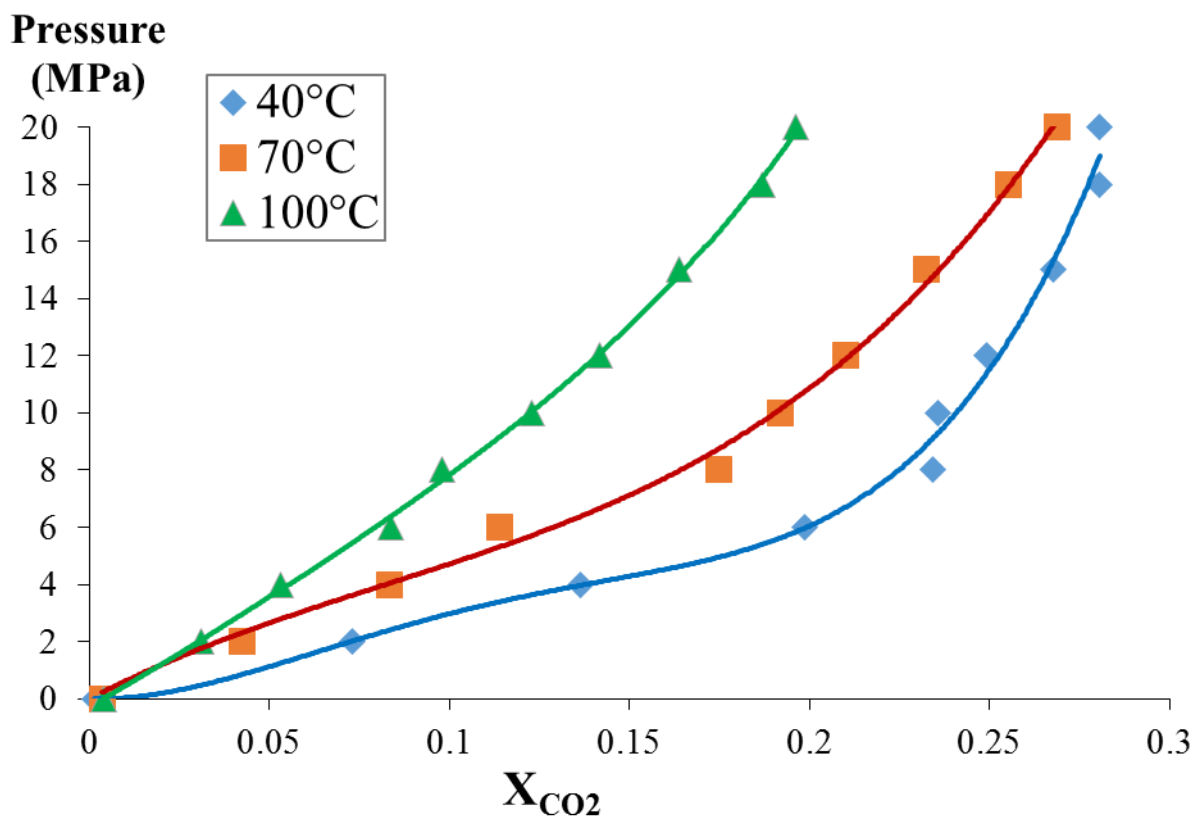


Figure 8: Molar fraction of CO<sub>2</sub> in the ELSO rich phase as a function of pressure and temperature

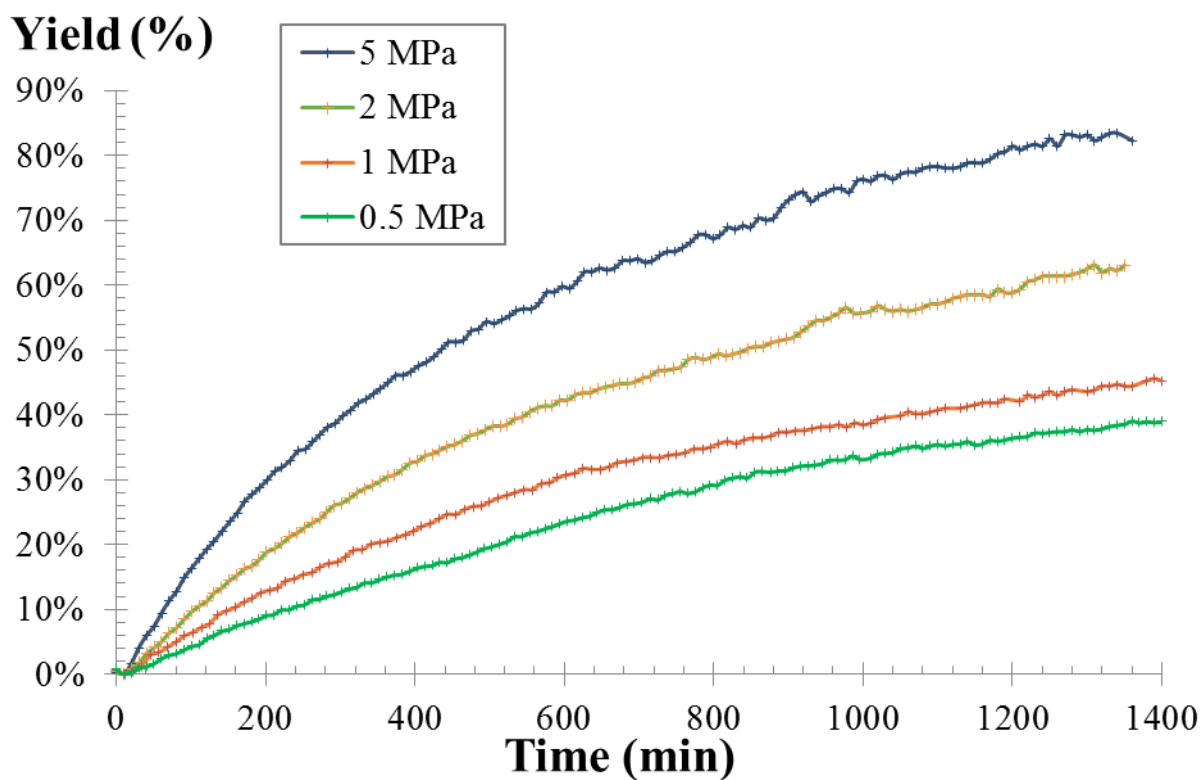


Figure 9: Kinetic study of the TBABr/HBD 15 promoted coupling of CO<sub>2</sub> with ELSO: Pressure effect. Conditions: T = 80°C, TBABr = 2.2 mol%, [TBABr]/[HBD 15] = 1

Finally, the impact of the HBD15 concentration on the ELSO/CO<sub>2</sub> coupling was studied under optimized experimental conditions, i.e. a temperature of 120°C and a pressure of 5 MPa using 2.2 mol% of TBABr as catalyst. HBD 15 was chosen as a model activator as it was the cheapest HBD that showed one of the most efficient co-catalytic activity. Figure 10 shows the typical kinetic curves for a co-catalyst loading ranging from 0 to 3.7 mol%. If the addition of 0.5 equivalent of HBD 15 only slightly improved the TBABr promoted coupling of CO<sub>2</sub> with ELSO, the kinetic was doubled when TBABr and HBD 15 were used in equimolar amount and the reaction was complete within 600 minutes instead of 1200 minutes without HBD 15. However, addition of an excess of HBD 15 (1.5 equivalent) compared to TBABr, had a detrimental effect on the kinetic as evidenced by a decrease of the rate constant compared to experiment conducted using an equimolar amount. This observation was related to the acidity of the proton of perfluoro-*tert*-butanol that decreased the nucleophilicity of the halide anion by strong solvation.<sup>53</sup>

### Yield (%)

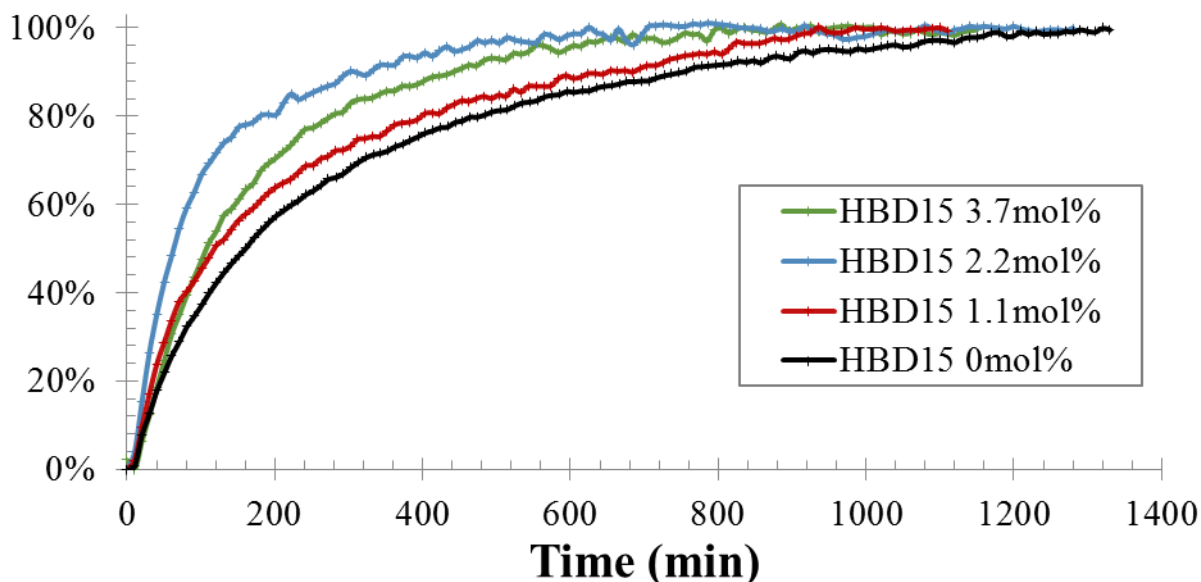


Figure 10: Kinetic study of the TBABr/HBD 15 promoted coupling of CO<sub>2</sub> with ELSO: effect of HBD content. Conditions: T = 120°C, P = 5 MPa, TBABr = 2.2 mol%.

## Conclusions

Cyclocarbonated linseed oil was synthesized by coupling CO<sub>2</sub> with epoxidized linseed oil (ELSO) using a catalytic platform composed of an organic halide salt or ionic liquid as organocatalyst, and a hydrogen bond donor as activator. We first screened the catalytic activity of various organo-catalysts and found that guanidinium salt showed the best catalytic efficiency. The improvement of the CO<sub>2</sub>/epoxidized vegetable oil coupling reaction was then investigated by adding various activators to the reaction medium containing TBABr as organocatalyst. Amongst all tested activators, 1,3-bis(2-hydroxyhexafluoroisopropyl)benzene, hexafluoro-2-(*p*-tolyl)isopropanol, perfluoro-*tert*-butanol and pyrocatechol are the most efficient with a doubling of the conversion of epoxide groups into cyclic carbonates compared to the same reaction carried out without the activator. The coupling of CO<sub>2</sub> with ELSO was optimized through detailed kinetic studies highlighting the positive impact of the pressure, the amount of CO<sub>2</sub> dissolved in ELSO, the temperature and the co-catalyst loading on the reaction rate. Optimal conditions deduced from kinetic studies (TBABr/HBD = 1, [TBABr] = 2.2 mol%, 120°C, 5 MPa) provides quantitative conversion of ELSO into CLSO in about 600 min without using any organic solvent. Therefore, when comparing the reaction conditions and kinetics previously reported<sup>46</sup> (> 30 h, 140°C, 1.5 MPa) with our optimized conditions (10h, 120°C, 5 MPa), we emphasize that the organocatalytic system composed of TBABr and hydrogen bond donor activator is particularly suitable to speed up the production of cyclocarbonated vegetable oils. However, the thermodynamic conditions still remain rather harsh and further research efforts are needed in order to develop more efficient catalysts that are active under mild conditions for the production of cyclocarbonated vegetable oils.

## References

1. M. Aresta, A. Dibenedetto and A. Angelini, *Chemical Reviews*, 2014, **114**, 1709-1742.
2. R. Martín and A. W. Kleij *ChemSusChem*, 2011, **4**, 1259-1263.
3. T. Sakakura, J.-C. Choi and H. Yasuda, *Chemical Reviews*, 2007, **107**, 2365-2387.
4. K. Nogi, T. Fujihara, J. Terao and Y. Tsuji, *Chemical Communications*, 2014, **50**, 13052-13055.
5. B. Yu, Z.-F. Diao, C.-X. Guo, C.-L. Zhong, L.-N. He, Y.-N. Zhao, Q.-W. Song, A.-H. Liu and J.-Q. Wang, *Green Chemistry*, 2013, **15**, 2401-2407.
6. D. Yu, M. X. Tan and Y. Zhang, *Advanced Synthesis & Catalysis*, 2012, **354**, 969-974.
7. M. Arndt, E. Risto, T. Krause and L. J. Gooßen, *ChemCatChem*, 2012, **4**, 484-487.
8. T. Zevaco and E. Dinjus, in *Carbon Dioxide as Chemical Feedstock*, ed. M.Aresta, Wiley-VCH Verlag GmbH & Co. KGaA, 2010, pp. 89-120.
9. A. Behr and V. A. Brehme, *Journal of Molecular Catalysis A: Chemical*, 2002, **187**, 69-80.
10. A. Behr and M. Heite, *Chemical Engineering & Technology*, 2000, **23**, 952-955.
11. A. Behr and K.-D. Juszak, *Journal of Organometallic Chemistry*, 1983, **255**, 263-268.
12. G. Fiorani and A. W. Kleij, *Angewandte Chemie International Edition*, 2014, **53**, 7402-7404.
13. M. Tamura, M. Honda, Y. Nakagawa and K. Tomishige, *Journal of Chemical Technology & Biotechnology*, 2014, **89**, 19-33.
14. W. Xiong, C. Qi, H. He, L. Ouyang, M. Zhang and H. Jiang, *Angewandte Chemie International Edition*, 2015, **54**, 3084-3087.
15. S. Pulla, C. M. Felton, P. Ramidi, Y. Gartia, N. Ali, U. B. Nasini and A. Ghosh, *Journal of CO<sub>2</sub> Utilization*, 2013, **2**, 49-57.
16. Y.-N. Zhao, Z.-Z. Yang, S.-H. Luo and L.-N. He, *Catalysis Today*, 2013, **200**, 2-8.
17. M. Tamura, M. Honda, K. Noro, Y. Nakagawa and K. Tomishige, *Journal of Catalysis*, 2013, **305**, 191-203.
18. M. Honda, S. Sonehara, H. Yasuda, Y. Nakagawa and K. Tomishige, *Green Chemistry*, 2011, **13**, 3406-3413.
19. T. E. Waldman and W. D. McGhee, *Journal of the Chemical Society, Chemical Communications*, 1994, **699**, 957-958.
20. D. Saylik, M. J. Horvath, P. S. Elmes, W. R. Jackson, C. G. Lovel and K. Moody, *The Journal of Organic Chemistry*, 1999, **64**, 3940-3946.
21. P. P. Pescarmona and M. Taherimehr, *Catalysis Science & Technology*, 2012, **2**, 2169-2187.

22. J. Łukaszczyk, K. Jaszcz, W. Kuran and T. Listos, *Macromolecular Rapid Communications*, 2000, **21**, 754-757.
23. D. J. Darensbourg and W.-C. Chung, *Macromolecules*, 2014, **47**, 4943-4948.
24. S. Kumar, S. L. Jain and B. Sain, *Catalysis Letters*, 2012, **142**, 615-618.
25. C. Martín, G. Fiorani and A. W. Kleij, *ACS Catalysis*, 2015, **5**, 1353-1370.
26. G. Fiorani, W. Guo and A. W. Kleij, *Green Chemistry*, 2015, **17**, 1375-1389.
27. C. J. Whiteoak, A. H. Henseler, C. Ayats, A. W. Kleij and M. A. Pericàs, *Green Chemistry*, 2014, **16**, 1552-1559.
28. C. J. Whiteoak, A. Nova, F. Maseras and A. W. Kleij, *ChemSusChem*, 2012, **5**, 2032-2038.
29. T. Werner, N. Tenhumberg and H. Büttner, *ChemCatChem*, 2014, **6**, 3493-3500.
30. M. E. Wilhelm, M. H. Anthofer, M. Cokoja, I. I. E. Markovits, W. A. Herrmann and F. E. Kühn, *ChemSusChem*, 2014, **7**, 1357-1360.
31. T. Werner and N. Tenhumberg, *Journal of CO<sub>2</sub> Utilization*, 2014, **7**, 39-45.
32. Y. Zhang, S. Yin, S. Luo and C. T. Au, *Industrial & Engineering Chemistry Research*, 2012, **51**, 3951-3957.
33. L. Han, H.-J. Choi, S.-J. Choi, B. Liu and D.-W. Park, *Green Chem.*, 2011, **13**, 1023-1028.
34. J. Tharun, G. Mathai, A. C. Kathalikkattil, R. Roshan, J.-Y. Kwak and D.-W. Park, *Green Chem.*, 2013, **15**, 1673-1677.
35. S. Gennen, M. Alves, R. Méreau, T. Tassaing, B. Gilbert, C. Detrembleur, C. Jerome and B. Grignard, *ChemSusChem*, 2015, **8**, 1845-1849.
36. A. M. Hardman-Baldwin and A. E. Mattson, *ChemSusChem*, 2014, **7**, 3275-3278.
37. E. G. D. Miloslavskiy, O. Figovsky, D. Pashin, *International Letters of Chemistry, Physics and Astronomy*, 2014, **27**, 20-29.
38. P. G. Parzuchowski, M. Jurczyk-Kowalska, J. Ryszkowska and G. Rokicki, *J. Appl. Polym. Sci.*, 2006, **102**, 2904-2914.
39. M. Bähr and R. Mülhaupt, *Green Chemistry*, 2012, **14**, 483-489.
40. B. Tamami, S. Sohn and G. L. Wilkes, *Journal of Applied Polymer Science*, 2004, **92**, 883-891.
41. I. Javni, W. Zhang and Z. S. Petrović, *Journal of Applied Polymer Science*, 2003, **88**, 2912-2916.
42. A. R. Mahendran, N. Aust, G. Wuzella, U. Müller and A. Kandelbauer, *Journal of Polymers and the Environment*, 2012, **20**, 926-931.
43. K. M. Doll and S. Z. Erhan, *Green Chemistry*, 2005, **7**, 849-854.
44. N. Mann, S. K. Mendon, J. W. Rawlins and S. F. Thames, *IAOCS, Journal of the American Oil Chemists' Society*, 2008, **85**, 791-796.
45. P. Mazo and L. Rios, *IAOCS, Journal of the American Oil Chemists' Society*, 2013, **90**, 725-730.
46. Z. Li, Y. Zhao, S. Yan, X. Wang, M. Kang, J. Wang and H. Xiang, *Catalysis Letters*, 2008, **123**, 246-251.
47. A. Lee and Y. Deng, *European Polymer Journal*, 2015, **63**, 67-73.



48. A. Boyer, E. Cloutet, T. Tassaing, B. Gadenne, C. Alfes and H. Cramail, *Green Chem.*, 2010, **12**, 2205-2213.
49. L. Maisonneuve, A. S. More, S. Foltran, C. Alfes, F. Robert, Y. Landais, T. Tassaing, E. Grau and H. Cramail, *RSC Adv.*, 2014, **4**, 25795-25803.
50. S. Foltran, L. Maisonneuve, E. Cloutet, B. Gadenne, C. Alfes, T. Tassaing and H. Cramail, *Polym. Chem.*, 2012, **3**, 525-532.
51. S. Foltran, R. Mereau and T. Tassaing, *Catalysis Science and Technology*, 2014, **4**, 1585-1597.
52. S. Foltran, J. Alsarraf, F. Robert, Y. Landais, E. Cloutet, H. Cramail and T. Tassaing, *Catalysis Science and Technology*, 2013, **3**, 1046-1055.
53. N. Aoyagi, Y. Furusho and T. Endo, *Tetrahedron Letters*, 2013, **54**, 7031-7034.

---

## Chapter V:

A comprehensive Density Functional Theory study of the key role of fluorination and dual hydrogen bonding in the activation of the epoxide/CO<sub>2</sub> coupling by fluorinated alcohols

---

The results presented in this chapter were published in *RSC Advances*, 2016, **6**, 36327 - 36335

## Abstract

The activation mechanism of the CO<sub>2</sub>/propylene oxide coupling catalysed by a bicomponent organocatalyst combining the use of TBABr with (multi)phenolic or fluorinated hydrogen bond donors (HBDs) was investigated using Density Functional Theory (DFT). Thus, it was shown that increasing the number of electron withdrawing trifluoromethyl substituents in HBDs strengthens their proton donor capability and allows a better stabilization by hydrogen bonding of the intermediates and transition states. In addition, the high efficiency of fluorinated monoalcohol activators is related to a dual hydrogen bonding mechanism by two fluorinated molecules that cooperatively contribute to the CO<sub>2</sub>/propylene oxide coupling.

## Table of contents

Introduction.....	149
Experimental .....	150
Computational details.....	150
Results and discussion.....	150
1. CO <sub>2</sub> /PO coupling without HBDs .....	151
2. CO <sub>2</sub> /PO coupling using (multi)phenolic HBDs .....	153
3. CO <sub>2</sub> /PO coupling using fluorinated monoalcohols as HBDs.....	155
4. CO <sub>2</sub> /PO coupling using fluorinated HBDs: the key role of the CF <sub>3</sub> groups.....	159
5. CO <sub>2</sub> /PO coupling using fluorinated diols as HBDs.....	162
Conclusions.....	163

## Introduction

The synthesis of five-membered cyclic carbonates *via* the catalytic coupling of CO<sub>2</sub> with epoxides is currently the subject of numerous studies.<sup>1-11</sup> Although specific transition metal catalysts have proven to be efficient even under atmospheric pressure and ambient temperature,<sup>2, 10, 12</sup> some of these complexes are highly sensitive to hydrolysis and oxidation, poorly selective and potentially toxic. To overcome these limitations, less/non-toxic and eco-friendly organocatalysts such as (functional) ionic liquids and halide salts have been extensively developed in the past years.<sup>13-26</sup> If these organocatalysts allow the selective formation of cyclic carbonates from CO<sub>2</sub> and epoxides, they usually display low activity and only show reasonable efficiency at high catalyst loading, at high pressure and high temperature ( $T > 100^{\circ}\text{C}$ ) favoring their degradation.<sup>4, 10, 27-30</sup> The catalytic activity of organocatalysts can be drastically enhanced by using suitable co-catalysts such as hydrogen bond donors (HBDs) which, as shown in several theoretical investigations, (i) interact with the O-donor group of epoxides facilitating the ring-opening by the nucleophilic attack of the halide counter-anion of the halide salt or ionic liquid and, (ii) stabilize, by hydrogen bonding, the oxyanion formed after the epoxide ring-opening step.<sup>6, 31-33</sup> Phenolic derivatives<sup>31, 34, 35</sup>, (amino)alcohols<sup>36-38</sup>, fluorinated alcohols<sup>39-41</sup>, carboxylic acids<sup>42-44</sup>, lecithin<sup>45</sup>, cellulose<sup>46, 47</sup>, chitosan<sup>48-51</sup>, tannic acid<sup>52</sup> and silanols<sup>53</sup> have been proposed as potential hydrogen bond donors to fasten the CO<sub>2</sub>/epoxide coupling under mild experimental conditions. Among these HBDs, phenol derivatives, fluorinated alcohols and silanols were found to be the most efficient co-catalysts. Kleij *et al.* proposed a very efficient (multi)phenolic compound/ammonium iodide organocatalytic system that fastened the coupling of CO<sub>2</sub> with epoxides at low temperature (25 - 45°C) and pressure (1 MPa).<sup>31</sup> Mattson *et al.* reported recently on the use of silanols as a new class of HBDs allowing the synthesis of cyclic carbonates at 0.1 MPa and 25°C although the reaction rate was very low (18h) despite the use of a very high catalyst (TBAI) and co-catalyst (silanol) loading (10 mol%).<sup>53</sup> Recently, we reported a novel combination of onium salts with catalytic amount of fluorinated HBDs allowing the fast synthesis of cyclic carbonates within a few minutes under solvent free and mild experimental conditions.<sup>41</sup>

In a recent comparative study highlighting the co-catalytic activity of a series of commercially available HBDs, we demonstrated that fluorinated alcohols were the most efficient HBDs for the synthesis of cyclic carbonates from CO<sub>2</sub> and epoxides under mild experimental conditions.<sup>39</sup> From preliminary DFT calculations reported in reference<sup>41</sup>, we evidenced that two different HBDs diols (pyrogallol and 1,3-bis(2-hydroxyhexafluoroisopropyl)benzene) strongly reduced the relative energy of the reaction in comparison with the system without activator. A hydrogen-bond stabilization mechanism that impacted the energy of the epoxide ring-opening step was proposed. However, the origin of the high efficiency of fluorinated mono-alcohols in comparison with non-fluorinated (multi)phenolic activators was not understood. This prompted us to understand the origin of the unprecedented catalytic activity of

fluorinated alcohols in comparison with other HBDs proposed in the literature. In this paper, we therefore report on the detailed mechanistic investigation, through molecular modeling, of the fluorinated HBDs/halide salts catalysed CO<sub>2</sub>/propylene oxide coupling.

## Experimental

### Computational details

Preliminary calculations of equilibrium structures were performed using a semi-empirical model (AM1-D<sub>3</sub>H<sub>4</sub> <sup>54, 55</sup>) to determine the most stable conformations of the reactants, the catalysts and the products. These semi-empirical calculations were performed using the AMPAC software.<sup>56</sup> Using the same semi-empirical model (AM1-D<sub>3</sub>H<sub>4</sub>), the CHAIN algorithm <sup>57</sup> implemented in the AMPAC software was used for locating along the reaction path the conformations that were identified as intermediates and transition states. The lowest energy structures of the intermediates and transition states obtained at the AM1-D<sub>3</sub>H<sub>4</sub> level were further investigated using the Density Functional Theory method (DFT) implemented in the Gaussian 09 package.<sup>58</sup> DFT calculations of geometries, energies, and vibrational frequencies reported in this paper were carried out with the Mo6-2X functional <sup>59</sup> using the 6-311G(d,p) basis set. All frequencies of each structure have been calculated to verify the presence of a single imaginary frequency for transition states and the absence of imaginary frequency for ground states. The intrinsic reaction coordinate (IRC) method has been used to verify that the obtained transition states were effectively connected to the desired minima. For all catalysts, a wide range of possible configurations and interactions have been modelled and the more stable of them are reported in this work. To consider entropic effects, the energies mentioned in this study correspond to the Gibbs free energy ( $\Delta G$ ).

Although CO<sub>2</sub>, PO, the bromine ion and the different hydrogen bond donor activators will be represented using the Ball-and-Stick model, the tetrabutylammonium cation will be represented using the skeleton model in order to improve the visualization of those complex systems described below.

## Results and discussion

The mechanistic study through DFT simulation was realized for a model reaction involving the coupling of CO<sub>2</sub> with propylene oxide (PO) catalysed by tetrabutylammonium bromide (TBABr) in presence or not of HBDs. As previous reports <sup>60-64</sup> figured out that the most probable pathway in the reaction mechanism involves the activation of the epoxide by the catalyst before addition of CO<sub>2</sub>, this activation mode was privileged in the present discussion. On the other hand, as it will be illustrated in this paper, the epoxide ring-opening step corresponds to the highest energy transition state and is assumed to be the Rate Determining Step (RDS), in line with previous reports.<sup>65, 66</sup> This is further supported by the following arguments:

i) we consider that the initial energy of the reactants is conserved within the "system" along the reaction path even though the line dramatically dips down to some intermediates indicating a strong decrease in energy. Indeed, even if the energy leaves the reactants as they are transformed into an intermediate in an exergonic step, the released energy remains in solution and dissipated heat is consumed by the intermediates to overcome their subsequent energy barriers.

ii) when the reaction occurs in a solvent, a putative intermediate may only become a true detectable intermediate when the solvent fully stabilizes it. However, some intermediates might be "bypassed" because the dynamics of the solvent equilibration might be slower than the molecular reaction dynamics allowing the following elementary reaction step to occur before reaching the intermediate state of low energy.<sup>67</sup> It is especially true for the systems studied in this work. Indeed, after the first elementary reaction, everything is in place to proceed until the formation of the end products. The activated intermediate (IR1; Figure 1) is surrounded by CO<sub>2</sub> molecules allowing a fast addition (compare to its stabilization) and the last step of the reaction (ring closure) is an intramolecular rearrangement which is fast as the "excess" energy is already available in the degrees of freedom involved in the reaction coordinate of this final step. The "bypass" of low energy intermediates is supported by the fact that we do not experimentally detect (in our *in-situ* kinetic studies) the very low energy intermediates reported in our DFT study.

Considering this discussion, the first step of the reaction, thus the ring-opening of the epoxide, is the RDS, whatever the catalytic system investigated.

## 1. CO<sub>2</sub>/PO coupling without HBDs

Schematic potential energy profiles obtained at the Mo6-2X/6-311G(d,p) level and schematic Lewis structures for the CO<sub>2</sub>/PO coupling catalysed by TBABr are depicted in Figure 1. After having fully optimized the TBABr, PO, propylene carbonate (PC) and CO<sub>2</sub> structures, the overall cycloaddition pathway between PO and CO<sub>2</sub> has been modelled by a three-step mechanism. The initial state corresponds to the sum of the free energies of each compound (PO, CO<sub>2</sub>, TBABr) which is taken as the zero energy. The first transition state TS1 corresponds to the nucleophilic attack of the epoxide by the bromine ion of the organocatalyst inducing the opening of the C-O-C bond (Figure 2) and the stabilization of the resulting oxy-anion by the alkyl chains of TBA<sup>+</sup> by Van der Waals interactions. The nucleophilic attack on the secondary carbon of PO was only considered as it was reported to be the most favourable.<sup>64</sup> Then, a bromohydrin ion corresponding to the intermediate IR1 is obtained by formation of a C-Br bond between Br<sup>-</sup> and the non-substituted carbon atom of the epoxide. As IR1 is not stabilized by strong interactions, the insertion of CO<sub>2</sub> onto the oxy-anion occurs without the existence of a transition state (TS2) and leads to a more stable bromo-alkylcarbonate intermediate (IR2) that is stabilized by Van der Waals interactions between the carbonate ion and the alkyl chains of TBA<sup>+</sup>. Finally, a second transition step (TS3), which consists in the breaking of the C-Br bond and the intramolecular

ring-closure of the intermediate IR2, provides propylene carbonate (PC) while regenerating the ammonium salt.

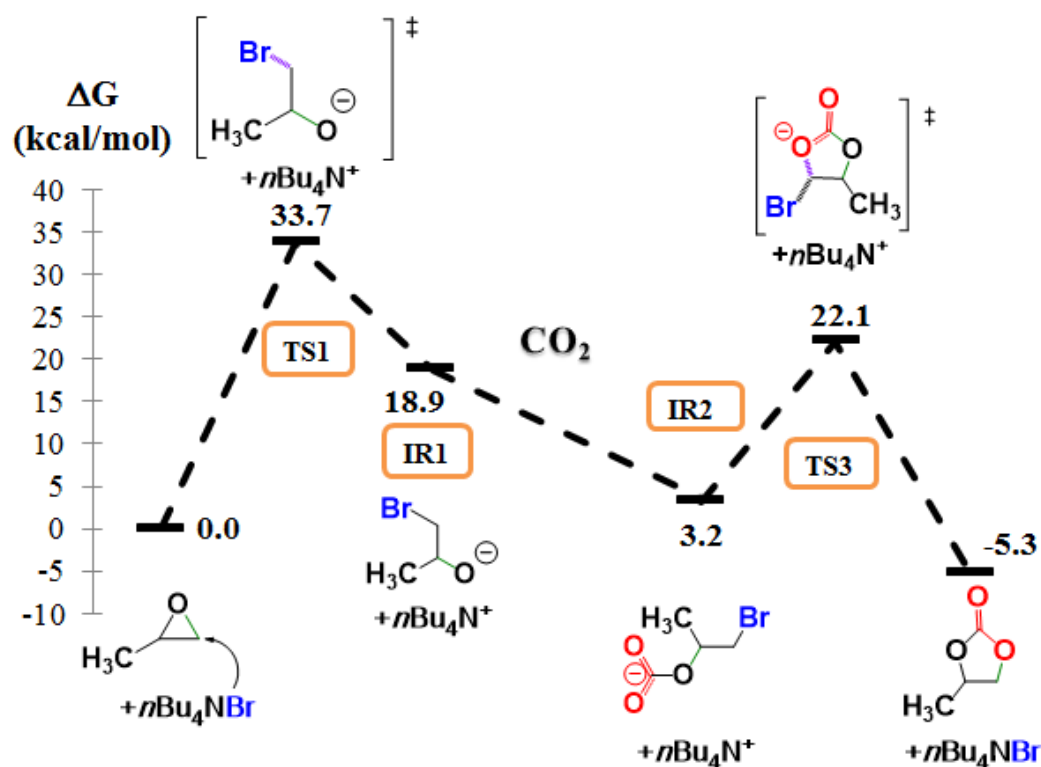


Figure 1: Free energy profiles (Mo6-2X/6-311G(d,p)) and Lewis structures for the propylene oxide/ $\text{CO}_2$  coupling catalysed by TBABr

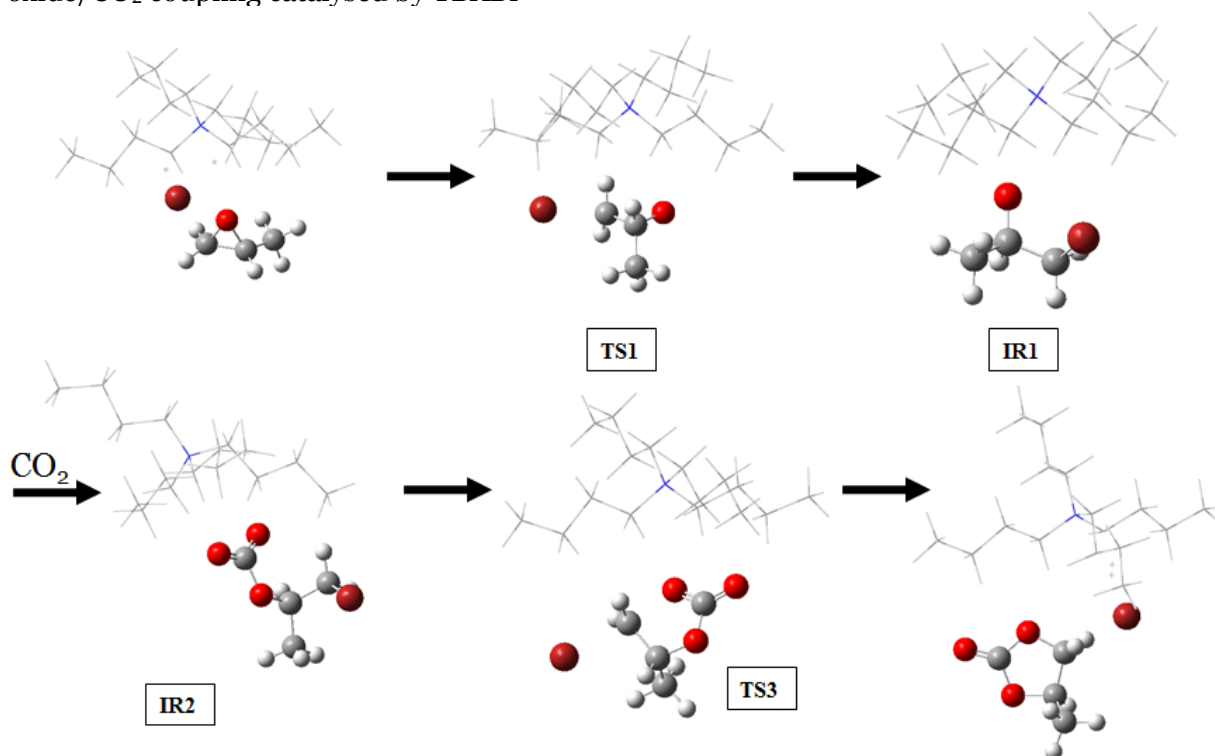


Figure 2: Optimized geometries (Mo6-2X/6-311G(d,p)) of the structures of the  $\text{CO}_2/\text{PO}$  coupling in the presence of TBABr (skeleton).

Note that this “backbiting” step is named TS3 instead of TS2 for an easier comparison of the reaction pathway with that obtained using hydrogen bond activators (see below). From the DFT calculations, the formation of the first transition state (TS1) corresponds to the rate-determining step and  $\Delta G = 33.7$  kcal.mol<sup>-1</sup> are required to obtain propylene carbonate with TBABr. In view of this high activation energy value, the energy barrier is too high for the non-activated CO<sub>2</sub>/PO coupling to happen under mild conditions. Thus, efficient activators able to significantly decrease the energy barrier for the formation of TS1 have to be identified.

## 2. CO<sub>2</sub>/PO coupling using (multi)phenolic HBDs

(Multi)phenolic derivatives were reported amongst the most efficient HBDs for the TBAI catalysed coupling of CO<sub>2</sub> with epoxides.<sup>43, 47</sup> In Kleij's study, the beneficial role of such HBDs that activate the epoxide and reduce the energy barrier of the limiting step was highlighted through a detailed DFT study. However, the presence of the TBA<sup>+</sup> counter-ion was not taken into account in the initial study. For coherence with our DFT results, we reinvestigated the overall reaction pathway for which the energy profiles are depicted in Figure 3 for phenol (blue), pyrocatechol (magenta) and pyrogallol (red). The sum of free energies of isolated reactants (CO<sub>2</sub>, PO) and catalysts (TBABr, phenol derivative) is taken as zero.

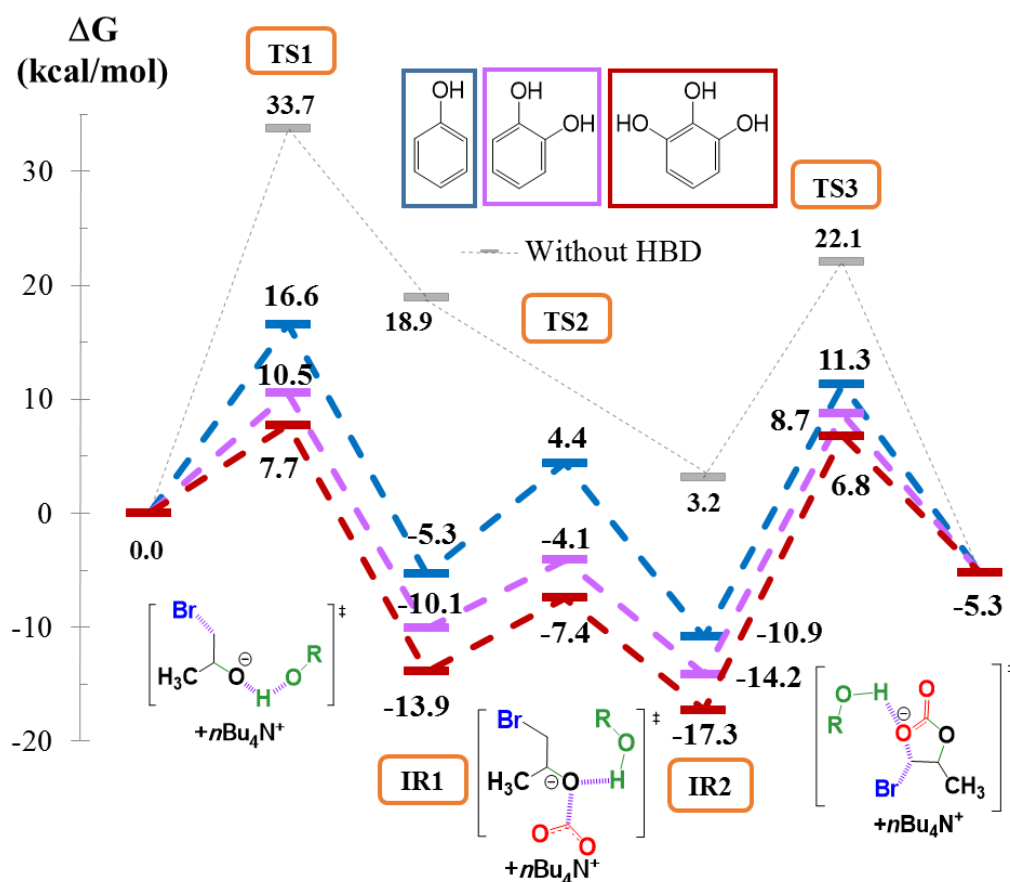


Figure 3: Free energy profiles (Mo6-2X/6-311G(d,p)) and Lewis structures of the transition states for CO<sub>2</sub>/PO coupling catalysed by TBABr (---), TBABr plus phenol (blue), TBABr plus pyrocatechol (purple) and TBABr plus pyrogallol (red)



As reported by Kleij, whatever the phenolic HBD, a three-step mechanism (instead of two when TBABr is used as sole catalyst) whose energy depends on the nature of the phenol derivative is observed. As the mechanisms are similar for all (multi)phenolic derivatives, the reaction pathway will be only described for pyrogallol (Figure 4). In a first step, the nucleophilic Br<sup>-</sup> anion attacks the less-substituted C atom of PO leading to the epoxide ring-opening (TS1). Pyrogallol and TBA<sup>+</sup> have a huge impact on the stabilization of TS1 *via* the formation of hydrogen bonds and Van der Waals interactions. Indeed, the central OH group of the pyrogallol transfers its proton to the bromohydrin (1.47 Å) creating an O-H bond. The first vicinal hydroxyl function allows for the stabilization of the O atom of the bromohydrin ion (1.78 Å) and the second one stabilizes the central O atom of pyrogallol (2.04 Å), consistently with Kleij's observations. However, the presence of the TBA<sup>+</sup> ion induces a new stabilization by covering the complex *via* creation of Van der Waals interactions with the aromatic ring of pyrogallol. This overall stabilization mechanism decreases importantly the energy of the first step compared to the pathway described previously without HBD. From TS1, the formation of the bromohydrin and the phenoxide anion leads to the stable intermediate IR1. In a second step, the C atom of the CO<sub>2</sub> approaches the O atom of the bromohydrin implying the breaking of the O-H bond previously created (TS2). The bromo-alkylcarbonate (IR2) is formed by the formation of a bond between CO<sub>2</sub> and the bromohydrin. IR2 is stabilized through a similar mechanism that the one discussed for the formation of IR1. The final step involves a torsional deformation of the bromo-alkylcarbonate and the C-Br bond rupture (TS3). PC is formed by ring-closure of the alkylcarbonate with the release of TBABr and pyrogallol. The relative energy of this last path is drastically reduced in comparison with the one reported without HBD thanks to the hydrogen-bonding stabilization mechanism driven by pyrogallol.

From the DFT studies, the number of vicinal hydroxyl functions of the phenolic HBD has an important influence on the energy of this path (Figure 3) as the required Gibbs energies to overcome the energy barrier are 7.7 kcal.mol<sup>-1</sup>, 10.5 kcal.mol<sup>-1</sup> and 16.6 kcal.mol<sup>-1</sup> for pyrogallol, pyrocatechol and phenol, respectively, which is much lower than the value determined when TBABr is the sole catalyst ( $\Delta G_{TS1} = 33.7$  kcal.mol<sup>-1</sup>). If the general trends, i.e. the mechanism and the decrease of the activation energies, are fully consistent with Kleij's experiment, the Gibbs energies values determined in our study cannot be compared with the values mentioned in Kleij's work as the functional and the basis set that we selected are different.

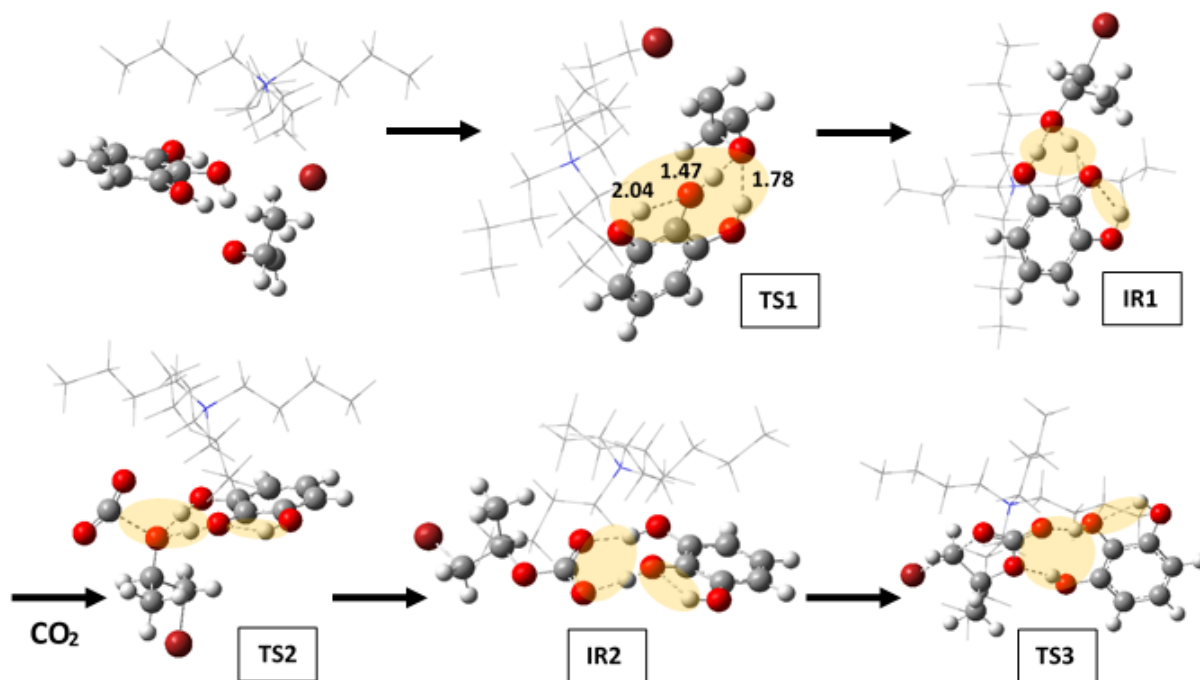


Figure 4: Optimized geometries of the structures (Mo6-2X/6-311G(d,p)) of the  $\text{CO}_2/\text{PO}$  coupling, in the presence of Pyrogallol/TBABr (skeleton) as catalysts. The dashed lines depict hydrogen bond interactions and intermolecular distances are given in angström.

### 3. $\text{CO}_2/\text{PO}$ coupling using fluorinated monoalcohols as HBDs

Recently, we reported that some fluorinated alcohols show very high co-catalytic activity for the TBABr promoted coupling of  $\text{CO}_2$  with epoxides and even proved to be more efficient than (multi)phenolic HBDs under similar experimental conditions.<sup>39, 41</sup> The reaction mechanism was then studied in detail and the energy profiles were reported on Figure 5 for fluorinated monoalcohols, i.e. 1,1,1-trifluoro-2-methyl-2-propanol (TFMP, yellow), hexafluoro-*tert*-butanol (HFB, purple), perfluoro-*tert*-butanol (PFB, light blue) and hexafluoro-(*p*-tolyl)-isopropanol (HFTI, orange). For illustration, the reaction pathway describing the structure of all intermediates and transitions states is reported in detail for perfluoro-*tert*-butanol in Figure 6 where the hydrogen-bonding stabilization mechanism driven by the activator and the Van der Waals interactions with  $\text{TBA}^+$  are clearly identified at each step of the reaction. Similarly to phenolic HBDs, we observe in Figure 5 that for all fluorinated alcohols, the reaction answers the three-step mechanism whose energy depends on the nature of the HBD. Whatever the fluorinated activator, the relative energy of the elementary paths, and more particularly regarding the energy of the epoxide ring-opening step, is significantly reduced in comparison with that reported without activator.

Figure 5 also highlights the positive influence of the increasing number of trifluoromethyl substituents in HBDs. Indeed, the Gibbs energy decreases in the order TFMP (1  $\text{CF}_3$ ) > HFB (2  $\text{CF}_3$ ) > PFB (3  $\text{CF}_3$ ). As fluorine atom is an electronegative element, the Natural Bond Orbital (NBO) analysis of TS1 reveals that the positive charge (qH) on the proton of the hydroxyl function increases with the number of electron withdrawing trifluoromethyl groups (Table 1).

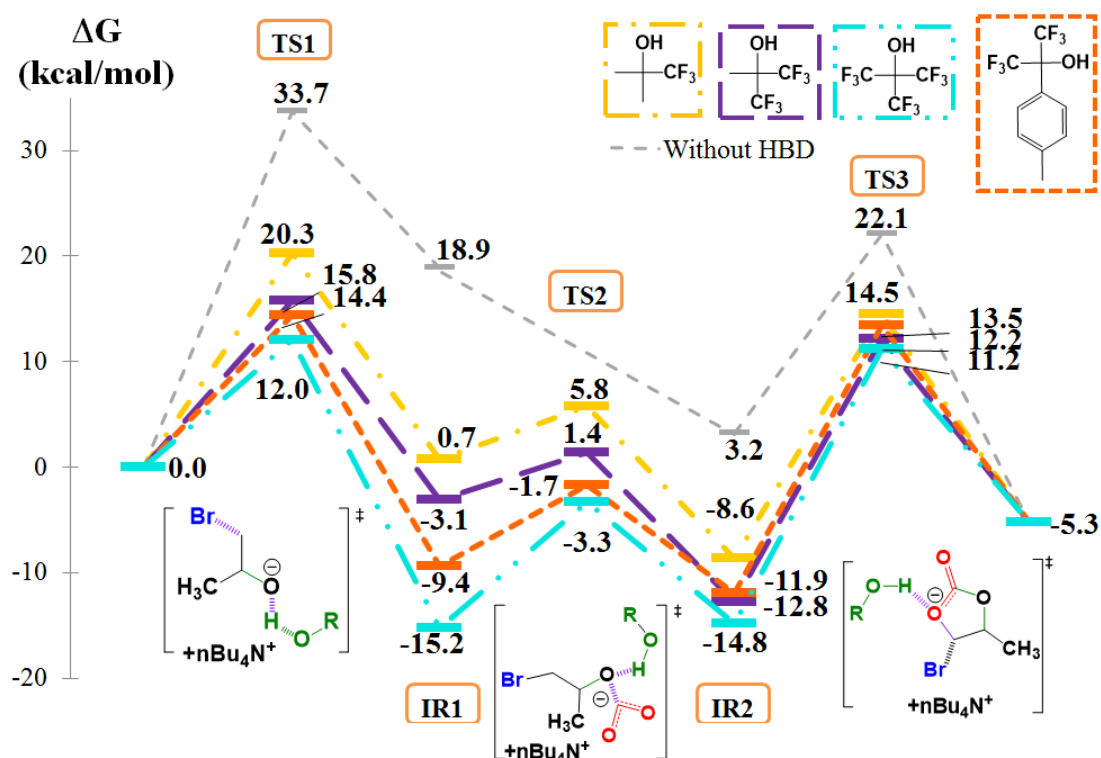


Figure 5: Free energy profile (Mo6-2X/6-311G(d,p)) and Lewis structures of transition states for the  $\text{CO}_2/\text{PO}$  coupling catalysed by TBABr (---), TBABr plus TFMP (---), TBABr plus HFB (—) TBABr plus PFB (-.-.-) and TBABr plus HFTI (- - -)

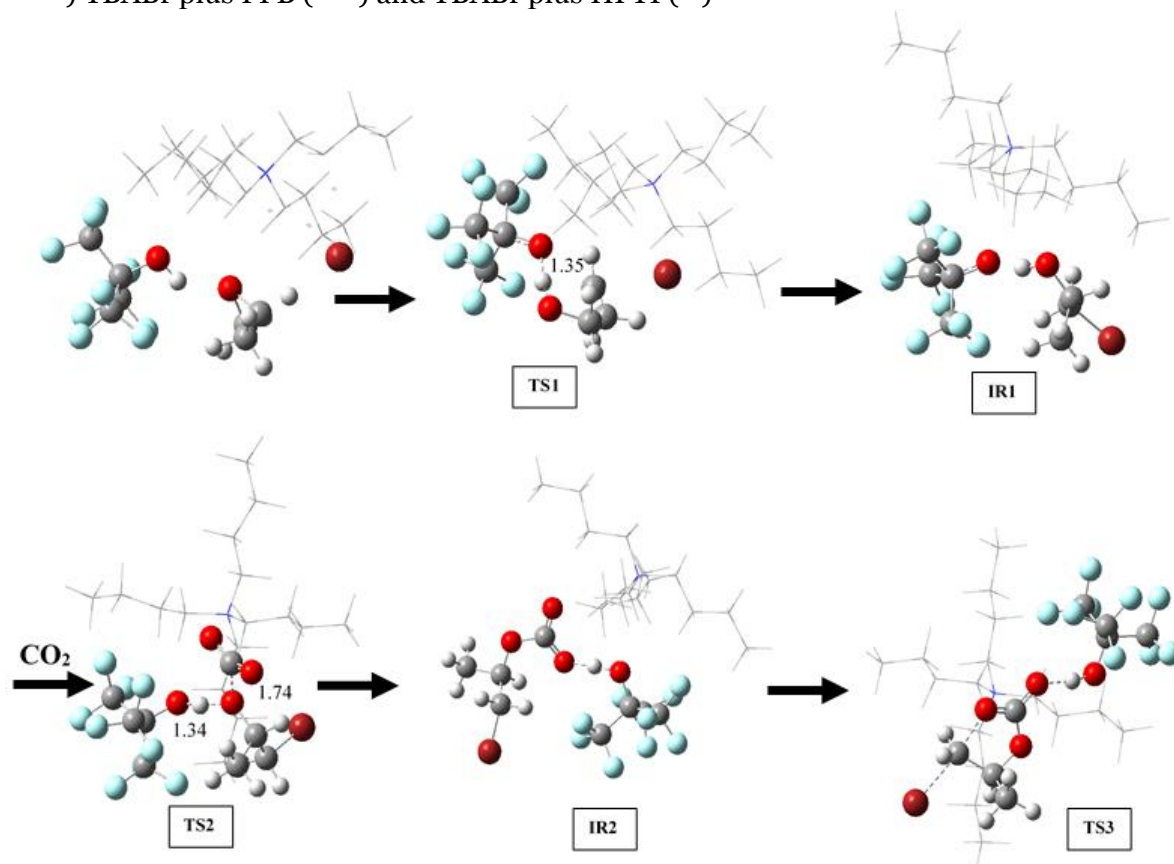


Figure 6: Optimized geometries (Mo6-2X/6-311G(d,p)) of the structures of the  $\text{CO}_2/\text{PO}$  coupling in the presence of TBABr (skeleton) plus PFB as catalysts. The dashed lines depict the intermolecular distances in angstrom.

Table 1: Charge on the proton of the (fluorinated) alcohol obtained by Natural Population Analysis (NBO) and O...H length between the epoxide and the (fluorinated) alcohol depending on the structure of the (fluorinated) alcohol for the transition state resulting from the nucleophilic attack of the bromine anion on the epoxide ring (TS1).

Fluorinated alcohol	qH (me)	-O...H-O- length (Å)
<i>Tert</i> -butanol	0.45	1.70
1,1,1-trifluoro-2-methyl-2-propanol (TFMP)	0.46	1.44
Hexafluoro- <i>tert</i> -butanol (HFB)	0.47	1.33
Hexafluoro-( <i>p</i> -tolyl)-isopropanol (HFTI)	0.48	1.26
Perfluoro- <i>tert</i> -butanol (PFE)	0.49	1.09

To further ascertain the positive role of the trifluoromethyl groups, the substitution of one CF<sub>3</sub> of PFB by a less attractive *p*-tolyl group (HFTI) induces a slight increase of the Gibbs energy required for the CO<sub>2</sub>/PO coupling, which value is intermediate to the ones reported for PFB and HFB. On the other hand, for the first transition state (TS1), the O...H distance between the O atom of the opened epoxide and the proton of the fluorinated alcohol decreases when the charge determined by the NBO analysis on the H atom increases (Table 1) highlighting stronger hydrogen bond interactions. Thus, the higher the hydrogen bond interaction between the opened epoxide and the fluorinated alcohol is, the lower the Gibbs energy is required for the first reaction step as confirmed by the Gibbs energy values determined for TFMP ( $\Delta G = 20.3$  kcal.mol<sup>-1</sup>), HFB ( $\Delta G = 15.8$  kcal.mol<sup>-1</sup>), HFTI ( $\Delta G = 14.4$  kcal.mol<sup>-1</sup>) and PFB ( $\Delta G = 12.0$  kcal.mol<sup>-1</sup>). Although the Gibbs energy corresponding to the first limiting step of the CO<sub>2</sub>/PO coupling using PFB ( $\Delta G = 12.0$  kcal.mol<sup>-1</sup>) is significantly lower than with phenol ( $\Delta G = 16.6$  kcal.mol<sup>-1</sup>), it remains higher than the value determined for pyrogallol ( $\Delta G = 7.7$  kcal.mol<sup>-1</sup>). This observation seems to contradict our experimental results that showed that fluorinated HBDs were better activators than the (multi)phenolic ones.<sup>39</sup>

To understand the origin of this disagreement, we supposed that dual hydrogen bonding activation mechanism involving two fluorinated monoalcohols could be responsible for an enhanced stabilization of the transition states and the intermediates. Indeed, Berkessel *et al.* reported that the boosting catalytic effect of fluorinated alcohols, used as solvents for the olefins epoxidation, was due to their aggregation and the formation of a multiple H-bond network.<sup>68, 69</sup> This assumption is also further supported by our previous NMR titrations experiments that highlighted the formation of complexes between the epoxide and more than one molecule of fluorinated HBD.<sup>41</sup> Both the reaction mechanism and the Gibbs energy were then investigated for the dual hydrogen bonding activation with TFMP, HFB, HFTI and PFB (Figure 7). As shown in Figure 8 (for PFB), two molecules participate to the stabilization of the O atom of the epoxide via H-bonds. Due to the steric hindrance caused by the methyl substituent of PO, the structure of TS1 exhibits two asymmetric

H-bonds (1.48 Å and 1.57 Å). For sake of comparison, DFT calculations on ethylene oxide provide a complete symmetric system with two identical H-bonds lengths. The resulting IR1 is characterized by a PFB-bromohydrin-PFB H-bonds sequence for which the O atom of the bromohydrin occupies a central position of the “IR1 complex”. In TS2, both PFB molecules play a different role. One interacts with one O atom of the former CO<sub>2</sub> while the second interacts with the oxygen of the former epoxide. Then, each PFB molecules stabilizes one terminal O atom of the carbonate group by hydrogen bonding until the formation of the cyclic carbonate (IR2 and TS3 on Figure 8). Besides these mechanistic considerations, the dual hydrogen bonding activation by two fluorinated monoalcohols impacts significantly the Gibbs energy profile (Figure 7) compared to the one with only one fluorinated alcohol molecule (Figure 5). This is clearly evidenced for the first - and limiting - step as the Gibbs energy is decreased by 6.5, 5.0, 4.5 and 8.3 kcal.mol<sup>-1</sup> for TFMP, HFB, HFTI and PFB, respectively. Thus, these DFT calculations highlight the origin of the high co-catalytic activity of fluorinated monoalcohol thanks to a dual hydrogen bonding activation by two fluorinated monoalcohols that cooperatively contribute to the coupling of CO<sub>2</sub> with PO.

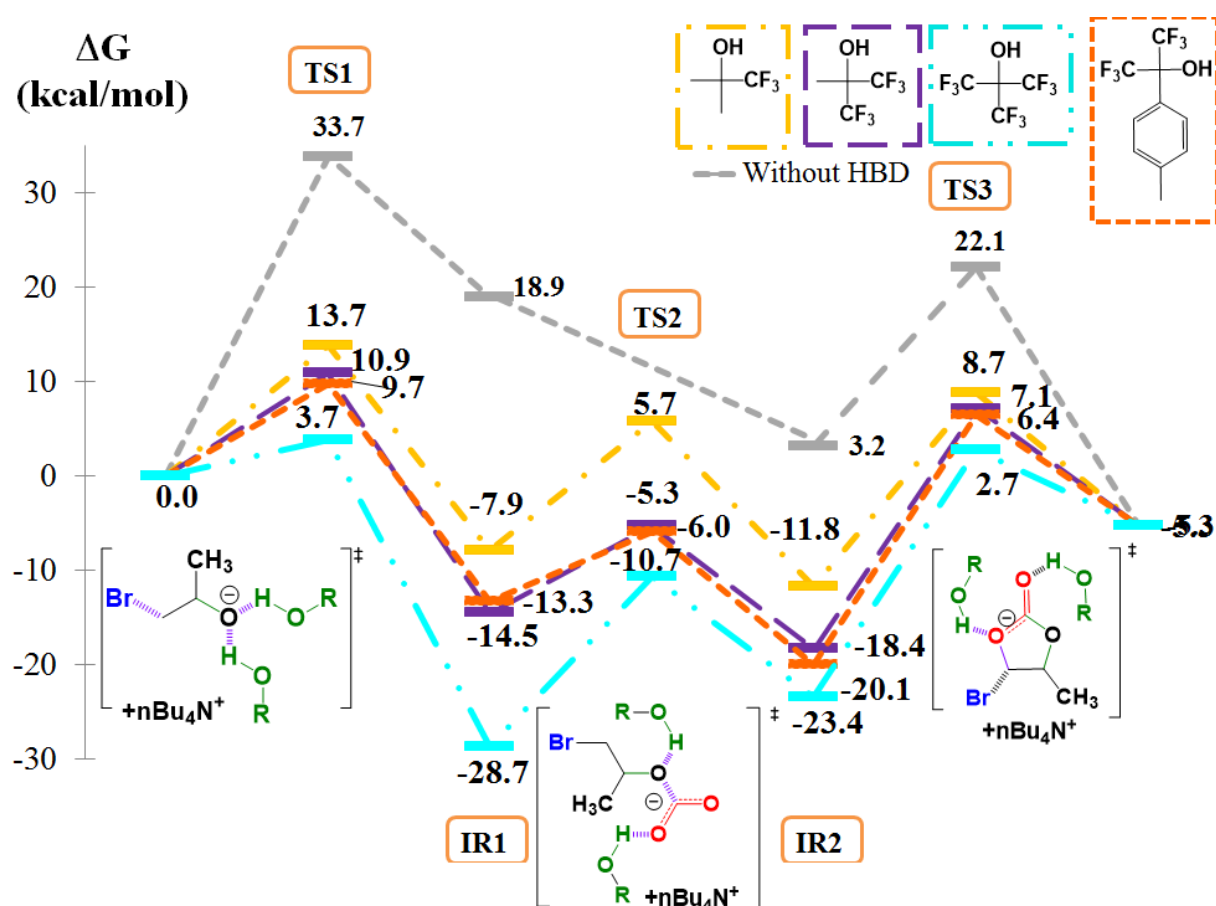


Figure 7: Free energy profiles (Mo6-2X/6-311G(d,p)) and Lewis structures of the transition states for the CO<sub>2</sub>/PO coupling catalysed by TBABr (---), TBABr plus two molecules of TFMP (---), TBABr plus two molecules of HFB (—) TBABr plus two molecules of HFTI (- -) and TBABr plus two molecules of PFB (- · - ·).

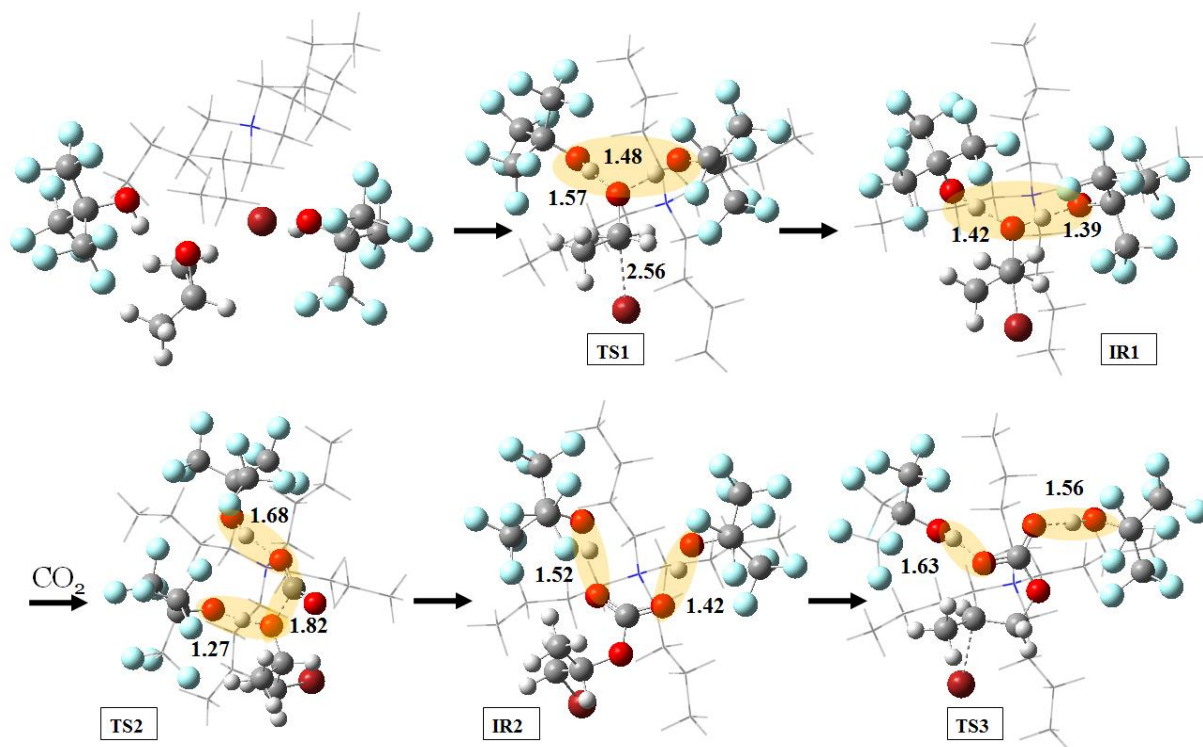


Figure 8: Optimized geometries (Mo6-2X/6-311G(d,p)) of the structures of the CO<sub>2</sub>/PO coupling in the presence of TBABr (skeleton) plus two molecules of PFB as catalysts. The dashed lines depict the intermolecular distances in angström.

#### 4. CO<sub>2</sub>/PO coupling using fluorinated HBDs: the key role of the CF<sub>3</sub> groups

To determine to which extent the substitution of a methyl group by a trifluoromethyl one impacts the capability of HBD to generate strong hydrogen bonding and efficient stabilization of the transition states and intermediates, we compared the Gibbs energy profiles of the TBABr promoted coupling of CO<sub>2</sub> with PO using two molecules of *tert*-butanol or PFB as co-catalysts.

From Figure 9, we observe that the relative energy of each transition states and intermediates is drastically reduced in the presence of PFB in comparison with the values reported for *tert*-butanol. Clearly, the non-fluorinated activator has a poor effect on the stabilization of both the intermediates and transitions states that results from its lower capability to generate strong hydrogen bonds. Indeed, if the modelled structures of transition states TS1 (epoxide ring-opening) and TS3 (carbonate ring closure) with *tert*-butanol and PFB are similar (Figure 8 and Figure 10), the hydrogen bond length between the proton of the HBDs and the reactive center are different. For TS1, the distances between the protons of the hydroxyl group and the O atom of the ring-opened epoxide are much longer for *tert*-butanol (1.70 Å and 1.74 Å, Figure 10) than for PFB (1.48 Å and 1.57 Å, Figure 8). The NBO analysis of both the TS1 reveals that the charge distribution is dissimilar. The atomic charges of the proton of the hydroxyl functionalities are 0.517e and 0.512e in the case of *tert*-butanol against 0.533e and 0.522e for PFB, in line with the more acidic character of PFB. Therefore,

the stabilization of the resulting bromohydrin IR1 is significantly weaker with *tert*-butanol and the proton transfer to the bromohydrin does not occur. This explains the significant difference in the Gibbs energy values of TS1 using *tert*-butanol ( $\Delta G = 19.9$  kcal.mol<sup>-1</sup>) or PFB ( $\Delta G = 3.7$  kcal.mol<sup>-1</sup>) as HBDs. The same marked difference exists between 1,3-bis(2-hydroxyhexafluoroisopropyl)-benzene (1,3-bis-HFAB) and its non-fluorinated counterpart ( $\alpha,\alpha'$ -dihydroxy-1,3-diisopropylbenzene, Figure 11).

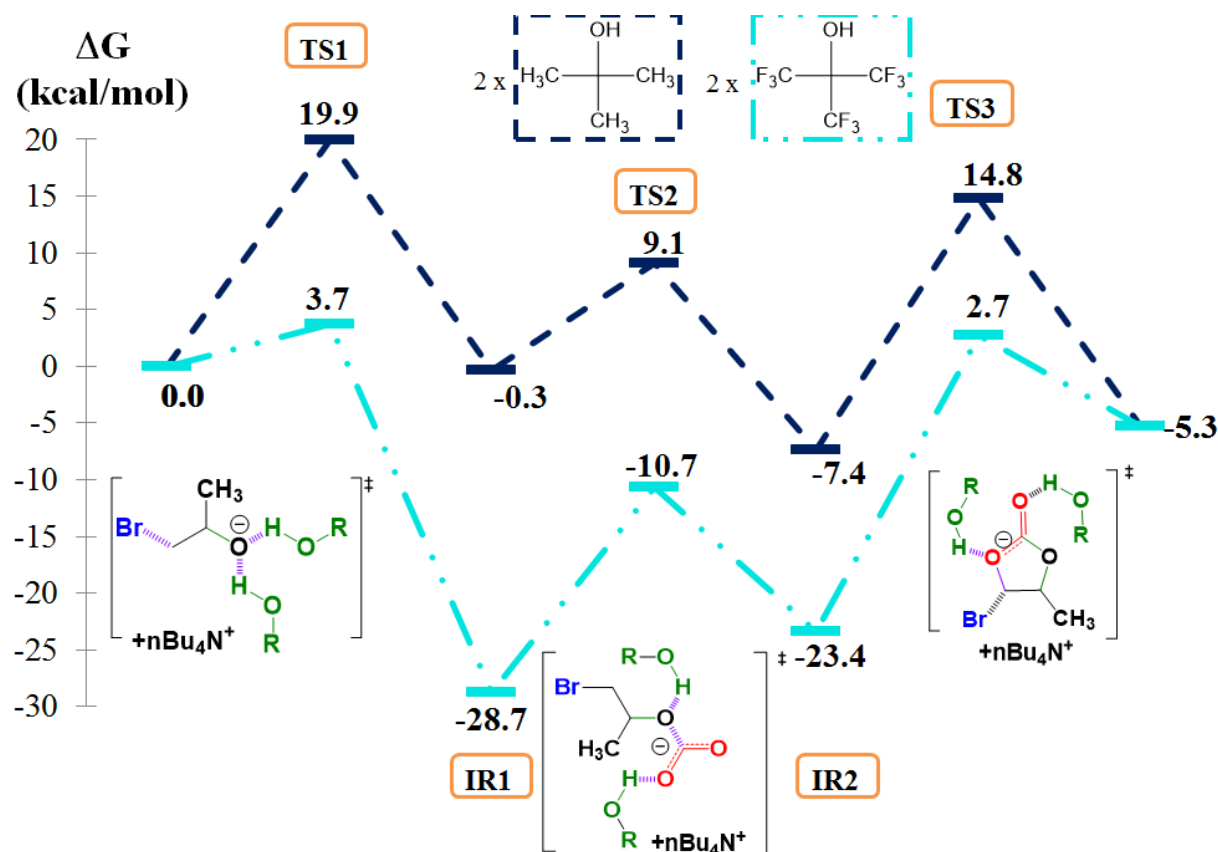


Figure 9: Free energy profiles (Mo6-2X/6-311G(d,p)) and Lewis structures of the transition states for the CO<sub>2</sub>/PO coupling catalysed by TBABr plus two molecules of *tert*-butanol (--) and TBABr plus two molecules of PFB (---).



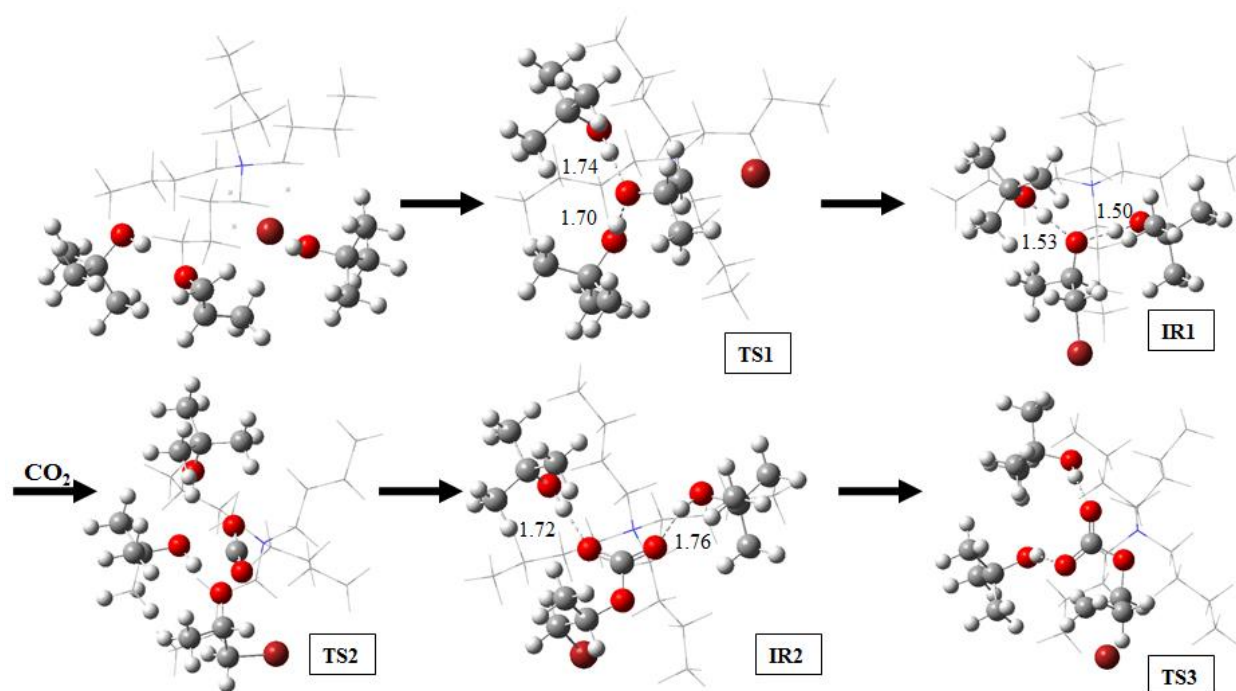


Figure 10: Optimized geometries (Mo6-2X/6-311G(d,p)) of the structures of the CO<sub>2</sub>/PO coupling in the presence of TBABr (skeleton) plus two molecules of *tert*-butanol as catalysts. The dashed lines depict the intermolecular distances in angström.

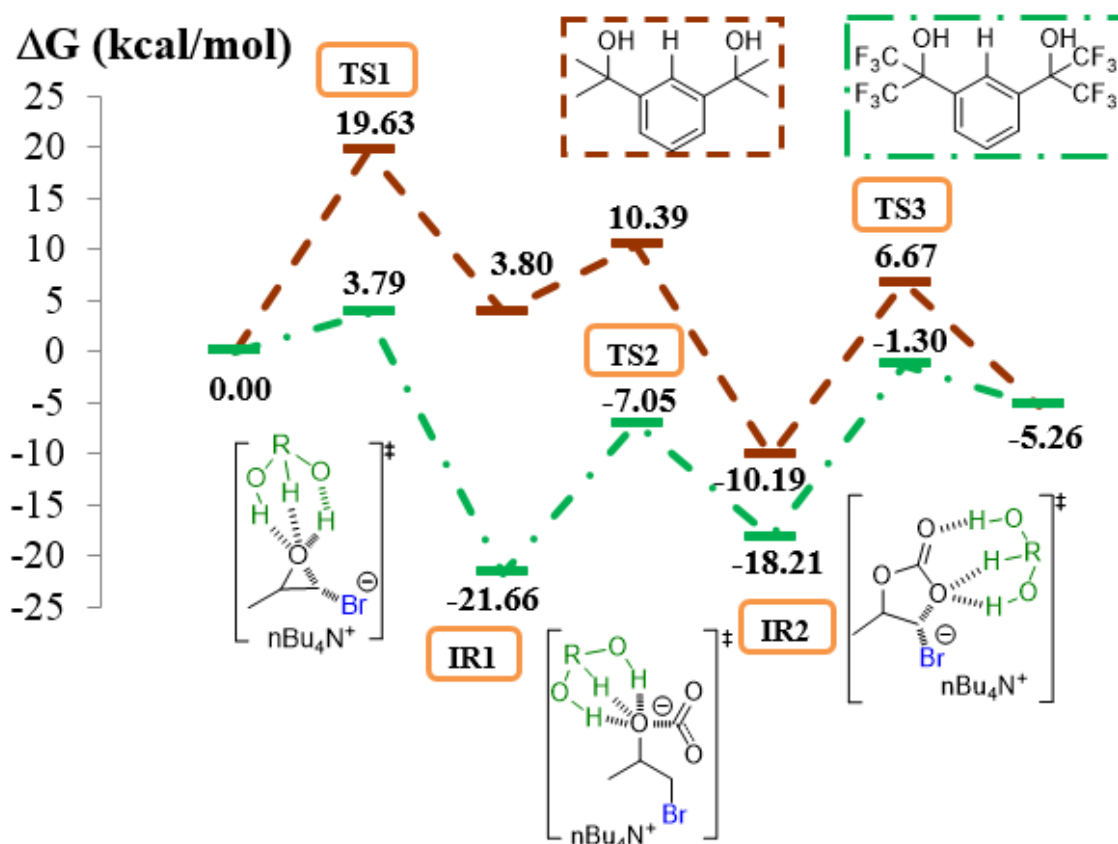


Figure 11: Free energy profiles (Mo6-2X/6-311G(d,p)) and Lewis structures of the transition states for the propylene oxide/CO<sub>2</sub> coupling catalysed by TBABr plus 1,3-bis-HFAB (green) or  $\alpha,\alpha'$ -dihydroxy-1,3-diisopropylbenzene (brown).



## 5. CO<sub>2</sub>/PO coupling using fluorinated diols as HBDs

In our previous work, we found that a fluorinated double hydrogen bond donor, i.e. 1,3-bis-HFAB, an alcohol bearing two hexafluoroisopropyl groups, showed an impressive co-catalytic activity for the TBABr promoted coupling of CO<sub>2</sub> with epoxides. The origin of this co-catalytic activity was elucidated by DFT calculations. Figure 12 reports on the detailed reaction mechanism answering the three elementary steps pathway. The molecular structures of the corresponding intermediates and transition states are displayed in Figure 13. To maximize clarity of the figure, the TBA<sup>+</sup> cation which stabilizes the system by Van der Waals interactions was represented using a skeleton model.

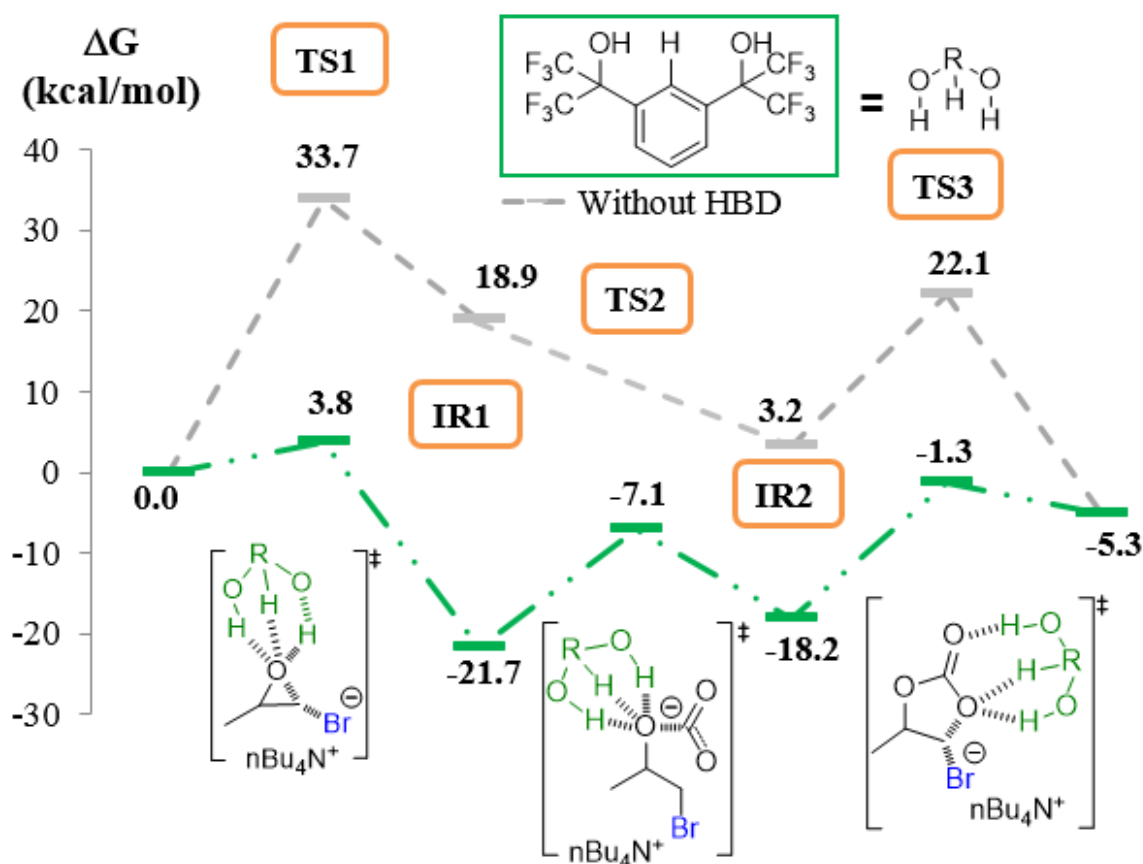


Figure 12: Free energy profiles (Mo6-2X/6-311G(d,p)) for the CO<sub>2</sub>/PO coupling catalysed by TBABr (---) and TBABr plus 1,3-bis-HFAB (---). Lewis structure of the transition states for the hydrogen-bond activation pathway.

First the nucleophilic attack of the bromine ion onto the non-substituted carbon atom of PO leads to the epoxide ring-opening. The resulting negatively charged O atom of the transition state (TS1) is stabilized by both hydroxyl functional groups of 1,3-bis-HFAB (1.44 Å and 1.92 Å). In addition, a weak C-H...O hydrogen bond interaction is formed between the O atom of the bromohydrin anion and the aromatic proton in *ortho* position of hexafluoro alcohol functionalities (2.32 Å) that contributes cooperatively with the two O-H...O hydrogen bonds to the stabilization of TS1. The intermediate IR1 is obtained after the formation of the C-Br bond and the proton

transfer from 1,3-bis-HFAB to the O atom. Consequently, the bromohydrin is stabilized by the second hydroxyl function of the hydrogen-bond donor (1.82 Å). Then, the attack of CO<sub>2</sub> by the O atom of the bromohydrin implies a concomitant breaking of the O-H bond previously created (TS2). Hydrogen-bonds are formed between 1,3-bis-HFAB and the bromo-alkyl carbonate leading to a stable intermediate (IR2). Finally, the torsional deformation of the bromo-alkylcarbonate occurs and both hydroxyl functions and the aromatic proton of 1,3-bis-HFAB stabilize the two O atoms of the inserted carbon dioxide (TS3). The concerted C-Br bond rupture and the carbonate ring-closing lead to the formation of propylene carbonate. The Gibbs energies required for the epoxide ring-opening and the carbonate ring-closing steps are significantly lower than that calculated with pyrogallol as activator. In particular, only 3.8 kcal.mol<sup>-1</sup> are necessary for the CO<sub>2</sub>/PO coupling (Figure 12) instead of 7.7 kcal.mol<sup>-1</sup> in the case of pyrogallol (Figure 3). These calculations are consistent with the experimental data showing that 1,3-bis-HFAB is a more efficient activator than pyrogallol.<sup>39</sup> This higher efficiency of 1,3-bis-HFAB might be related to the stabilization mechanism that involves three intermolecular H-bonds (see Figure 13-TS1) instead of only two for pyrogallol (see Figure 4-TS1). These results clearly highlight that the number of hydrogen atoms able to participate to the activation of epoxides and their ability to stabilize the transitions states and intermediates by hydrogen bonding are key parameters for optimizing the activity of the co-catalysts.

## Conclusions

A detailed mechanistic investigation by DFT calculations of the TBABr promoted coupling of CO<sub>2</sub> with propylene oxide using a series of hydrogen bond donors (HBDs) activators is reported. In particular, we have investigated phenol derivatives and fluorinated alcohols that have shown unprecedented catalytic activity in comparison with other HBDs proposed in the literature. Thus, we demonstrated how the substitution of alcohols with trifluoromethyl groups significantly improves the stabilization of transition states and the intermediates generated during the reaction by a significant decrease of the Gibbs energy of each step and especially, the one corresponding to the ring-opening of the epoxide. The results reveal that the trifluoromethyl groups strongly influence the charge distribution of HBDs and, in particular, the acidity of the hydroxyl groups that strengthens hydrogen-bond interactions. Indeed, the Gibbs energy decreases in the order TFMP (1 CF<sub>3</sub>) > HFB (2 CF<sub>3</sub>) > PFB (3 CF<sub>3</sub>). We also showed that for single HBDs, the stabilization of the transition states and intermediates was further improved in the presence of two molecules of fluorinated monoalcohols that contribute cooperatively to the catalytic mechanism through a dual hydrogen bonding activation. Finally, DFT calculations highlight that the double HBD, 1,3-bis-HFAB, is a better co-catalyst than pyrogallol, one of the most efficient (multi)phenolic activators, because three intermolecular H-bonds are involved with 1,3-bis-HFAB instead of only two in the case of pyrogallol.

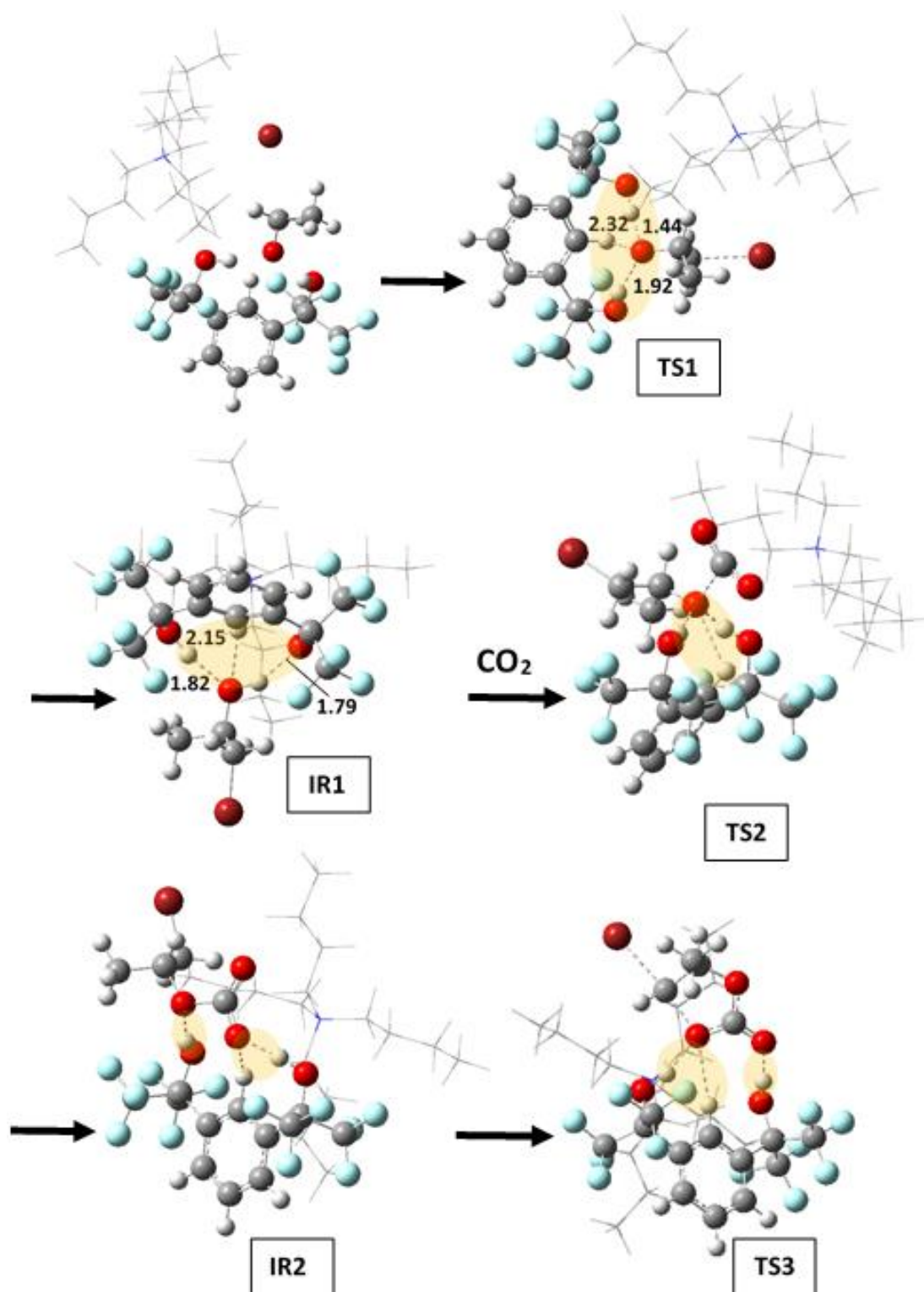


Figure 13: Optimized geometries of the structures (Mo6-2X/6-311G(d,p)) of the CO<sub>2</sub>/PO coupling in the presence of 1,3-bis-HFAB/TBABr (skeleton) as catalysts. The dashed lines depict hydrogen bond interactions and intermolecular distances are given in angström.

## References

1. M. Aresta, *Carbon Dioxide as Chemical Feedstock*, WILEY-VCH Verlag GmbH & Co. KGaA, Weinheim, edn., 2010.
2. M. North, R. Pasquale and C. Young, *Green Chemistry*, 2010, **12**, 1514-1539.
3. T. Sakakura, J. C. Choi and H. Yasuda, *Chemical Reviews*, 2007, **107**, 2365-2387.
4. P. P. Pescarmona and M. Taherimehr, *Catalysis Science & Technology*, 2012, **2**, 2169-2187.
5. A. Decortes, A. M. Castilla and A. W. Kleij, *Angew. Chem. Int. Ed.*, 2010, **49**, 9822-9837.
6. J.-Q. Wang, K. Dong, W.-G. Cheng, J. Sun and S.-J. Zhang, *Catalysis Science & Technology*, 2012, **2**, 1480-1484.
7. D. J. Darensbourg and S. J. Wilson, *Green Chemistry*, 2012, **14**, 2665-2671.
8. C. J. Whiteoak and A. W. Kleij, *Synlett*, 2013, **24**, 1748-1756.
9. Z.-Z. Yang, L.-N. He, J. Gao, A.-H. Liu and B. Yu, *Energy & Environmental Science*, 2012, **5**, 6602-6639.
10. C. Martín, G. Fiorani and A. W. Kleij, *ACS Catalysis*, 2015, **5**, 1353-1370.
11. A. H. Liu, Y. N. Li and L. N. He, *Pure and Applied Chemistry*, 2012, **84**, 581-602.
12. M. North and C. Young, *Catalysis Science & Technology*, 2011, **1**, 93-99.
13. J. Sun, S. I. Fujita and M. Arai, *Journal of Organometallic Chemistry*, 2005, **690**, 3490-3497.
14. T. Seki, J. D. Grunwaldt and A. Baiker, *Journal of Physical Chemistry B*, 2009, **113**, 114-122.
15. J. Li, L. Wang, F. Shi, S. Liu, Y. He, L. Lu, X. Ma and Y. Deng, *Catalysis Letters*, 2011, **141**, 339-346.
16. Z. Z. Yang, L. N. He, C. X. Miao and S. Chanfreau, *Advanced Synthesis and Catalysis*, 2010, **352**, 2233-2240.
17. H. Y. Ju, M. D. Manju, K. H. Kim, S. W. Park and D. W. Park, *Journal of Industrial and Engineering Chemistry*, 2008, **14**, 157-160.
18. S. Foltran, J. Alsarraf, F. Robert, Y. Landais, E. Cloutet, H. Cramail and T. Tassaing, *Catalysis Science & Technology*, 2013, **3**, 1046-1055.
19. W.-L. Wong, L. Y. S. Lee, K.-P. Ho, Z.-Y. Zhou, T. Fan, Z. Lin and K.-Y. Wong, *Applied Catalysis A: General*, 2014, **472**, 160-166.
20. D. Wei-Li, J. Bi, L. Sheng-Lian, L. Xu-Biao, T. Xin-Man and A. Chak-Tong, *Catalysis Today*, 2014, **233**, 92-99.
21. J. Sun, S. Zhang, W. Cheng and J. Ren, *Tetrahedron Letters*, 2008, **49**, 3588-3591.
22. W. L. Dai, J. Bi, S. L. Luo, X. B. Luo, X. M. Tu and C. T. Au, *Catalysis Science and Technology*, 2014, **4**, 556-562.
23. O. Coulembier, S. Moins, V. Lemaure, R. Lazzaroni and P. Dubois, *Journal of CO<sub>2</sub> Utilization*, 2015, **10**, 7-11.

24. J. Tharun, G. Mathai, R. Roshan, A. C. Kathalikkattil, K. Bomi and D.-W. Park, *Physical Chemistry Chemical Physics*, 2013, **15**, 9029-9033.
25. A. J. R. Amaral, J. F. J. Coelho and A. C. Serra, *Tetrahedron Letters*, 2013, **54**, 5518-5522.
26. M. H. Anthofer, M. E. Wilhelm, M. Cokoja, M. Drees, W. A. Herrmann and F. E. Kühn, *ChemCatChem*, 2015, **7**, 94-98.
27. J. Łukaszczyk, K. Jaszcz, W. Kuran and T. Listos, *Macromolecular Rapid Communications*, 2000, **21**, 754-757.
28. D. J. Darensbourg and W.-C. Chung, *Macromolecules*, 2014, **47**, 4943-4948.
29. S. Kumar, S. L. Jain and B. Sain, *Catalysis Letters*, 2012, **142**, 615-618.
30. G. Fiorani, W. Guo and A. W. Kleij, *Green Chemistry*, 2015, **17**, 1375-1389.
31. C. J. Whiteoak, A. Nova, F. Maseras and A. W. Kleij, *ChemSuschem*, 2012, **5**, 2032-2038.
32. J. Ma, J. Liu, Z. Zhang and B. Han, *Green Chemistry*, 2012, **14**, 2410-2420.
33. L. Wang, X. Jin, P. Li, J. Zhang, H. He and S. Zhang, *Industrial & Engineering Chemistry Research*, 2014, **53**, 8426-8435.
34. J. W. Huang and M. Shi, *Journal of Organic Chemistry*, 2003, **68**, 6705-6709.
35. Y. M. Shen, W. L. Duan and M. Shi, *European Journal of Organic Chemistry*, 2004, 3080-3089.
36. T. Werner, N. Tenhumberg and H. Büttner, *ChemCatChem*, 2014, **6**, 3493-3500.
37. M. E. Wilhelm, M. H. Anthofer, M. Cokoja, I. I. E. Markovits, W. A. Herrmann and F. E. Kühn, *ChemSusChem*, 2014, **7**, 1357-1360.
38. T. Werner and N. Tenhumberg, *Journal of CO<sub>2</sub> Utilization*, 2014, **7**, 39-45.
39. M. Alves, B. Grignard, S. Gennen, R. Mereau, C. Detrembleur, C. Jerome and T. Tassaing, *Catalysis Science & Technology*, 2015, **5**, 4636-4643.
40. M. Alves, B. Grignard, S. Gennen, C. Detrembleur, C. Jerome and T. Tassaing, *RSC Advances*, 2015, **5**, 53629-53636.
41. S. Gennen, M. Alves, R. Méreau, T. Tassaing, B. Gilbert, C. Detrembleur, C. Jerome and B. Grignard, *ChemSusChem*, 2015, **8**, 1845-1849.
42. W. Cheng, Z. Fu, J. Wang, J. Sun and S. Zhang, *Synthetic Communications*, 2012, **42**, 2564-2573.
43. L. Han, H.-J. Choi, S.-J. Choi, B. Liu and D.-W. Park, *Green Chemistry*, 2011, **13**, 1023-1028.
44. J. Tharun, G. Mathai, A. C. Kathalikkattil, R. Roshan, J.-Y. Kwak and D.-W. Park, *Green Chemistry*, 2013, **15**, 1673-1677.
45. J. Song, B. Zhang, P. Zhang, J. Ma, J. Liu, H. Fan, T. Jiang and B. Han, *Catalysis Today*, 2012, **183**, 130-135.
46. S. Liang, H. Liu, T. Jiang, J. Song, G. Yang and B. Han, *Chemical Communications*, 2011, **47**, 2131-2133.
47. J. Sun, W. Cheng, Z. Yang, J. Wang, T. Xu, J. Xin and S. Zhang, *Green Chemistry*, 2014, **16**, 3071-3078.

48. J. Sun, J. Wang, W. Cheng, J. Zhang, X. Li, S. Zhang and Y. She, *Green Chemistry*, 2012, **14**, 654-660.
49. J. Tharun, Y. Hwang, R. Roshan, S. Ahn, A. C. Kathalikkattil and D. W. Park, *Catalysis Science and Technology*, 2012, **2**, 1674-1680.
50. Y. Zhao, J. S. Tian, X. H. Qi, Z. N. Han, Y. Y. Zhuang and L. N. He, *Journal of Molecular Catalysis A: Chemical*, 2007, **271**, 284-289.
51. C. Jing-Xian, J. Bi, D. Wei-Li, D. Sen-Lin, C. Liu-Ren, C. Zong-Jie, L. Sheng-Lian, L. Xu-Biao, T. Xin-Man and A. Chak-Tong, *Applied Catalysis A: General*, 2014, **484**, 26-32.
52. S. Sopena, G. Fiorani, C. Martín and A. W. Kleij, *ChemSuschem*, 2015, **8**, 3179-3179.
53. A. M. Hardman-Baldwin and A. E. Mattson, *ChemSusChem*, 2014, **7**, 3275-3278.
54. M. J. S. Dewar, E. G. Zebisch, E. F. Healy and J. J. P. Stewart, *Journal of the American Chemical Society*, 1985, **107**, 3902-3909.
55. J. Řezáč and P. Hobza, *Journal of Chemical Theory and Computation*, 2012, **8**, 141-151.
56. AMPAC 10, *Journal*.
57. D. A. Liotard, *International Journal of Quantum Chemistry*, 1992, **44**, 723-741.
58. M. J. Frisch and A. D. Becke, *Gaussian 09, Revision A.02*, 2009, **98**, 5648-5652.
59. Y. Zhao and D. G. Truhlar, *Theoretical Chemistry Accounts*, 2008, **120**, 215-241.
60. J.-Q. Wang, J. Sun, W.-G. Cheng, K. Dong, X.-P. Zhang and S.-J. Zhang, *Physical Chemistry Chemical Physics*, 2012, **14**, 11021-11026.
61. H. Sun and D. Zhang, *Journal of Physical Chemistry A*, 2007, **111**, 8036-8043.
62. S. Marmitt and P. F. B. Gonçalves, *Journal of Computational Chemistry*, 2015, **36**, 1322-1333.
63. Y. Ren, C. H. Guo, J. F. Jia and H. S. Wu, *Journal of Physical Chemistry A*, 2011, **115**, 2258-2267.
64. S. Foltran, R. Mereau and T. Tassaing, *Catalysis Science & Technology*, 2014, **4**, 1585-1597.
65. S. Kozuch and J. M. Martin, *ChemPhysChem*, 2011, **12**, 1413-1418.
66. E. V. Anslyn and D. A. Dougherty, *Modern Physical Organic Chemistry*, University Science, Sausalito, 2004.
67. Z. Chen, Y. Nieves-Quinones, J. R. Waas and D. A. Singleton, *Journal of the American Chemical Society*, 2014, **136**, 13122-13125.
68. A. Berkessel, J. A. Adrio, D. Hüttenhain and J. M. Neudörfl, *Journal of the American Chemical Society*, 2006, **128**, 8421-8426.
69. A. Berkessel and J. A. Adrio, *Journal of the American Chemical Society*, 2006, **128**, 13412-13420.

Optimized Cartesian coordinates (Å) from Mo6-2X/6-311G(d) calculations are available following this link:

<http://www.rsc.org/suppdata/c6/ra/c6ra03427f/c6ra03427f1.pdf>

---

Chapter VI:  
Organocatalytic coupling of CO<sub>2</sub> with  
oxetane

---



The results presented in this chapter were accepted in *ChemSusChem* (2016).

### Abstract

The organocatalytic coupling of CO<sub>2</sub> with oxetanes is investigated under solvent-free conditions. The influence of the main reaction parameters (type of organocatalytic system, pressure and temperature) on the yield, the product formed and the selectivity of the reaction is discussed. An onium salt combined with a fluorinated alcohol promotes the efficient and selective organocatalytic synthesis of  $\alpha,\omega$ -hydroxyl oligocarbonates by coupling CO<sub>2</sub> with oxetanes at 130°C and at a CO<sub>2</sub> pressure as low as 2 MPa. NMR characterizations were correlated with MALDI-ToF analyses for elucidating the structure of the oligomers. Online FTIR studies under pressure, NMR titrations and DFT calculations allowed an in-depth understanding of the reaction mechanism. Finally, CO<sub>2</sub>-based poly(carbonate-co-urethane)s were synthesized by step-growth polymerization of hydroxyl telechelic oligocarbonates with MDI. The organocatalytic system described in this paper constitutes an innovative sustainable route to the selective preparation of hydroxyl telechelic carbonates, of high interest for many applications, notably for the polyurethane business, especially for coatings or foams.

## Table of contents

Introduction.....	173
Experimental Section .....	174
Materials .....	174
Experimental procedure .....	174
a) CO <sub>2</sub> /trimethylene oxide coupling.....	174
b) Chain extension. ....	177
c) Purification .....	177
d) Characterizations .....	177
e) Kinetic studies.....	178
f) Computational details.....	178
Results and Discussion .....	179
1- Oxetane/CO <sub>2</sub> coupling.....	179
a) Catalyst screening.....	179
b) Influence of the temperature.....	179
c) Influence of the pressure .....	181
d) HBD screening .....	181
e) Organocatalysed coupling of CO <sub>2</sub> with oxetanes .....	182
2- Oligocarbonate characterizations .....	182
3- Mechanistic investigations.....	184
4- Theoretical study of the TMO/CO <sub>2</sub> coupling catalysed by TBABr/1,3-bis-HFAB.....	189
5- CO <sub>2</sub> -based polyurethanes by chain extension of oligocarbonates .....	195
Conclusions.....	199
References.....	200

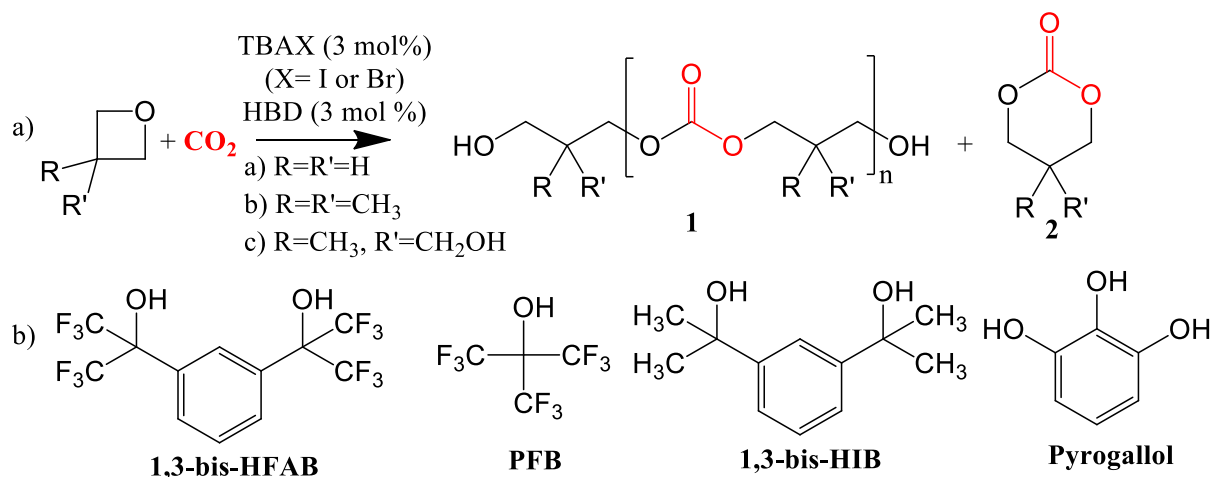


## Introduction

In the last years, significant works have been accomplished to substitute fossil carbon sources by CO<sub>2</sub> as a green and inexhaustible C1 feedstock. Among the sustainable reactions involving CO<sub>2</sub> conversion, the selective synthesis of five-membered cyclic carbonates or polycarbonates by (organo)catalytic coupling of CO<sub>2</sub> with epoxides has been extensively reviewed in the literature.<sup>1-6</sup> At the opposite, the synthesis of six-membered cyclic carbonates by oxetane/CO<sub>2</sub> coupling remains challenging because of i) the lower reactivity of four-membered ether rings compared to epoxides even under harsh experimental conditions and ii) a poor reaction selectivity.<sup>7</sup> For example, using a ternary organoaluminum catalyst<sup>8</sup> or bicomponent catalysts composed of Co(III), Cr(III) or Ca(II) salen complexes and ammonium salts<sup>9-11</sup>, the CO<sub>2</sub>/trimethylene oxide (TMO) coupling provided a mixture of trimethylene carbonate (TMC) and polycarbonate. By online FTIR studies, Darensbourg *et al.* discriminated two distinct reaction mechanisms for the CO<sub>2</sub>/oxetane coupling catalysed by Cr and Co salen complexes, i.e. the synthesis of the six-membered cyclic carbonate in the early stages of the process that competed with the direct alternating copolymerization of CO<sub>2</sub> with oxetane. They also highlighted that the direct copolymerization of oxetane with CO<sub>2</sub> lead to some defects in the polymer structure by the presence of some ether linkages.<sup>10-13</sup> The selectivity of the CO<sub>2</sub>/oxetane coupling can be improved by varying the temperature, by adding an organic base or by changing the nature of the catalyst and/or co-catalyst counter anion. Generally, the formation of six-membered cyclic carbonates is favoured at temperatures below 100°C. TMC was selectively produced from TMO and CO<sub>2</sub> by tetraphenylstibonium iodide<sup>14</sup> whereas polycarbonate was formed by the addition of tributyl phosphine as a base, without any cyclic carbonate by-products.<sup>15</sup> Kleij *et al.* developed series of efficient binary catalysts composed of aluminum and iron aminophenolate complexes and tetrabutylammonium bromide (TBABr) as co-catalyst that enabled the selective formation of six-membered cyclic carbonates under low pressure (0.2 - 1 MPa) and moderate temperature (70 - 85°C).<sup>16-18</sup> Darensbourg reported on a VO(acac) metal complex used in combination with various ammonium salts for the conversion of TMO into TMC under mild experimental conditions (T = 60°C, P = 3.5 MPa, t = 4h).<sup>19</sup> However, the conversion of substituted oxetanes requires much more demanding experimental conditions, presumably because of steric effects. Both organometallic catalytic systems developed by Kleij and Darensbourg allowed the conversion of 3,3-disubstituted oxetanes but the selectivity toward the cyclic carbonate formation dramatically decreased and longer reaction times were required for converting substituted oxetanes into the six-membered cyclic carbonates.<sup>16, 17, 19, 20</sup>

In this paper we describe the first organocatalytic coupling of oxetane with CO<sub>2</sub> under solvent-free conditions by using a binary catalytic system composed of a tetrabutylammonium salt and a hydrogen bond donor (HBD) (Scheme 1). The influence of the catalyst loading, the temperature, the pressure, and reaction time on the CO<sub>2</sub>/oxetane coupling efficiency is investigated, and the selectivity of the reaction

is explored. Under appropriate conditions, hydroxyl telechelic oligocarbonates were selectively synthesized using tetrabutyl ammonium iodide (TBAI) as the catalyst and fluorinated alcohols as co-catalysts. The mechanism of the reaction is discussed based on online FTIR under pressure studies, NMR titrations and DFT calculations. Finally, CO<sub>2</sub>-based poly(carbonate-co-urethane)s are synthesized by step-growth polymerization of the hydroxyl telechelic oligocarbonate with 4,4'-methyldiphenyldiisocyanate (MDI). These poly(carbonate-co-urethane)s have gained significant interest in the biomedical field to replace poly(ether-co urethane)s because of the increased oxidative stability of the oligocarbonate soft segment.<sup>21-24</sup>



Scheme 1: Organocatalytic coupling of CO<sub>2</sub> with oxetane (a) and structures of the hydrogen bond donors co-catalysts (b)

## Experimental Section

### Materials

Carbon dioxide N45 (purity: 99.95%) was supplied by Air Liquide. Tetrabutylammonium iodide (TBAI), tetrabutylammonium bromide (TBABr), 3,3-dimethyloxetane, 3-methyl-3-oxetanemethanol, pyrogallol, dibutyltin dilaurate and 4,4'-methylene diphenyl diisocyanate (MDI) were purchased from Sigma-Aldrich. 1,3-bis(2-hydroxyhexafluoroisopropyl)benzene (1,3-bis-HFAB) and perfluoro-*tert*-butanol (PFB) were purchased from Fluorochem. Trimethylene oxide (TMO) and  $\alpha,\alpha'$ -dihydroxy-1,3-diisopropylbenzene (1,3-HIB) were supplied by ABCR. All reactants or catalysts were used as received.

### Experimental procedure

#### a) CO<sub>2</sub>/trimethylene oxide coupling

In a typical experiment, TBAI (340.8 mg, 9.24  $\times 10^{-4}$  mol, 3 mol%) and HBD (9.24  $\times 10^{-4}$  mol, 3 mol%) are dissolved in 2 mL of trimethylene oxide (0.031 mol) in a high-pressure cell equipped with a mechanical stirrer. The cell is heated at 130°C before the addition of carbon dioxide till the pressure is equilibrated at 10 MPa. After 24 h,

the pressure is slowly released and the final product was collected as a highly viscous sample corresponding to oligocarbonate. An aliquot is analyzed by  $^1\text{H}$  NMR spectroscopy in  $\text{CDCl}_3$  to calculate the conversion (92%) from the integration values of the triplets (Figure 1 and 2) of TMO ( $\delta = 4.76$  ppm,  $-\text{O}-\underline{\text{CH}_2}-\text{CH}_2-\underline{\text{CH}_2}-$ , 4H), TMC ( $\delta = 4.47$  ppm,  $-\text{O}-\text{C}(\text{O})-\underline{\text{CH}_2}-\text{CH}_2-\underline{\text{CH}_2}-$ , 4H), and the oligocarbonates ( $\delta = 4.30$  ppm,  $-\text{O}-\text{C}(\text{O})-\underline{\text{CH}_2}-\text{CH}_2-\text{CH}_2-\text{OH}$ , 4H and  $\delta = 4.25$  ppm,  $-\text{O}-\text{C}(\text{O})-\underline{\text{CH}_2}-\text{CH}_2-\underline{\text{CH}_2}-$ , 4H) using Equation 1. The selectivity of TMC was calculated by the ratio between the integration values of TMC and the oligocarbonates (Figure 1 and 2).

$$\text{Conv (\%)} = \frac{I_{\delta=4.46\text{ppm}}}{I_{\delta=4.46\text{ppm}} + I_{\delta=4.47\text{ppm}} + I_{\delta=4.30\text{ppm}} + I_{\delta=4.25\text{ppm}}} * 100 \quad \text{Eq 1}$$

Another aliquot is dissolved in THF and injected in SEC (THF as eluent, polystyrene calibration) to determine the molar mass ( $M_n = 2000 \text{ g.mol}^{-1}$ ) and dispersity ( $M_w/M_n = 1.3$ ) of oligocarbonate. The oligomers were then purified by dialysis in methanol in order to remove TBAI and the HBD before drying under vacuum overnight at room temperature.

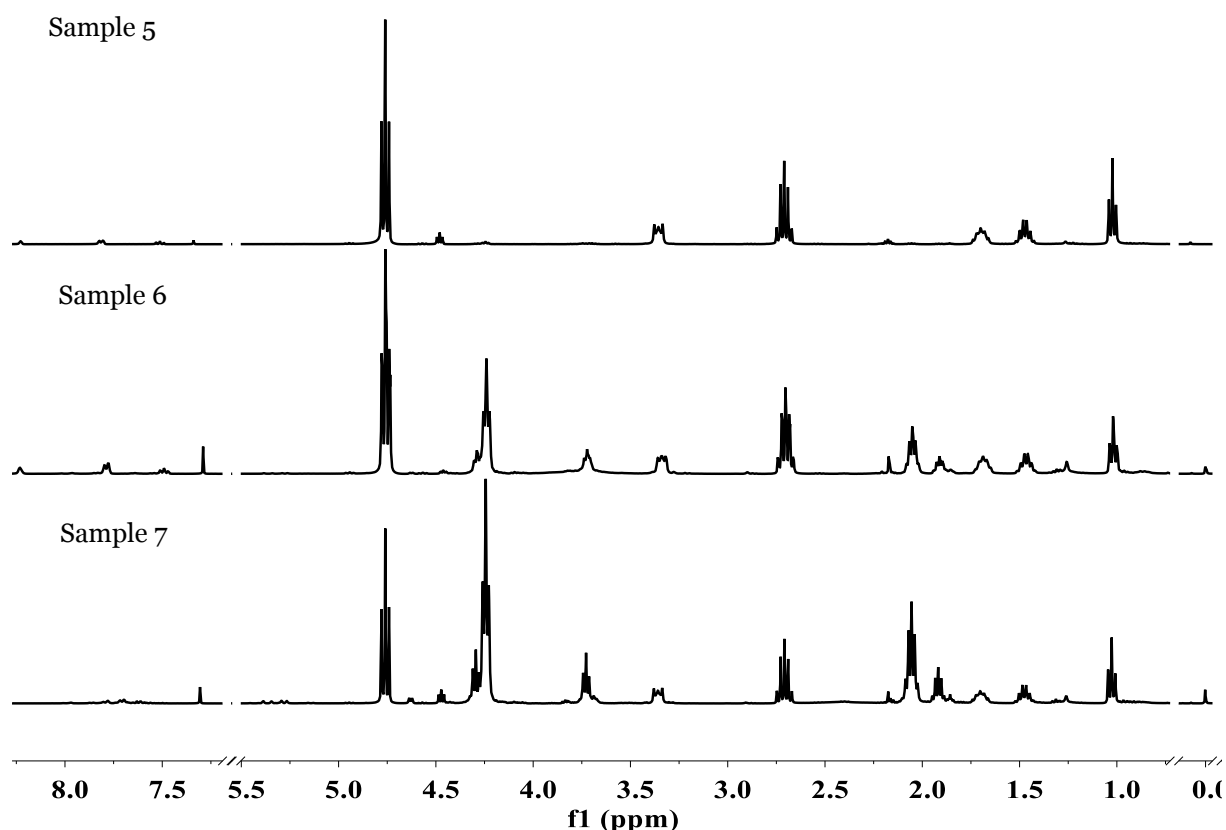
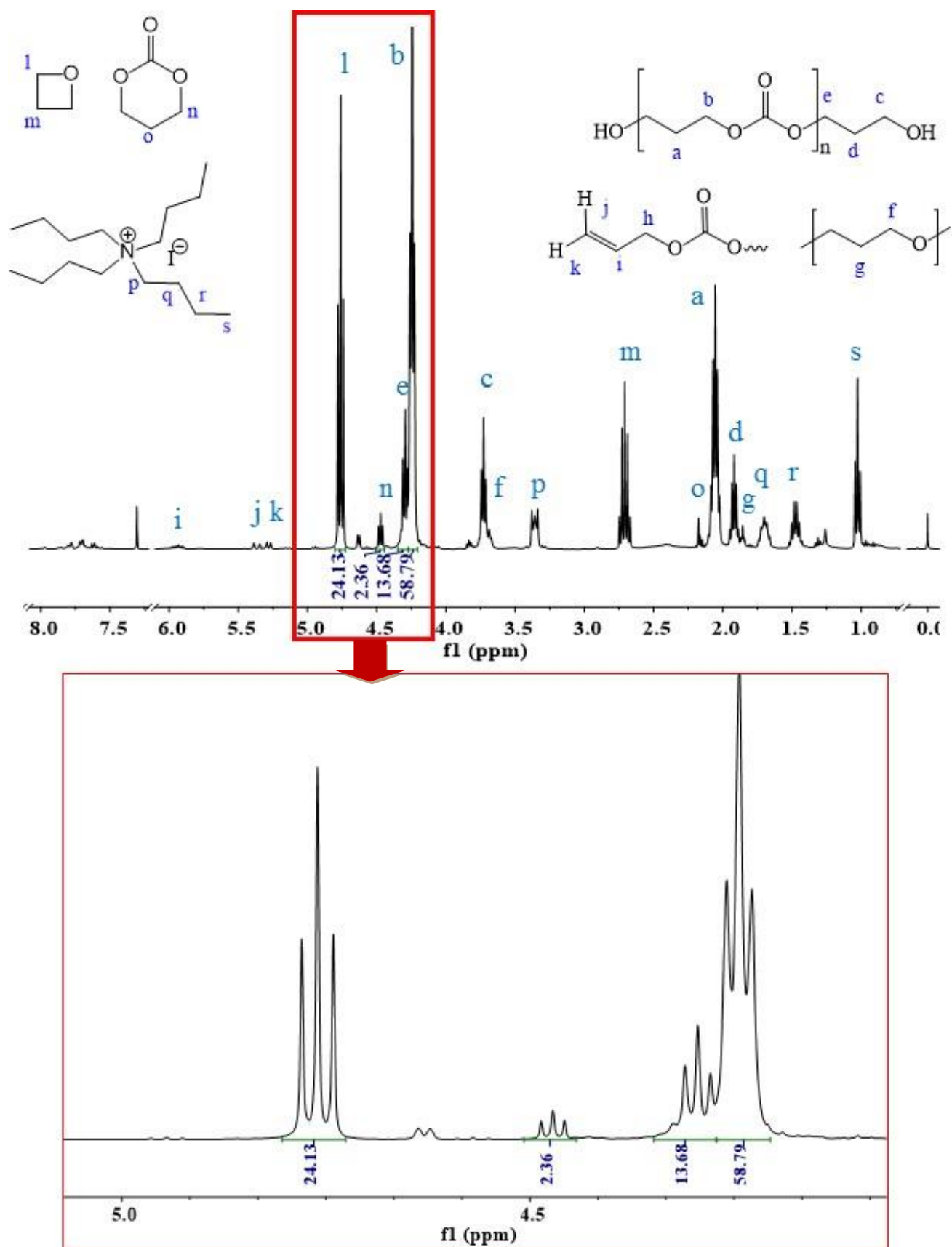


Figure 1: Overlay of the  $^1\text{H}$  NMR spectra in  $\text{CDCl}_3$  of the crude reaction mixture obtained by oxetane/ $\text{CO}_2$  coupling in the presence of 1,3-bis-HFAB/TBAI as catalytic system at  $80^\circ\text{C}$  (Sample 5 Table 1),  $100^\circ\text{C}$  (Sample 6, Table 1) and  $130^\circ\text{C}$  (Sample 7, Table 1).



**b) Chain extension.**

In a typical experiment, 0.5 g of oligocarbonate ( $M_n = 2000 \text{ g.mol}^{-1}$ ,  $2.5 \cdot 10^{-4} \text{ mol}$ ) were reacted with 4,4'-methyldiphenyldiisocyanate (MDI, 62.5 mg,  $2.5 \cdot 10^{-4} \text{ mol}$ ,  $[\text{Oligomer}]/[\text{MDI}] = 1$ ) using 1 wt% of dibutyltin dilaurate as catalyst and 2 mL of dried THF as solvent. The mixture was then degassed for 5 minutes by  $\text{N}_2$  bubbling before being stirred overnight at room temperature under  $\text{N}_2$  atmosphere. The resulting polyurethane was finally purified by precipitation into methanol and dried under vacuum before characterization. An aliquot is analyzed by  $^1\text{H}$  and  $^{13}\text{C}$  NMR spectroscopy in deuterated DMF while another aliquot is dissolved in THF and injected in SEC to determine the molar mass and dispersity.

**c) Purification**

Prior to analysis, oligomers were purified by dialysis in methanol according to the following procedure: oligomers were dissolved in THF, added into dialysis membrane (Spectra/Por®, cut-off: 1000 Da), and dialyzed against methanol for 48h. Methanol was replaced three times in order to completely remove the ammonium salt and HDB. Purified oligomers in the dialysis membrane were then collected, methanol was removed under vacuum at room temperature, and oligomers were finally dried under vacuum at room temperature for 24h.

**d) Characterizations**

NMR spectra were recorded in  $\text{CDCl}_3$  or  $\text{DMF-d}_7$  at 400 MHz in the FT mode with a Bruker AN 400 apparatus at 25°C.

The molar masses ( $M_n$ ) and dispersities ( $M_w/M_n$ ) of the polymers were determined by size exclusion chromatography (SEC) in tetrahydrofuran (THF) at 45°C at a flow rate of 1 mL/min with Viscotek 305 TDA liquid chromatograph equipped with 2 PSS SDV analytical linear M 8 mm columns protected by a PL gel 5  $\mu\text{m}$  guard column and calibrated with poly(styrene) standards.

Matrix-assisted Laser Desorption/Ionization Time-of-Flight (MALDI-ToF) mass spectra were recorded using a Waters QToF Premier mass spectrometer equipped with a Nd:YAG laser using the 3rd harmonic with a wave length of 355 nm. In the context of this study, a maximum output of ~65 J is delivered to the sample in 2.2 ns pulses at 50 Hz repeating rate. Time-of-flight mass analyses were performed in the reflection mode at a resolution of about 10 000. The matrix, trans-2-[3-(4-tert-butyl-phenyl)-2-methyl-2-propenylidene]malononitrile (DCTB), was prepared as a 40 mg/mL solution in chloroform. The matrix solution (1  $\mu\text{L}$ ) was applied to a stainless-steel target and air-dried. Polymer samples were dissolved in THF to obtain 1 mg/mL solutions and 100  $\mu\text{L}$  of NaI solution (2 mg/mL in acetonitrile) are added as source of cationization agent. Then, 1  $\mu\text{L}$  aliquots of these solutions were applied onto the target area (already bearing the matrix crystals) and then air-dried.



### **e) Kinetic studies**

The synthesis of trimethylene carbonate and poly(carbonate) were monitored *in situ* by IR spectroscopy using a home-made Ge ATR accessory suitable for high-pressure measurements (up to 5 MPa) and high temperature (up to 100 °C) coupled with a ThermoOptek interferometer (type 6700) equipped with a global source, a KBr/Ge beamsplitter and a DTGS (Deuterated TriGlycine Sulphate) detector. Single beam spectra recorded in the spectral range (400 - 4000 cm<sup>-1</sup>) with a 4 cm<sup>-1</sup> resolution were obtained after the Fourier transformation of 100 accumulated interferograms. Spectra were recorded every ten minutes for 24 h. The stainless-steel cell with a volume of about 3 mL screwed above the Ge crystal provides one port for the inlet of mixture and CO<sub>2</sub>. A magnetic stirrer was placed into the cell to ensure good homogenization of the mixture. The ATR cell was heated using cartridge heaters disposed in the periphery of its body. A thermocouple was used and located close to a cartridge heater for the temperature regulation with an accuracy of about 2°C. The cell was connected directly to the CO<sub>2</sub> tank allowing the pressure to be raised up to 5 MPa.

### **f) Computational details**

Preliminary calculations of equilibrium structures were performed using a semi-empirical model (AM1-D<sub>3</sub>H<sub>4</sub><sup>25, 26</sup>) to determine the most stable conformations. These semi-empirical calculations were performed using the AMPAC software<sup>27</sup>. The CHAIN algorithm was used for locating intermediates and transition states along the reaction path. The lowest energy structures obtained at the AM1-D<sub>3</sub>H<sub>4</sub> level were further investigated using the Density Functional Theory method (DFT) implemented in the Gaussian 09 package.<sup>28</sup> DFT calculations of geometries, energies, and vibrational frequencies reported in this paper were carried out with the M06-2X functional<sup>29</sup> using the 6-311G(d,p) basis set.

All frequencies of each structure have also been calculated to verify the presence of a single imaginary frequency for transition states and the absence of imaginary frequency for ground states. The intrinsic reaction coordinate (IRC) method has been used to verify that the obtained transition states were effectively connected to the desired minima. For all catalysts, a wide range of possible configurations and interactions have been modelled and the more stable of them are reported in this work. To consider entropic effects, the energies mentioned in this study correspond to the Gibbs free energy ( $\Delta G$ ).

## Results and Discussion

### 1- Oxetane/CO<sub>2</sub> coupling

#### a) Catalyst screening.

The TMO/CO<sub>2</sub> coupling was first investigated in the presence of TBAI or TBABr (3 mol% compared to TMO) as the catalyst at 100°C and 10 MPa for 24h (Table 1, entries 1 and 3). Under these conditions, the conversion of TMO was very low (below 5%) and only traces of cyclic carbonates and oligocarbonates in a 80:20 molar ratio were formed with the two organocatalysts. In order to speed-up the reaction, 1,3-bis(2-hydroxyhexafluoroisopropyl)benzene (1,3-bis-HFAB; Scheme 1) was added as a co-catalyst. Indeed, as previously demonstrated by us, this fluorinated diol drastically accelerated the coupling of CO<sub>2</sub> with various epoxides.<sup>30-32</sup> Similarly to the CO<sub>2</sub>/epoxide coupling, 1,3-bis-HFAB is expected to facilitate the oxetane ring opening by hydrogen-bonding interactions, and therefore to accelerate the CO<sub>2</sub>/oxetane reaction, as it will be discussed in the section devoted to the mechanism study (see later). In the presence of an equimolar amount of ammonium salt and 1,3-bis-HFAB (Table 1, entries 2 and 6), the TMO conversion reached values of 17% and 39% when TBABr and TBAI were used as catalysts, respectively. As observed for the epoxide/CO<sub>2</sub> coupling, the higher conversion of TMO with TBAI was attributed to the higher nucleophilicity and better leaving character of iodide compared to bromide.<sup>33,34-38</sup> Importantly, additionally to favor the CO<sub>2</sub>/oxetane coupling, 1,3-bis-HFAB strongly increased the selectivity in low molar mass oligocarbonate over TMC. An oligocarbonate/TMC selectivity of 90/10 was noted for TBABr as catalyst that was further increased to 98/2 for TBAI.

#### b) Influence of the temperature

The impact of the temperature on the TMO/CO<sub>2</sub> coupling catalysed by the TBAI/1,3-bis-HFAB binary catalyst ([TBAI]/[1,3-bis-HFAB] = 1, [TBAI] = 3 mol%) was investigated at a fixed pressure of 10 MPa by varying the temperature from 80°C to 130°C (Table 1, entries 5-7). At 80°C, the TMO conversion was low (7%) and only traces of TMC and oligomers were obtained. The main product was the 6-membered cyclic carbonate (TMC) that was produced with 71% selectivity. By increasing the temperature to 100°C or 130°C, TMO conversion increased to 39% and 92%, respectively, and the selectivity reversed as low molar mass oligocarbonate was produced in a near quantitative way ([oligocarbonate]/[TMC] = 98/2). Moreover, the molar mass of the oligomers increased when raising the temperature to reach 2000 g.mol<sup>-1</sup> at 130°C (Table 1, entry 7). These results are consistent with those reported by Darensbourg *et al.* who showed that lowering the operating temperature favored the selective formation of TMC from TMO and CO<sub>2</sub> when a chromium salen complex/TBABr system was used as dual catalyst.<sup>11</sup>

Table 1: Chemical fixation of CO<sub>2</sub> onto TMO catalysed by tetrabutylammonium salts (X = I<sup>-</sup>, Br<sup>-</sup>) and HBDs. Conditions: t = 24h, [HBDs]/[TBAX] = 1.

Entry	Catalyst	HBD	[Catalyst]/ [TMO] (mol%)	T (°C)	P (MPa)	Conv (%) <sup>a</sup>	Selectivity (oligocarbonate: TMC) <sup>a</sup>	Mn (g/mol) <sup>b</sup>	Mw (g/mol) <sup>c</sup>
1	TBABr	/	3	100	10	< 5	20:80	<1000	<1000
2	TBABr	1,3-bis-HFAB	3	100	10	17	90:10	<1000	1050
3	TBAI	/	3	100	10	< 5	20:80	<1000	<1000
4	TBAI	/	3	130	10	5	49:51	<1000	<1000
5	TBAI	1,3-bis-HFAB	3	80	10	7	29:71	<1000	<1000
6	TBAI	1,3-bis-HFAB	3	100	10	39	98:2	1000	1150
7	TBAI	1,3-bis-HFAB	3	130	10	92	98:2	2000	2600
8	TBAI	1,3-bis-HFAB	3	130	5	72	95:5	1500	2000
9	TBAI	1,3-bis-HFAB	3	130	2	25	96:4	<1000	<1000
10	TBAI	PFB	3	100	10	17	75:25	<1000	1000
11	TBAI	PFB	3	130	10	87	99:1	1600	2100
12	TBAI	Pyrogallol	3	100	100	33	88:12	<1000	<1000
13	TBAI	Pyrogallol	3	130	100	28	90:10	<1000	1300
14	TBAI	1,3-HIB	3	130	100	11	15:85	<1000	<1000
15 <sup>d</sup>	TBAI	1,3-bis-HFAB	3	130	100	10	/	<1000	<1000
16 <sup>e</sup>	TBAI	1,3-bis-HFAB	3	130	100	8	/	<1000	<1000

<sup>a</sup> Conversion and selectivity determined by <sup>1</sup>H NMR.<sup>b</sup> Apparent number average molar mass determined by SEC using THF as eluent and a polystyrene calibration<sup>c</sup> Apparent weight average molar mass determined by SEC using THF as eluent and a polystyrene calibration<sup>d</sup> oxetane = 3,3-dimethyloxetane<sup>e</sup> oxetane = 3-methyl-3-oxetanemethanol

### c) Influence of the pressure

The impact of the pressure on the TMO/CO<sub>2</sub> coupling catalysed by TBAI/1,3-bis-HFAB ([TBAI]/[1,3-bis-HFAB] = 1, [TBAI] = 3 mol%) was evaluated at a fixed temperature of 130°C in a pressure range from 2 to 10 MPa. As highlighted in Table 1 (entries 7-9), the CO<sub>2</sub>/TMO organocatalytic coupling was CO<sub>2</sub> pressure dependent as the TMO conversion decreased from 92% to 72% and 25% at 10, 5 and 2 MPa, respectively. As the TMO/CO<sub>2</sub> medium is biphasic (liquid/gas) under our experimental conditions, the conversion depends on the concentration of CO<sub>2</sub> dissolved in the TMO phase that decreases with the decrease of the CO<sub>2</sub> pressure. Under the CO<sub>2</sub> pressure conditions investigated here, the synthesis of low molar mass oligocarbonate ( $\sim 800 < M_n < 2000 \text{ g.mol}^{-1}$ ;  $M_w/M_n < 1.35$ ) was nearly selective and only traces of TMC were produced ([oligocarbonate]/[TMC]  $\geq 95/5$ ).

### d) HBD screening

The co-catalytic activity of series of hydrogen bond donors was screened at 100°C or 130°C and 10 MPa for 24h by using TBAI as catalyst (3 mol% compared to TMO). As highlighted in Table 1 (entry 10), perfluoro-*tert*-butanol (PFB) also fastened the TMO/CO<sub>2</sub> coupling but, at 100°C, the TMO conversion was twice lower (17%) than that one determined for the same reaction co-catalysed by 1,3-bis-HFAB (39%). The reaction was poorly selective as a TMC/oligocarbonate mixture was produced in a 25/75 molar ratio. The lower co-catalytic activity of PFB is consistent with our previous results reported for the CO<sub>2</sub>/epoxide coupling.<sup>30</sup> By increasing the temperature to 130°C, the TMO conversion reached 87% and the oligocarbonate was selectively produced (Table 1, entry 11). These results are similar to the ones obtained by using 1,3-bis-HFAB, which suggests that a reaction time of 24h for the TMO/CO<sub>2</sub> coupling co-catalysed by 1,3-bis-HFAB was probably overestimated and that the conversion already reached the plateau.

The co-catalytic activity of 1,3-bis-HFAB was also compared with the one of pyrogallol that was identified by Kleij's group as one of the most efficient activator for the selective synthesis of five-membered cyclic carbonates from CO<sub>2</sub> and epoxide.<sup>39</sup> At 100°C, pyrogallol enabled the conversion of TMO into oligocarbonate with a catalytic activity similar to that noted for 1,3-bis-HFAB (Table 1, entries 6 and 12). However, whereas 1,3-bis-HFAB led to a nearly selective synthesis of oligocarbonate, a mixture of oligocarbonate and TMC in a 88/12 molar ratio was obtained in the presence of pyrogallol. An increase of the temperature from 100°C to 130°C had a detrimental effect on the TMO conversion that decreased to 28% (Table 1, entry 13). As already evidenced by Kleij for the CO<sub>2</sub>/epoxide coupling, the lower TMO conversion probably arose from the deactivation of the pyrogallol/TBAI catalyst at high temperature.<sup>40, 41</sup>

Finally, 1,3-HIB, the non-fluorinated analogue of 1,3-bis-HFAB, displayed only marginal co-catalytic activity as evidenced by a low TMO conversion of 11%. As

expected for such low conversion, TMC was identified as the major product that was synthesized with a selectivity of 85% (Table 1, entry 14).

Importantly, all reactions reported in this paper were carried out with products/reagents used as received and were reproducible, highlighting the robustness of the developed organocatalytic system.

### e) Organocatalysed coupling of CO<sub>2</sub> with oxetanes

Converting 3,3-disubstituted oxetanes into the corresponding six-membered cyclic carbonates has been shown very challenging, as these cyclic ethers are known to be less reactive than TMO. The coupling of 3,3-dimethyloxetane and 3-methyl-3-oxetanemethanol (Scheme 1, b and c) with CO<sub>2</sub> was then investigated using the most efficient TBAI/1,3-bis-HFAB bicomponent organocatalyst ([TBAI] = 3 mol%, [TBAI]/[1,3-bis-HFAB] = 1) at 130°C and 10 MPa for 24h. For both reactions, the oxetane conversion was close to 10% and a mixture of 4,4-disubstituted cyclic carbonates and low molar mass oligocarbonates ( $M_n < 1000 \text{ g.mol}^{-1}$ ) was produced whereas under the same experimental conditions, the conversion of TMO was high (92%) and oligocarbonate was selectively formed (Table 1, entries 7, 15 and 16). These results are consistent with those reported by Kleij or Darensbourg for the coupling of substituted oxetane with CO<sub>2</sub> using metal complexes as co-catalysts.<sup>16, 17, 19, 20</sup>

## 2- Oligocarbonate characterizations

To elucidate the exact structure of the oligocarbonate and the nature of its chains ends, <sup>1</sup>H NMR characterizations were correlated with MALDI-ToF analyses. Prior to analysis, oligomers were purified by dialysis in methanol in order to remove unreacted TMO, TBAI and 1,3-bis-HFAB.

MALDI mass spectra of Sample 7 (Table 1) are composed of one main distribution with a maximum at  $m/z$  1629 (Figure 3A). This main population is characterized by peak to peak separation of 102 mass units that is consistent with the presence of poly(trimethylene carbonate) (poly(TMC)). A fine investigation confirms that chains are  $\alpha,\omega$ -hydroxyl telechelic corresponding to poly(TMC) initiated by 1,3-propanediol and cationized by Na<sup>+</sup> (Figure 3B).

<sup>1</sup>H NMR spectroscopy also confirmed this structure with signals characteristic of the repeating units of poly(TMC) at  $\delta = 4.25 \text{ ppm}$  (CH<sub>2</sub>-O-C(O)-O-) and  $\delta = 2.04 \text{ ppm}$  (-CH<sub>2</sub>-CH<sub>2</sub>-CH<sub>2</sub>-O-C(O)-O-), and of the chain ends at  $\delta = 4.30 \text{ ppm}$  (CH<sub>2</sub>),  $\delta = 1.91 \text{ ppm}$  (CH<sub>2</sub>) and  $3.73 \text{ ppm}$  (CH<sub>2</sub>-OH) (Figure 4). At 18 mass unit lower, a second less intense population was observed. This distribution was attributed to polymer ions having lost a molecule of water during the polymerization process. This assumption was supported by <sup>1</sup>H NMR spectroscopy with signals characteristic of olefinic group at  $\delta = 5.92 \text{ ppm}$ ,  $\delta = 5.37 \text{ ppm}$ ,  $\delta = 5.28 \text{ ppm}$ , and the signal characteristic of a methylene adjacent to the carbonate group and the olefinic chain end at  $\delta = 4.62 \text{ ppm}$ .

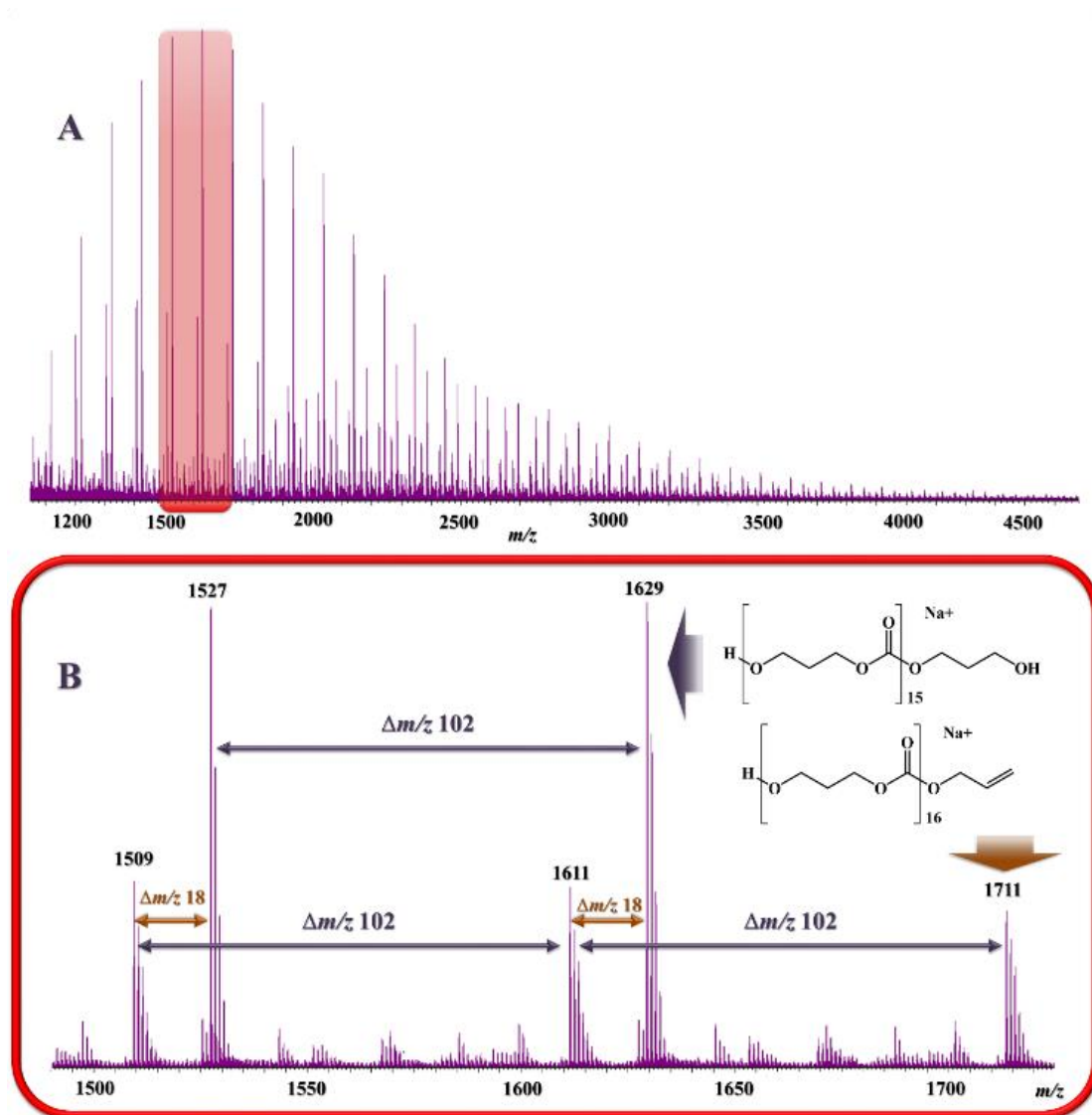


Figure 3: (A) Global MALDI mass spectrum recorded for the CO<sub>2</sub>/TMO coupling catalysed by TBAI plus 1,3-bis-HFAB (Sample 7, Table 1), (B) magnification of the mass spectrum between  $m/z$  1500 and 1750.

This olefin chain-end was formed by random chain scission of the chain with decarboxylation that was identified as one of the two mechanisms of degradation of the polycarbonates by unzipping reaction.<sup>42, 43</sup> By comparison of the relative intensities of the peak characteristic of both hydroxyl and olefinic chain ends, about 90% of the oligomers were bearing the hydroxyl groups at both chain-ends, and only 10% contained the olefin at one of the chain-end. Finally, the mass spectrum highlights a peak at  $m/z = 1585$  g.mol<sup>-1</sup> of very low intensity corresponding to a loss of a 44 mass units. This population was attributed to the formation of ether links in the  $\alpha,\omega$ -hydroxyl oligo(carbonates) structure. This was confirmed by the presence in the <sup>1</sup>H NMR spectrum of peaks of the methylene groups of ring opened TMO at  $\delta = 3.67$  ppm and  $\delta = 1.84$  ppm. However, these ether linkages are negligible (~1%) and can be considered as defects in the oligocarbonate structure.

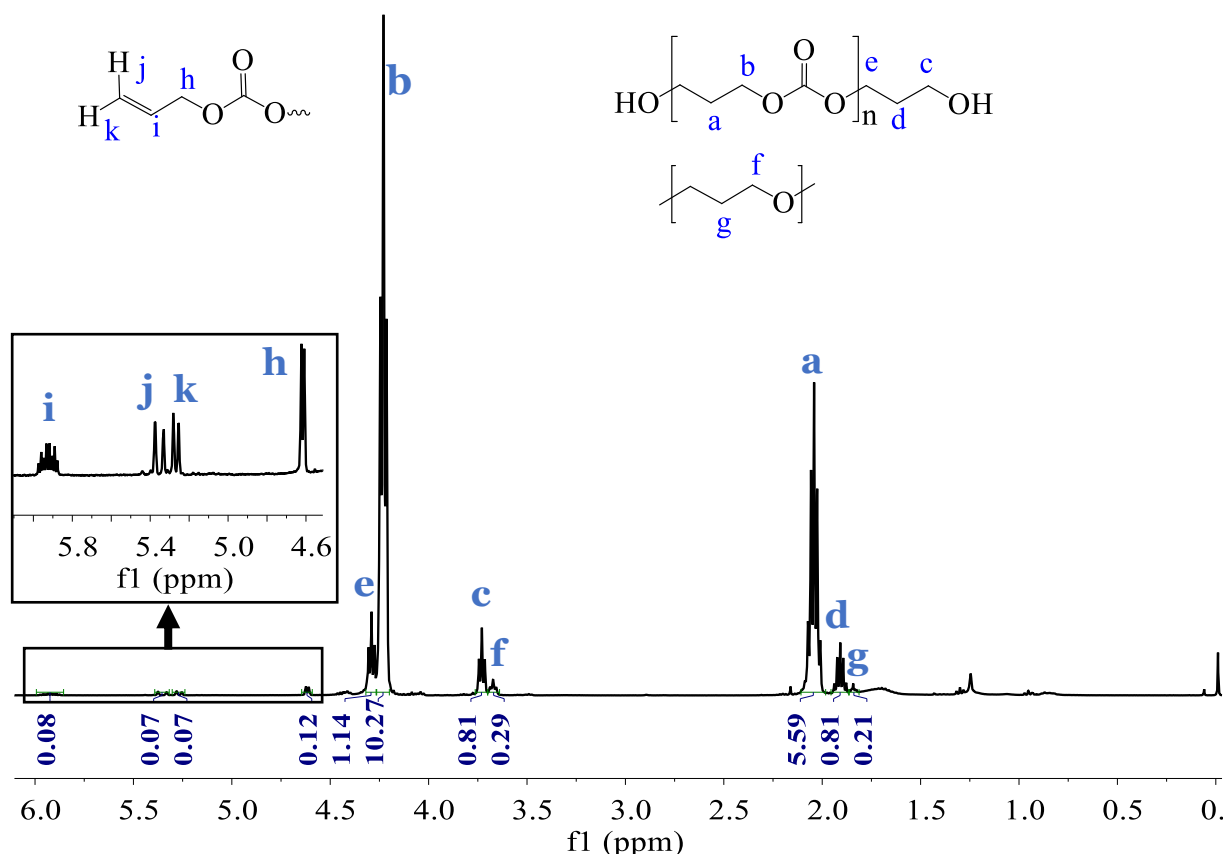


Figure 4:  $^1\text{H}$  NMR spectrum in  $\text{CDCl}_3$  of poly(TMC) obtained by oxetane/ $\text{CO}_2$  coupling in the presence of 1,3-bis-HFAB/TBAI as the catalytic system (Sample 7, Table 1). Polymer was purified by dialysis in methanol.

### 3- Mechanistic investigations

Two distinct mechanisms can be proposed for the formation of the oligomers, either by ring opening polymerization (ROP) of TMC or by direct copolymerization of TMO with  $\text{CO}_2$ . In order to elucidate the main reaction pathway, the coupling of TMO with  $\text{CO}_2$  promoted by the TBAI/1,3-bis-HFAB dual catalytic system was first monitored by online FTIR spectroscopy under pressure by using a homemade ATR experimental set-up.

In order to detect the possible presence of TMC, the study was realized at a moderate temperature ( $100^\circ\text{C}$ ) and a  $\text{CO}_2$  pressure of 3 MPa. Figure 5 depicts the typical time evolution of the absorbance. At the early stages of the reaction, ATR spectra showed the appearance of a peak at  $1760\text{ cm}^{-1}$  typical of the  $\nu_{\text{C}=\text{O}}$  of TMC that rapidly disappeared. This disappearance coincided with the appearance of a peak at  $1750\text{ cm}^{-1}$  attributed to the  $\nu_{\text{C}=\text{O}}$  of linear carbonate, attesting for the formation of oligocarbonate. However, the small separation between these two peaks ( $\Delta\nu < 10\text{ cm}^{-1}$ ) did not enable their proper deconvolution and quantification. Based on those observations, we assumed that TMC was first produced and that its ring opening polymerization (ROP) then rapidly occurred to provide the hydroxyl telechelic oligocarbonate (Scheme 2, Path 1).

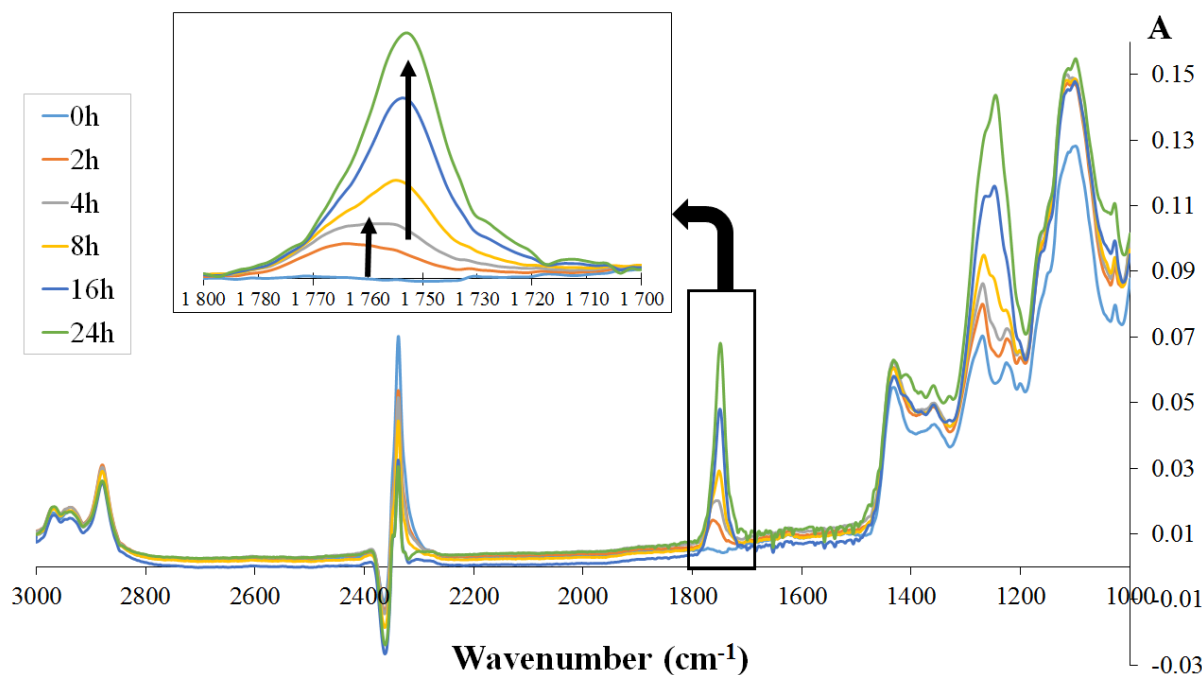
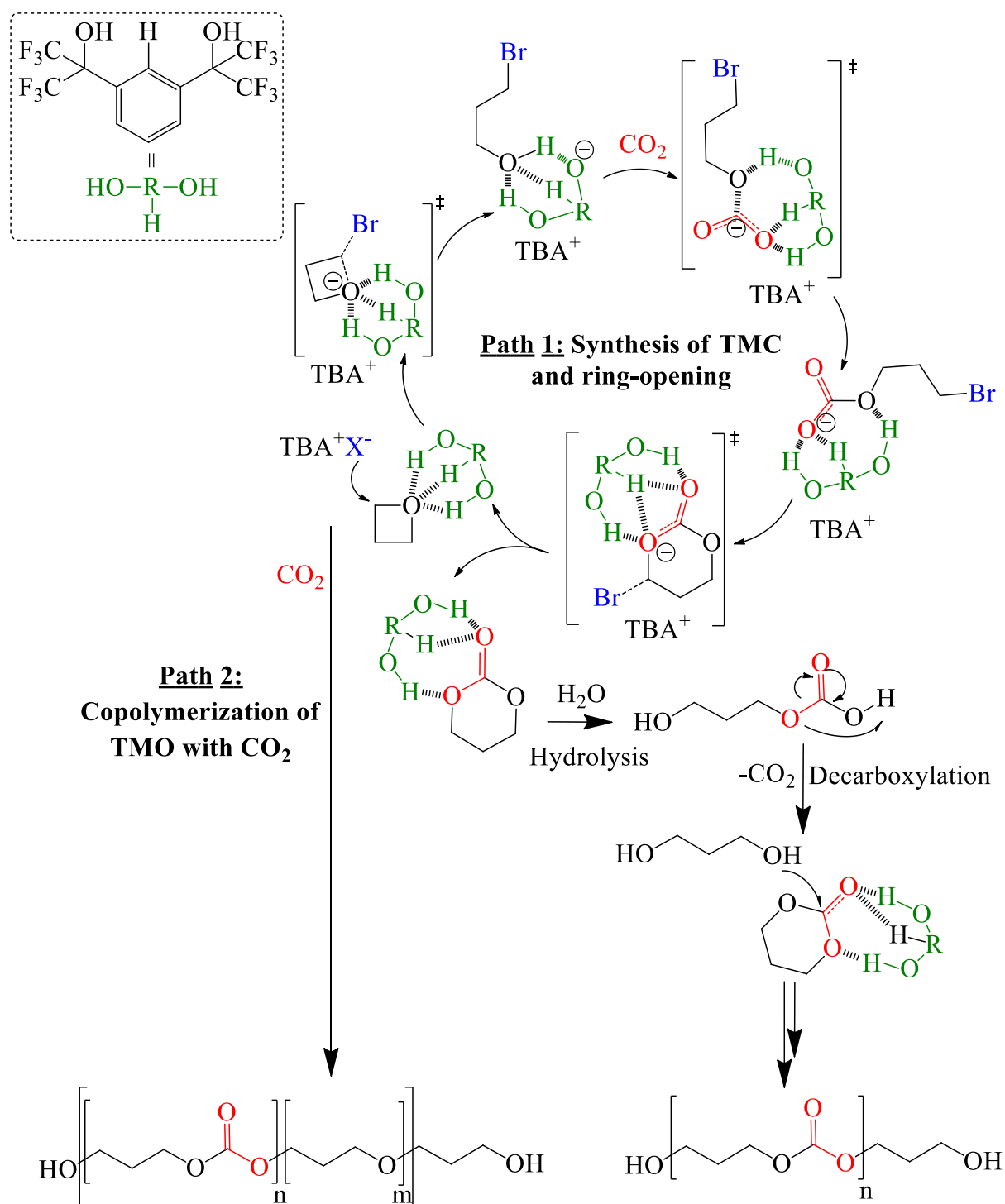


Figure 5: Time evolution of the infrared spectra for the TMO/CO<sub>2</sub> coupling at T = 100 °C and P = 3 MPa, [TBAI] = 3 mol%, [1,3-bis-HFAB] = 3 mol%

MALDI-ToF and <sup>1</sup>H-NMR analyses of the polymer have evidenced that both chain-ends of the polymer are mainly constituted by a –CH<sub>2</sub>CH<sub>2</sub>CH<sub>2</sub>-OH group, suggesting that ROP of TMC was initiated by 1,3-propanediol. The most probable origin of this initiator was the *in-situ* hydrolysis of TMC by residual water into the corresponding carbonic acid, followed by its fast decarboxylation (Scheme 2, Path 1). The hydrolysis of TMC and the nucleophilic attack of hydroxyl groups of 1,3-propanediol onto the carbonyl group of TMC were facilitated both by the high temperature and the presence of 1,3-bis-HFAB that not only activated TMO for coupling with CO<sub>2</sub> but also strongly interacted with the six-membered cyclic carbonate through hydrogen bonding. This interaction between TMC and 1,3-bis-HFAB was supported by <sup>1</sup>H-NMR titration experiments that highlighted shifts of the protons of the hexafluoroalcohol groups of 1,3-bis-HFAB (δOH) and the aromatic proton in *ortho* position of those two groups (δHo) (Figure 6a and 7). <sup>1</sup>H-NMR titrations of TMC by 1,3-bis-HFAB evidence the hydrogen-bonding interaction between the two components by the large change in the chemical shift of the OH resonance of 1,3-bis-HFAB from 3.1 ppm for pure 1,3-bis-HFAB to 6.8 ppm for the TMC/1,3-bis-HFAB mixture with a 1.52 molar ratio. The aromatic proton Ho in *ortho* position of the two fluorinated substituents is also interacting with the cyclic carbonate as indicated by the change in its chemical shift. This hydrogen bonding also slightly affects the chemical shift of all the other aromatic protons as a result of the deformation of the electronic density of the aromatic ring.





Scheme 2: Mechanism proposals for the synthesis of oligocarbonates from  $\text{CO}_2$ /TMO coupling catalysed by the dual TBAI/1,3-bis-HFAB organocatalyst.  $\text{RH}(\text{OH})_2$  represents 1,3-bis(2-hydroxyhexafluoroisopropyl)benzene. The energy of an isolated molecule of  $\text{CO}_2$  was included in the IRO, IR1, TS1 energies.

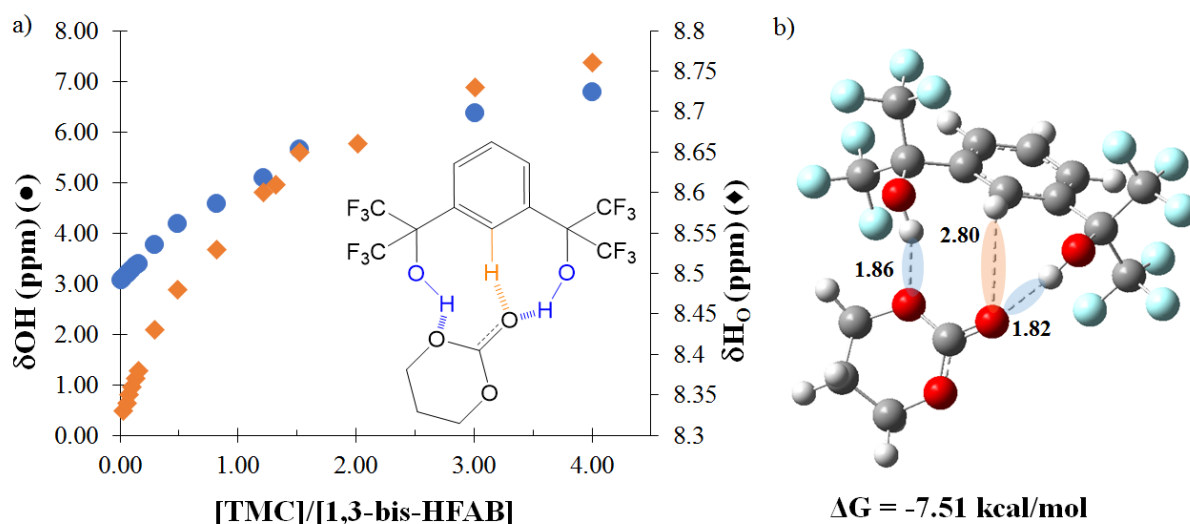


Figure 6: a) Variation of the chemical shift on the  $^1H$  spectrum of the hydroxyl protons ( $\delta_{OH}$ ) and the proton  $H_o$  ( $\delta_{H_o}$ ) with the [TMC]/[1,3-bis-HFAB] molar ratio, b) Optimized structure of the TMC/1,3-bis-HFAB adduct at the Mo6-2X level using the 6-311G(d,p) basis set. The dashed lines depict the intermolecular distances in angstrom.

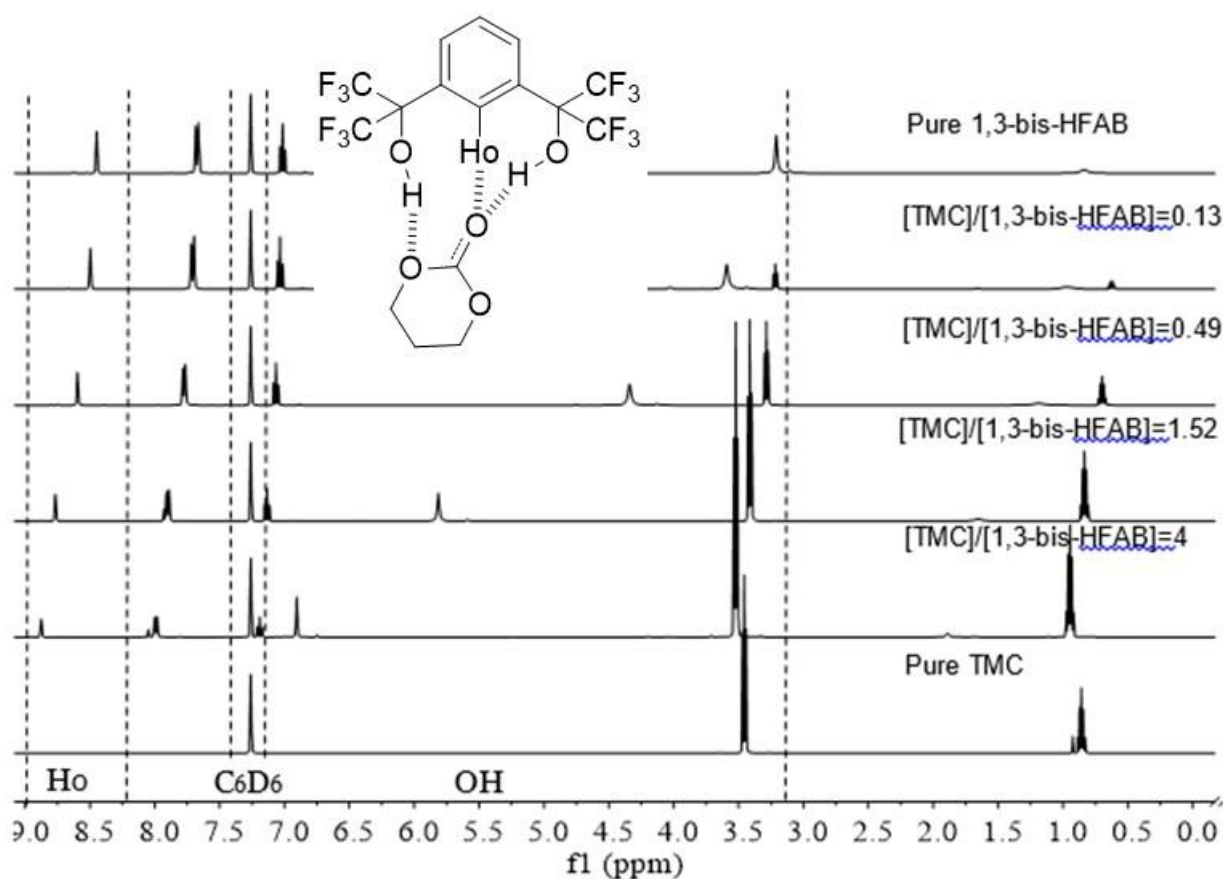


Figure 7:  $^1H$  NMR titration of TMC by 1,3-bis-HFAB in  $C_6D_6$

This was further confirmed by DFT calculations that evidence the formation of a TMC/1,3-bis-HFAB adduct by three strong H-bonds interactions. Figure 6b illustrates the optimized structure of the TMC/1,3-bis-HFAB adduct at the Mo6-2X level using the 6-311G(d,p) basis set and shows that one hydroxyl group of the hexafluoroalcohol moiety interacts with the O atom of the carbonyl of TMC (1.82 Å) while the second hydroxyl group stabilizes the O atom adjacent to the carbonyl (1.86 Å). Furthermore, a third weaker hydrogen bond exists between the aromatic proton in *ortho* position of the two fluorinated substituents and the O atom of the carbonyl (2.80 Å). Therefore, it is likely that the activation barrier of both the hydrolysis of TMC and the oxetane ring-opening polymerization are decreased in presence of 1,3-bis-HFAB. Therefore, TMC has to be viewed as an *in-situ* generated intermediate that directly enters the synthesis of the oligocarbonate that is initiated by 1,3-propanediol and catalysed by 1,3-bis-HFAB. The presence of ether linkages in the oligomer structure might be explained by the ring opening of oxetane resulting from the attack of the hydroxyl chain-ends of the growing chains. However, this side reaction seems disfavoured as evidenced by the ether linkage content as low as 1% and could be considered as defects in the oligomer structure.

This mechanism investigation highlights the origin of the selectivity towards the formation of oligo(ether-*co*-carbonate) that arises from the strong activation of TMC by 1,3-bis-HFAB. According to the proposed mechanism and the observation that about 90% of the formed oligomers were bearing hydroxyl groups at both chain-ends, at least an equimolar amount of water with respect to the oligomers was expected to be present in the reaction medium. It is here important to note that all the reagents (CO<sub>2</sub>, TMO, TBAI, HBD activator) were used as received and were not dried. Moreover, some compounds are highly hygroscopic such as TBAI that contains about 4 wt% water (as determined by thermogravimetric analysis; TGA). Substantial amount of water is therefore present in the reactor before starting the experiments.

Determining the structure of the product formed under strict anhydrous conditions would have been interesting. However, it is impossible to work under these conditions with our pressure cell equipped for online FTIR analysis. In order to tentatively limit the water content in the reaction medium, the same CO<sub>2</sub>/TMO coupling reaction catalysed by TBAI/1,3-bis-HFAB (under identical conditions than Entry 7, Table 1), was thus performed in a conventional high pressure cell by using dried TMO (distilled over CaH<sub>2</sub>), 1,3-bis-HFAB (dried on molecular sieves), and TBAI (dried under vacuum at 50°C for 24h in the reactor). However similar results were obtained compared to the experiment carried out with reagents used as received: similar selectivity in oligomers, yield and chain-end content and structures. At this stage, we cannot draw any reliable conclusions from this experiment because the exact content of remaining water in the reactor is unknown. Indeed, although TMO, 1,3-bis-HFAB and TBAI were dried, removing adsorbed water from the stainless-steel reactor is challenging and the water content in the CO<sub>2</sub> line is unknown.

#### 4- Theoretical study of the TMO/CO<sub>2</sub> coupling catalysed by TBABr/1,3-bis-HFAB

The mechanism of the synthesis of trimethylene carbonate (TMC) from the TMO/CO<sub>2</sub> coupling was investigated using DFT calculations performed at the Mo6-2X/6-311G(d,p) level. To the best of our knowledge, the catalytic chemical fixation of CO<sub>2</sub> onto TMO has never been investigated using DFT calculations.

As reported for the epoxide/CO<sub>2</sub> coupling, the most probable mechanism is composed of three key elementary steps involving the epoxide ring opening, the CO<sub>2</sub> electrophilic attack, and the intramolecular cyclization step. Therefore, TBABr was chosen as catalyst instead of TBAI for an easy comparison with the results recently reported with propylene oxide.<sup>31, 44</sup> We compared the reaction between TMO and CO<sub>2</sub> catalysed by (1) TBABr, (2) TBABr plus pyrogallol and (3) TBABr plus 1,3-bis-HFAB. The Gibbs energy profiles and the schematic intermediates and transition states structures for the catalysis with 1,3-bis-HFAB are depicted on Figure 8.

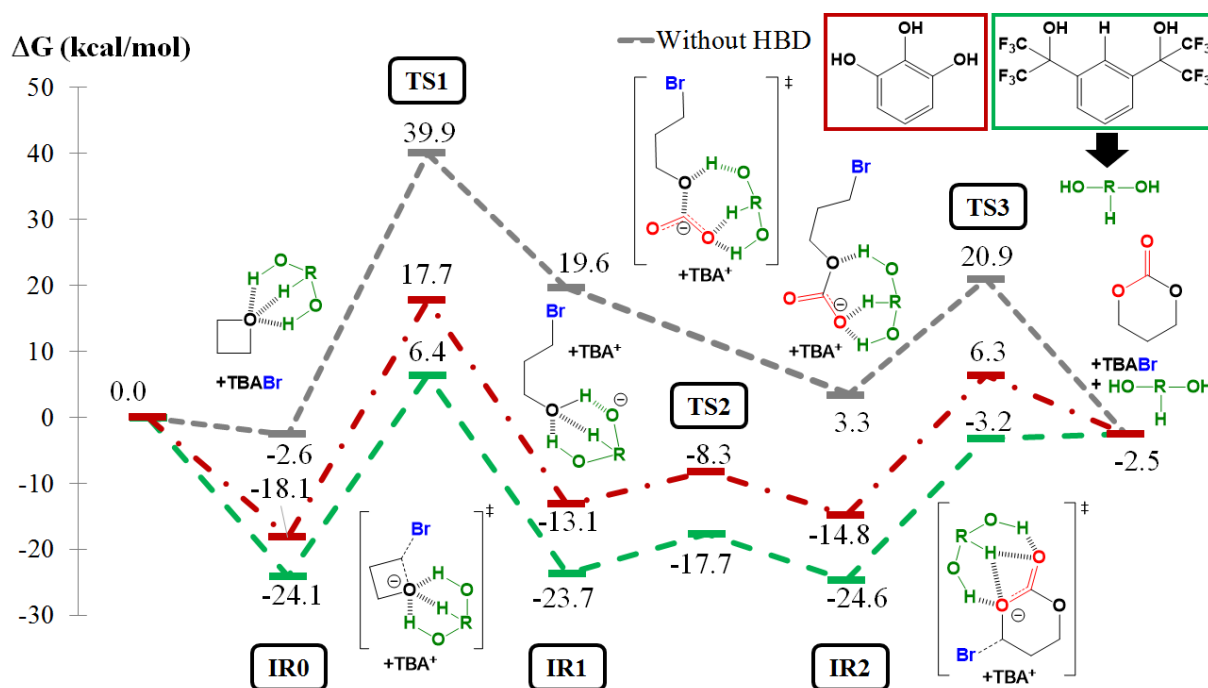


Figure 8: Free energy profiles (Mo6-2X/6-311G(d,p)) for the CO<sub>2</sub>/TMO coupling catalysed by TBABr (grey), TBABr plus pyrogallol (red) and TBABr plus 1,3-bis-HFAB (green). Lewis structure for the triple hydrogen-bond activation pathway. RH(OH)<sub>2</sub> represents 1,3-bis(2-hydroxyhexafluoroisopropyl)benzene. The energy of an isolated molecule of CO<sub>2</sub> was included in the IR0, IR1, TS1 energies.

Initial state (zero energy) corresponds to the sum of the Gibbs energy of each compound (TBABr/TMO/CO<sub>2</sub>/Pyrogallol or 1,3-bis-HFAB) fully optimized whereas IR0 corresponds to the Van der Waals complex that results from the interactions between the reactants (except for CO<sub>2</sub>). The CO<sub>2</sub>/TMO coupling catalysed by TBABr is exothermic by 2.5 kcal/mol and the oxetane ring opening is the rate-determining step ( $\Delta G = 42.5$  kcal/mol) (Figure 8, grey). As the intermediate IR1 resulting from the epoxide ring-opening by the bromine anion is not stable, the addition of carbon

dioxide is instantaneous and reaches a more stable intermediate (IR2). Finally, the intramolecular backbiting (TS3) leads to the synthesis of trimethylene carbonate (Figure 9).

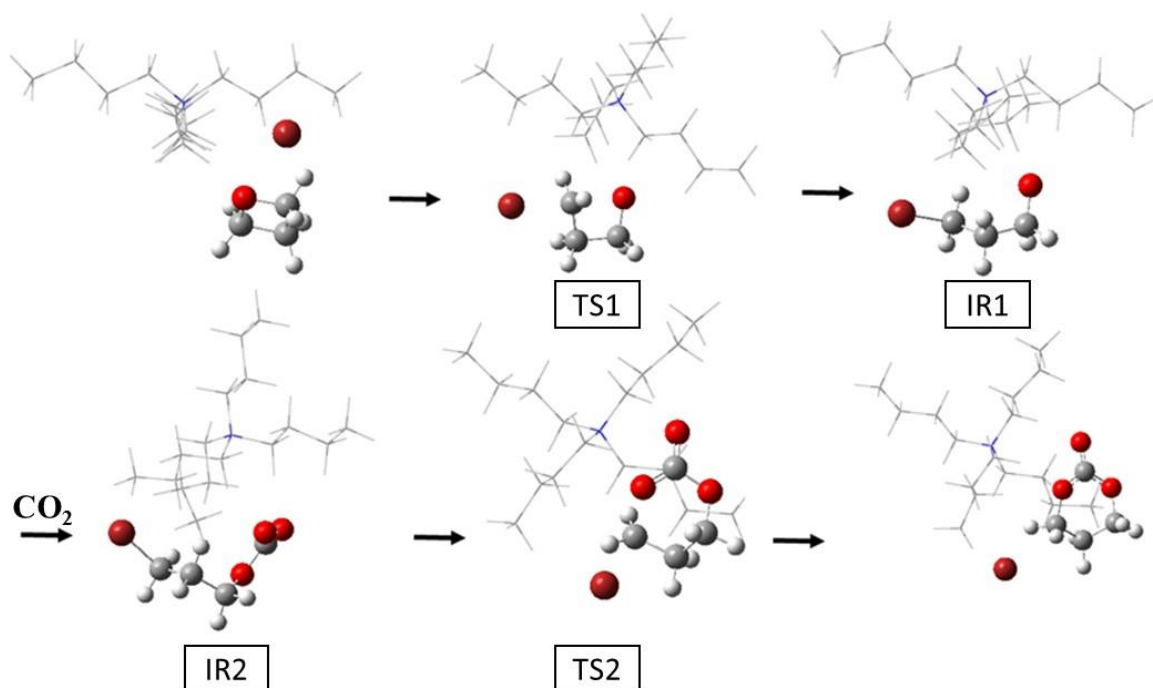


Figure 9: Optimized geometries (Mo6-2X/6-311G(d,p)) of the structures of the CO<sub>2</sub>/TMO coupling in the presence of TBABr (represented using the skeleton model for better clarity).

For the bicomponent catalyst composed of TBABr and 1,3-bis-HFAB (Figure 8, green and Figure 10), the low free energy ( $\Delta G = -24.1$  kcal/mol) of the Van der Waals complex (IRO) demonstrated a strong interaction between the oxetane and the fluorinated diol. To probe this interaction, <sup>1</sup>H titration experiments were done following a previously reported procedure<sup>31, 45</sup> (Figure 11). A downfield shift was observed for both protons of the hexafluoroalcohol moieties and the aromatic proton in *ortho* of these groups. These observations suggest that 1,3-bis-HFAB interacts with TMO and that each hydroxyl group is engaged in a H-bond as found by DFT calculations. Both hexafluoroalcohol moieties activated the O atom of TMO (1.90 and 1.96 Å). Moreover, TMO is stabilized by a third weaker H-bond interaction (2.66 Å) between the O atom and the aromatic proton in *ortho* position of the hexafluoroalcohol groups (Figure 12).

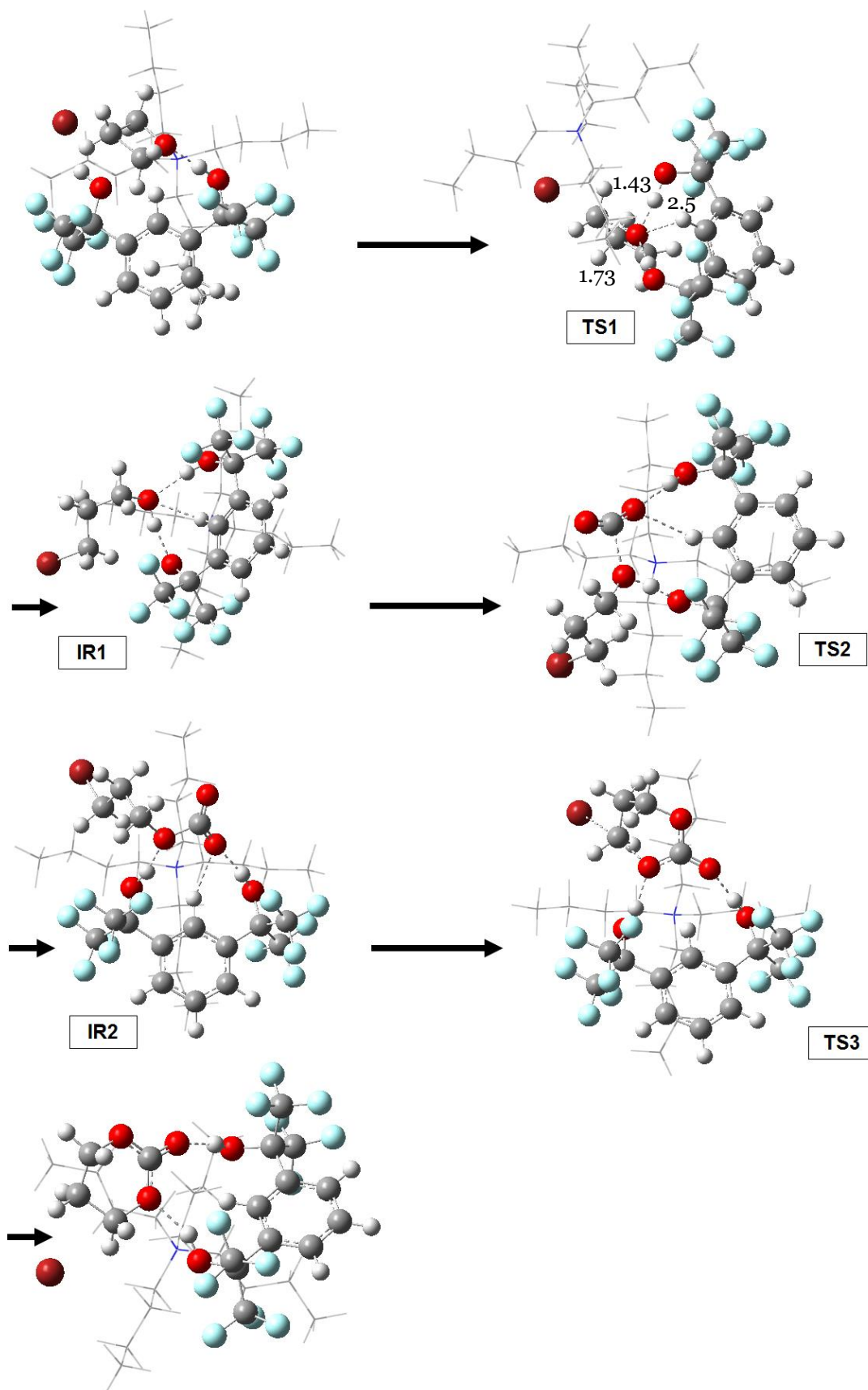


Figure 10: Optimized geometries (Mo6-2X/6-311G(d,p)) of the structures of the CO<sub>2</sub>/TMO coupling in the presence of TBABr (represented using the skeleton model for better clarity) plus 1,3-bis-HFAB as co-catalyst. The dashed lines depict the intermolecular distances in angström.

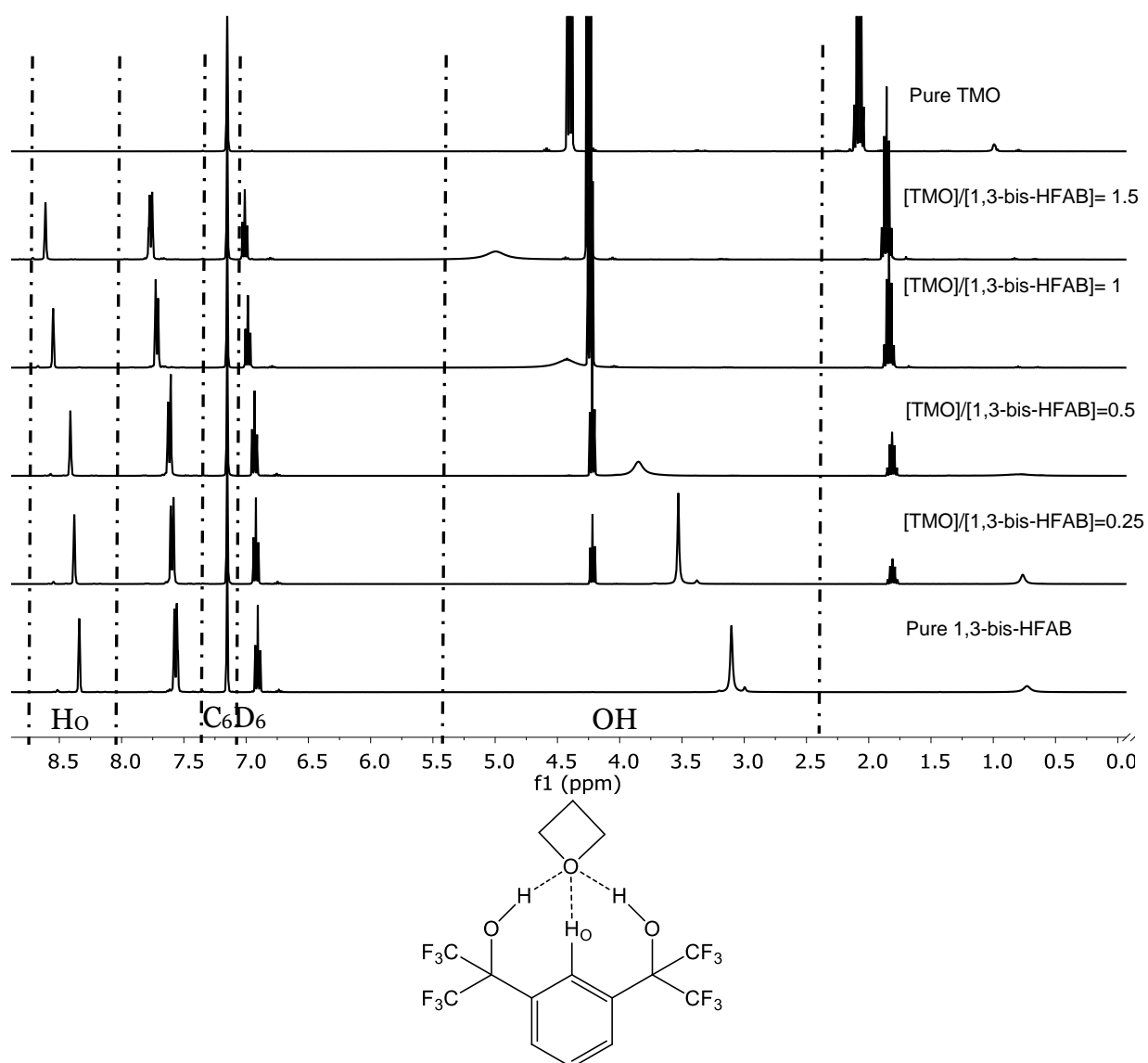
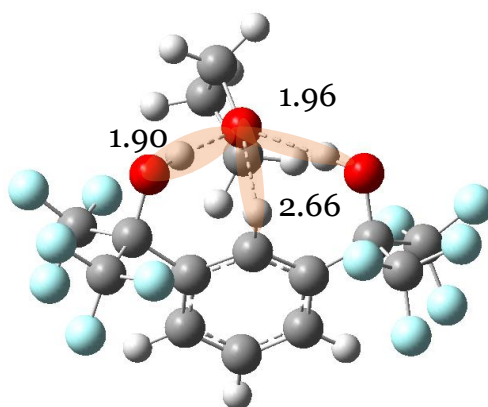


Figure 11:  $^1\text{H}$  NMR titration of TMO by 1,3-bis-HFAB in  $\text{C}_6\text{D}_6$



$$\Delta G = -6.5 \text{ kcal/mol}$$

Figure 12: Optimized structure of the 1,3-bis-HFAB-TMO adduct at the Mo6-2X level using the 6-311G(d,p) basis set. The dashed lines depict the intermolecular distances in angström.

The overall energy of the reaction required to form trimethylene carbonate is lower ( $\Delta G = 31.4$  kcal/mol, Figure 8) than without HBD. The rate-determining step is the TMO ring opening (TS1). In TS1, the fluorinated diol stabilizes the oxygen of the TMO by three intermolecular hydrogen bonds (Figure 10): two strong H-bonds with the OH groups (1.43 and 1.73 Å) and one weak H-bonding with the proton in the *ortho* position (2.50 Å). The ring opening of the oxetane leads to a bromohydrin after the transfer of a H atom from 1,3-bis-HFAB (IR1). As this intermediate is stable, a transition state is observed for the electrophilic attack of CO<sub>2</sub> and the proton migrates back to the fluorinated diol (TS2). The intermediate IR2 is formed and stabilized by hydrogen bonding. The first OH group of 1,3-bis-HFAB interacts with the terminal oxygen while the second OH group stabilizes the O between the two carbons. Finally, the intramolecular ring closure of the bromocarbonate (TS3) regenerates TBABr and TMC is formed.

The mechanism is the same for pyrogallol (Figure 8, red and Figure 13) but the overall energy required for the reaction is higher ( $\Delta G = 35.8$  kcal/mol) than the one reported for 1,3-bis-HFAB. This is due to the stronger interaction with 1,3-bis-HFAB because three intermolecular hydrogen bonds are involved instead of only two for pyrogallol. The conclusions are the same than previously reported for the CO<sub>2</sub>/propylene oxide coupling, *i.e.* the addition of a HBD strongly reduced the Gibbs energy of the reaction in comparison with the system without activator.



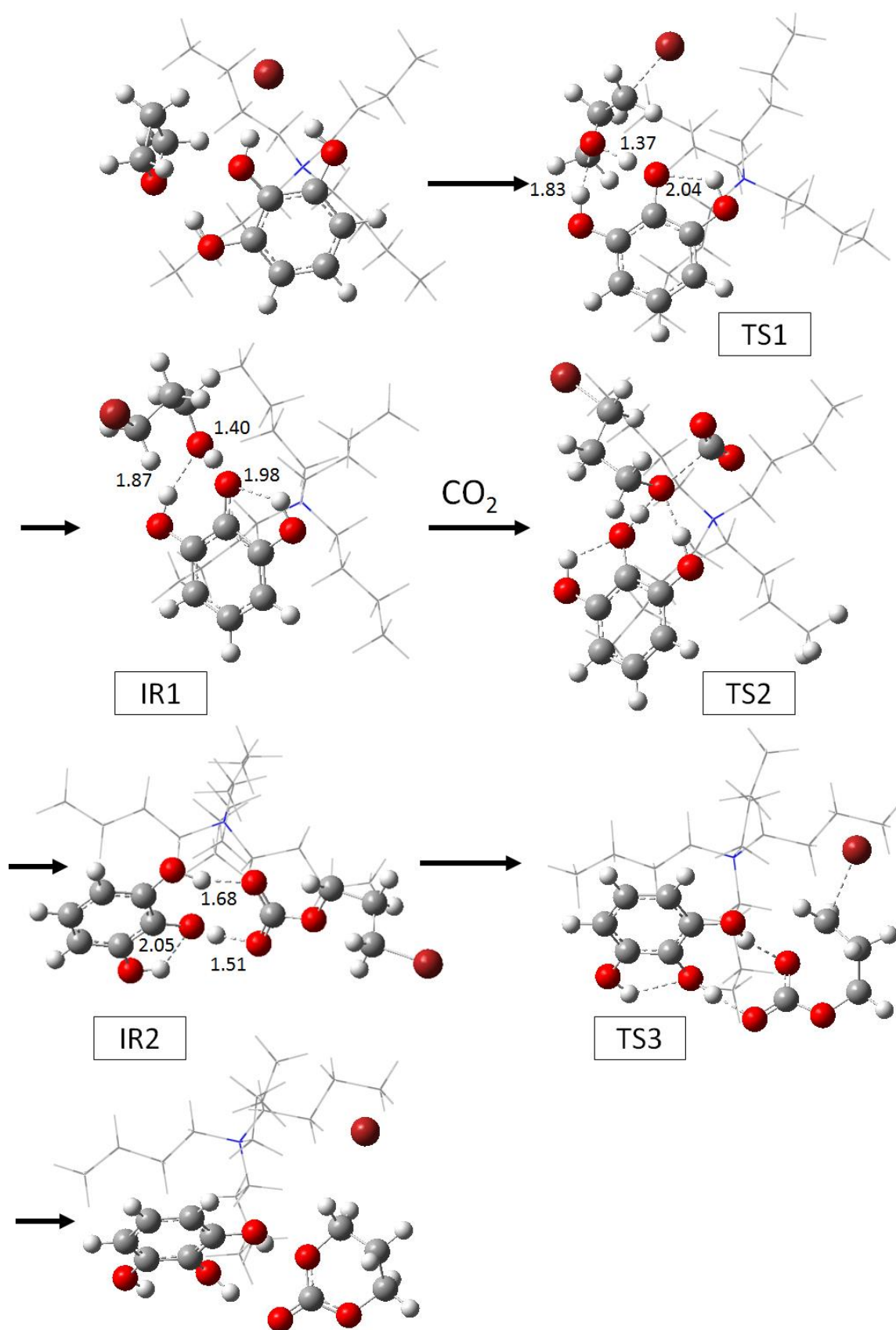
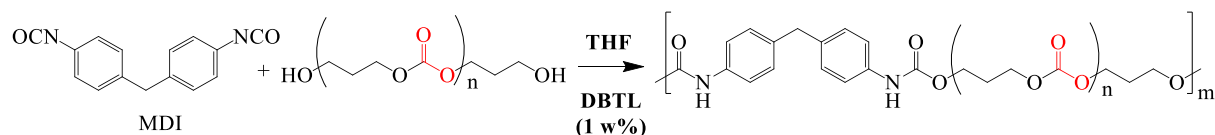


Figure 13: Optimized geometries (Mo6-2X/6-311G(d,p)) of the structures of the CO<sub>2</sub>/TMO coupling in the presence of TBABr (represented using the skeleton model for better clarity) plus pyrogallol as co-catalyst. The dashed lines depict the intermolecular distances in angström.

## 5- CO<sub>2</sub>-based polyurethanes by chain extension of oligocarbonates

CO<sub>2</sub>-based polyurethanes were then synthesized by step-growth polymerization of purified hydroxyl telechelic oligocarbonates ( $M_n = 2000 \text{ g.mol}^{-1}$ ,  $M_w/M_n = 1.3$ ) with 4,4'-methylene diphenyl diisocyanate (MDI) (Scheme 3) in THF using dibutyltin dilaurate (DBTL) as catalyst (1 wt%) under N<sub>2</sub> atmosphere.



Scheme 3: Synthesis of polyurethanes by step-growth polymerization between MDI and the oligocarbonate.

Three formulations with different [oligomers]/[MDI] ratios of 0.67, 1, 1.5 were investigated and the reactions occurred at room temperature overnight. The polycondensation was evidenced by the shift of the SEC trace of oligocarbonate towards lower elution time and the formation of polymers with an apparent  $M_n$  comprised between  $5700 \text{ g.mol}^{-1}$  and  $9200 \text{ g.mol}^{-1}$  and a dispersity between 1.65 and 2.64 (Figure 14). <sup>13</sup>C NMR analysis of the polymer shows the presence of the urethane bond with the signal at 154 ppm that is characteristic of the C=O group of this bond (Figure 15). The <sup>1</sup>H NMR spectrum (Figure 16) also confirms the structure of the main chain of PU with characteristic signals at 4.21 ppm ( $\text{CH}_2\text{-O-C(O)NH-}$ ), 3.89 ppm ( $\text{Ph-CH}_2\text{-Ph}$ ), 7.50 ppm and 7.19 ppm (aromatic protons).

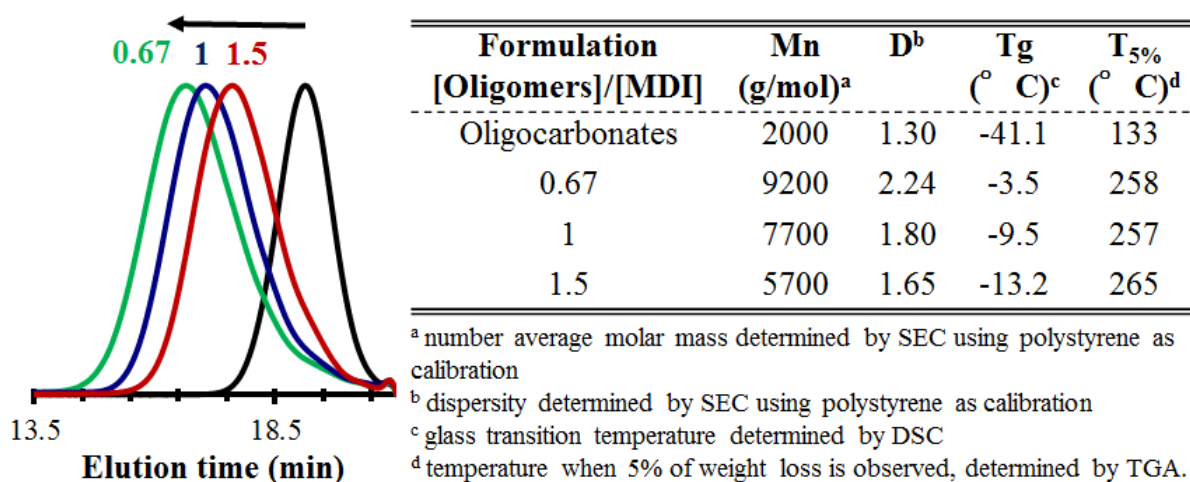


Figure 14: a) Evolution of SEC traces after chain extension of oligocarbonates as a function of the [Oligomer]/[MDI] molar ratio, b) Macromolecular characteristics and thermal properties of oligocarbonate and poly(carbonate-co-urethane)s prepared by step-growth polymerization of telechelic oligocarbonate and 4,4'-MDI using different formulations.

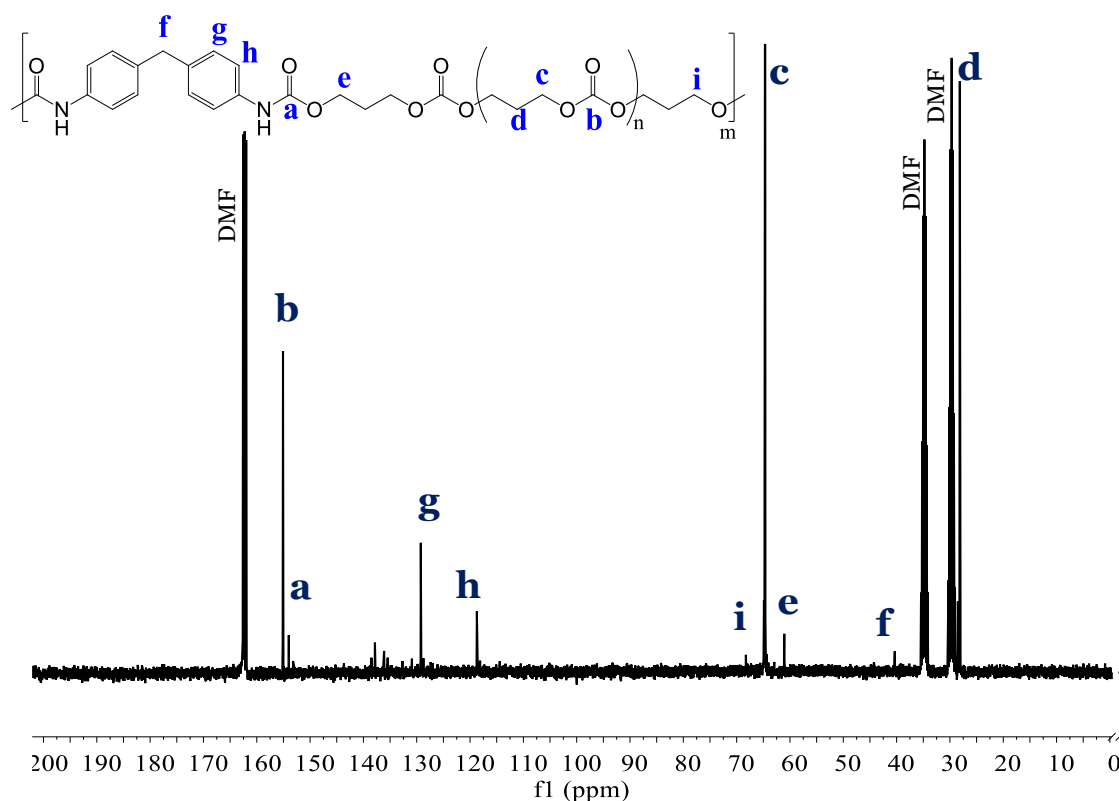


Figure 15:  $^{13}\text{C}$  NMR spectrum in DMF of copolymer poly(carbonate-co-urethane) obtained by chain extension of the oligocarbonate polyol with MDI ([oligomers]/[MDI] = 0.67) catalysed by DBTL. Polymer was purified by precipitation in methanol.

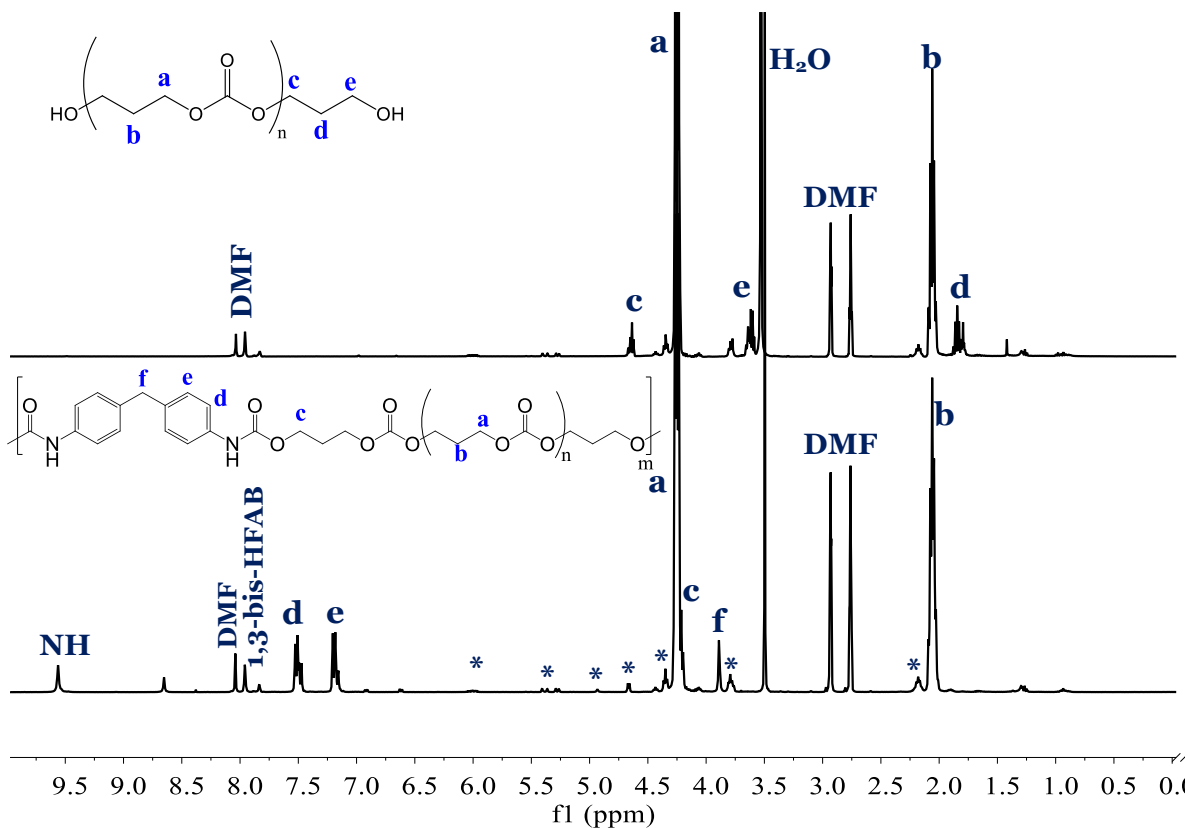


Figure 16: Overlay of  $^1\text{H}$  NMR spectra in  $\text{DMF-d}_7$  of oligocarbonate and copolymer poly(carbonate-co-urethane) obtained by chain extension of the oligocarbonates polyols with MDI ([oligomers]/[MDI] = 0.67) catalysed by DBTL. Polymer was purified by precipitation in methanol. \* oligocarbonates defects (ether links and alkylene chain-ends).

The overlay of the SEC traces highlights that the PU molar mass increased with the decrease of the [oligomer]/[MDI] molar ratio (MDI in excess). This was assigned to i) the presence of side reactions during the PU formation because of the presence of water traces that react with the diisocyanate to produce amines; ii) to the use of an apparent oligocarbonate  $M_n$  in the calculation of the optimum oligomer/MDI molar ratio and/or iii) the absence of quantification of the OH chain-ends by titration. Moreover, the disappearance of the signals corresponding to hydroxyl chain-ends of the oligomers at 1.84 ppm ( $-\text{CH}_2-\text{CH}_2-\text{CH}_2-\text{OH}$ ) and 3.62 ppm ( $-\text{CH}_2-\text{CH}_2-\text{CH}_2-\text{OH}$ ) for the [oligomer]/[MDI] molar ratio of 0.67 confirms that all the chain-end reacted to form urethane bonds (Figure 16).

The specific defects of the oligocarbonate chain (ether linkages and some alkene chain-end) are still visible in the  $^1\text{H}$  spectrum of the poly(carbonate-co-urethane)s. Furthermore, characteristic signals at 7.96 and 7.83 ppm and 136 - 138 ppm in the  $^1\text{H}$  and  $^{13}\text{C}$  NMR spectra, respectively, evidenced the presence of traces of fluorinated alcohol (1,3-bis-HFAB) that was difficult to completely remove by dialysis. These poly(carbonate-co-urethane)s were found stable to a temperature up to 250°C whereas the starting oligocarbonate already decomposed at 135°C (Figure 17). The glass transition temperature also shifted from -41°C for oligocarbonate to -3°C for PU of  $M_n = 9200 \text{ g.mol}^{-1}$  as the result of the incorporation of the aromatic hard segment (Figure 14b and Figure 18). This preliminary study shows that the formulation enables to modulate the final properties of the  $\text{CO}_2$ -based PUs by using the same starting products, facilitating the tailor-made production of materials dedicated to a precise application.

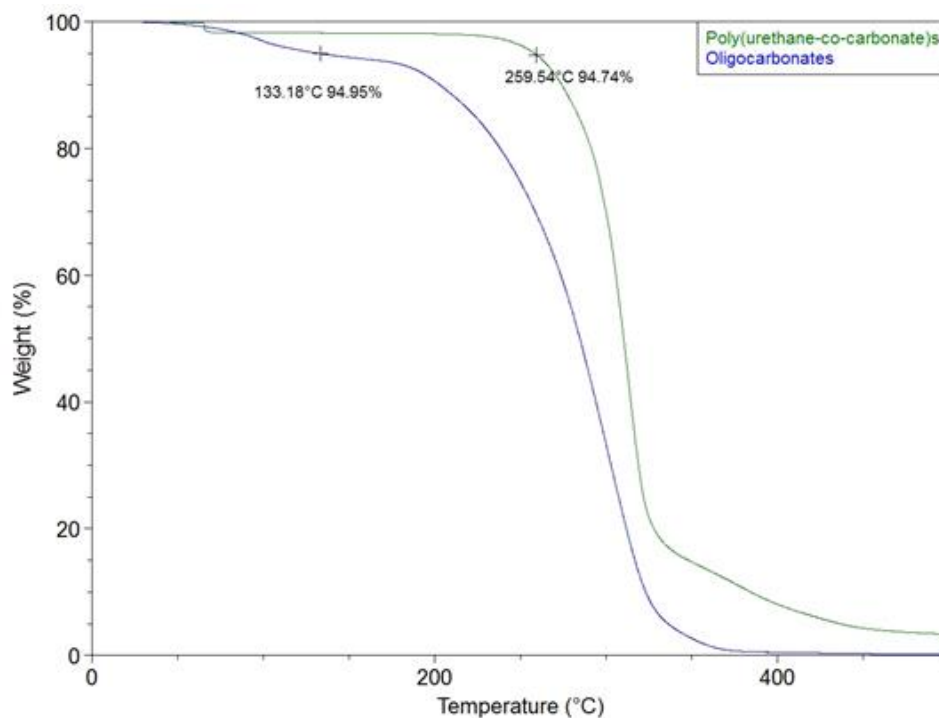


Figure 17: Thermogravimetric analysis of telechelic oligocarbonate (blue) and poly(carbonate-co-urethane) produced by chain extension of oligocarbonate with MDI ([oligocarbonate]/[MDI]=0.67) (green).

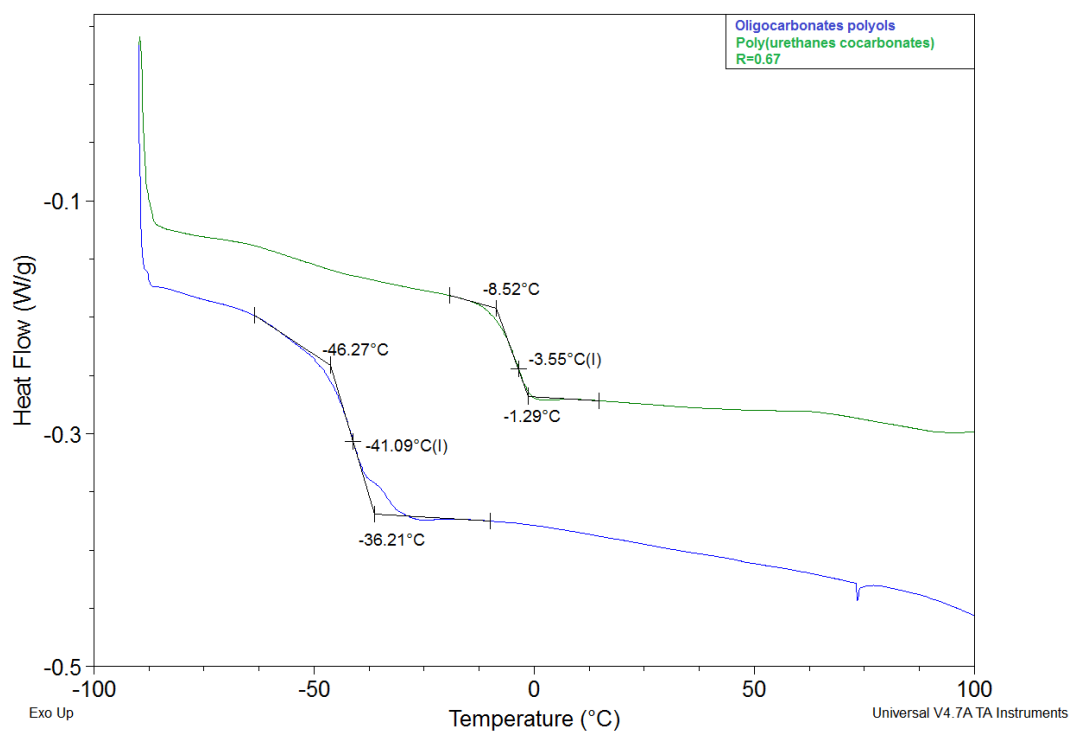


Figure 18: DSC thermograms of telechelic oligocarbonate (blue) and poly(carbonate-co-urethane) produced by chain extension of oligocarbonate with MDI ([oligocarbonate]/[MDI]=0.67) (green)

## Conclusions

In this contribution, we have reported the first metal-free oxetane/ $\text{CO}_2$  coupling using an organocatalytic system composed of an ammonium salt as catalyst and a hydrogen bond donor (HBD) as co-catalyst. Amongst the different HBDs tested, 1,3-bis-(hydroxyhexafluoroisopropyl)-benzene (1,3-bis-HFAB) was found to be the most efficient one. After optimizing the reaction conditions (mainly the temperature and the pressure), the combination of 1,3-bis-HFAB with tetrabutylammonium iodide produced  $\alpha,\omega$ -hydroxyl telechelic oligocarbonate with a high selectivity ( $\sim 98\%$ ) at  $130^\circ\text{C}$ , as demonstrated by  $^1\text{H}$  NMR analysis and supported by MALDI-ToF characterizations. A detailed kinetic study by ATR-IR combined with DFT calculations and  $^1\text{H}$  NMR titrations allowed us to propose a reaction mechanism for the formation of this  $\alpha,\omega$ -hydroxyl telechelic oligocarbonate. The six-membered cyclic carbonate (trimethylene carbonate, TMC) was *in-situ* generated in the first step of the process by coupling trimethylene oxide (TMO) with  $\text{CO}_2$ . Its hydrolysis rapidly produced 1,3-propanediol that initiated the ring-opening polymerization of TMC to form the telechelic oligomers. Both the TMO/ $\text{CO}_2$  coupling and TMC hydrolysis steps are facilitated by activation of TMO and TMC by hydrogen bondings with 1,3-bis-HFAB. Finally,  $\text{CO}_2$ -based poly(carbonate-co-urethane)s were synthesized by step-growth polymerization of the hydroxyl telechelic oligocarbonate with MDI. The organocatalytic system described in this paper constitutes therefore an innovative route to the preparation of hydroxyl telechelic carbonates, of high interest for many applications, notably for the polyurethane business, especially for coatings or foams. This system proved to be robust and efficient because commercially available starting products were used as received, and the process did not require prior reagents purification or drying.

## References

1. A. C. Kathalikkattil, R. Babu, J. Tharun, R. Roshan and D.-W. Park, *Catalysis Surveys from Asia*, 2015, **19**, 223-235.
2. P. P. Pescarmona and M. Taherimehr, *Catalysis Science & Technology*, 2012, **2**, 2169-2187.
3. C. Maeda, Y. Miyazaki and T. Ema, *Catalysis Science and Technology*, 2014, **4**, 1482-1497.
4. M. North, R. Pasquale and C. Young, *Green Chemistry*, 2010, **12**, 1514-1539.
5. Q. He, J. W. O'Brien, K. A. Kitselman, L. E. Tompkins, G. C. T. Curtis and F. M. Kerton, *Catalysis Science and Technology*, 2014, **4**, 1513-1528.
6. M. Cokoja, M. E. Wilhelm, M. H. Anthofer, W. A. Herrmann and F. E. Kühn, *ChemSusChem*, 2015, **8**, 2436-2454.
7. C. Martín, G. Fiorani and A. W. Kleij, *ACS Catalysis*, 2015, **5**, 1353-1370.
8. H. Koinuma and H. Hirai, *Die Makromolekulare Chemie*, 1977, **178**, 241-246.
9. D. J. Darensbourg, W. Choi, P. Ganguly and C. P. Richers, *Macromolecules*, 2006, **39**, 4374-4379.
10. D. J. Darensbourg and A. I. Moncada, *Macromolecules*, 2009, **42**, 4063-4070.
11. D. J. Darensbourg and A. I. Moncada, *Macromolecules*, 2010, **43**, 5996-6003.
12. D. J. Darensbourg, A. I. Moncada, W. Choi and J. H. Reibenspies, *Journal of the American Chemical Society*, 2008, **130**, 6523-6533.
13. D. J. Darensbourg and A. I. Moncada, *Inorganic Chemistry*, 2008, **47**, 10000-10008.
14. A. Baba, H. Kashiwagi and H. Matsuda, *Tetrahedron Letters*, 1985, **26**, 1323-1324.
15. A. Baba, H. Meishou and H. Matsuda, *Die Makromolekulare Chemie, Rapid Communications*, 1984, **5**, 665-668.
16. C. J. Whiteoak, N. Kielland, V. Laserna, E. C. Escudero-Adán, E. Martin and A. W. Kleij, *Journal of the American Chemical Society*, 2013, **135**, 1228-1231.
17. C. J. Whiteoak, E. Martin, M. M. Belmonte, J. Benet-Buchholz and A. W. Kleij, *Advanced Synthesis and Catalysis*, 2012, **354**, 469-476.
18. J. Rintjema, W. Guo, E. Martin, E. C. Escudero-Adán and A. W. Kleij, *Chemistry – A European Journal*, 2015, **21**, 10754-10762.
19. D. J. Darensbourg, A. Horn Jr and A. I. Moncada, *Green Chemistry*, 2010, **12**, 1376-1379.
20. D. J. Darensbourg, A. I. Moncada and S. H. Wei, *Macromolecules*, 2011, **44**, 2568-2576.
21. A. Edwards, R. J. Carson, M. Szycher and S. Bowald, *Journal of Biomaterials Applications*, 1998, **13**, 23-45.
22. E. M. Christenson, M. Dadsetan, M. Wiggins, J. M. Anderson and A. Hiltner, *Journal of Biomedical Materials Research Part A*, 2004, **69A**, 407-416.
23. K. L. Kull, R. W. Bass, G. Craft, T. Julien, E. Marangon, C. Marrouat and J. P. Harmon, *European Polymer Journal*, 2015, **71**, 510-522.

24. B. Ochiai, H. Amemiya, H. Yamazaki and T. Endo, *Journal of Polymer Science Part A: Polymer Chemistry*, 2006, **44**, 2802-2808.
25. J. Řezáč and P. Hobza, *J. Chem. Theory Comput.*, 2012, **8**, 141-151.
26. M. J. S. Dewar, E. G. Zoebisch, E. F. Healy and J. J. P. Stewart, *Journal of the American Chemical Society*, 1985, **107**, 3902-3909.
27. AMPAC 10, © 1992-2013 Semichem, Inc. PO Box 1649, Shawnee, KS 66222
28. M. J. Frisch and A. D. Becke, Gaussian 09, Revision A.02, 2009, 98, 5648-5652
29. Y. Zhao and D. G. Truhlar, *Theoretical Chemistry Accounts*, 2008, **120**, 215-241.
30. M. Alves, B. Grignard, S. Gennen, R. Mereau, C. Detrembleur, C. Jerome and T. Tassaing, *Catalysis Science and Technology*, 2015, **5**, 4636-4643.
31. S. Gennen, M. Alves, R. Méreau, T. Tassaing, B. Gilbert, C. Detrembleur, C. Jerome and B. Grignard, *ChemSusChem*, 2015, **8**, 1845-1849.
32. M. Alves, B. Grignard, S. Gennen, C. Detrembleur, C. Jerome and T. Tassaing, *RSC Advances*, 2015, **5**, 53629-53636.
33. The activity order of the the halide cannot be generalized and depends of many parameters (nature of the epoxide, nature of the cocatalyst, solvent, etc.). However, the same order was found for some catalytic systems.
34. H. Büttner, K. Lau, A. Spannenberg and T. Werner, *ChemCatChem*, 2015, **7**, 459-467.
35. L. Wang, G. Zhang, K. Kodama and T. Hirose, *Green Chemistry*, 2016, **18**, 1229-1233.
36. M. E. Wilhelm, M. H. Anthofer, M. Cokoja, I. I. E. Markovits, W. A. Herrmann and F. E. Kühn, *ChemSusChem*, 2014, **7**, 1357-1360.
37. A. M. Hardman-Baldwin and A. E. Mattson, *ChemSusChem*, 2014, **7**, 3275-3278.
38. H. Büttner, J. Steinbauer and T. Werner, *ChemSusChem*, 2015, **8**, 2655-2669.
39. C. J. Whiteoak, A. Nova, F. Maseras and A. W. Kleij, *ChemSusChem*, 2012, **5**, 2032-2038.
40. C. J. Whiteoak, A. H. Henseler, C. Ayats, A. W. Kleij and M. A. Pericàs, *Green Chemistry*, 2014, **16**, 1552-1559.
41. L. Martínez-Rodríguez, J. Otalora Garmilla and A. W. Kleij, *ChemSusChem*, 2016, **9**, 749-755.
42. Y. Márquez, L. Franco and J. Puiggali, *Thermochimica Acta*, 2012, **550**, 65-75.
43. S. Honda and H. Sugimoto, *Journal of Polymer Science, Part A: Polymer Chemistry*, 2016, **54**, 3336-3342.
44. M. Alves, R. Mereau, B. Grignard, C. Detrembleur, C. Jerome and T. Tassaing, *RSC Advances*, 2016, **6**, 36327-36335.
45. O. Coulembier, D. P. Sanders, A. Nelson, A. N. Hollenbeck, H. W. Horn, J. E. Rice, M. Fujiwara, P. Dubois and J. L. Hedrick, *Angewandte Chemie - International Edition*, 2009, **48**, 5170-5173.





---

## General conclusions and outlooks

---



In an effort to valorise CO<sub>2</sub> as a cheap and inexhaustible C<sub>1</sub> source of carbon, this work aimed at developing new efficient and versatile homogeneous organocatalysts enabling the fast and selective cycloaddition of CO<sub>2</sub> onto series of oxiranes (terminal epoxides, epoxidized vegetable oils) and oxetanes under mild experimental conditions. As synergisms exist between hydrogen bond donors compounds and organic salts or ionic liquids for the CO<sub>2</sub>/epoxides, the new binary catalyst that we proposed combined the use of onium salts or ionic liquids with fluorinated alcohols to boost the reactions. This approach was quite challenging and risky as previous works showed that hexafluoroisopropanol had a detrimental effect on the epoxide/CO<sub>2</sub> coupling when it was used as solvents as no product was formed.

Catalytic amounts of fluorinated alcohols used as HBDs combined with nBu<sub>4</sub>N<sup>+</sup>X<sup>-</sup> salts (with X<sup>-</sup> = I<sup>-</sup> or Br<sup>-</sup>) efficiently promoted the neat epoxides conversion into the corresponding cyclic carbonates. As CO<sub>2</sub> was used in large excess and no by-products were formed, the CO<sub>2</sub>/epoxide coupling reactions followed a pseudo-first order kinetics. Using online Raman and *in-situ* FTIR spectroscopy under pressure, reaction kinetics of the CO<sub>2</sub>/epoxide coupling catalysed by the bicomponent catalytic system composed of nBu<sub>4</sub>N<sup>+</sup>X<sup>-</sup> salts and HBD were monitored and kinetic rates constants were extracted. For a model epoxide (1,2-epoxydodecane), the kinetics were increased by 300% by simple addition of 1 equivalent of 1,1,1-trifluoro-2-methyl-2-propanol (compared to tetrabutylammonium iodide (TBAI)). The co-catalytic activity of fluorinated alcohols increased with an increasing number of trifluoromethyl substituents of the HBDs in the order 1,1,1-trifluoro-2-methyl-2-propanol < hexafluoro-*tert*-butanol < perfluoro-*tert*-butanol. Interestingly, online kinetic studies show that 1,3-bis-(2-hydroxyhexafluoroisopropyl)benzene (1,3-bis-HFAB), a fluorinated diol, was the most efficient hydrogen bond donor and displayed the highest co-catalytic activity enabling the remarkably fast and selective CO<sub>2</sub>/epoxide coupling under moderate temperature (60 - 80°C) and even at atmospheric pressure. For sake of comparison, the non-fluorinated counterpart of 1,3-bis-HFAB had no co-catalytic activity assessing for the positive impact of replacing methyl group by trifluoromethyl substituents to boost the reaction.

In an effort to assess for the better co-catalytic performances of fluorinated alcohols compared to existing HBDs, a rational investigation of the co-catalytic activity of commercially available hydrogen bond donors reported in the literature for fastening the conversion of model epoxides was conducted using *in-situ* near FTIR spectroscopy under mild conditions (60°C, 2 MPa). The co-catalytic performances of fluorinated alcohols, especially 1,3-bis-HFAB impressively surpassed the ones of triethanolamine, fructose or phenol derivatives. The kinetics of CO<sub>2</sub>/PO coupling were systematically and significantly faster with perfluoro-*tert*-butanol, hexafluoro-(*p*-tolyl)-isopropanol and 1,3-bis-HFAB. Remarkably, the kinetic rate constant was increased by 230% with 1,3-bis-HFAB compared to pyrogallol reported as the most performant co-catalyst in the literature. At 60°C and 2 MPa, the PO conversion was quantitative after only 100 minutes. As expected, increasing the temperature and the pressure significantly fasten the CO<sub>2</sub>/epoxide coupling. Then, the scope of epoxide

was enlarged to styrene oxide, glycidol, cyclohexene oxide. The binary TBABr/fluorinated alcohol catalytic system always fastened the reaction compared to the CO<sub>2</sub>/epoxide coupling catalysed by TBABr as sole catalyst and allowed for the selective formation of the corresponding cyclic carbonate. However, the conversion of disubstituted internal epoxides such as cyclohexene oxide was slower than the ones of terminal epoxides consistently with results reported in the literature.

Then, the use of these new binary catalysts was extended with success to the organocatalytic synthesis of carbonated linseed oil (CLSO) by CO<sub>2</sub>/epoxidized linseed oil (ELSO) coupling. First, a series of organic salts and ionic liquids were screened as catalyst. The catalytic activity evolved with the cation structure and decreased in the order: guanidinium > ammonium ~ imidazolium > phosphonium ~ amidinium > pyrrolidinium > pyridinium. Besides, the influence of the halide anion on the kinetics was also studied. Bromine was the most efficient anion because it offers the best size/nucleophilicity compromise. Even though bromide is less nucleophilic than iodine, its smaller size favours its faster diffusion into the viscous oil toward the internal epoxides function. Then, the bicomponent organocatalytic platforms composed of TBABr and commercially available (multi)phenolic derivatives or fluorinated alcohols were screened. Multiphenolic activators derived from catechol or pyrogallol and fluorinated alcohols displayed the highest activity (excepted for trifluoro-*tert*-butanol). A detailed kinetic study by *in-situ* FTIR spectroscopy demonstrated that 1,3-bis-HFAB still remained the most efficient co-catalyst among those hydrogen-bond donor activators. The impact of several parameters (temperature, pressure, catalyst loading, amount of CO<sub>2</sub> dissolved on the ELSO) on the kinetics was then also investigated by online FTIR spectroscopy. The reaction was favoured at high temperature (120°C) and high pressure (5 MPa) even if the concentration of CO<sub>2</sub> in the oil phase decreases by increasing the temperature. The synthesis of CLSO was quantitative after 600 minutes. But, even at high temperature and pressure, the conversion of ELSO bearing internal disubstituted epoxides into CLSO was slower than the one of model terminal epoxides because of the increased steric hindrance. However, our catalytic system is suitable to speed up the CO<sub>2</sub>/epoxidized vegetable oil coupling compared to other binary organocatalysts reported in the literature.

A DFT study was then conducted to elucidate the activation mechanism and the key parameters influencing the co-catalytic activity of fluorinated alcohols. The most favourable mechanism is a three steps pathway composed of the epoxide ring-opening, the CO<sub>2</sub> insertion and the carbonate ring-closure. The DFT calculations correlated with the NMR titrations demonstrate that a strong multiple interaction exists between the 1,3-bis-HFAB and the O atom of the epoxide. Aside from the two strong hydrogen-bonds with both hexafluoroalcohol groups, a third weak interaction exists between the O donor atom of the epoxide and the aromatic proton in *ortho* position of the hexafluoroalcohol groups. This triple interaction enables the strong epoxide activation and stabilization of each transition states (TS) and intermediates of reaction (IR) and decreases the Gibbs energy. The Gibbs energy of the rate

determining step of the reaction, i.e. the epoxide ring-opening, is reduced from 33.7 kcal.mol<sup>-1</sup> with TBABr to 3.8 kcal.mol<sup>-1</sup> with the binary catalyst composed of TBABr and 1,3-bis-HFAB. The activation mechanism was similar with pyrogallol but only two hydroxyl groups were engaged in the stabilization of the epoxide. The third OH groups stabilized the vicinal one by intramolecular hydrogen bond. The superior activity of 1,3-bis-HFAB compared to pyrogallol probably arises from the stronger stabilization mechanism. Besides, the co-catalytic efficiency of fluorinated mono-alcohols is attributed to the activation of the epoxide and the cooperative stabilization of all TSs and IRs by two fluorinated molecules. DFT calculations also highlight that trifluoromethyl groups significantly influence the charge distribution of the hydrogen bond donor and, notably, the acidity of the hydrogen of the hydroxyl moiety that strengthens the interactions.

Finally, we took profit of the versatility and unprecedented catalytic activity of the binary ammonium salt/fluorinated catalytic platform to selectively synthesize telechelic  $\alpha,\omega$ -hydroxyl oligocarbonates by the CO<sub>2</sub>/oxetane coupling. This catalytic system is the first enabling the conversion of oxetanes into added value products by metal-free catalysis. As oxetanes are less reactive than epoxides, higher temperature and pressure (130°C, 10 MPa) were used. 1,3-bis-HFAB was thermally stable under those optimized conditions whereas others organic co-catalysts such as pyrogallol degrades themselves. First, NMR titrations and DFT calculations highlighted that the fluorinated diol, 1,3-bis-HFAB, strongly interacted with the less reactive oxetanes by hydrogen bonding and significantly reduced the Gibbs energy of the rate determining oxetane ring-opening step to 6.4 kcal.mol<sup>-1</sup> compared to the reaction using TBABr as sole catalyst (39.9 kcal.mol<sup>-1</sup>). The detailed investigation of the mechanism by online FTIR reveals that trimethylene carbonate (TMC) is formed. However, the six-membered cyclic carbonate is decomposed into 1,3-propanediol by hydrolysis in the presence of water residues. Then, 1,3-propanediol acts as an initiator that induced the ring opening of TMC to form oligocarbonates ( $M_n = 2000$  g.mol<sup>-1</sup>,  $\bar{D} = 1.3$ ). In addition, as 1,3-bis-HFAB also strongly interacts with the six-membered cyclic carbonate, it is likely that it could catalysed the ring-opening of TMC. The fine structure of oligocarbonates was elucidated by combining NMR and Mass spectroscopy analysis highlighting that around 10% of the chain-ends are olefinic. In a second step, CO<sub>2</sub>-based poly(urethane-co-carbonate)s were synthesized by chain extension of oligocarbonates with a diisocyanate. CO<sub>2</sub>-sourced polymers with a molar mass up to 9200 g.mol<sup>-1</sup> ( $\bar{D} = 2.24$ ) were synthesized. The poly(urethane-co-carbonate)s are stable up to 250°C whereas the oligocarbonates start to decompose at 135°C. Similarly, the glass transition temperature is shifted from -41°C ( $M_n = 2000$  g.mol<sup>-1</sup>) for the oligocarbonates to -3°C for PU ( $M_n = 9200$  g.mol<sup>-1</sup>). Therefore, the insertion of a hard segment onto the polymer backbone improves the properties of the poly(urethane-co-carbonate)s and opens the door to their use for coating or foam applications.

Even if the fluorinated diol is used in catalytic amount (3 mol%) and the tetrabutylammonium salts are cheap and readily available, the TBABr/1,3-bis-HFAB

bicomponent system is homogeneous and the catalyst cannot be easily extracted and recycled. Therefore, heterogeneous catalysts would be more profitable for easy recycling or performing reactions under continuous flow conditions. The outlooks of this thesis concern the development of a bicomponent supported organocatalyst by grafting the fluorinated diol and the ammonium salts onto a solid support such as silica or polystyrene beads. However, the activity of supported catalysts is generally reduced compared to the homogenous analogues and harsher conditions or a solvent are used to afford reasonable epoxides conversion in short reaction times. Such experimental conditions could favour the thermal degradation of the ammonium salts. Therefore, the performances of homogeneous/heterogeneous combined catalysts consisting of thermally stable fluorinated alcohols immobilized onto a support used in combination with free ammonium salts could be evaluated. Besides, this project also demonstrates that molecular modelling using DFT calculations is a powerful tool to determine the activation mechanism of catalysts and quantitatively compare their activity. Therefore, computational studies should be continued to guide and fasten the development of new efficient metal- and halide-free catalysts as competitive as metal-based ones under room temperature and atmospheric pressure. This would avoid the presence of metal residues in the product and prevent the corrosion of the process installations. Finally, elaboration of new valorising routes of CO<sub>2</sub>-based products should be investigated, for example by using (bio-based) cyclic carbonates as intermediates for the synthesis of CO<sub>2</sub>-based polymers such as polycarbonates and polyurethanes.

---

## Appendix:

DFT investigation of the reaction mechanism for the guanidine catalysed ring-opening of cyclic carbonates by aromatic and alkylamines

---



## Abstract

The guanidine catalyzed aminolysis of propylene carbonate has been investigated using the density functional theory (DFT) and highlights that different reaction pathways are involved depending on the aromatic or aliphatic nature of the amine. The structural ability of 1,5,7-triazabicyclo[4.4.0]dec-5-ene (TBD) to simultaneously give and receive protons was demonstrated by a detailed mechanistic investigation. The bifunctional activity (base/H-bond donor) of TBD significantly reduces the Gibbs energy of the reaction and allows understanding its higher efficiency compared to its methyl counterpart (MTBD).

## Table of contents

Introduction.....	211
Experimental .....	212
Computational details.....	212
Results and discussion.....	213
1. Cyclic carbonate – amine coupling without catalyst.....	213
2. Cyclic Carbonate – aniline coupling with TBD and MTBD catalyst .....	215
3. Cyclic Carbonate – methylamine coupling with TBD and MTBD catalyst .....	219
4. Cyclic Carbonate – cyclohexylamine coupling with TBD catalyst .....	222
Conclusion .....	224
References.....	225

## Introduction

In the last years, developing greener and safer alternatives to the conventional synthesis of polyurethanes (PUs) from isocyanates and polyols has attracted increasing interest to respond to regulation and environmental changes. The most frequently studied and promising route relies on the polyaddition of bis-5-membered cyclic carbonates with diamines, leading to the formation of PolyHydroxyUrethanes (PHUs)<sup>1-7</sup> that are mainly exploited for coating applications or as cross-linked materials for thermosets or elastomers<sup>8-10</sup> or as foamed materials<sup>11</sup>. Beside the improved mechanical and chemical properties of PHUs over conventional PUs<sup>12</sup>, this chemical pathway also offers the benefit of substituting toxic isocyanates and their phosgene precursors by CO<sub>2</sub>, an abundant, renewable and environmentally friendly chemical to produce cyclic carbonate precursors entering the synthesis of PHUs.<sup>13-18</sup> The addition of amines onto cyclic carbonates is governed by several parameters such as the temperature, the nature of the solvent, the solubility, the concentration and the chemical structure of the reactants. In particular, the chemical structure of the amine has a significant impact on the reaction/polymerization rates and yields.<sup>19-22</sup> Moreover it was shown that aryl amines are less reactive or even non-reactive towards cyclic carbonates compared to the aliphatic ones. Although nucleophilic alkylamines induce ring opening of cyclic carbonates, this aminolysis reaction is generally slow and the use of catalysts able to activate the cyclic carbonate is generally required to accelerate the reaction. Many catalysts have been proposed to promote the hydroxyurethane formation at low temperature within short reaction time.<sup>19, 20, 22-25</sup> Maisonneuve *et al.*<sup>24</sup> screened various catalysts (Schreiner catalyst, LiCl, DBU, ZnAc, MTBD) for a model solvent-free reaction between propylene carbonate and hexylamine. If these catalysts were effective at the early stage of the reaction, they were deactivated after 1 h with conversions that were similar to those noted for the uncatalyzed model reaction. This could be due to the high H-bonds density progressively formed during the conversion in the bulk phase. Blain *et al.*<sup>20</sup> carried out a rational investigation of catalytic systems for the aminolysis of model cyclic carbonates by amines in organic solvents. Organocatalysts such as TBD (1,5,7-triazabicyclo[4.4.0]dec-5-ene), phosphines, phosphazenes, cyclohexylphenyl thiourea and more recently urea<sup>26</sup> were found to display a higher efficiency than inorganic Lewis acids (MgBr<sub>2</sub>, FeCl<sub>3</sub>, Fe(OTf)<sub>3</sub>...). The same conclusion was drawn from the investigation of Lambeth *et al.*<sup>19</sup> who found TBD as the most potent organocatalyst to fasten the step-growth polymerization of bis-cyclic carbonates and amines. In addition, PHUs synthesized in the presence of TBD at room temperature showed higher molar mass than the corresponding polymers produced in the absence of catalyst.<sup>27</sup> However, with or without catalyst, the so-produced PHUs exhibited low molar masses which probably arised from side reactions as recently proposed by Caillol *et al.*<sup>28</sup> To explain the higher catalytic efficiency of TBD, the authors proposed that this guanidine derivative could potentially act as a bifunctional nucleophilic catalyst as reported previously in quantum chemical studies for the Ring Opening

Polymerization (ROP) of esters,<sup>29-31</sup> the intramolecular aldol reaction of acyclic ketoaldehyde<sup>32</sup> or the hydrolysis of acetonitrile.<sup>33</sup> The mechanism of the uncatalysed hydroxyurethane formation by aminolysis of carbonate was previously investigated in detail by Zabalov *et al.*<sup>34-36</sup> using DFT calculations. They established that the reaction might progress notably throughout a six-centre ring intermediate based on the 5-membered cyclic carbonate and two amine molecules, one playing a catalytic role. Moreover, they highlighted that acetic acid could act as a bifunctional catalyst decreasing the activation energy by concerted protons transfers.<sup>37</sup> More recently, Kleij *et al.*<sup>22, 38</sup> reported that TBD was an effective organocatalyst for the challenging formation of N-aryl carbamates from cyclic carbonates and aromatic amines. In addition, they reported a DFT investigation that evidenced the differences in the TBD mediated mechanisms with aniline and butylamine. Although the catalytic role of TBD as proton donor and acceptor was highlighted, the activation pathway differs from previous DFT calculations studies involving concerted proton transfer.<sup>30, 32, 33</sup>

In our continuous effort to promote the organocatalytic synthesis of PHUs and to fully understand the origin of the high catalytic activity of TBD organocatalyst, we report a detailed mechanistic study of the guanidine organocatalysed ring-opening of propylene carbonate by amines using DFT calculations. In order to highlight the influence of the amine nucleophilicity, the uncatalysed model reaction between propylene carbonate and aniline, methyl amine and cyclohexylamine was first considered. Then, the same reactions were reinvestigated using TBD as catalyst and compared with the ones promoted by 7-methyl-TBD (MTBD). For all pathways, detailed structural and energetic information of transition states and intermediates have been optimized. We emphasize that our “gas phase” DFT calculations that consider one molecule of carbonate reacting with one amine molecule is appropriate to model reactions carried out with the reactants diluted in an aprotic organic solvent. For a proper modelling of reactions performed in the bulk, we should have taken into account explicitly in our calculations additional reactant molecules such as two or three amine molecules which is beyond the scope of the paper.

## Experimental

### Computational details

Preliminary calculations of equilibrium structures were performed using a semi-empirical model (AM1-D<sub>3</sub>H<sub>4</sub>)<sup>39, 40</sup> to determine the most stable conformations. These semi-empirical calculations were performed using the AMPAC software.<sup>41</sup> Using the same semi-empirical model (AM1-D<sub>3</sub>H<sub>4</sub>), the CHAIN algorithm<sup>42</sup> implemented in the AMPAC software was used for locating along the reaction path the conformations that were identified as intermediates and transition states. The lowest energy structures obtained at the AM1-D<sub>3</sub>H<sub>4</sub> level were further investigated using the Density Functional Theory method (DFT) implemented in the Gaussian 09 package.<sup>43</sup> DFT calculations of geometries, energies, and vibrational frequencies

reported in this paper were carried out with the Mo6-2X functional<sup>44</sup> using the 6-311G(d,p) basis set.

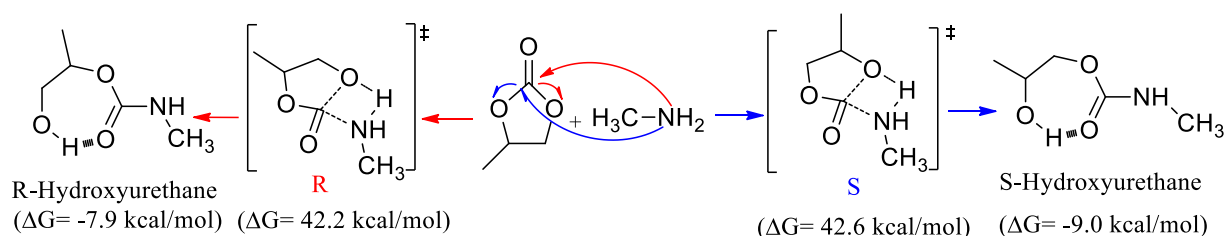
All frequencies of each structure have also been calculated to verify the presence of a single imaginary frequency for transition states and the absence of imaginary frequency for ground states. The intrinsic reaction coordinate (IRC) method has been used to verify that the obtained transition states were effectively connected to the desired minima. For all catalysts, a wide range of possible configurations and interactions have been modeled and the more stable of them are reported in this work. To consider entropic effects, the energies mentioned in this study correspond to the Gibbs free energy ( $\Delta G$ ).

## Results and discussion

The mechanistic study through DFT simulation was realized for a model aminolysis reaction between propylene carbonate (PC) and an amine. Only the most favorable pathway is reported.

### 1. Cyclic carbonate – amine coupling without catalyst

A racemic mixture is obtained by aminolysis of the racemic propylene carbonate (Scheme 1). Depending of the regio-selectivity of the ring-opening, a primary (R) or a secondary (S) alcohol is synthesized.



Scheme 1: Racemic aminolysis of propylene carbonate by methylamine

It can be noted that the aminolysis of propylene carbonate by methylamine is exothermic and that the Gibbs energy for the synthesis of R-hydroxyurethane ( $\Delta G = 42.2$  kcal.mol<sup>-1</sup>) and S-hydroxyurethane ( $\Delta G = 42.6$  kcal.mol<sup>-1</sup>) is similar (Figure 1). The most stable isomer of hydroxyurethane is cyclic due to hydrogen-bonding between the alcohol and the O atom of the carbonyl group.<sup>36</sup> However, the Gibbs energy of the S- product, 2-hydroxypropyl methylcarbamate, is lower ( $\Delta G = -9.0$  kcal.mol<sup>-1</sup>) than for the R-product ( $\Delta G = -7.9$  kcal.mol<sup>-1</sup>). Therefore, the following results will focus only on the pathway leading to the synthesis of the S-hydroxyurethane (secondary alcohol).

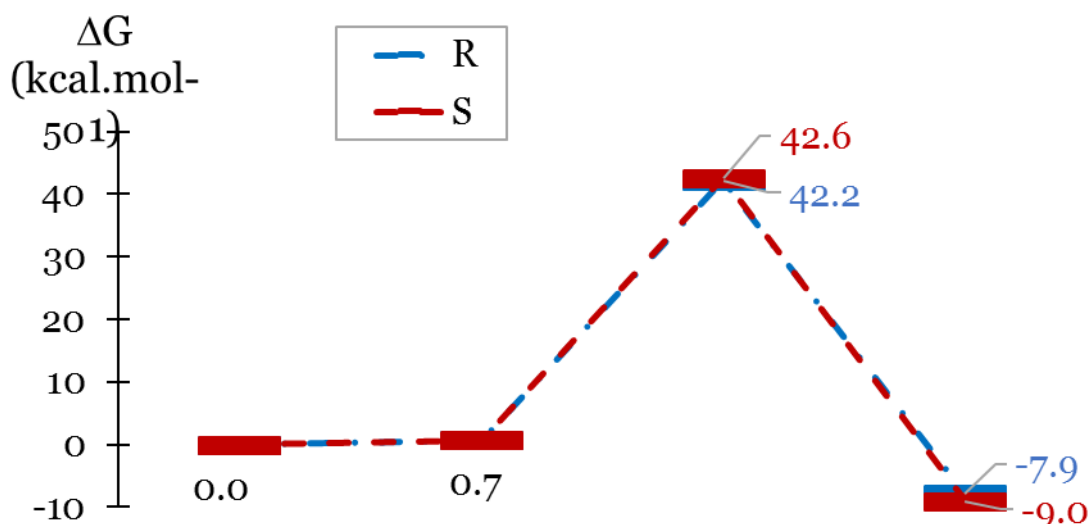


Figure 1: Free energy profiles (Mo6-2X/6-311G(d,p)) for the racemic aminolysis of propylene carbonate by methylamine.

Schematic potential energy profiles obtained at the Mo6-2X/6-311G(d,p) level and schematic Lewis structures for the aminolysis of PC by methylamine, aniline and cyclohexylamine are depicted in Figure 2. After having fully optimized independently PC, methylamine, cyclohexylamine, aniline and the corresponding S-hydroxyurethane structures, the overall aminolysis pathway between PC and the amines has been modelled by a one-step mechanism. The initial state corresponds to the sum of the Gibbs free energies of each compound (PC, amine) which is taken as the zero energy.

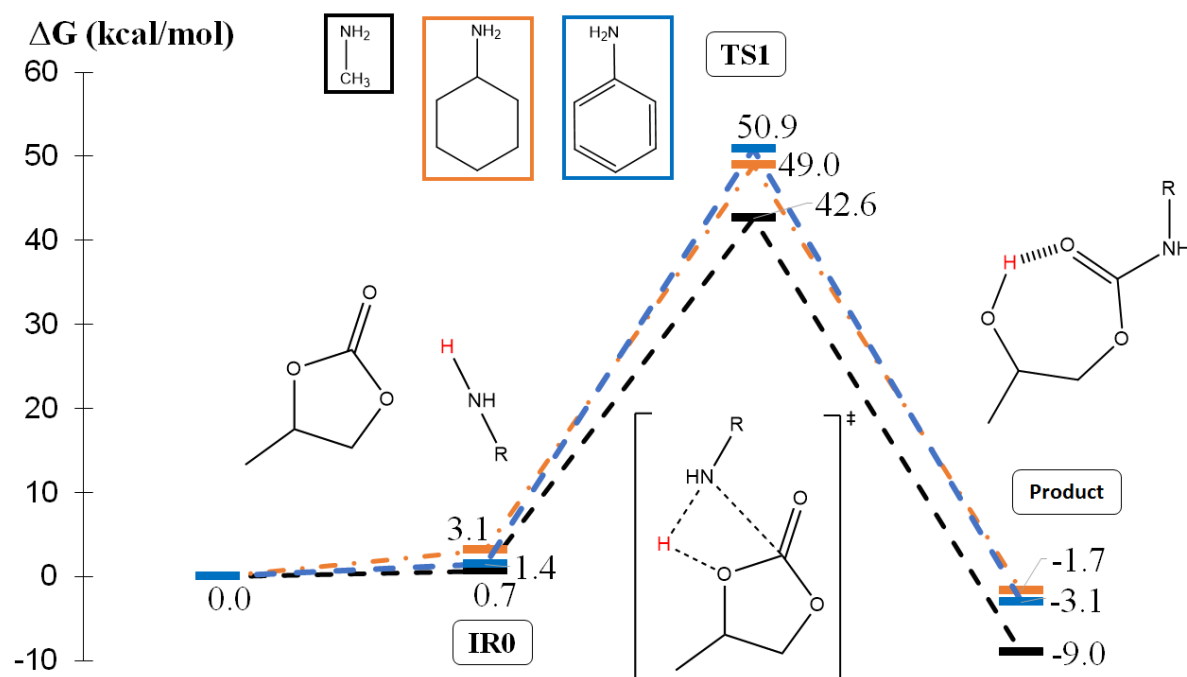


Figure 2: Free energy profiles (Mo6-2X/6-311G(d,p)) and Lewis structures for the aminolysis of propylene carbonate by methylamine (black), cyclohexylamine (orange) and aniline (blue) without catalyst.

The complexes resulting from the Van der Waals interactions and H-bonds (IRO) between the amines and PC have a positive Gibbs free energy of 0.7 kcal.mol<sup>-1</sup>, 1.4 kcal.mol<sup>-1</sup> and 3.1 kcal.mol<sup>-1</sup> for methylamine, aniline and cyclohexylamine, respectively. The transition state corresponds to the concerted addition of the amine onto the C atom of the carbonate group of PC, transfer of the proton of the amine to the adjacent O atom of the carbonate group and the ring-opening of PC (Figure 3). The reaction is exothermic and the Gibbs energy of the product depends of the nature of the amine. It can be noted that this mechanism is favored compared to a two-step pathway involving a zwitterionic intermediate, ammonium alkoxide, resulting from the addition of the amine and the transfer of its proton to the O atom of the carbonyl. The Gibbs energy for the uncatalyzed aminolysis of PC evolves in the following order  $\Delta G(\text{methylamine}) < \Delta G(\text{cyclohexylamine}) < \Delta G(\text{aniline})$ . Those results are consistent with previous experimental studies<sup>20, 22, 45</sup> reporting that linear alkylamines are more reactive than cyclic and aromatic amines. The higher  $\Delta G$  value determined for the ring opening of PC by less nucleophilic aniline is related to the lower partial charge on the nitrogen atom of the aromatic amines compared to the aliphatic ones.<sup>41</sup>

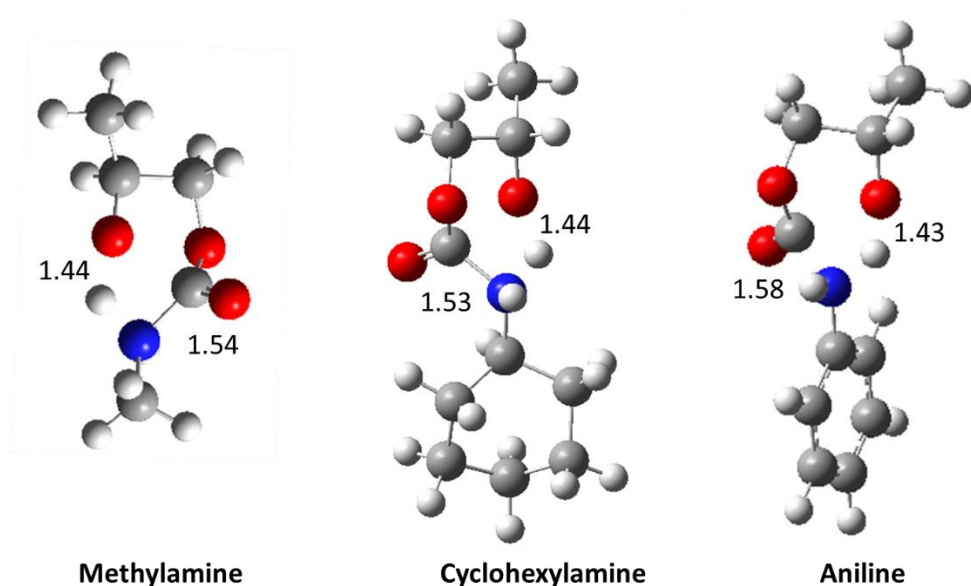


Figure 3: Optimized geometries of the structures (Mo6-2X/6-311G(d,p)) of the transition state for the aminolysis of propylene carbonate by methylamine (left), cyclohexylamine (center) and aniline (right) without catalyst. The intermolecular distances are given in angstrom.

## 2. Cyclic Carbonate – aniline coupling with TBD and MTBD catalyst

The mechanism of the TBD catalyzed aminolysis of propylene carbonate by aniline was investigated at the Mo6-2X/6-311G(d,p) level. The most probable activation mechanism by TBD answers a two-step pathway (Figure 4). The molecular structures of the corresponding intermediates and transition states are displayed in Figure 4.

The pre-reaction complex IRO has a negative Gibbs energy meaning that the reagents are weakly linked together by Van der Waals interactions and hydrogen bonds.

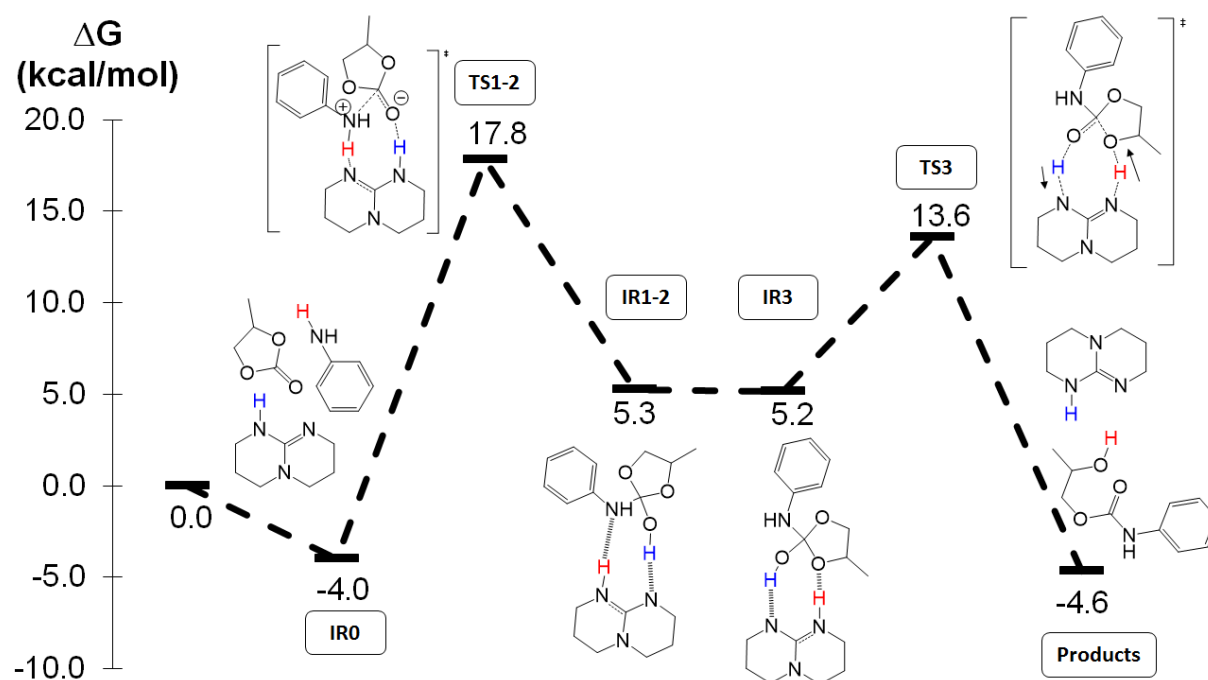


Figure 4: Free energy profiles (M06-2X/6-311G(d,p)) and Lewis structures for the aminolysis of propylene carbonate by aniline catalyzed by TBD.

The initial step (TS1-2) corresponds to the nucleophilic attack of aniline onto the carbonate group of PC (1.64 Å) with a concerted exchange of protons from aniline towards the N atom of TBD (1.41 Å) and from TBD to the O atom of the carbonyl (1.67 Å) (Figure 5). This concerted transfer of protons is possible because of the two nitrogen available sites on the structure of TBD. The intermediate IR1-2 is a cyclic aminoalcohol interacting with TBD by two H-bonds. However, the structure of this intermediate is unfavorable for the ring-opening step. Thus, a rotation of TBD creating a hydrogen bond with the adjacent O atom of the alcohol group leads to IR3 which has a similar Gibbs energy. In the final step, TS3 corresponds to the C-O bond cleavage and the simultaneous dual protons transfer between TBD and the adjacent O atom of the carbonate and between the aminoalcohol and TBD. Finally, TBD is regenerated and the phenyl S-hydroxyurethane is the resulting product. The formation of the first reactive intermediate IR1-2 is the rate determining step of the reaction as it displays the highest energy transition state of the process. TBD acts as proton donor and acceptor and consequently decreases the Gibbs energy of the reaction between PC and aniline from  $\Delta G = 50.9 \text{ kcal.mol}^{-1}$  to  $\Delta G = 17.8 \text{ kcal.mol}^{-1}$ . The proton shuttle activation mechanism pathway of TBD is consistent with the previous study of Kleij *et al.*<sup>22</sup> although their reaction pathway involves a larger number of intermediates and formation of an ion-pair association composed of TBDH<sup>+</sup> and an alkoxide.

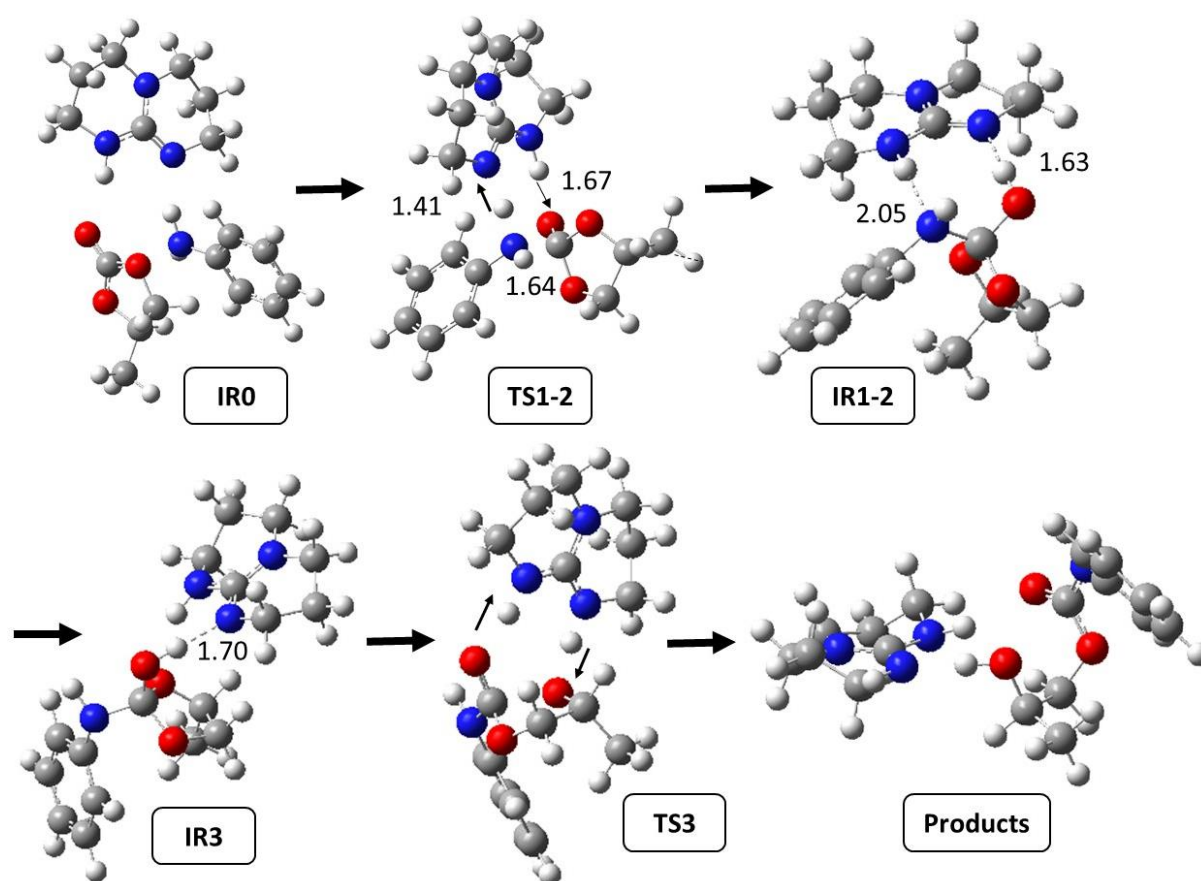


Figure 5: Optimized geometries of the structures (Mo6-2X/6-311G(d,p)) of the propylene carbonate/aniline coupling in the presence of TBD as catalyst. The dashed lines depict hydrogen bond interactions, the arrows represent the concerted proton transfer and intermolecular distances are given in angstrom.

To highlight the importance of the dual proton exchange on the catalytic activity of TBD, the NH proton of TBD was substituted by a methyl substituent and the mechanism of the MTBD catalyzed aminolysis of PC by aniline was investigated (Figure 6). The activation mechanism is different as it answers a three elementary steps pathway. The molecular structures of the corresponding intermediates and transition states are displayed in Figure 7. To improve the visualization of the systems, MTBD was represented using the stick model. The pre-reaction complex (IR0) has a positive Gibbs energy of 1.6 kcal.mol<sup>-1</sup>. The first elementary step corresponds to the nucleophilic attack of aniline onto the C atom of the carbonate group of PC (TS1) resulting in an increase of the electron density on this atom. The electron density excess is then distributed between adjacent O atoms of the ring. The instable zwitterionic first intermediate IR1, *i.e.* an ammonium alkoxide, interacts with MTBD by formation of H-bonds. The proton of the ammonium is then transferred to the nitrogen atom of MTBD (TS2) with a low activation energy barrier ( $\Delta G = 0.2$  kcal.mol<sup>-1</sup>) relatively to the calculation error leading to an ion-pair composed of MTBDH<sup>+</sup> and an alkoxide (IR2). To reach a lower Gibbs energy and favor the last step, IR2 undergoes a rearrangement where the proton of MTBDH<sup>+</sup> interacts with the O atom adjacent of the carbonyl of the carbonate group (IR3).



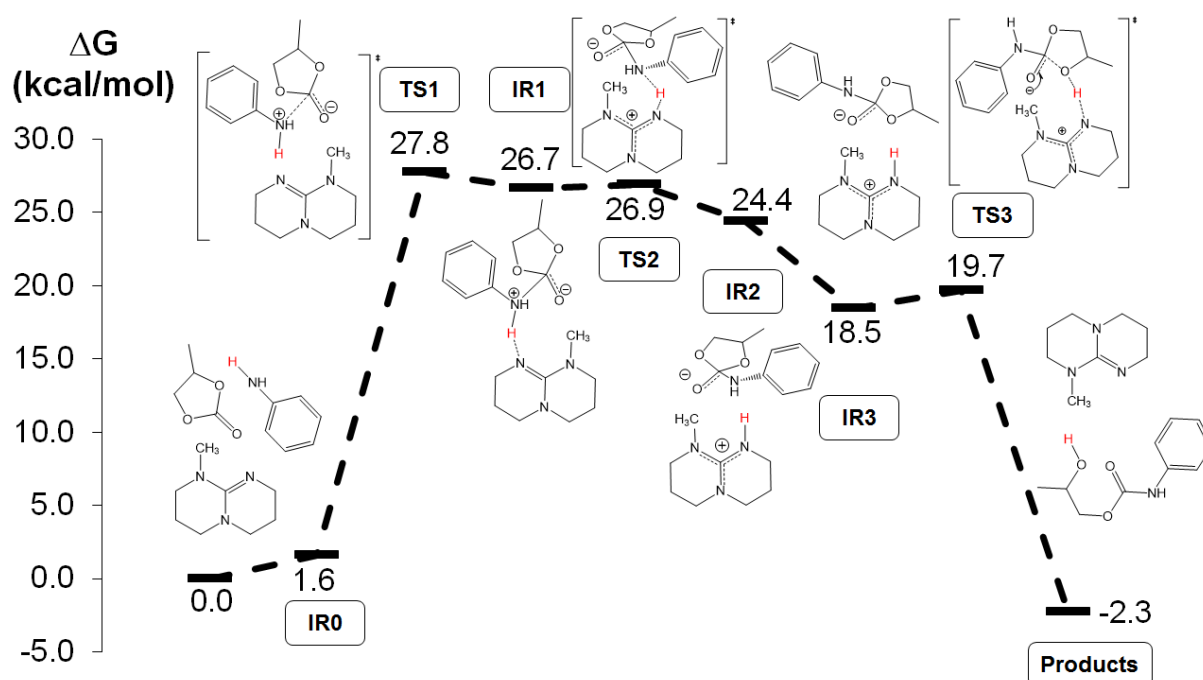


Figure 6: Free energy profiles (Mo6-2X/6-311G(d,p)) and Lewis structures for the aminolysis of propylene carbonate by aniline catalysed by MTBD.

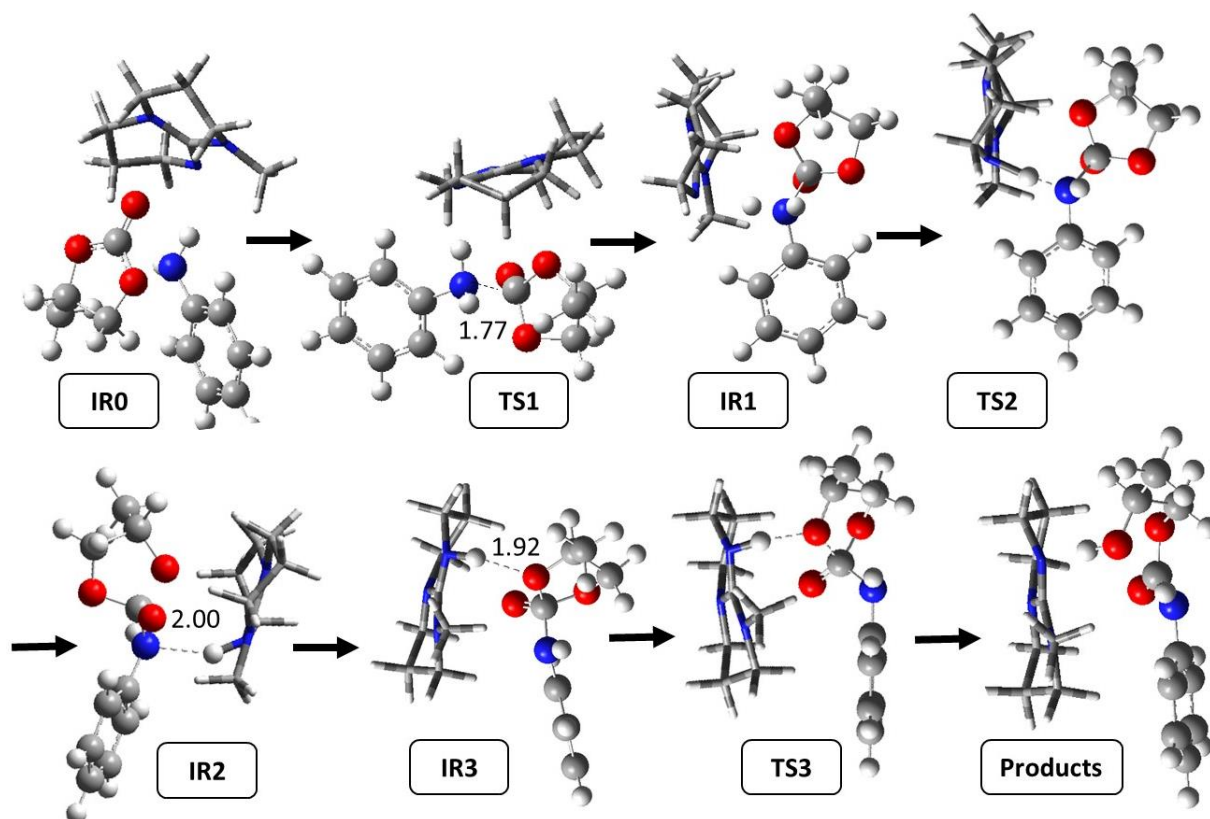


Figure 7: Optimized geometries of the structures (Mo6-2X/6-311G(d,p)) of the propylene carbonate/aniline coupling in the presence of MTBD as catalyst. The dashed lines depict hydrogen bond interactions, intermolecular distances are given in angstrom.

Finally, the concerted transfer of the same proton from MTBD to the adjacent O atom of the carbonyl and the ring-opening of the five-membered ring (TS3) lead to the synthesis of the S-hydroxyurethane derivative and the regeneration of MTBD. The rate determining step is the addition of the aniline onto PC that represents the highest energy transition state of the process. The MTBD catalyst drastically decreases the Gibbs energy of the aminolysis of PC by aniline from  $\Delta G = 50.9$  kcal.mol<sup>-1</sup> to  $\Delta G = 27.8$  kcal.mol<sup>-1</sup>. However, the Gibbs energy value is higher than for the TBD-promoted reaction ( $\Delta G = 17.8$  kcal.mol<sup>-1</sup>) as the methyl group of MTBD prevents the concerted proton exchange to occur as it was observed for the most efficient TBD catalyst.

### 3. Cyclic Carbonate – methylamine coupling with TBD and MTBD catalyst

In a first step, the activation mechanism of the TBD catalyzed aminolysis of PC with methylamine was investigated (Figure 8).

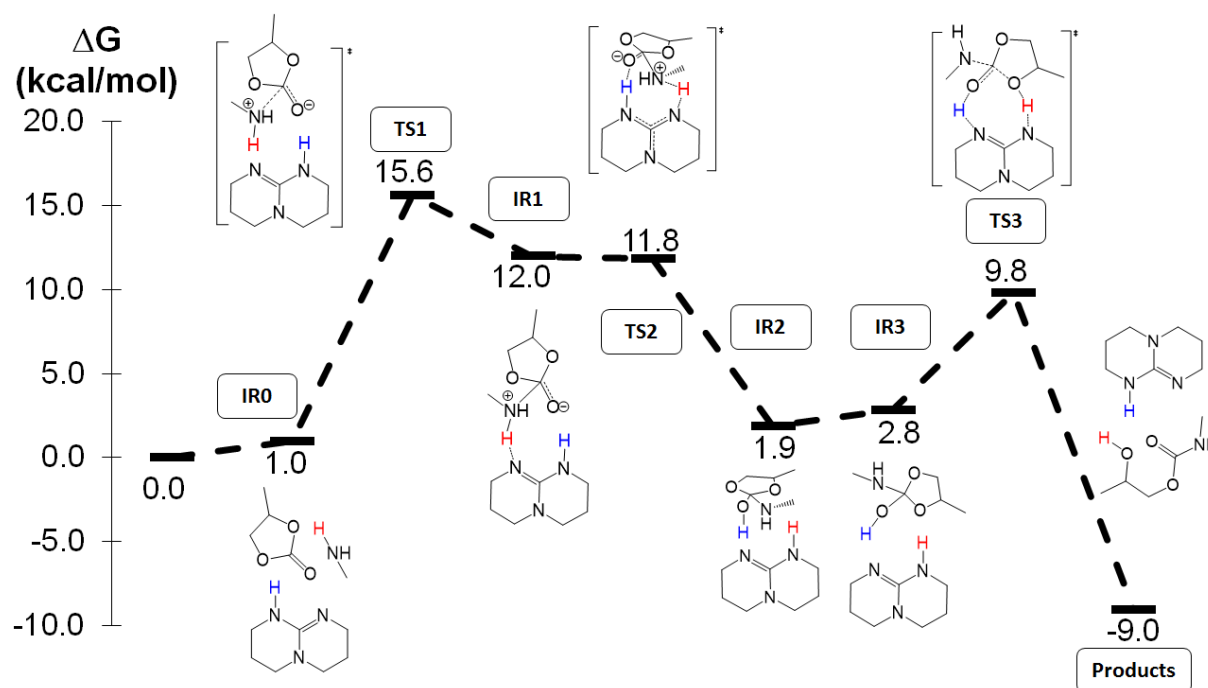


Figure 8: Free energy profiles (Mo6-2X/6-311G(d,p)) and Lewis structures for the aminolysis of propylene carbonate by methylamine catalysed by TBD.

In contrast to the analogous reaction with aniline, the reaction follows a three elementary steps pathway with methylamine and the pre-reaction complex has a positive Gibbs energy. The first transition state (TS1) corresponds to the nucleophilic attack of the amine onto the C atom of the carbonate of PC (Figure 9). The distance between the amine and the C atom of the carbonyl group of PC is longer (1.87 Å) than for aniline (1.64 Å, Figure 5). As aliphatic amines are more nucleophilic than the aromatic ones, the nucleophilic attack of the cyclic carbonate by methylamine and the concerted transfer of protons are dissociated in two independent steps. The ammonium alkoxide (IR1) is stabilized by H-bonds formation between the N atom of TBD and the proton of the ammonium (1.61 Å) and between the O atom of the

carbonyl group of PC and the proton of TBD (1.74 Å). The concerted transfer of both protons involved in the H-bond occurs in a second step (TS2). It should be noted that the ammonium alkoxide (IR1) has a higher Gibbs energy than TS2. However, the IRC confirmed that the electronic energy of IR1 is lower than for TS2 but the thermal and entropic contributions reversed the trend. The aminoalcohol (IR2) which is in interaction with TBD rotates (IR3) to create a H-bond between the proton of TBD and the adjacent O atom of the alcohol group (1.92 Å). However, this rotation increases the H-bond distances implying a rise of the Gibbs energy but favors the second concerted protons transfer between TBD and the aminoalcohol (TS3) leading to the S-hydroxyurethane and regenerating TBD.

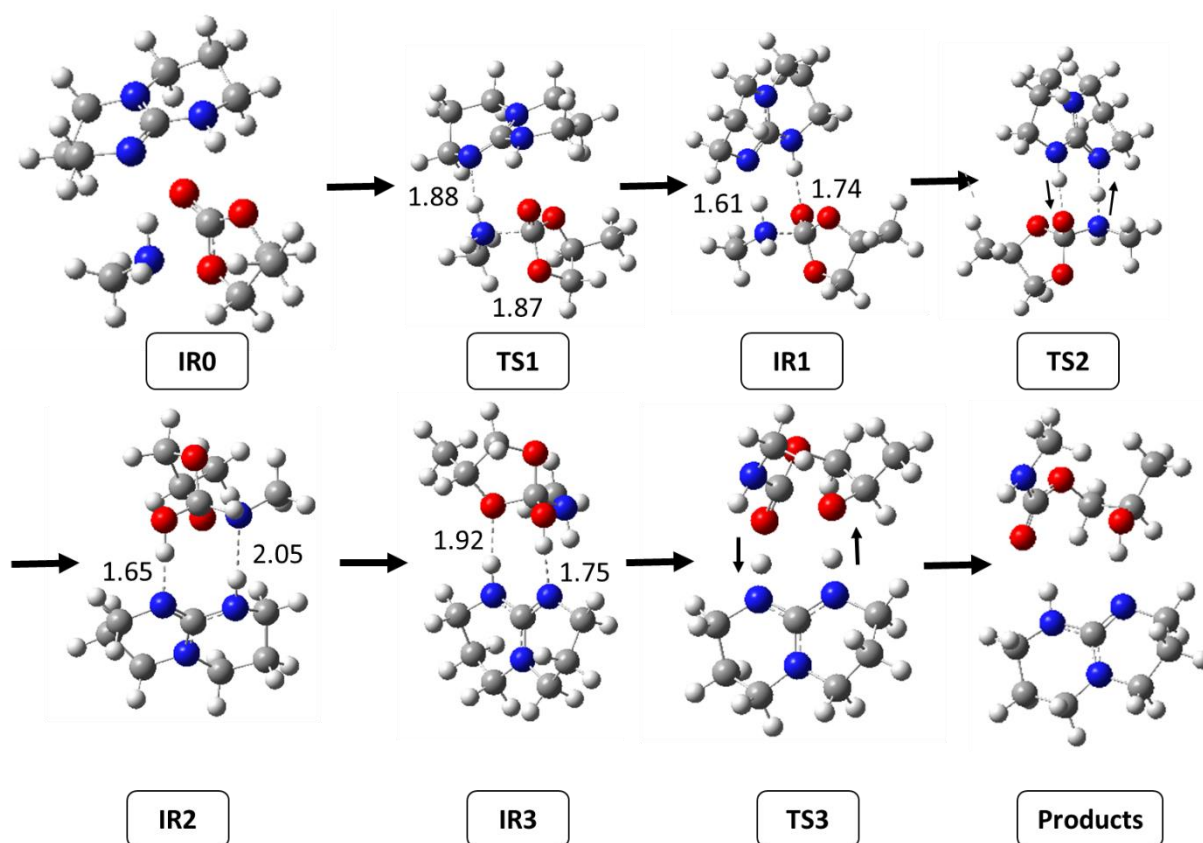


Figure 9: Optimized geometries of the structures (Mo6-2X/6-311G(d,p)) of the propylene carbonate/methylamine coupling in the presence of TBD as catalyst. The dashed lines depict hydrogen bond interactions, the arrows represent the concerted proton transfer and intermolecular distances are given in angstrom.

The addition of methylamine onto the cyclic carbonate is the rate determining step ( $\Delta G = 15.6 \text{ kcal.mol}^{-1}$ ). TBD acts as a proton-relay with concerted protons transfers. As already observed with aniline, TBDH<sup>+</sup> was not identified as an intermediate for the aminolysis of PC by methylamine in contrary to the mechanism suggested by Kleij *et al.* with butylamine.<sup>22</sup> However, the aminoalcohol intermediate was also reported by Tiger *et al.* using acetic acid as bifunctional catalyst for the mechanism involving one amine molecule although two steps of the mechanism differed.<sup>37</sup>

For sake of comparison, the influence of the methyl group of MTBD on the catalyst activity for the propylene carbonate/methylamine coupling was investigated. The MTBD catalyzed synthesis of 2-hydroxypropyl methylcarbamate answers a three-step pathway (Figure 10), similarly to the one previously reported with aniline. The pre-reaction complex composed of methylamine/MTBD/PC has a positive Gibbs free energy ( $\Delta G = 1.8 \text{ kcal.mol}^{-1}$ ). The first transition state (TS1) corresponds to nucleophilic attack of the amine onto the C atom of the carbonate of PC (1.86 Å) (Figure 11). The instable ammonium alkoxide (IR1) transfers the proton of the amine to MTBD (TS2). The resulting ion pair association [MTBDH<sup>+</sup>-alkoxide] (IR2) has a higher Gibbs energy than TS2 (we checked that the electronic energy of IR2 is lower than that of TS2 and this seldom behavior is due to the fact that the thermal and entropic contributions to the Gibbs energy is higher for IR2 than TS2). After the rotation of MTBDH<sup>+</sup>, the Gibbs energy is decreased by 2 kcal.mol<sup>-1</sup> (IR3) while MTBDH<sup>+</sup> interacts with the adjacent O atom rather than the alkoxide. Finally, the concerted proton transfer and the ring-opening (TS3) regenerate MTBD and lead to the hydroxyurethane.

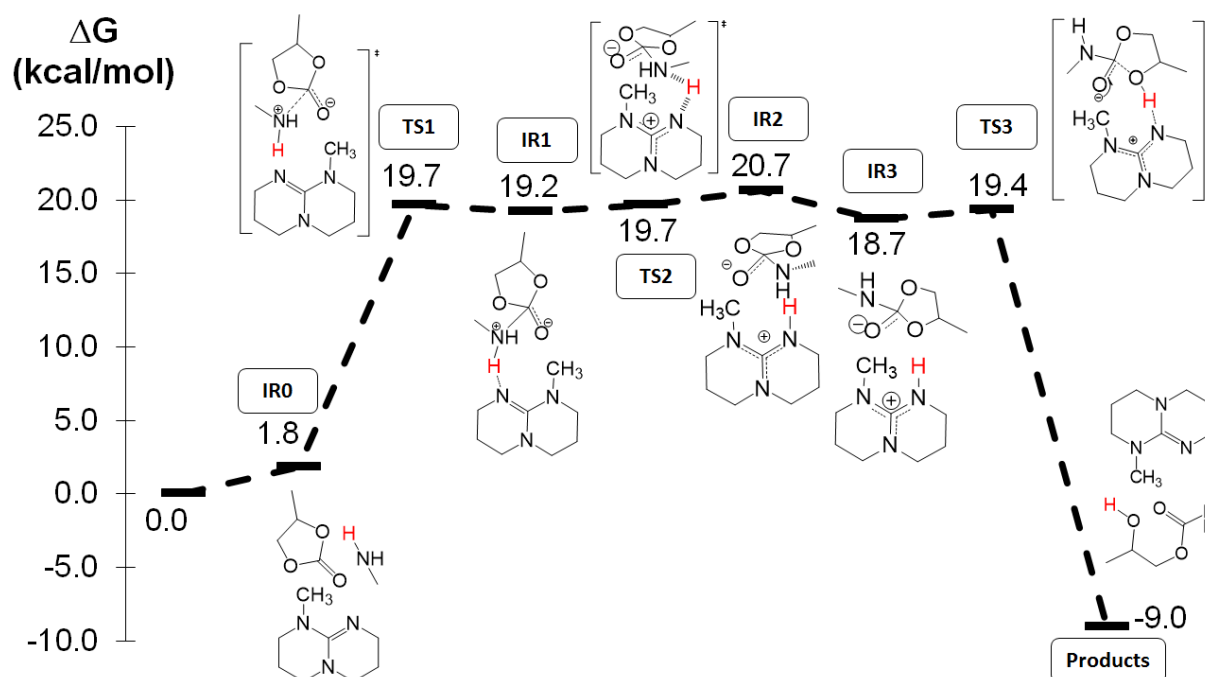


Figure 10: Free energy profiles (Mo6-2X/6-311G(d,p)) and Lewis structures for the aminolysis of propylene carbonate by methylamine catalysed by MTBD.

The first step corresponding to the nucleophilic attack of the amine onto the carbonate can be considered as the rate determining step ( $\Delta G = 19.7 \text{ kcal.mol}^{-1}$ ). It may be noted that the next two following steps occur with a Gibbs energy barrier lower than 1 kcal.mol<sup>-1</sup>. The activation barrier of the aminolysis of PC by methylamine catalyzed by MTBD is substantially lower compared to the one-step uncatalyzed reaction ( $\Delta G = 42.6 \text{ kcal.mol}^{-1}$ ) but still higher than for the TBD-activated pathway ( $\Delta G = 15.6 \text{ kcal.mol}^{-1}$ ). This conclusion is in line with the one hold for the aminolysis of PC by aniline catalyzed by TBD and MTBD. Similarly, the methyl group of MTBD prevents both concerted protons exchanges as one nitrogen of the guanidine site is

blocked. Therefore, TBD is a more efficient catalyst than MTBD for the aminolysis of propylene carbonate with alkylamines and aromatic amines.

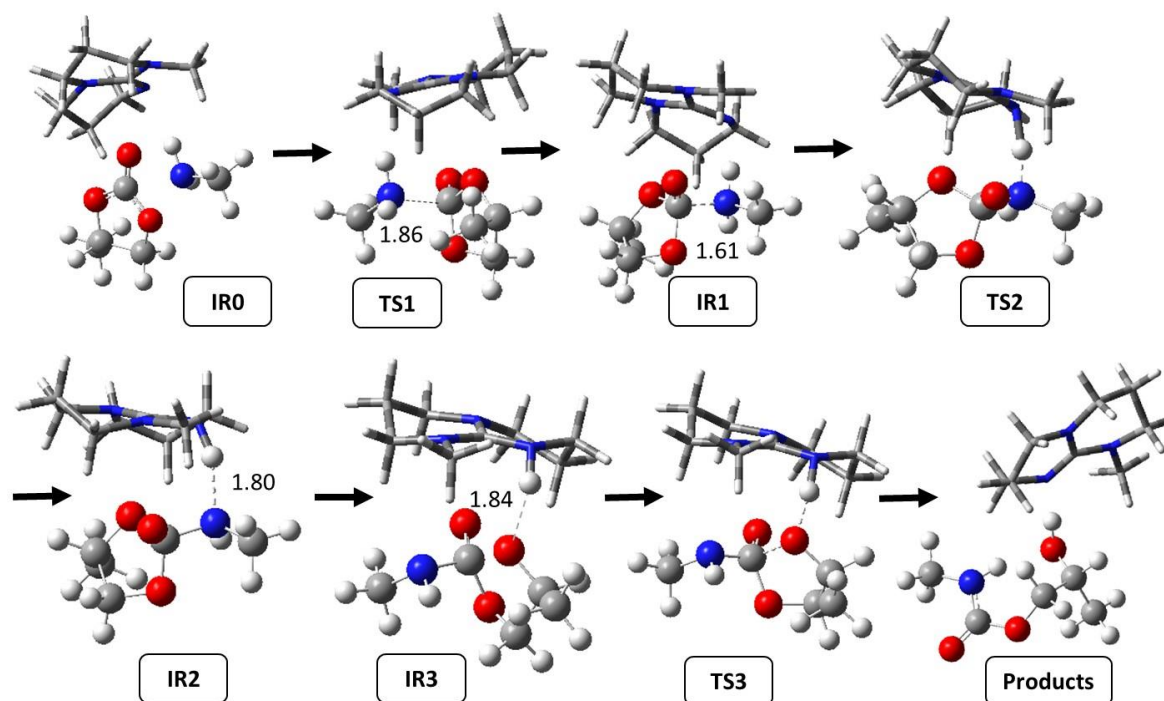


Figure 11: Optimized geometries of the structures (Mo6-2X/6-311G(d,p)) of the propylene carbonate/methylamine coupling in the presence of MTBD as catalyst. The dashed lines depict hydrogen bond interactions, intermolecular distances are given in angstrom.

#### 4. Cyclic Carbonate – cyclohexylamine coupling with TBD catalyst

In order to determine if the aromaticity of the benzene ring of aniline has an influence on the mechanistic pathway, the TBD catalyzed aminolysis of PC was studied using cyclohexylamine. The reaction answers a three-step pathway depicted on Figure 12. As previously reported for methylamine, the nucleophilic attack of cyclohexylamine onto PC is an independent elementary step (TS1). Indeed, the distance between the N atom of the amine and the C atom of the carbonate is longer (1.80 Å) than for aniline (1.64 Å, Figure 5) (Figure 13). The ammonium alkoxide, IR1, is stabilized by two hydrogen bonds between TBD and the O atom of the carbonate (1.74 Å) and the amine group (1.62 Å). In a second step, TBD acts as donor and acceptor of those protons in interaction for the concerted protons transfer between TBD and the ammonium alkoxide (TS2). The resulting aminoalcohol is stabilized by TBD (IR2) and rearranges to favor the last step (IR3) by interaction between TBD and the adjacent O atom of the carbonate (1.71 Å). Then, the second concerted protons exchange between TBD and the aminoalcohol (TS3) allows the synthesis of the hydroxyurethane and the recovery of TBD. The nucleophilic attack of cyclohexylamine onto PC is the rate determining step ( $\Delta G = 19.7 \text{ kcal.mol}^{-1}$ ). Consequently, the activation barrier is decreased when TBD is used as catalyst for the aminolysis of PC by cyclohexylamine compared to the non-catalyzed reaction ( $\Delta G = 49 \text{ kcal.mol}^{-1}$ ). The TBD-activation mechanism with cyclic alkylamines such as



cyclohexylamine follows a three-step pathway like the aliphatic amines highlighting the special case of aromatic amines. The Gibbs energy for the reaction is lower for methylamine than for cyclohexylamine probably because of steric effect and the nucleophilicity. Besides, these results are consistent with experimental investigations on the aminolysis of propylene carbonate by aromatic and (cyclic) aliphatic amines.<sup>19</sup>

20, 22

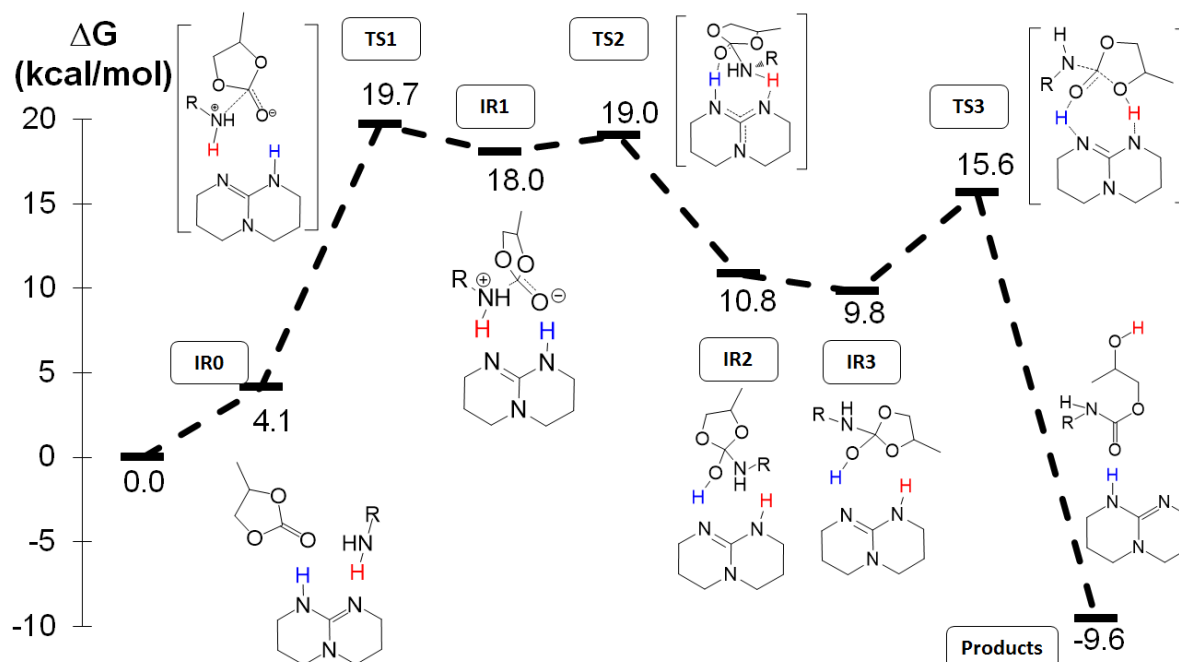


Figure 12: Free energy profiles (M06-2X/6-311G(d,p)) and Lewis structures for the aminolysis of propylene carbonate by cyclohexylamine catalyzed by TBD.

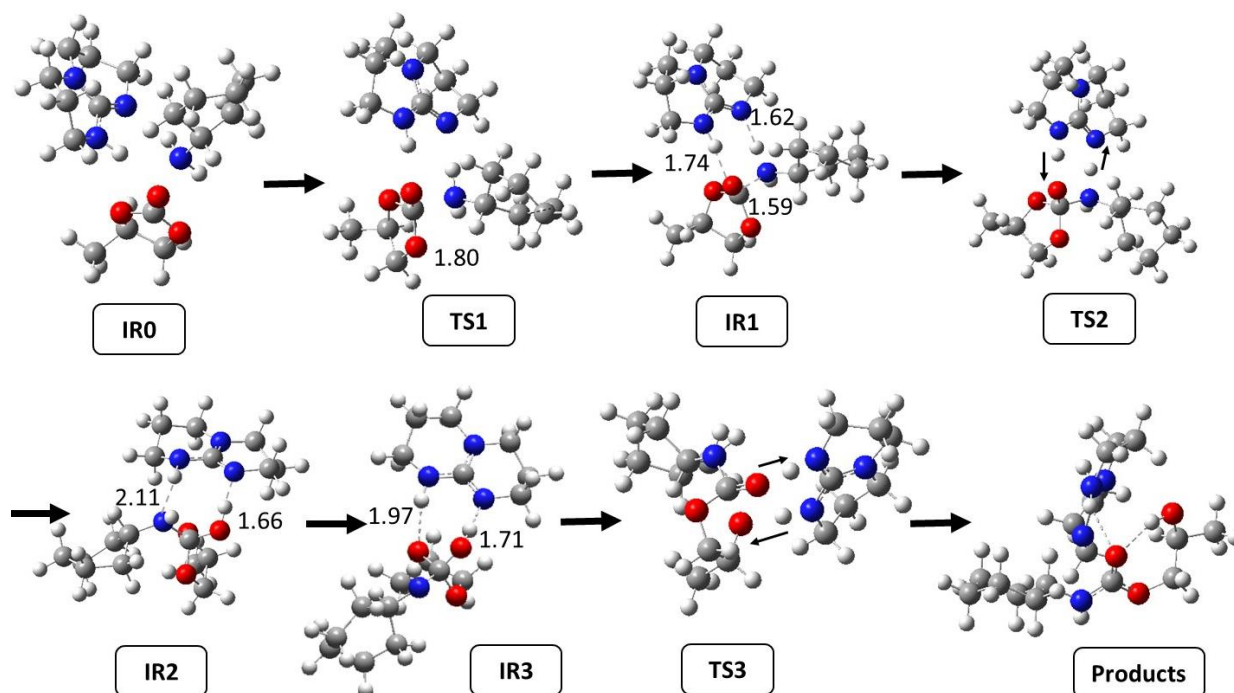


Figure 13: Optimized geometries of the structures (M06-2X/6-311G(d,p)) of the propylene carbonate/cyclohexylamine coupling in the presence of TBD as catalyst. The dashed lines depict hydrogen bond interactions, the arrows represent the concerted proton transfer and intermolecular distances are given in angstrom

## Conclusion

A detailed mechanistic investigation of the synthesis of hydroxyurethanes by reaction between propylene carbonate and (cyclic) alkylamines and aromatic amines has been performed. The non-catalyzed reaction answers a concerted one-step mechanism. The Gibbs energy depends of the nucleophilicity of the amine and was found to evolve in the order  $\Delta G(\text{aniline}) > \Delta G(\text{cyclohexylamine}) > \Delta G(\text{methylamine})$ . As a general trend, the guanidine-catalyzed reaction answers a three-step pathway associated to the nucleophilic attack of the amine onto the carbonate, a proton transfer and hydrogen bonding interaction between the catalyst and the reactant, and finally a ring opening leading to the hydroxyurethane. In the case of TBD, the two first steps, *i.e.* the nucleophilic attack of the amine onto the carbonate and the concerted proton transfer, occur simultaneously in the case of aniline because of its low nucleophilicity compared to methyl amine and cyclohexylamine. Besides, the activation of TBD is linked to a proton-relay mechanism with two successive concerted protons exchanges decreasing drastically the Gibbs free energy of the reaction. Such proton-relay activation is not possible in the case of MTBD hence explaining why TBD is a more efficient catalyst than MTBD as it was evidenced experimentally.

## References

1. J. Guan, Y. Song, Y. Lin, X. Yin, M. Zuo, Y. Zhao, X. Tao and Q. Zheng, *Industrial & Engineering Chemistry Research*, 2011, **50**, 6517-6527.
2. M. Bahr and R. Mulhaupt, *Green Chemistry*, 2012, **14**, 483-489.
3. M. S. Kathalewar, P. B. Joshi, A. S. Sabnis and V. C. Malshe, *RSC Advances*, 2013, **3**, 4110-4129.
4. G. Rokicki, P. G. Parzuchowski and M. Mazurek, *Polymers for Advanced Technologies*, 2015, **26**, 707-761.
5. O. Kreye, H. Mutlu and M. A. R. Meier, *Green Chemistry*, 2013, **15**, 1431-1455.
6. L. Maisonneuve, O. Lamarzelle, E. Rix, E. Grau and H. Cramail, *Chemical Reviews*, 2015, **115**, 12407-12439.
7. B. Grignard, J. M. Thomassin, S. Gennen, L. Poussard, L. Bonnaud, J. M. Raquez, P. Dubois, M. P. Tran, C. B. Park, C. Jerome and C. Detrembleur, *Green Chemistry*, 2016, **18**, 2206-2215.
8. C. Carre, L. Bonnet and L. Averous, *RSC Advances*, 2014, **4**, 54018-54025.
9. L. Poussard, J. Mariage, B. Grignard, C. Detrembleur, C. Jérôme, C. Calberg, B. Heinrichs, J. De Winter, P. Gerbaux, J. M. Raquez, L. Bonnaud and P. Dubois, *Macromolecules*, 2016, **49**, 2162-2171.
10. J. Nanclares, Z. S. Petrović, I. Javni, M. Ionescu and F. Jaramillo, *Journal of Applied Polymer Science*, 2015, **132**, DOI: 10.1002/app.42492.
11. A. Cornille, S. Dworakowska, D. Bogdal, B. Boutevin and S. Caillol, *European Polymer Journal*, 2015, **66**, 129-138.
12. E. K. Leitsch, G. Beniah, K. Liu, T. Lan, W. H. Heath, K. A. Scheidt and J. M. Torkelson, *ACS Macro Letters*, 2016, **5**, 424-429.
13. C. Maeda, Y. Miyazaki and T. Ema, *Catalysis Science and Technology*, 2014, **4**, 1482-1497.
14. G. Fiorani, W. Guo and A. W. Kleij, *Green Chemistry*, 2015, **17**, 1375-1389.
15. M. Alves, B. Grignard, S. Gennen, R. Mereau, C. Detrembleur, C. Jerome and T. Tassaing, *Catalysis Science & Technology*, 2015, **5**, 4636-4643.
16. S. Gennen, M. Alves, R. Méreau, T. Tassaing, B. Gilbert, C. Detrembleur, C. Jerome and B. Grignard, *ChemSusChem*, 2015, **8**, 1845-1849.
17. S. Foltran, J. Alsarraf, F. Robert, Y. Landais, E. Cloutet, H. Cramail and T. Tassaing, *Catalysis Science & Technology*, 2013, **3**, 1046-1055.
18. S. Foltran, R. Mereau and T. Tassaing, *Catalysis Science & Technology*, 2014, **4**, 1585-1597.
19. R. H. Lambeth and T. J. Henderson, *Polymer*, 2013, **54**, 5568-5573.
20. M. Blain, L. Jean-Gerard, R. Auvergne, D. Benazet, S. Caillol and B. Andrioletti, *Green Chemistry*, 2014, **16**, 4286-4291.
21. F. Camara, S. Benyahya, V. Besse, G. Boutevin, R. Auvergne, B. Boutevin and S. Caillol, *European Polymer Journal*, 2014, **55**, 17-26.
22. W. Guo, J. Gönzalez-Fabra, N. A. G. Bandeira, C. Bo and A. W. Kleij, *Angewandte Chemie - International Edition*, 2015, **54**, 11686-11690.
23. M. Fleischer, H. Blattmann and R. Mulhaupt, *Green Chemistry*, 2013, **15**, 934-942.



24. L. Maisonneuve, A. S. More, S. Foltran, C. Alfos, F. Robert, Y. Landais, T. Tassaing, E. Grau and H. Cramail, *RSC Advances*, 2014, **4**, 25795-25803.
25. V. M. Lombardo, E. A. Dhulst, E. K. Leitsch, N. Wilmot, W. H. Heath, A. P. Gies, M. D. Miller, J. M. Torkelson and K. A. Scheidt, *European Journal of Organic Chemistry*, 2015, **2015**, 2791-2795.
26. M. Blain, H. Yau, L. Jean-Gérard, R. Auvergne, D. Benazet, P. R. Schreiner, S. Caillol and B. Andrioletti, *ChemSusChem*, 2016, DOI: 10.1002/cssc.201600778, n/a-n/a.
27. Q. Chen, K. Gao, C. Peng, H. Xie, Z. K. Zhao and M. Bao, *Green Chemistry*, 2015, **17**, 4546-4551.
28. V. Besse, F. Camara, F. Méchin, E. Fleury, S. Caillol, J.-P. Pascault and B. Boutevin, *European Polymer Journal*, 2015, **71**, 1-11.
29. M. K. Kiesewetter, M. D. Scholten, N. Kirn, R. L. Weber, J. L. Hedrick and R. M. Waymouth, *Journal of Organic Chemistry*, 2009, **74**, 9490-9496.
30. L. Simón and J. M. Goodman, *Journal of Organic Chemistry*, 2007, **72**, 9656-9662.
31. I. Nifant'ev, A. Shlyakhtin, V. Bagrov, B. Lozhkin, G. Zakirova, P. Ivchenko and O. Legon'kova, *Reaction Kinetics, Mechanisms and Catalysis*, 2016, **117**, 447-476.
32. P. Hammar, C. Ghobril, C. Antheaume, A. Wagner, R. Baati and F. Himo, *The Journal of Organic Chemistry*, 2010, **75**, 4728-4736.
33. J. Ma, X. Zhang, N. Zhao, F. Xiao, W. Wei and Y. Sun, *Journal of Molecular Structure: THEOCHEM*, 2009, **911**, 40-45.
34. M. A. Levina, V. G. Krashenninnikov, M. V. Zabalov and R. P. Tiger, *Polym. Sci. Ser. B*, 2014, **56**, 139-147.
35. M. V. Zabalov, R. P. Tiger and A. A. Berlin, *Dokl Chem*, 2011, **441**, 355-360.
36. M. V. Zabalov, R. P. Tiger and A. A. Berlin, *Russ. Chem. Bull.*, 2012, **61**, 518-527.
37. M. V. Zabalov, M. A. Levina, V. G. Krashenninnikov and R. P. Tiger, *Russ. Chem. Bull.*, 2014, **63**, 1740-1752.
38. S. Sopena, V. Laserna, W. Guo, E. Martin, E. C. Escudero-Adán and A. W. Kleij, *Advanced Synthesis and Catalysis*, 2016, **358**, 2172-2178.
39. M. J. S. Dewar, E. G. Zebisch, E. F. Healy and J. J. P. Stewart, *Journal of the American Chemical Society*, 1985, **107**, 3902-3909.
40. J. Řezáč and P. Hobza, *J. Chem. Theory Comput.*, 2012, **8**, 141-151.
41. AMPAC 10, © 1992-2013 Semichem, Inc. PO Box 1649, Shawnee, KS 66222
42. D. A. Liotard, *International Journal of Quantum Chemistry*, 1992, **44**, 723-741.
43. M. J. Frisch and A. D. Becke, *Gaussian 09, Revision A.02*, 2009, **98**, 5648-5652.
44. Y. Zhao and D. G. Truhlar, *Theoretical Chemistry Accounts*, 2008, **120**, 215-241.
45. R. H. Lambeth and T. J. Henderson, *Polymer (United Kingdom)*, 2013, **54**, 5568-5573.



## Valorisation du CO<sub>2</sub> et d'huiles végétales pour la synthèse de monomères biosourcés

**Résumé :** Bien que thermodynamiquement et cinétiquement stable, le dioxyde de carbone est une molécule qui peut être convertie en carbonates cycliques à cinq ou six atomes respectivement au départ d'époxydes ou d'oxétanes moyennant l'utilisation d'un catalyseur approprié. Ces carbonates cycliques sont utilisés comme solvants verts, électrolytes pour les batteries au lithium ou comme intermédiaires pour la synthèse de polymères. Cependant, les performances catalytiques doivent être améliorées en particulier pour le couplage du CO<sub>2</sub> avec les huiles végétales époxydées ou les oxétanes. Dans ce contexte, nous avons développé un nouveau catalyseur homogène bicomposant organique composé d'un sel d'ammonium jouant le rôle de catalyseur et d'un co-catalyseur fluoré simple ou double donneur de liaison hydrogène. Dans un premier temps, l'efficacité de ces nouveaux catalyseurs a été évaluée et optimisée pour le couplage entre un époxyde terminal et le CO<sub>2</sub> via des études cinétiques par spectroscopie FTIR ou Raman *in-situ* sous pression. Ces études ont démontré que l'utilisation combinée de sels d'ammonium et d'alcools fluorés induit un effet synergique permettant la fixation rapide et sélective du CO<sub>2</sub> sur les époxydes modèles et les huiles végétales époxydées dans des conditions douces et sans solvant. L'utilisation de cette plateforme catalytique performante a ensuite été exploitée pour la synthèse d'oligocarbonates hydroxyles téléchéliques au départ d'oxétanes nettement moins réactifs que les époxydes. Ces oligocarbonates ont finalement été valorisés pour la synthèse de polyuréthanes CO<sub>2</sub>-sourcés par extension de chaînes en présence de diisocyanates. En complément de ces travaux, une compréhension fine des mécanismes réactionnels a été réalisée via calculs DFT qui ont mis en évidence que l'efficacité catalytique de ces catalyseurs était liée à la stabilisation multiple des intermédiaires et états de transition par liaisons hydrogènes. A ce jour, via une étude comparative, nous avons mis en évidence que ce système catalytique bicomposant constitue un des catalyseurs organiques les plus performants pour le couplage du CO<sub>2</sub> et d'époxydes et le seul système organique permettant la conversion d'oxétanes en synthons d'intérêt.

**Mots clés :** Transformation chimique du CO<sub>2</sub>, carbonates cycliques, organocatalyse, spectroscopie FTIR *in-situ*, suivi cinétique, calculs DFT, polycarbonates, alcools fluorés, huiles végétales carbonatées

---

## Carbon dioxide and vegetable oil for the synthesis of bio-based polymer precursors

**Abstract:** Although it is a thermodynamically and kinetically stable molecule, carbon dioxide can be converted into five- and six-membered cyclic carbonates by coupling with epoxides or oxetanes, respectively, using appropriate catalysts. Cyclic carbonates are used as green solvents, electrolytes for Li-ion batteries or intermediates for the synthesis of polymers. However, the catalytic performance must be further enhanced in particular for the coupling of CO<sub>2</sub> with epoxidized vegetable oils or oxetanes. In this context, we developed a new highly efficient bicomponent homogeneous organocatalyst composed of an ammonium salt as the catalyst and fluorinated single or double hydrogen bond donors as co-catalysts. First, a screening of onium-based catalysts and hydrogen-bond donors was performed. Performances of the catalysts and optimization of the reaction was realized through detailed kinetics studies using *in-situ* FTIR/Raman spectroscopy under pressure. We demonstrated that fluorinated alcohols showed unexpected co-catalytic activity due to synergisms between the onium salt and fluorinated co-catalysts enabling the fast and selective addition of CO<sub>2</sub> onto model epoxides and epoxidized vegetable oils under solvent-free and mild experimental conditions. The use of this powerful dual catalyst was then extended to the first organocatalytic coupling of CO<sub>2</sub> with less reactive oxetanes to produce hydroxyl telechelic oligocarbonates that were used as precursor of CO<sub>2</sub>-based polyurethanes by chain-extension with a diisocyanate. In addition, a fine comprehension of the mechanisms was investigated by DFT calculations highlighting that the co-catalytic performance of the onium salt/fluorinated alcohol binary catalyst arose from the strong stabilization of the intermediates and transitions states by hydrogen-bonding. To date, through comparative studies, we evidenced that this new catalyst is one of the most performing and versatile system enabling the coupling of CO<sub>2</sub> both with epoxides or oxetanes.

**Keywords :** Chemical transformation of CO<sub>2</sub>, cyclic carbonates, organocatalysis, *in-situ* FTIR, kinetic monitoring, DFT calculations, polycarbonates, fluorinated alcohols, carbonated vegetable oils

---

### Unités de recherche

Institut des Sciences Moléculaires (ISM), UMR 5255 CNRS – Université de Bordeaux, 351 cours de la libération, 33405 Talence Cedex, France

Center for Education and Research on Macromolecules (CERM), CESAM Research Unit, University of Liège, 13, Allée du 6 Août, Agora square, Building B6a - third floor, B-4000 Liège, Belgium